Analysis, Estimation and Prediction of Fading for a Time-Variant UAV-Ground Control Station Wireless Channel for Cognitive Communications

by

Rafi Mahabbat Bin Belal

A Thesis submitted to the Faculty of Graduate Studies of
The University of Manitoba
in partial fulfilment of the requirements of the degree of

Master of Science

Department of Electrical and Computer Engineering
University of Manitoba
Winnipeg, Manitoba

This page intentionally left blank

This page intentionally left blank

Abstract

The wireless communication channel between an *Unmanned Aerial Vehicle* (UAV) and a ground control station poses severe challenges in estimation and prediction of its characteristics. Its time variant dynamic nature, coupled with the high-speed, complex aerial maneuvers of the UAV, creates severe limitations in the estimation of large scale and small scale fading properties. When operated in a dense urban environment, the dynamic nature of high rise structures in the propagation path, pointing errors of the ground station antenna and orientation change (roll, pitch and yaw) of the UAV antennas contribute heavily to the unpredictable nature of the wireless signal propagation. Recent developments of communication subsystems for these unmanned aerial systems rely on fixed channel models and fading distributions to estimate the level of fading existent in the channel. Consequently, a fixed transmission power is employed by the radios to compensate for this fading. However, the time-variant nature of an urban environment demands an instantaneous estimation of channel coefficients for a better approximation of the channel's fading properties. Moreover, the transmission power should be optimized to increase the range of operation of those UAVs which is cognizant of the channel's fadingdistributions.

This thesis presents a design and implementation of a long-range communication subsystem for a UAV and a ground control station. The subsystem is a low-cost alternative employing a line of sight, local communication network for optimal communications between a low-altitude UAV and a portable ground control station. In this thesis, real world experiments are conducted to model the time-variant wireless channel between a low-altitude micro-UAV and a portable ground control station operating in an urban environment. The large-scale and small-scale fading coefficients are calculated and analyzed for this dynamic channel. The channel properties, along with the fading distribution parameters, are computed and analyzed for two most popular antenna configurations for UAV systems (Yagi to omnidirectional and omnidirectional to omnidirectional). For the Yagi-to-omnidirectional link, the effects of three major impacting factors i.e. propagation distance, antenna gains in specific spherical angles and polarization mismatch factor on the overall fading distribution is investigated. Through regression analysis, a multiple-regression model is derived that estimates the instantaneous fading parameter, given these channel conditions. For this model, a modified particle-swarm optimization algorithm is designed and implemented to estimate the underlying model coefficients, given the instantaneous fading information. The implementation of this algorithm, along with the regression model, demonstrates that a sufficient approximation of the fading parameter can be provided for any given wireless channel when the impacting factors and instantaneous fading information is available.

Visual Abstract

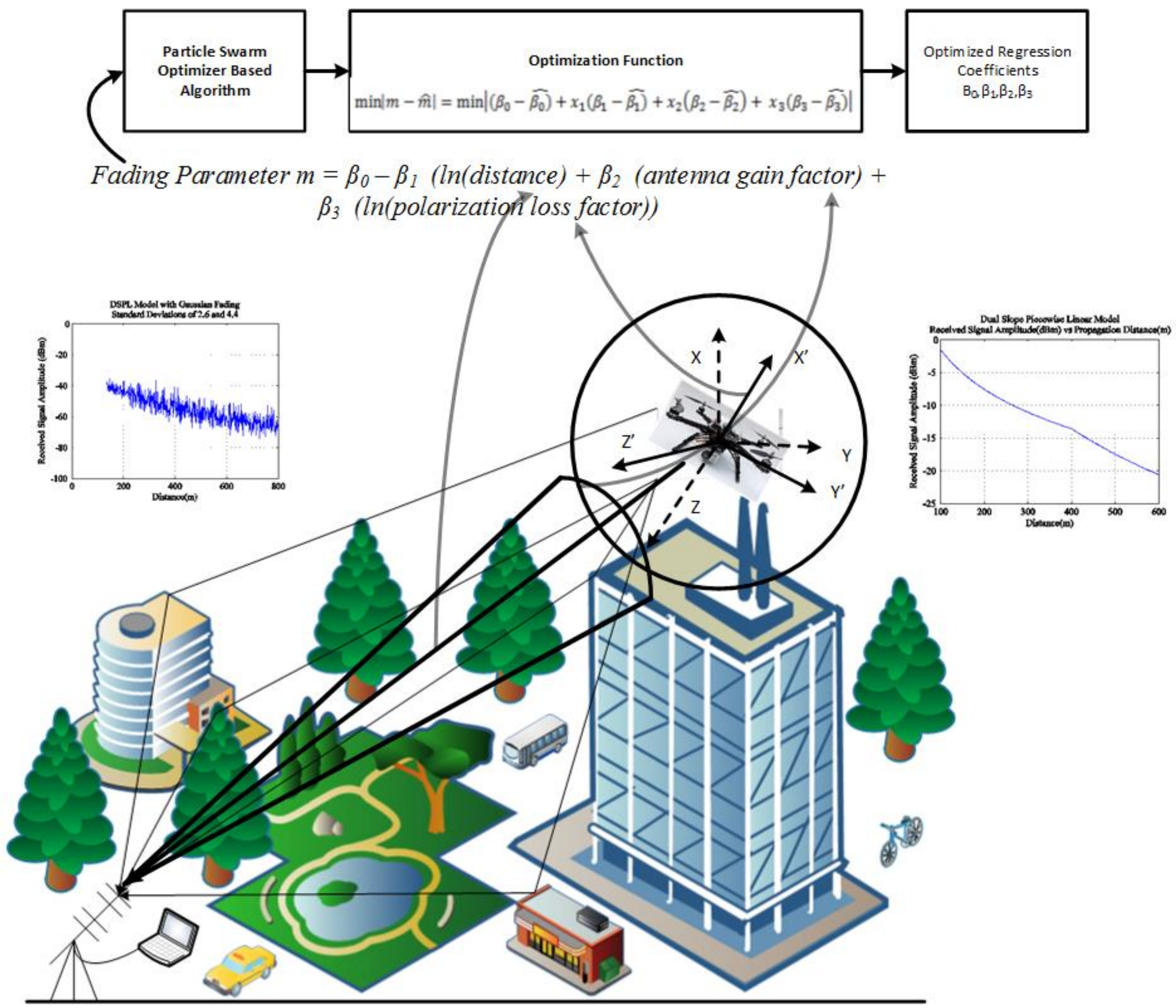

Acknowledgement

This thesis is the result of direct and indirect contributions from some wonderful people who enriched my life by their presence. I would like to take this opportunity to express my humble gratitude towards them who helped me unconditionally during my times of need.

First and foremost, I would like to thank Professor Witold Kinsner for his supervision throughout my Master degree. His knowledge, vision, philosophy towards life and work ethics enriched my life in so many ways that is hard to put down on paper. Working with him was not just a privilege, but an experience of a lifetime. I am honored and proud to have been able to work with him and consider this as the best thing I ever did in my life.

I would like to express my gratitude to my beloved wife, Nishi Hossain, for her love and support throughout this endeavor. She was the strongest pillar, whom I could always lean on during good and bad times. I would like to thank my loving parents, Belal Ahmed and Salma Parveen for their love, encouragement and care throughout my life which helped me most in my life abroad. I cherished the wise words from my father and inspirational words from my mother which guided me through times of distress.

Two very special persons touched my life and contributed immensely throughout this endeavor, Myra Friesen and Aidan Topping. I thank Myra for believing in me and supporting me and my family through difficult times. Words can never express the amount of respect I feel towards her. Working with Aidan Topping was an extremely rewarding experience in my life. She was just not my boss, but a mentor and a friend. The valuable things I learned from her deserve a separate book in its own right.

I would also like to take this opportunity to thank my friend, colleague, mentor and overall a person with whom I could share everything, Mohamed Temam Nasri. He is a wonderful person who poured out his big heart with help, advice and suggestions whenever I needed. I can never thank him enough for his contributions in my life. I would also like to thank Hieu Van Dang for all his technical support and knowledge during this wonderful journey.

I would like to thank all the faculty members of the ECE department of University of Manitoba, who provided me with knowledge and support throughout my courses and research. Special thanks to Dr. Greg Bridges for his technical support during the experimentation stage. Also, special thanks to Glen Kolansky, Sinisa Janic and Amy Dario for all their support and hard work in helping me succeed in my goals and aspirations.

This acknowledgement page would be nevertheless incomplete without mentioning the names of Dr. Barry Prentice, Dale George and all the team members of BASI (Buoyant Aircraft Systems International). I thank them with all my heart for their technical and financial support throughout this research assignment.

Table of Contents

List of Figures

List of Tables

List of Acronyms

UAV	Unmanned aerial vehicle
GCS	Ground control station
BASI	Buoyant Aircraft Systems International
FAA	Federal Aviation Administration
US	United States
GPS	Global positioning system
IMU	Inertia monitoring unit
IEEE	Institute of Electrical and Electronics Engineers
AODV	Advanced on-demand vector
DSR	Dynamic source routing
ANOVA	Analysis of variance
PSO	Particle swarm optimization
RSS	Received signal strength
DSPL	Dual slope piecewise linear
AWSN	Aerial wireless sensor network
ISM	Industrial, scientific and medical
ERP	Effective radiated power
UDAAN	Utilizing directional antennas for *ad hoc*
PCB	Printed circuit board
SIR	Signal-to-interference ratio
CDMA	Code division multiple access
MAC	Media access control
RTS	Request to send
ACK	Acknowledgement
CTS	Clear to send
DRTS	Directional request to send
ORTS	Omnidirectional request to send

ITU	International Telecommunication Union
FSPL	Free space path loss
LOS	Line of sight
CSI	Channel side information
AWGN	Additive white Gaussian noise
SNR	Signal to noise ratio
VHF	Very high frequency
UHF	Ultra high frequency
NEC	Numerical electromagnetic code
RSSI	Received signal strength indicator
PRR	Packet reception ratio
ETR	Effective transmission range
PER	Packet error rate
MMSE	Minimum mean squared error
WCDMA	Wideband code division multiple access
FHSS	Frequency hopping spread spectrum
AES	Advanced encryption standard
GPU	Graphics processing unit
MB	Mega bytes
GB	Giga bytes
GFLOPS	Giga floating-point operations per second
CPU	Central processing unit
GPIO	General Purpose Input/Output
UART	Universal Asynchronous Receiver/Transmitter
SPI	Serial Peripheral Interface
USB	Universal Serial Bus
IC	Integrated circuit
EEPROM	Electrically erasable programmable read-only memory
RF	Radio frequency

VSWR	Voltage standing wave ratio
MPH	Miles per hour
RP-SMA	Reversed polarized subminiature version A
SMA	Subminiature version A
DC	Direct current
LED	Light emitting diode
SD	Secure digital
FPV	First person view
LCD	Liquid crystal display
VGA	Video graphics array
CSI	Camera serial interface
API	Application programming interface
VNA	Vector network analyzer
JPEG	Joint Photographic Experts Group
PVC	Polyvinyl chloride
UDP	User datagram protocol
SE	Standard error
MIMO	Multiple input multiple output
DSSS	Direct sequence spread spectrum

List of Symbols

$s(t)$	Transmit signal model
$u(t)$	Complex baseband signal
$x(t)$	In-phase component of signal
$y(t)$	Quadrature component of signal
B	Bandwidth
p_t	Power of transmit signal
f_c	Carrier frequency
$\emptyset_0$	Initial phase offset
$r(t)$	Received signal model
p_r	Power of received signal
P_L	Path loss
$\sqrt{G_l}$	Product of transmit and receive antenna field radiation pattern in LOS direction
$e^{-j\left(\frac{2\pi d}{\lambda}\right)}$	Phase shift experienced by the wave for distance d
K	Constant path loss factor for Dual Slope Piecewise Linear channel model
γ_1	Path loss exponent for Dual Slope Piecewise Linear channel model
d_0	Reference distance

d_c	Critical distance
γ_2	Path loss exponent after the critical distance
$p(\psi)$	Path loss in Log Normal Shadowing channel model
ξ	$\frac{10}{\ln 10}$
ψ_{dB}	$10\log_{10}\psi$ in dB
$\mu_{\psi dB}$	Mean of ψ_{dB} in dB
$\sigma_{\psi dB}$	Standard deviation of ψ_{dB} in dB
$r_I(t)$	In-phase component of the signal in received signal model
$r_Q(t)$	Quadrature component of the signal in received signal model
$z(t)$	Received signal envelope
$pz(z)$	Probability distribution of the signal envelope
m	Nakagami fading parameter
f_D	Doppler frequency shift
θ	Arrival angle of the received signal relative to the direction of motion given by Eq. (3.15)
v	Velocity of the receiver
λ	Wavelength of received signal in Eq. (3.15)
C	Channel capacity given by Eq. (3.16)
γ	The instantaneous received signal-to-noise ratio (SNR) in Eq. (3.16)

$\bar{S}$	Average transmit signal power in Eq. (3.16)
$\bar{g}$	Average channel power gain in Eq. (3.16)
N_0	Noise spectral density of the AWGN noise $n[i]$ in Eq. (3.16)
$p(\gamma)$	Probability distribution of the received signal-to-noise ratio in Eq. (3.16)
E_b	Signal energy per bit in Eq. (3.17)
T_b	Bit time in Eq. (3.17)
P_{out}	Outage probability given by Eq. (3.18)
γ_s	SNR per symbol given in Eq. (3.18)
$\overline{P_s}$	Average probability of error given in Eq. (3.19)
$P_s(\gamma)$	Probability of symbol error in an AWGN channel with SNR γ in Eq. (3.19)
E_y	Electric field oscillating along the y axis of an electromagnetic wave given in Eq. (3.20)
E_x	Electric field oscillating along the x axis of an electromagnetic wave given in Eq. (3.21)
E_1	Amplitude of wave linearly polarized in x direction given in Eq. (3.21)
E_2	Amplitude of wave linearly polarized in y direction given in Eq. (3.22)
δ	Time-phase angle given in Eq. (3.22)
E	Instantaneous total vector field E given in Eq. (3.23)
2τ	Longitude of polarization ellipse given in Eq. (3.25)
2ε	Latitude of polarization ellipse given in Eq. (3.26)

τ	Tilt angle of the polarization ellipse
V	Voltage response of the antenna given in Eq. (3.28)
MM_a	Angle subtended by great circle line from polarization state of wave M to the polarization state of the antenna M_a given in Eq. (3.28)
F	Polarization mismatch factor given in Eq. (3.29)
$\Delta\tau$	Difference between the tilt angles of wave and antenna given in Eq. (3.30)
AF	Yagi antenna array factor given in Eq. (3.31)
I_0, I_1, I_2	Current excitations at the element centers given in Eq. (3.31)
$F(\theta, \varphi)$	Radiation pattern in azimuth and elevation plane given in Eq. (3.32)
$D_{yagi}(\theta, \varphi)$	Directivity of antenna given in Eq. (3.36)
$G_{yagi}(\theta, \varphi)$	Gain in azimuth and elevation angle given in Eq. (3.37)
$\vec{x_i}(t)$	Position vector of particles in Particle swarm optimization algorithm given in Eq. (3.38)
$\vec{v_i}(t)$	Velocity vector of particles in Particle swarm optimization algorithm given in Eq. (3.39)
A_{eff}	Antenna aperture
P_0	Power transferred to the load of the antenna during signal reception
PFD	Power flux density of the incoming radio waves
X_σ	Zero mean Gaussian random variable with standard deviation of σ given in Eq. (6.4)
$f(x; \mu, \omega)$	Nakagami fading distribution given in Eq. (6.7)

plf	Polarization loss factor given in Eq. (6.10)

This page intentionally left blank

CHAPTER 1

INTRODUCTION

An *Unmanned Aerial Vehicle* (UAV) is a flying object that performs flight operations without any human intervention on board. It can be flown by a human operator by remote control from a *ground control station* (GCS), or it can be pre-programmed for a flight plan and fly without any remote controlling unit. Recently, the term UAV has been replaced by a more descriptive term to *unmanned aircraft system* (UAS) by *Federal Aviation Administration* (FAA) to recognize the fact that these vehicles employ complex ground control station and other elements besides the actual vehicle itself [Theu09]. However, the term UAV, or "drones", is widely recognized throughout the media and general population.

Depending on the type of flight dynamics used, UAVs can be categorized into two main classes: (i) fixed wing and (ii) rotary wing. A fixed wing UAV has fixed wings with a certain wingspan. A rotary wing UAV employs a rotary blade or a propeller based system and has the advantage of flying in every direction (horizontal or vertical) with the ability to hover, when compared with their fixed wing counterparts. These configurations of UAVs are chosen according to their specific applications and each has its own advantages and disadvantages based on their application.

Based on their applications, UAVs can be categorized into five main classes [Wiki14]. **Target and Decoy** UAVs provide ground and aerial gunnery to a target that simulates an enemy aircraft or missile. These are widely used in military operations and aerial warfare. **Reconnaissance** UAVs are mainly used for acquiring battlefield intelligence, coastal area patrol and monitoring. **Combat** UAVs have the ability to search and destroy multiple ground and aerial targets and is used in typical aerial warfare. **Research and development** UAVs are employed by various research organizations for research in remote and dangerous areas such as radiation sources, volcano eruption, and wildlife monitoring. **Civil and commercial** UAVs are employed for commercial purposes such as providing communication backbone in remote and rural areas, and aerial photography.

Based on the degree of autonomy, UAVs are mainly divided into three classes: (i) human controlled UAVs, (ii) semi-autonomous UAVs, and (iii) full autonomous UAVs. Autonomy is a term that is used to define the ability to make decisions without human intervention. Early UAVs were not autonomous and were controlled via a radio link by a human operator. All the necessary operations were controlled by the human pilot. As time progressed, more levels of autonomy were introduced in modern UAVs combining remote control and computerized automation, capable of autonomous control and guidance to perform low level human pilot duties such as speed, flight-path stabilization, and waypoint following. Full autonomous UAVs are also capable of taking off, flying through waypoints and landing in a fully computerized environment, without any human intervention. These sophisticated machines employ complex algorithms to achieve sensor fusion, communications, path planning, trajectory generation, trajectory regulation, task allocation, scheduling, and co-operative tactics.

1.1. History of UAV Development

Military research was the dominant factor in the field of development of unmanned aerial vehicles for the most of the 20th century. Research and development on UAVs can be dated as early as 1916 when Hewitt-Sperry Automatic Airplane conducted some test flights confirming the idea of a flying platform without a human pilot on-board [Mahm07]. In 1917, the US army started working on an aerial torpedo implementing the main principles of flight without human pilot. By October 4th, 1918, 20 complete pilotless aircrafts were developed by a joint venture of different aerospace companies and a successful test flight was conducted. In September 15th 1924, during a test flight of a pilotless plane, the aircraft was damaged during landing and sank. This halted the research into UAVs for a short while. However, with advances in electronics, a major program was started by US Naval Research Laboratory which conducted its first test flight of a UAV in November 15th 1937. The US military re-started its UAV program during early 1950s and employed an Air Force drone named Lightning Bug in the Vietnam war [Myli07]. In early 1980's, Israeli forces used UAVs to track Syrian radar and missile sites in the Bekaa Valley. More recently, US Air Force's high end UAVs such as the Predator and Global Hawk operated over airspaces of Iraq, Bosnia, Kosovo, Afghanistan, and provided reconnaissance, target and destroy functionalities.

Civilian and commercial UAVs of today employ state of the art microcontrollers with digital signal processing techniques as the autopilot, or, the brain of the system. *Global* *positioning system* (GPS) receivers are used to determine its co-ordinates and to measure the speed of the UAV. Gyroscopes and accelerometers are used to compute the spatial orientation and the acceleration of the vehicle. An *inertia monitoring unit* (IMU) is used to monitor the inertia of the vehicle. For communications, digital radio modems with transceivers are used with an antenna for communicating with the ground control station or other UAVs. Moreover, different sensors and actuators are also used based on the application of the UAV.

Most civilian and commercial UAVs of today have maximum flight duration of 1 hour [RFGL13]. These UAVs employ the IEEE 802.11 a/b/g/n standard based WiFi technology to communicate with other UAVs or the ground station [LIED08]. However, WiFi has a limited range of 70m (indoor) to 300m (outdoor) when used with common omnidirectional antennas [Mamm13]. Incorporating high gain directional antennae increases the range although sophisticated tracking mechanism is required to point the antenna in the desired position of the UAV. This drastically increases the complexity of the system adding to the already complex wireless communication channel. Additionally, a lot of UAVs are using the 900 MHz frequency band with high gain directional antennae for telemetry and data communication between the UAV and ground control stations. This frequency band introduces less propagation loss although limiting the data rate and capacity. However, some commercial UAVs are using a hybrid of 900 MHz and 2.4 GHz frequencies to send telemetry using the former and multimedia data using the latter.

Research is being undertaken to increase the flight duration of these unmanned aerial systems for a better application to different fields mentioned above. One of the main constraints in achieving that goal is the limited battery power. Being of a small form factor, these vehicles have a limited power resource for flight operations and communications. Long range communications can be a resource hungry component for these systems with radios operating at maximum power for a longer communication range. Limitation and regulation of the transmission power for these radios can reduce the power consumption for long range communication for these systems and hence, increase power efficiency to achieve a longer flight range. To regulate the transmission power of the radios, large scale and small scale fading of the wireless channel need to be estimated and predicted to vary the transmission power according to the channel conditions. Moreover, sudden altitude and orientation change of UAVs further degrades the wireless channel because of polarization mismatch factor and change in antenna spherical angles. Last but not the least, the distance (and the density of buildings, cars) between the UAV and a ground control station severely impacts the small scale fading of the wireless channel.

This thesis presents a study on the wireless channel between a UAV and a ground control station in a typical urban environment. The main objectives are to choose the best wireless channel model for this environment, estimate the large scale and small scale fading parameters, investigate the relationship of the severity of fading with distance and orientation of UAVs and lastly, to design an algorithm which can estimate the level of fading for different wireless channel given certain channel parameters. Various power control algorithms can then be applied to vary the transmission power of the radios according to the severity of fading in the channel to increase power efficiency and thus increase flight and communication range of UAVs.

1.2. Problem Statement

There are a number of problems and challenges associated with the modeling and estimation of fading of a wireless channel between a UAV and a ground control station in an urban environment. This section provides the main motivation behind the characterization of fading of a wireless channel to achieve a long range UAV flight, factors affecting the fading distribution of the channel and the solutions proposed by this thesis for a proper estimation of fading to determine the instantaneous behavior of the channel.

1.2.1. Motivation

Employment of civilian UAVs are increasing rapidly for various civil duties such as firefighting, police surveillance, scientific and environmental studies, and communication backbone. A lot of countries are looking into the deployment of small UAVs for coastal area patrol and monitoring of major oil and gas pipelines. News reporting agencies are looking into deployment of UAVs for news gathering and video transmission replacing more expensive alternatives such as news helicopters. Real estate and tourism industries are also employing UAVs for aerial photography. For search and rescue missions, UAVs have tremendous advantages due to its capabilities of penetrating dangerous and remote places and monitoring. More recently Amazon and Google have teamed up to come up with a fully autonomous fleet of UAVs to deliver items to customers. Agriculture has enormous potentials for UAV deployment in counting stocks, checking dam levels, and monitoring of crops and resources.

Another major civil application that can benefit from UAV deployment is transportation. Countries with vast territories (e.g. Canada) have many remote and isolated communities in its vast territory. These remote communities need to be connected to the city with terrestrial means. For a big country like Canada, this is not an easy measure. Moreover, severe weather conditions degrade the quality of the roads every year and these become unusable repeatedly. One good alternative for terrestrial connections would be through airspace and employment of UAVs for transportation of goods. However, this is not an easy task since, a lot of challenges lie ahead for fully autonomous UAVs to acquire a long range capability in terms of both flight path and communications. A new class of UAVs is being designed by Buoyant Aircraft Systems International (BASI) in Manitoba to overcome the challenges of long range UAV flight and communication to provide transportation to various remote communities in northern Manitoba. The UAV, still in its development phase can be seen in Fig. 1.1.

Fig. 1.1: The development phase of the hexacopter named “ORBO” by Buoyant Aircraft Systems International (BASI).

1.2.2. Problem Definition

Although current civilian UAVs are restricted to a flight range of maximum 1 hour, research is being undertaken by different companies to increase that range. One of the main constraints is power. As civilian UAVs are smaller in size, they are limited by the battery capacity that puts an upper bound on the flight range it can achieve. However, recent advances in battery capacity, electric motor technology and solar cell efficiency have increased the range of solar powered UAVs tremendously. QinetiQ's Zephyr (a solar powered UAV) flew more than two weeks continuously, demonstrating the range of operations solar UAVs can achieve [Qine10].

In order to have a long range flight, one of the key components needed is effective communication between UAVs and ground control stations. There are two ways the effective range of communication can be extended: (i) having a network of ground control stations to provide long range communication support to a single UAV, and (ii) having a swarm of UAVs and employing a network of communication between them.

For a successful and long range operation of UAVs, we need to ensure the stability of wireless communication links between the UAV and ground control stations. Most of civilian UAVs in use today are limited by battery power which introduces a limit in their transmission power. Sudden altitude and orientation changes in UAVs due to high speed maneuvers and sharp banking also degrades the signal quality and decreases signal strength. Limitations on antenna deployment on the UAV also introduce some constraints on achieving a long range communication link between UAVs and ground control stations. These problems need to be addressed in order to design and implement an effective, long range communication network for a UAV and ground control stations.

In order to achieve a reliable high speed communication, the wireless radio channel itself acts as the biggest technical challenge. The wireless channel is usually degraded by noise and interference. Moreover, these changes and effects are time variant due to the high mobility of UAVs. As the UAV moves with high speed, the environment of the wireless channel between the UAV and ground control station also change rapidly, which introduce non-stationary channel impediments. The variation in received power is caused by these channel impediments as well as path loss and shadowing [Gold04]. Path loss is associated with the dissipation of power radiated by the transmitter with the adverse effects the channel has on the signal. Shadowing is caused by things that absorb the power of the transmitted signal and exists between the transmitter and receiver. These are referred to as large scale propagation effects as variations due to them occur in large distances. Small scale propagation effects occur because of variations due to the constructive and destructive addition of multipath signal components. This is also known as multipath fading. In order to achieve a reliable communication link, we need to model the propagation environment accurately. An accurate representation of the channel impulse response will enable correct prediction of channel quality and help to compensate for degraded wireless communication link.

To determine the reliability and stability of these wireless channels, we also need to determine the capacity limits of these channels. Capacity limit is associated with the maximum data rate that can be supported by the channel [Gold04]. Claude Shannon, in his pioneering work in channel capacity in the late 1940s, developed a mathematical model of communication based on the notion of mutual information between the input and output of a channel. Moreover, the Shannon capacity for these time-variant wireless channels with channel side information at both the transmitter and receiver is an important component for system design and performance analysis. Adaptive and cognitive techniques to compensate for channel variation can then be designed by adapting the transmission power or data rate according to these capacity measures.

In order to establish and maintain a reliable communication link, the communication framework should be able to predict the link quality and link breakage probability [Myli07]. Detailed study on the broadside and endfire radiation patterns for the antennas considered for this communication sub-system is of paramount importance. For an accurate prediction of the wireless signal quality, measures such as directivity, gain, polarization, polarization mismatch factors of the antennas and atmospheric attenuation of the transmitted signal need to be calculated. Noise temperature onboard the UAV and ground station antenna needs to be calculated to measure the signal to noise ratio of the channel.

For achieving a long range of operation, the UAV should be linked with a network of ground control stations to provide it with communication support. Beyond line-of-sight communication can be achieved by employing multiple ground control stations and can act as a less expensive alternative to satellite communication. Different ad hoc multi-hop routing protocols such as Advanced On-Demand Vector (AODV) and Dynamic Source Routing (DSR) need to be studied for implementation in the multiple ground control station and UAV network [Mamm13].

One of the major constraints of UAV communications is limited battery power. This directly affects the long range capabilities of UAV operations as these systems rely on battery power alone. One of the major improvements of such UAV systems will be to have a cognitive and adaptive power control algorithm to vary the transmission power according to the distance and link quality metrics. This will reduce the power consumption by power hungry radio transmission and at the same time improve signal quality.

1.2.3. Proposed Solution

The proposed solution is to accurately estimate the level of fading a channel suffers from between a UAV and a ground control station to employ an effective transmission power control algorithm. In order to achieve that, the wireless channel in an urban environment needs to be analyzed and modeled properly. Five sets of received signal amplitude versus distance data are obtained through experiments. A UAV node and a ground control station node is positioned in different places on campus with varying degrees of orientation of UAV node antenna to capture the power fall off versus polarization mismatch and antenna spherical angles. The experiment data are modeled with different state-of-the art wireless channel models and compared. The best performing model is chosen to accurately represent the wireless channel. The large scale and small scale fading distribution parameters are analyzed for this model and compared with different antenna configurations. Through regression analysis, individual relationships between the severity of small scale fading and parameters such as distance, UAV antenna orientation and polarization mismatch factor are analyzed. These individual relationships are superimposed on the overall fading to get a linear approximation of the data through multiple linear regression analysis. This multiple linear regression model is evaluated through statistical measures to test how well this model explains the variation of fading in the data. A simple particle swarm optimization based algorithm is designed and tested to estimate the actual fading parameter of any given channel based on this model. The data presented in this study could also be used by policymakers to regulate data communications schemes and techniques between UAVs and ground control stations operating in dense urban environment.

1.3. Thesis Formulation

This section provides the main statement this thesis attempts to address along with its key objectives. It also gives an overview of the key research questions this thesis tries to answer.

1.3.1. Thesis Statement

This thesis aims to develop a linear approximation model of the severity of fading for any given wireless channel between a UAV and a ground control station against channel parameters such as distance, antenna spherical angles, polarization mismatch factors to accurately estimate and predict the instantaneous behavior of the channel.

1.3.2. Thesis Objectives

This thesis has three main objectives:

1. Modeling of the wireless channel between a UAV and a portable ground control station in an urban environment for an accurate representation of the channel, including:
    a) Conduct experiments to acquire the received signal amplitude versus distance between the UAV and ground control station;
    b) Conduct experiments to capture the received signal amplitude falloff with varying degrees of antenna spherical angles and polarization mismatch factor;

  c) Model the experiment data with different wireless channel models through regression analysis and choose the best performing model for further analysis.

2. Analysis of the large scale and small scale fading of the channel and comparison with different UAV-GCS antenna configurations, including:
   a) Analyze and investigate the correlation of large scale fading with distance;
   b) Analyze and investigate the small scale fading with distance;
   c) Compare large and small scale fading with different UAV-GCS antenna configurations.
3. Linear approximation of fading against distance, antenna spherical angles and polarization mismatch factor between UAV and ground control station, including:
   a) Investigate the individual relationship between the fading parameter and distance;
   b) Investigate the individual relationship between the fading parameter and antenna spherical angles of the UAV antenna;
   c) Investigate the individual relationship between the fading parameter and polarization mismatch factor; and
   d) Through multiple linear regression, develop a model that approximates the fading parameter given certain channel parameters.
4. Design and test of a particle swarm optimization based algorithm to estimate the fading of a channel based on this model given the channel parameters

1.3.3. Research Questions

This thesis presents a number of research questions on the fading wireless channel that exists between a low altitude UAV and a portable ground control station in an urban scenario. The questions that are addressed in this thesis are provided below.

1. For a low altitude UAV equipped with an omnidirectional antenna and a portable ground control station equipped with a directional Yagi antenna in an urban environment, what is the correlation of received signal amplitude with distance?
2. How does the mean and standard deviation of the received signal amplitude vary with the distance for this particular environment?
3. How does received signal amplitude, its mean and standard deviation, vary with distance when the UAV and ground control station is both equipped with an omnidirectional antenna?
4. For a portable ground control station equipped with a directional Yagi antenna and a low altitude UAV equipped with an omnidirectional antenna operating in an urban environment, which wireless channel model best describes the path loss against distance?
5. For a dual slope piecewise linear model, how does the path loss exponent vary when we have directional-to-omnidirectional and omnidirectional-to-omnidirectional antenna configurations?
6. For a log normal shadowing model, how does the path loss exponent vary when we have directional-to-omnidirectional and omnidirectional-to-omnidirectional antenna configurations?

7. For a portable ground control station equipped with a directional Yagi antenna and a low altitude UAV equipped with an omnidirectional antenna operating in an urban environment, which fading model best describes the small scale fading of the channel?
8. In the case of modeling the fading as Gaussian fading, how does the standard deviation of the Gaussian fading vary when modeled with dual slope piecewise linear model for directional-to-omnidirectional and omnidirectional-to-omnidirectional antenna configurations?
9. In the case of modeling the fading as Gaussian fading, how does the standard deviation of the Gaussian fading vary when modeled with log normal shadowing model for directional-to-omnidirectional and omnidirectional-to-omnidirectional antenna configurations?
10. How does the Nakagami shape parameter of the small scale fading vary when modeled with dual slope piecewise linear model against distance for a directional-to-omnidirectional antenna configuration?
11. What are the impacts of polarization mismatch factor between the antennas, directional gain of antennas in specific spherical angles and multipath propagation due to buildings, cars, roads on the Nakagami shape parameter of small scale fading?
12. For a portable ground control station equipped with a directional Yagi antenna situated 3.5 feet from the ground, how does the far field radiation pattern change as the polarization of the antenna is changed from vertical to horizontal?
13. Can we derive a linear approximation model for the overall impact of the above mentioned three factors on the Nakagami shape parameter of the small scale fading? What are the boundary conditions on the parameters?

14. What does this linear approximation model suggest about the channel?
15. In terms of percentage, how much of the variation of the fading parameter can be explained by this linear model?
16. In terms of Analysis-of-Variance (ANOVA), how does this model perform in fitting the experimental data?
17. Can Particle Swarm Optimization (PSO) be applied to design an algorithm that will be able to accurately estimate the fading parameter for a channel given certain channel parameters based on this model? If yes, what modifications need to be made in the particle swarm optimization method?

1.4. Thesis Organization

This thesis presents an analysis of the fading wireless channel between a UAV and a portable ground control station. It investigates the impacts of several channel parameters on the fading distribution in this wireless channel. It derives a linear approximation model that is able to explain the variation of the fading parameter in this channel as the channel parameters change. It designs an algorithm based on particle swarm optimization technique that can accurately estimate the fading parameters of the channel given the channel parameters. Chapter 2 of this thesis provides an overview of the state-of-the-art technologies and research being used in different aspects of UAV to ground control station communications. Chapter 3 provides a theoretical background on large scale and small scale fading in a wireless channel along with the effects of polarization mismatch factor, directional gain and multipath propagation in wireless communications. It also provides a brief overview of the particle swarm optimization method and antenna modeling tools. Chapter 4 provides detailed information about the design and implementation of a line-of-sight communication sub-system between a UAV and a portable ground control station. Chapter 5 provides a detailed description on the methodology of the experiments conducted, equipment used and data collection procedures. Chapter 6 presents the results of the experiments and provides a detailed discussion on the observations. Chapter 7 states the main conclusions drawn from this research assignment.

1.5. Summary

This chapter provides an introduction to this research work with a brief overview of unmanned aerial systems and their history of development. The main motivations behind this new technology and its advancements are also given. It provides a short summary of what problems currently exist in achieving a longer range of operation of this technology to be implemented in various applications. The proposed solutions that can mitigate these problems are also introduced in this section. Lastly, this section provides the thesis statement, main objectives of this thesis and the key research questions addressed in this thesis. The scope of this thesis is limited to a direct point-to-point communication between a UAV and a ground control station. The main aim of this research is to analyze this time-variant wireless link in terms of large scale and small scale fading. The core of the research is to characterize the fading parameter's variation with respect to the channel impediments for correct prediction of fading in any given environment.

The next chapter provides the reader with a brief overview of the current techniques being employed to increase the range of communication and operation between UAVs and ground control stations.

This page intentionally left blank

CHAPTER 2

LITERATURE REVIEW OF UAV COMMUNICATIONS

In the previous chapter, an introduction to this thesis is provided along with the motivation behind this research, main problems, and the solutions proposed. This chapter provides the reader with an overview of the recent development in research for some of these areas. It also highlights the observations, findings of these research assignments and discusses some of the limitations. Lastly, this chapter provides what this thesis proposes to overcome the problems faced in a point-to-point wireless link between a UAV and a ground control station.

2.1. Selection Criteria of Pertinent Research

A detailed study of the literature reveals significant amount of research relevant to communication strategies between unmanned aerial vehicles and ground control stations. This section provides the methodology of selecting pertinent research and development reviewed in this thesis. Recent research involving digital signal processing techniques employing digital radios to communicate between UAVs and ground control stations is reviewed. A review of different research work related to the communication frequencies is included, focusing on single and hybrid frequency allocation. Research involving UAVs used as communication relays to extend the range of traditional communication backbone and emergency situations is reviewed. A short overview of recent developments in using cellular links to provide communication between UAVs and ground control stations is provided. Detailed review of research work concerning the modeling of the time varying wireless channel between UAVs and ground control station is conducted involving different channel models. Vehicle-to-vehicle (V2V), air-to-ground and aerial networks of communication are also investigated involving these propagation environments, providing majority of focus to large and small scale fading effects. A short review of different antenna selection, configuration and design for UAV-GCS wireless channel is provided. Specifically, research work involving directional antennas, their effects and limitations are reviewed in detail. The implementation of cognitive communication techniques are reviewed in recent literature for UAV-GCS and UAV-UAV links with their performance characteristics. Special focus is provided in optimal transmission power control strategies employed to extend the range of communications for civilian UAV systems. Various media access control and network layer protocols are reviewed for UAV-GCS communication links and their performance are evaluated. Moreover, a short review on ionospheric attenuation on radio waves involving high altitude VHF links is provided along with the higher attenuation reported in melting layer regions. In addition, research findings of excess signal attenuation due to snowfall in certain frequencies are reviewed for cold weather regions. The next section provides a detailed discussion on the above mentioned research work reviewed in this thesis.

2.2. Review of Pertinent Research

Modern UAVs employed in civil purposes today use a ground control station to communicate with a single UAV or, a network of UAVs. The communication sub-system for an unmanned aerial system is one of the key components for a safe and stable flight operation. This chapter discusses some of the implementations of this communication sub-system employed by different research initiatives and their limitations. Most of the civil UAVs today employ digital signal processing techniques incorporating digital radios to communicate with the ground control station for control and monitoring purposes. In [Roch99], Rochus shows that in terms of wireless communications, digital signal processing demonstrates superior performance for noise and interference immunity when compared to their analog counter parts.

For communication frequencies, different unmanned aerial systems incorporate various frequencies for controlling and data communication schemes. In literature, a combination of different frequencies has also been reported to provide a better performance for wireless data communications between a ground control station and UAVs. Among them, Zhou et al. in [ZhZa07] incorporates a hybrid transmission scheme employing the 72 MHz frequency for manual flight control and the 900 MHz frequency for multimedia streaming with a low resolution. In [ShKS00], the authors proposed a hybrid communication scheme by employing both the 900 MHz frequency and the 2.4 GHz frequency for data communications between the ground station and the UAV. The scheme is able to switch between these two frequencies for different scenarios. When a longer range is needed, the radio operates in the 900 MHz frequency band for its higher propagation distance. When, faster data rate is needed for multimedia streaming, the system switches to the 2.4 GHz frequency band.

Various applications of UAVs in different fields of the civilian domain have been reported in the literature. In telecommunications, UAVs can play a key role in enhancing the communication range of a telecommunication network significantly by acting as communication relays. In natural disaster or emergency situations, traditional communication infrastructure might fail and UAVs can play a major role in restoring communication in the affected areas. In [Sarr01], the authors employ UAVs as communication satellites to provide a longer communication range for the existing telecommunication network.

Using cellular links for data communication between UAVs and ground control stations has also been reported in the literature. Goddemeier et al. used a fixed wing UAV to measure cellular link properties in different altitudes based on their Received Signal Strength (RSS) values in [GoDW10]. Their study concluded that within an altitude limit of 500m, cellular links could be used reliably to control a UAV from a ground control station. Moreover, Wzorek et al. in [WzLD06], operated a Yamaha RMAX helicopter using cellular links with a maximum altitude of 25-35 meters.

To understand the complex time-varying dynamics of the propagation environment of the wireless link between a UAV and a ground control station, accurate models are needed in order to appropriately model the uncertainties. In [CHSB07] and [CHBS08], the authors modeled the wireless channel for their vehicle-to-vehicle (V2V) network using the Dual Slope Piecewise Linear (DSPL) model. The large scale fading such as propagation loss and shadowing is modeled with a path loss exponent that can be varied according to the environment. In [GPRB10], the authors employed the DSPL model to measure the path loss exponent in an urban scenario with varying vehicle speed. Short scale fading or, multipath fading is also an important factor when modeling a wireless channel. Due to high speed maneuvers of UAVs, the propagation environment changes rapidly and it is almost impossible to model this environment deterministically. In [Gold04], Goldsmith states that the multipath propagation channel can be characterized statistically with parameters representing the severity of the fading. The author provided different statistical models to model the short scale fading environment with distributions such as Rayleigh distribution, Rician distribution and Nakagami distribution. In [BeCh01], Beaulieu et al. show that with the Nakagami-m distribution, the fading can be appropriately modeled by varying the fading parameter for different types of fading environment. In [Isla13], Tarikul Islam modeled his V2V wireless channel with the Nakagami-m distribution with the m fading parameter to represent the fading from light, moderate and severe.

Antennas are a key component in the wireless system design for an unmanned aerial system. In [StTh98], the author provides a taxonomy on different kinds of antennas used in wireless systems today and also states that it is a key component of all mobile communications. In [Bala97], the author puts an emphasis on a good antenna design that can improve the performance of wireless channels. For the communication sub-system employed by an unmanned aerial system, various types of antennas are implemented and reported in the literature. In [PaJu10], Park et al. conducted a simulation study on the suitability of antennas deployed in an unmanned aerial system. They installed an omnidirectional antenna on the UAV and the ground station was equipped with a directional antenna and an omnidirectional antenna. During a UAV flyby, the authors show that omnidirectional antenna showed superior performance in maintaining the communication due to the highly directional nature of directional antennas. However, the tests were conclusive for a short range of communication as omni-directional antennas provide a shorter range than the directional ones. Moreover, other characteristics of an antenna such as orientation and elevation also affect the wireless system performance. In [CHKV06], Cheng et al. measured the 802.11a link performance for 32 pairs of UAV-to-ground station antenna configurations with their RSS values. They state that to achieve maximum throughput for the communication subsystem, both the ground station and the UAV should be equipped with an omnidirectional dipole antenna with horizontal orientation. Allred et al. in [AHPP07], measured the link characteristics of 802.15.4 networks in an aerial wireless sensor network (AWSN) test bed equipped with Xbee Pro mounted SensorFlock platform. They conclude that using quarter wave whip antenna, the best performance of the wireless link was found when the antenna orientation was close to 90 degrees.

As seen in the literature, most of the communication sub-systems employed by civilian unmanned aerial systems use the license free Industrial, Scientific and Medical (ISM) radio bands for communications. However, the maximum power is regulated by government inside these bands. This is a direct constraint to achieve a longer range of communications in these bands between a ground control station and a UAV. According to [Cana07], Industry Canada regulates the Effective Radiated Power (ERP) to a maximum of 4 watts for frequencies between 902 and 928 MHz in Canada. To mitigate this challenge and achieve a longer range using the ISM bands, highly directional antennas are used with a precision tracking mechanism in ground control stations. In [SPSM12], Shivaldova et al. conducted detailed simulation studies on the impact of directional antennas in vehicle-to-infrastructure communications and concluded that significant performance improvements can be achieved when employed in 802.11p networks. Jasani et al. in [JaYe06] proposed a scheme to maintain a stable link created by directional antennas by changing the directional antenna pattern based on the received power of the receiver. If the received power falls below a given threshold, the adaptive scheme changes the antenna pattern to produce higher gain for the directional antenna and thus extends the link that is about to break. Ramanathan et al. in [RRSW05] proposes a complete solution for systems employing directional antennas with novel mechanisms such as neighbor discovery with beam forming, link characterization for an ad hoc communication network. Their scheme is called Utilizing Directional Antennas for Ad Hoc (UDAAN). Tracking is an important component for systems employing directional antennas due to their highly directional nature. Balzano et al. used an advanced gimbal system for precision tracking of the mobile unit for a stable pointing operation in [BRMD07]. Jenvey et al. in [JeGH07] uses an omnidirectional antenna on the UAV and a directional 2.4 GHz antenna mounted on a rotating mechanical platform for tracking the UAV node. Other antenna configurations and their performance are also reported in the literature for unmanned aerial systems. In [TMCH08], Teh et al. performed some link performance and range measurements on an AWSN test bed employing Fleck systems with external 900 MHz antenna mounted on fixed wing UAVs. In [Mems14], Ahmed et al. uses the off-the-shelf TelosB platform with a PCB mounted inverted F antenna to conduct link characterization experiments.

Cognitive radios has been well known for its efficiency in adapting its properties based on the dynamic wireless channel and maximize performance with limited resources. According to our knowledge, there are not much work reported in the literature about implementing cognitive radio techniques for spectrum and resource sharing for unmanned aerial system communications. Lee in [Lee12] used a link-budget based signal-to-interference ratio (SIR) estimate to come up with a power control algorithm for code division multiple access (CDMA) communications between a base station and multiple UAVs. However, the main motivation behind the work was to calculate the UAV distance using linearity between speed and consecutive transmit power control ratio. Transmission power control is a well-known technique employed by cognitive radio systems to achieve maximum throughput with limited resources. In [NBRG02], the authors use game theory to change the transmission power level of secondary users to limit the interference caused by them to the primary user. In [MaSW01], the authors employ a transmission power control technique in an ALOHA network where the secondary users set their own transmission power levels. In [Hayk05], Haykin proposed a cognitive power control scheme for secondary users based on water filling technique. However, the transmission powers are all known and lies within a permissible rate region. In [HoSa05], the authors varied the transmission power of secondary users according to the received signal to noise ratio which they used as a proxy for distance.

Various *media access control* (MAC) layer protocols have been proposed in literature for optimal communications between ground control stations and UAVs. Wang et al. in [WaFW06] proposed a novel MAC timing structure to solve different mac layer problems such as the deafness problem, hidden terminal problem, exposed terminal problem and head-of-line blocking problem using directional antennas. In [KoSV00], the authors propose a novel mac layer scheme which involves transmission of *request-to-send* (RTS), *acknowledgement* (ACK) and data packets with a directional antenna and *clear-to-send* (CTS) packets with omnidirectional antenna. They also propose two types of RTS packets with one being a *directional request-to-send* (DRTS) using directional antenna and the other being *omnidirectional request-to-send* (ORTS) using an omnidirectional antenna. Multiple antenna technique has also been employed in [TMRB02] by Takai et al. which takes the advantage of a caching mechanism. Their work calculates the angular location of receiving nodes and according to that location transmits to that node using either directional or omnidirectional antenna.

Various network layer methods have been proposed by researchers for an optimal control and coordination of a network of UAVs using evolutionary algorithms and reinforcement learning in the literature. In [CBTA08], an optimal UAV path planning mechanism is proposed using a game theoretic approach for single and multiple UAVs. In [RiWB05], authors proposed a collaborative search technique for a swarm of UAVs using genetic algorithms. Authors in [MiDJ07] used an ant colony based swarm intelligence technique for optimal coordination of a swarm of UAVs for automatic target recognition in reconnaissance tasks. In case of limited communication constraints, authors in [BaOS08] proposed a genetic programming based multi-task allocation mechanism for a swarm of UAVs to maximize the output.

The wireless channel between a UAV and a ground control station is also affected by weather. Rain drops cause additional fading for wireless links which gave rise to rain-fade prediction models in the Recommendation ITU-R P.530 [InTU13]. Melting snow or ice particles situated in the melting layer are the source of rain drops. These are known as wet snow particles and Kerker showed in [AdKe51] that these particles scatter the electromagnetic signal much more than rain drops. Gunn and East in [GuEa54] stated that a larger attenuation and more scattering is experienced by the electromagnetic wave when it passes through this lower density water covered particles. Takada and Nakamura in [TaNa66] reported larger fading being experienced by electromagnetic waves from wet snow than it would for rain precipitation rate only. Moreover, snowfall creates more attenuation and fading in wireless signals than rainfall. Nishitsuji in [Nish71] conducted experiments in radio links and measured higher attenuation rate in snowfall than rainfall alone. In Canada, Kharadly *et al.* reported excess specific attenuation which was 40 times higher than specific attenuation due to rain in dB/km for certain frequency bands [KOSM83]. Hendry *et al.* also reports higher attenuation suffered by wireless signals in an earth-satellite wireless link due to melting layer [HASO81]. In [InTU02], Bacon and Eden provides the Bacon and Eden combined rain and wet snow attenuation prediction method which takes the melting layer height variability into account.

To achieve an optimal communication framework between a ground control station and a UAV, the range of the wireless link is a key factor. A lot of research work presented above operates in a limited range due to the limited range of omnidirectional antennas. For a longer range, some of the works proposed to have a network of UAVs connected with each other in an ad hoc fashion. In this thesis, we focus on a communication framework for an unmanned aerial system which employs a highly directional Yagi antenna at the ground control station and an omnidirectional antenna on board the UAV to achieve a long range of communication. We also aim to extend the wireless coverage of the link by employing a network of portable ground control stations linked to the UAV. Maintaining a stable link with a constant data rate is also a challenge for the dynamic behavior of the wireless link between the ground station and the UAV. This thesis analyzes and models the large scale and small scale fading of this time varying wireless link to maintain a stable wireless connection between the UAV and the ground control station. Many of the research work mentioned above investigates the correlation of received signal strength (RSS) value with distance with omnidirectional antenna on UAV and ground control station. In this thesis, a comparative study is conducted between the correlation of received signal amplitude and fading parameter with distance for different antenna configurations. Some of the research assignments mentioned above investigate the relationship of the severity of fading with distance only. This might be adequate for a vehicle to vehicle communication channel. However, for a low altitude UAV, other factors need to be taken into account. This thesis investigates the individual and overall relationship between fading parameter and distance, directional gain, polarization mismatch factor of antennas. A linear approximation model of the fading parameter is developed in this thesis given the channel parameters mentioned above. Battery power is one of the most important resources for civilian unmanned aerial systems and most of the research work presented above does not take into account of that fact. Moreover, cognitive power control techniques are not implemented for UAV transmission schemes to the best of our knowledge to maximize the battery power. This thesis designs a particle swarm optimization based algorithm which accurately estimates the fading parameter of a channel given certain channel parameters based on the linear approximation model. Further suggestion is made in this thesis to use cognitive transmission power control schemes based on the estimation of instantaneous fading in the channel. This ensures the optimal use of the scarce battery power for both the UAV and portable ground control stations and in the same time, maximizes the throughput of data communication.

This chapter provides a detailed review of pertinent research reported in literature concerning wireless communications between UAVs and ground control stations. Critical findings of these research along with their limitations are discussed. The next chapter discusses some of the theory behind the fading wireless channel which is the main topic of research in this thesis. Moreover, factors that affect this wireless channel are discussed in detail. A short overview of the particle swarm optimization algorithm is also provided.

This page intentionally left blank

CHAPTER 3

BACKGROUND ON UAV-GCS COMMUNICATION

In the previous chapter, a short review of the research undertaken to increase the range and quality of wireless communication between a UAV and a ground control station is provided. This chapter discusses the details of this point-to-point wireless link along with the transmitted and received signal models. The characterization of different types of fading suffered by this channel is elaborated. Different channel models are discussed with their advantages and disadvantages in modeling the actual channel. The factors that affect this wireless channel such as multipath fading, shadowing, path loss, directional gain of antennas and polarization mismatch factor are investigated. Moreover, the particle swarm based optimization technique is discussed in detail.

The wireless channel between a UAV and a ground control station is a challenge in its own right for reliable communication. This channel suffers from noise, interference, large scale and small scale fading. Moreover, these channel impediments are not stationary. They change rapidly due to the high mobility and complex aerial maneuvers of UAVs. This changes the channel characteristics abruptly and can cause severe channel degradation. To analyze this time varying wireless channel, further discussion of the basic principles of radio wave propagation is needed.

Radio wave propagation has been approximated by various propagation models. These models attempt to characterize the signal propagation for a certain environment of wireless communication. It is well known that radio waves suffer from reflection, scattering and diffraction by objects such as walls, buildings, roads, and cars that exist in its propagation path. Maxwell's equations with boundary conditions can be used to obtain the detailed characteristics of this propagation by using radar cross-section of large and complex structures [Gold04]. However, these details are not always available and an approximation to the signal propagation is enough to capture the characteristics of the channel.

Ray tracing techniques are one of the most common methods of approximating the signal propagation. It represents the signal wavefronts as simple particles that traverse through the medium. The reflection and refraction of waves is adequately represented by this method for a specific signal propagating in a certain environment. However, the phenomenon of signal scattering is ignored.

In order to capture the scattering and diffraction of electromagnetic waves during propagation, more complex models are employed which are based on empirical measurements.

These models which are called empirical models are discussed in detail in the subsequent sections. However, deterministic channel models do not always capture the characteristics of the actual propagation environment due to the complex and time-varying nature of the wireless medium. In these cases, statistical models are employed where the path loss, shadowing and multipath fading of the propagating signal are characterized statistically. These statistical models are also discussed in detail.

3.1. Model of the Transmitted and Received Signal

In this section, we model transmitted and received signal for the wireless link between the ground control station and the UAV. We consider the signals as real signals. The transmitted signal is modeled according to [Gold04] as

$$
\begin{aligned}
s(t) &= \Re\left\{u(t)e^{j(2\pi f_c t+\emptyset_0)}\right\} \\
&= \Re\{u(t)\}\cos(2\pi f_c t+\emptyset_0) - \Im\{u(t)\}\sin(2\pi f_c t+\emptyset_0) \\
&= x(t)\cos(2\pi f_c t+\emptyset_0) - y(t)\sin(2\pi f_c t+\emptyset_0) \qquad (3.1)
\end{aligned}
$$

where, $u(t) = x(t) + jy(t)$ is the complex baseband signal, $x(t) = \Re\{u(t)\}$ is the in-phase component, $y(t) = \Im\{u(t)\}$ is the quadrature component, B is the bandwidth, $P_t = P_u/2$ is the power of the transmit signal, f_c is the carrier frequency, and $\emptyset_0$ is the initial phase offset of the signal.

The received signal can be modeled as

$$
r(t) = \Re\left\{v(t)e^{j(2\pi f_c t+\emptyset_0)}\right\} \qquad (3.2)
$$

As the transmitted signal traverses through the wireless medium, it suffers from path loss, shadowing, multipath fading and Doppler shift which are introduced by the channel. The subsequent sections discuss the theory behind each of these phenomena.

3.2. Path Loss

In [Rapp01], the author calculated the linear path loss of a transmitted signal as the ratio of transmit power to the received power and can be defined as

$$P_L = \frac{P_t}{P_r} \tag{3.3}$$

where, P_t is the power of transmitted signal, and P_r is the power of received signal. The path loss is usually defined as the dB value of the linear path loss [Rapp01]. It is given by

$$P_L(dB) = 10log_{10} \frac{P_t}{P_r} \tag{3.4}$$

In order to appropriately model the signal propagation in the wireless channel, one of the models that will be considered is the *Free Space Path Loss* (FSPL) model. According to [Gold04], the FSPL models the received signal in a communication system where the transmitter and receiver are located at a distance d and there is a direct *line-of-sight* (LOS) between them. The received signal can then be modeled as given in [Gold04] as

$$r(t) = \Re\left\{\frac{\lambda\sqrt{G_l}e^{-j\left(\frac{2\pi d}{\lambda}\right)}}{4\pi d} u(t)e^{j2\pi f_c t}\right\} \tag{3.5}$$

where, $\sqrt{G_l}$ is the product of transmit and receive antenna field radiation pattern in the LOS direction, and $e^{-j\left(\frac{2\pi d}{\lambda}\right)}$ is the phase shift experienced by the wave for distance d. According to [Gold04], the received power in the FSPL model can be given in dBm as

$$P_r(dBm) = P_t(dBm) + 10log_{10}(G_l) + 20log_{10}(\lambda) - 20log_{10}(4\pi) - 20log_{10}(d)$$

Moreover, the ratio of received to transmit power is also given in [Gold04] as

$$\frac{P_r}{P_t} = \left[\frac{\sqrt{G_l}\lambda}{4\pi d}\right]^2 \tag{3.6}$$

As seen above, the FSPL model models the received signal power to reduce in an inversely proportional way to the square of the distance of the path length of the signal. We can also see that for higher operating frequency, the received power decreases due to the fact that received signal power is proportional to the square of the signal wavelength [Gold04].

Another popular method to model indoor and outdoor propagation channel is *Dual Slope Piecewise Linear* (DSPL) model [Patz02]. This is a special case of the widely known Piecewise Linear model. In this model, the received power in dB is plotted against the log-distance. There are number of segments in the plot and the number and locations of the breakpoints in the plot are usually obtained by different methods [Patz02]. The DSPL model can be characterized as follows [Gold04],

$$P_r(dB) = \begin{cases} P_t + K - 10\gamma_1 log_{10}\left(\frac{d}{d_0}\right) & d_0 \leq d \leq d_c \\ P_t + K - 10\gamma_1 log_{10}\left(\frac{d}{d_0}\right) - 10\gamma_2 log_{10}\left(\frac{d}{d_c}\right) & d > d_c \end{cases} \tag{3.7}$$

where, K is the constant path loss factor, γ_1 is the path loss exponent, d_0 is the reference distance, d_c is the critical distance, and γ_2 is the path loss exponent after the critical distance. In Fig. 3.1, a generalized Piecewise Linear Model can be seen [Gold04].

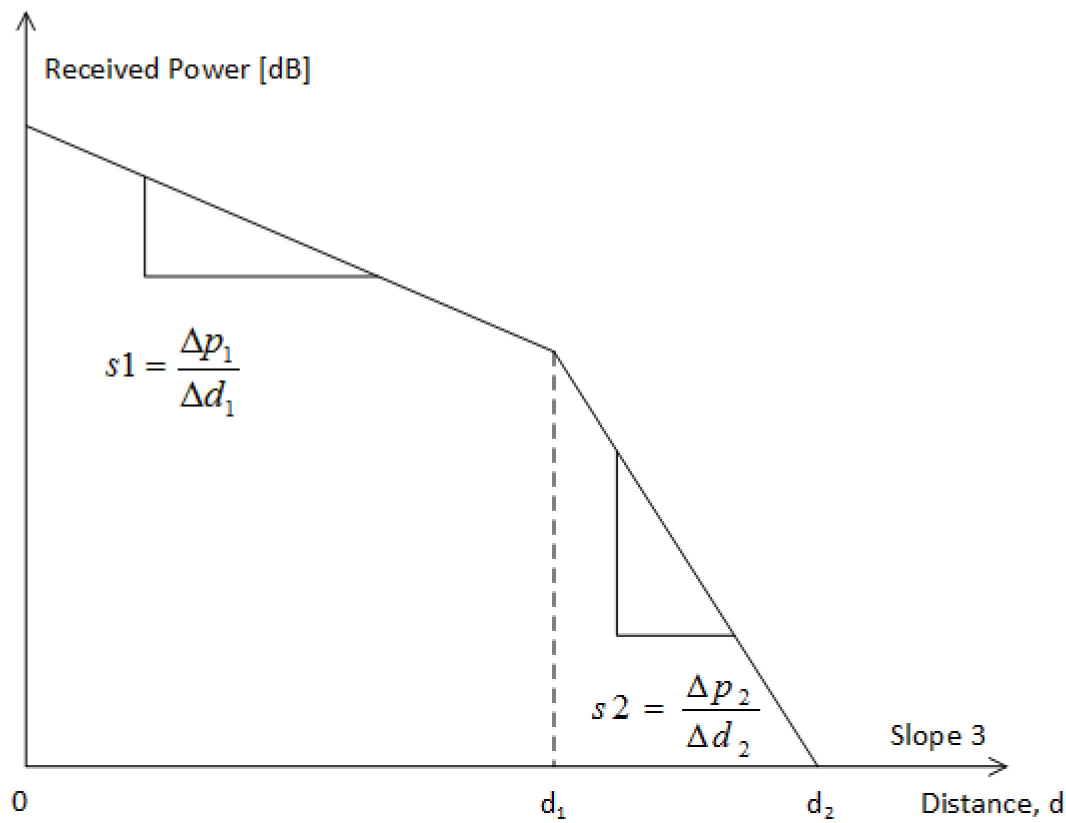

Fig. 3.1: Piecewise linear channel model.

3.3. Shadow Fading

There are other factors that cause random variation to a signal other than propagation loss. Shadow fading is the result of random variation to a signal due to blockage from objects which are situated in the signal path between the transmitter and receiver [Patz02]. Also, the signal is usually reflected by the surface of the earth and refracted by scattering objects. For a dynamic propagation environment between a fast moving UAV and a stationary ground control station, the location and size of scattering objects are always changing rapidly. In these kinds of scenarios, it is appropriate to model the attenuation by some statistical models [Gold04]. In [EGTP99] and [GGKS03], the authors introduce log-normal shadowing to model the shadow fading. In this model, the path loss can be given by

$$p(\psi) = \frac{\xi}{\sqrt{2\pi}\sigma_{\psi dB}\psi} exp\left[-\frac{\left(10log_{10}\psi - \mu_{\psi dB}\right)^2}{2\sigma_{\psi dB}^2}\right], \psi > 0 \tag{3.8}$$

where, $\xi = \frac{10}{ln10}$, $\psi_{dB} = 10log_{10}\psi$ in dB, $\mu_{\psi dB}$ is the mean of ψ_{dB} in dB, and $\sigma_{\psi dB}$ is the standard deviation of ψ_{dB} in dB.

In this thesis, one of the models that is considered to model the signal attenuation is the combined path loss and shadowing model. This is a widely used model to capture the power variation due to path loss and shadowing. In [Gold04] the author states that, this model characterizes the path loss by the simplified path loss model and shadow fading by the log-normal model stated above. In this combined model, the ratio of received to transmit power in dB can be given by

$$\frac{P_r}{P_t}(dB) = 10log_{10}K - 10\gamma log_{10}\frac{d}{d_0} + \psi_{dB} \tag{3.9}$$

where, ψ_{dB} is the Gauss-distributed random variable with zero mean and variance of $\sigma_{\psi dB}^2$, and γ is the path loss exponent.

3.4. Multipath Fading

Multipath fading is caused by random variation of signals due to constructive and destructive addition of different multipath components introduced by the channel [Gold04]. This sort of fading occurs over short distances and thus they are also called small scale propagation effects [Patz02]. For a signal transmitted by the transmitter, the receiver will receive multiple components of that signal due to scattering, reflection and refraction due to different objects in its path. One of the components corresponds to the line-of-sight component and the others are said to be multipath components. These components introduce a delay in the received signal which is called the delay spread. This delay spread plays an important role in characterizing the nature of multipath fading the signal is experiencing. If the inverse delay spread of the signal is small compared to the channel bandwidth, then the fading is known as narrowband fading. If it is larger, it is called wideband fading. In this thesis, we focus on narrowband fading effects of the wireless channel between the UAV and the ground control station. In Fig. 3.2, the multipath fading due to a single reflector and a cluster of reflectors is depicted.

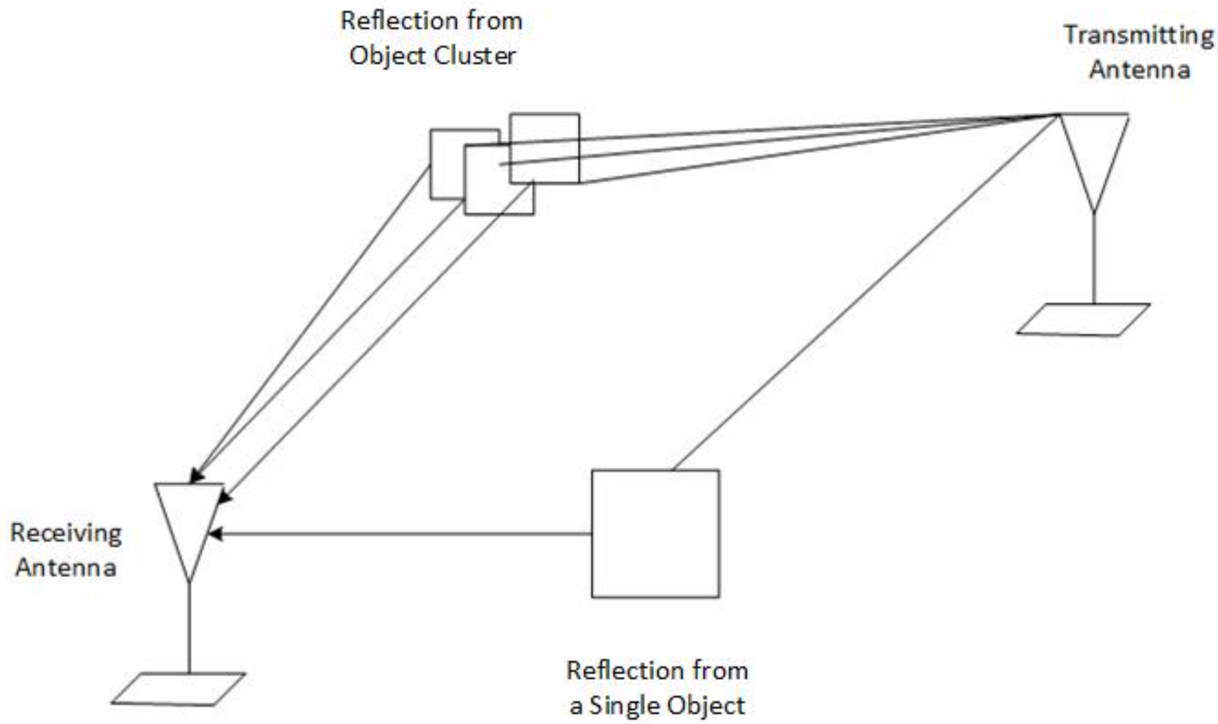

Fig. 3.2: Multipath fading of wireless signals due to objects in propagation path.

In [Gold04], the author models the received signal in a time-variant wireless channel as

$$r(t) = \Re\left\{\left[\sum_{n=0}^{N(t)} \alpha_n(t) e^{-j\emptyset_n(t)}\right] e^{j2\pi f_c t}\right\} = r_I(t) cos2\pi f_c t + r_Q(t) sin2\pi f_c t \qquad (3.10)$$

where, $r_I(t) = \sum_{n=1}^{N(t)} \alpha_n(t) cos\emptyset_n(t)$ is the in-phase component of the signal, and $r_Q(t) = \sum_{n=1}^{N(t)} \alpha_n(t) sin\emptyset_n(t)$ is the quadrature component of the signal.

From the Central Limit Theorem, it can be approximated that the components $r_I(t)$ and $r_Q(t)$ are jointly Gaussian random processes. For these two Gaussian random variables, it can be shown that $\sqrt{{r_I}^2 + {r_Q}^2}$ is Rayleigh-distributed [Gold04]. The square of this Rayleigh-distributed variable is exponentially distributed. Based on this principle, the received signal's envelope can be given by

$$z(t) = |r(t)| = \sqrt{{r_I}^2(t) + {r_Q}^2(t)} \tag{3.11}$$

The Rayleigh-distributed probability distribution of this signal envelope is also given by

$$pz(z) = \frac{2z}{P_r}\exp\left[-\frac{z^2}{P_r}\right] = \frac{z}{\sigma^2}exp\left[-\frac{z^2}{2\sigma^2}\right], \quad x \geq 0, \tag{3.12}$$

If the channel between the ground control station and the UAV has a fixed line-of-sight component, then the in-phase and quadrature components are not zero mean Gaussian random processes. In that case, the signal envelope is Rician distributed [Gold04] and can be given by

$$pz(z) = \frac{z}{\sigma^2}exp\left[\frac{-(z^2+s^2)}{2\sigma^2}\right]I_0\left(\frac{zs}{\sigma^2}\right), \quad x \geq 0, \tag{3.13}$$

Nakagami distribution is widely used to characterize the fading distribution for time-variant wireless channels [Gold04]. It is well known for its ability to model the fading with different degrees of severity. The fading parameter m is used to represent the fading severity of the channel. Nakagami distributions can model from most severe Rayleigh fading with $m = 1$ to no fading at $m = \infty$. This fading distribution can be given by [Gold04]

$$pz(z) = \frac{2m^m x^{2m-1}}{\Gamma(m)P_r^m}exp\left[\frac{-mz^2}{P_r}\right], \quad m \geq .5, \tag{3.14}$$

In this thesis, the Rayleigh, Rician and Nakagami distributions are considered to model the multipath fading of the time-variant wireless channel between the UAV and the ground control station. Figure 3.3 shows the combined effect of shadowing, narrowband fading and path loss in a typical wireless channel.

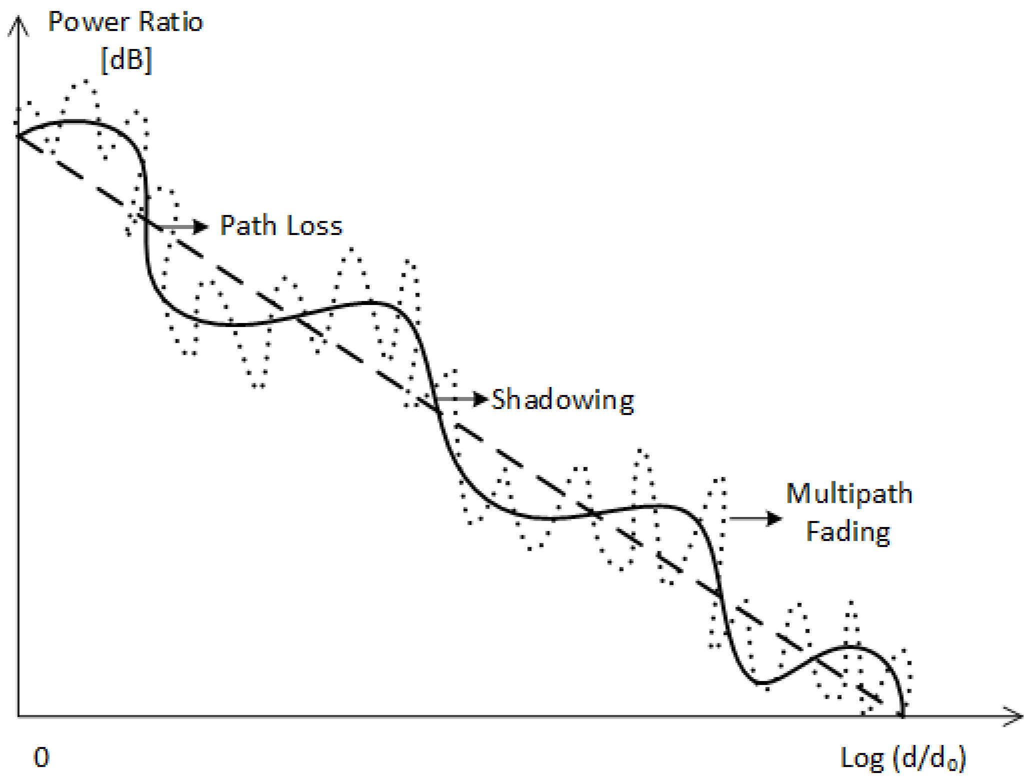

Fig. 3.3: Combined effect of shadowing, narrowband fading and propagation loss in a typical wireless channel.

3.5. Doppler Shift

Doppler shift occurs due to the relative movement of transmitter and receiver over a short time interval. The rapid change in position causes the signal path to vary and that introduces a phase change on the received signal. The Doppler shift can be obtained from [Gold04] as

$$f_D = \frac{1\Delta\emptyset}{2\pi\Delta t} = v cos\theta/\lambda \tag{3.15}$$

where, θ is the arrival angle of the received signal relative to the direction of motion, v is the velocity of the receiver, and $\lambda = c/f_c$ is the wavelength of the received signal. The geometry behind the calculation of Doppler shift can be seen in Fig. 3.4.

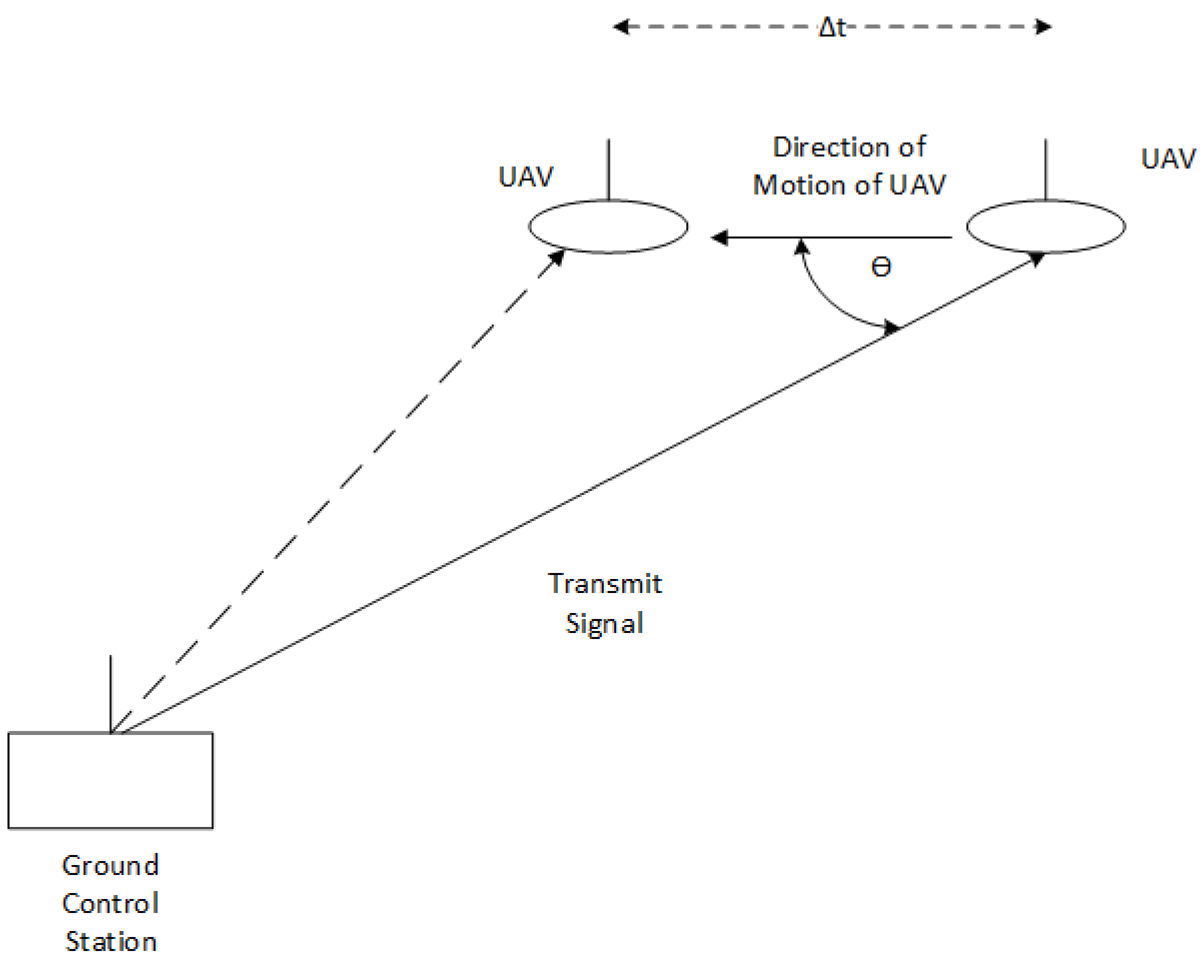

Fig. 3.4: The geometry of Doppler shift.

In [Gold04], the author states that for moving vehicles where the velocity is below 60 miles per hour and the operating frequency is around 1 GHz, the Doppler shift is less than 70 Hz which is negligible for most systems. Moreover, the main focus of this thesis is to investigate the fading characteristics of a wireless channel between a UAV and a ground control station. To reduce additional complexities, Doppler shift of the signal from a UAV to the ground control station is ignored.

In the sections mentioned above, some of the negative impacts the channel imposes on the wireless signal, are discussed. To design an optimal data communication link, these effects need to be considered in computing the capacity and performance of this wireless channel. The subsequent sections discusses some of the measures to evaluate the performance and capacity of a wireless channel between a UAV and a ground control station.

3.6. Channel Capacity

Channel capacity represents the maximum data rate that the channel can provide for data communications between the transmitter and the receiver without additional constraints on delay or complexity of the encoder or decoder [CoTh91]. To design an optimal data communication subsystem for the unmanned aerial system, we need to calculate the channel capacity for the time-variant wireless channel. Claude Shannon in the late 1940s developed the mathematical theory of channel capacity based on the mutual information between the transmitter and receiver of the channel. The main contribution of the theory is a coding scheme that allows to achieve maximum data rate in a channel with very low probability of error and for any data rate higher than that, the error probability increases.

For the communication subsystem of the designed unmanned aerial system, the capacity of the time varying wireless channel is examined. For this thesis, we focus on the flat fading channel where we assume that the fading distribution of the channel is known to the transmitter and receiver. An optimal power control algorithm can then be designed with this *Channel side information* (CSI) known at the transmitter and receiver to achieve maximum capacity.

Flat fading corresponds to the fading condition when the coherence bandwidth of the channel is larger than the signal bandwidth [CoTh91]. This causes all the frequency components of the transmitted signal to experience the same amount of fading and hence the name flat fading. In our channel model, we assume a stationary and ergodic time-varying gain and an *additive white Gaussian noise* (AWGN) added to the channel. The gain varies with time and is assumed to be an *independent and identically distributed* (i.i.d) process. The flat fading channel model adopted from [Gold04] is shown in Fig. 3.5.

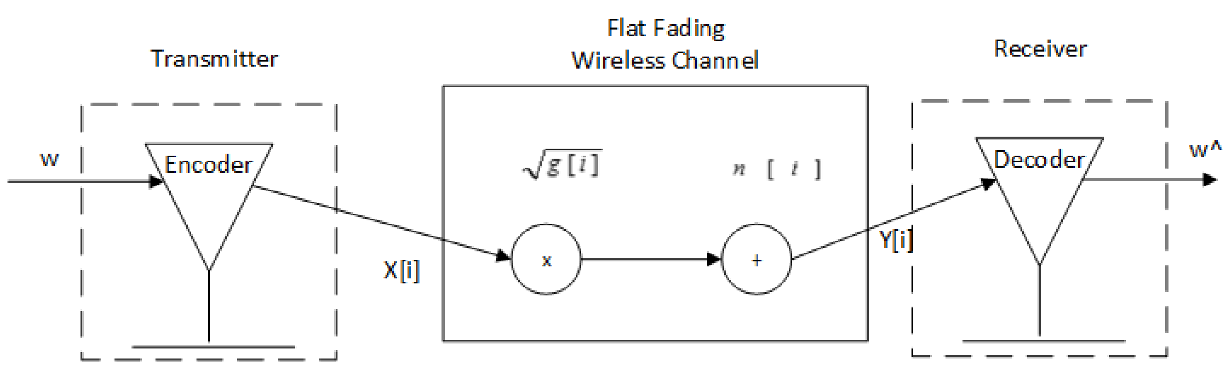

Fig. 3.5: Flat fading channel model.

We assume that the channel power gain is known to the transmitter and receiver at a certain point of time. Armed with this information, the channel capacity for this time-varying, flat fading channel can be given by [Gold04]

$$C = \int_0^{\infty} C_{\gamma} p(\gamma) d\gamma = \int_0^{\infty} B log_2(1+\gamma) p(\gamma) d\gamma \quad (3.16)$$

where, B is the bandwidth of the channel, $\gamma = \bar{S}\bar{g}/(N_0 B)$ is the instantaneous received signal-to-noise ratio (SNR), $\bar{S}$ is the average transmit signal power, $\bar{g}$ is the average channel power gain, N_0 is the noise spectral density of the AWGN noise $n[i]$, and $p(\gamma)$ is the probability distribution of the received signal-to-noise ratio.

3.7. Performance Measures of Wireless Channel

In this section, we provide detail information on the performance measures of the flat-fading wireless channel between the ground control station and the UAV. Performance measures such as signal-to-noise power ratio, probability of error and outage probability are considered in the performance evaluation of the wireless channel.

3.7.1. Signal-to-Noise Ratio (SNR)

The signal-to-noise ratio (SNR) is defined in [CoTh91] as the ratio of the received signal power to the noise power in the transmitted signal. In order to calculate the received signal power, we consider the transmitted power by the transmitter as well as path loss, shadowing and multipath fading. The noise power is calculated from the bandwidth of the transmitted signal and the spectral properties of noise. In [CoTh91], the author calculates the SNR as

$$SNR = \frac{P_r}{N_0 B} = \frac{E_b}{N_0 B T_b} \tag{3.17}$$

where, P_r is the received power of the transmitted signal, E_b is the signal energy per bit, and T_b is bit time. For binary signaling, SNR reduces to E_b/N_0 and this is often termed as SNR per bit, γ_b.

3.7.2. Outage Probability

The outage probability is defined in [CoTh91] as the probability that the instantaneous signal-to-noise ratio falls below a certain threshold. This threshold γ_0 is defined as the minimum SNR needed for acceptable performance depending on the application of the wireless system. The outage probability can be given by,

$$P_{out} = p(\gamma_s < \gamma_0) = \int_0^{\gamma_0} p_{\gamma_s}(\gamma)d\gamma \tag{3.18}$$

where, $\gamma_s = E_s/N_0$ is the SNR per symbol.

3.7.3. Average Probability of Error

The average probability of error is defined in [Gold04] as the probability of error in a single symbol or bit. The average probability of error is usually affected by the flat fading channel and can vary drastically depending on the severity of fading. The average probability of error is given by [Gold04]

$$\overline{P_s} = \int_0^{\infty} P_s(\gamma)p_{\gamma s}(\gamma)d\gamma \tag{3.19}$$

where, $P_s(\gamma)$ is the probability of symbol error in an AWGN channel with SNR γ.

In the previous sections, the transmitted and received signal models, behavior of the wireless channel, large scale and small scale fading suffered by the signals are discussed in detail. Moreover, some of the methods to measure the capacity and performance of this fading wireless channel are elaborated. In the next sections, two other factors that affect a wireless channel between a UAV and a ground control station are described: (i) directional gain of antenna and (ii) polarization mismatch factor.

3.8. Directional Gain of Antenna

To understand the directivity of a highly directional antenna, we need to elaborate some of the antenna parameters and properties. They are discussed in the sections below.

3.8.1. Radiation Pattern

The radiation pattern of an antenna are the three dimensional quantities that tries to express the variation of field or power of the electromagnetic wave radiated from the antenna as a function of azimuth and elevation angles. The direction in which maximum power is radiated is called the main lobe of the antenna. There are also minor lobes which radiates less power.

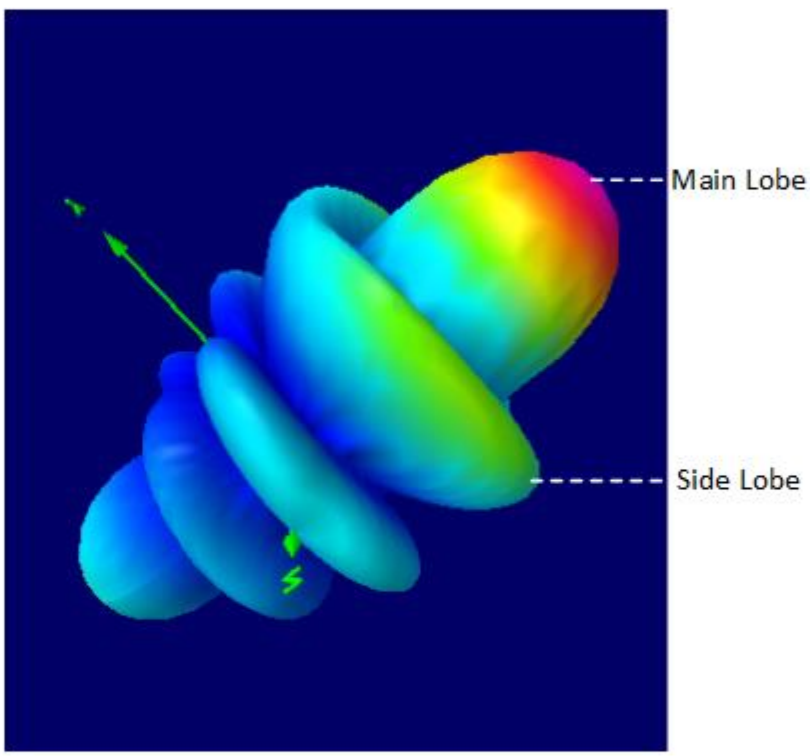

Fig. 3.6: Radiation pattern of a directional antenna.

In Fig. 3.6, we can see a three dimensional representation of a radiation pattern of a directional antenna. Here, we can see that the maximum direction is in the z direction at $\theta = 0°$.

It is apparent from this figure. that the main lobe carries most of the radiation where minor lobes also contribute but in lesser portions. Between the lobes in the pattern, there are empty spaces where the amount of radiation goes to zero. These are called antenna nulls. To represent the amount of radiation in any direction, the azimuth ($\emptyset$) and elevation (θ) angles are used. For example, a point Q represents the direction where the angles are $\emptyset = 85°$ and $\theta = 30°$.

The main goal of an antenna radiation pattern is to plot the radiation intensity over the 360 degrees in the azimuth or elevation plane. Directional antennas have highly directional beams which mean that their radiation pattern will closely resemble a flashlight beam. A typical radiation plot represents the relative radiation intensity of an antenna realized in the far field. For frequencies belonging to the VHF/UHF and microwave region, the ground reflections are negligible and thus not included in the radiation plots. The radiation pattern of an antenna is reciprocal which means it transmits and receives in the same direction. The radiation plot is generally expressed in dB value. These plots are also usually normalized to the outer edge of the coordinate system.

Radiation plots provide a clear map of the electromagnetic radiation radiated and received by an antenna. For wireless links employing directional antennas, radiation plots help to identify the degradation in case of misalignment and pointing errors. These plots also help to aim directional antennas properly for maximum wireless performance. For directional antenna with a narrower beam, the pointing becomes more complex. Moreover, interfering signals and their effects can also be realized with the help of a radiation plot.

3.8.2. Half-Power Beamwidth

The half-power beamwidth of an antenna is the angle between the two points on the main lobe where the effective radiated power becomes half of the peak effective radiated power.

3.8.3. Null to Null Beamwidth

The null to null beamwidth is the angular separation between two points in the antenna radiation pattern where both points radiate zero power.

3.8.4. Beam Area

The beam area of an antenna is the solid angle through which all the electromagnetic waves would radiate if the direction of the main beam is fixed. It is given by the integral of the normalized power pattern over a sphere.

3.8.5. Beam Efficiency

The beam efficiency of an antenna is given by the ratio of the main beam area to the total beam area. The total beam area of an antenna consists of the main beam and the side lobes.

3.8.6. Directivity

The directivity of an antenna is the ratio of the maximum power density to the average power density over the sphere observed from the far field radiation pattern of the antenna. For different types of antenna, directivity is different. The ideal isotropic antenna has the lowest directivity of 1. The short dipole antenna has a directivity of 1.5.

3.8.7. Gain

Gain of antenna is an actual quantity which is always less than the directivity of antenna due to different types of losses incurred in the system. Antenna efficiency factor is given by the ratio of gain to its directivity.

3.8.8. Azimuth Angle

“The azimuth angle is the angle between a celestial body and the north, measured clockwise around the observer’s horizon” [Pons15]. For an antenna, “the azimuth refers to the rotation of the whole antenna around a vertical axis” [Sats04].

3.8.9. Elevation Angle

“The elevation is the vertical angular distance between a celestial body and the observer’s local horizon or, also called, the observer’s local plane” [Pons15]. For an antenna, “the elevation refers to the angle between the beam pointing direction and the local horizontal plane” [Sats04].

In this section, different antenna parameters and characteristics were discussed which are relevant to the directivity and gain of a highly directional antenna. The next section provides an in-depth discussion on the polarization of waves and polarization mismatch factor.

3.9. Polarization

For any wireless communication system, the polarization of waves and antenna is an important factor. Most of the communication systems today use vertical, horizontal or circular polarized waves. However, it is important to understand the difference between them and how they affect the performance of the system.

As electric current is fed into an antenna, it converts it to electromagnetic waves and radiates them into free space. This electromagnetic wave has an electric field and a magnetic field. The polarization of this wave is determined from this electric field's orientation. Three types of polarization are considered in this thesis: (i) linear polarization, (ii) circular polarization and (iii) elliptical polarization.

3.9.1. Linear Polarization

For an electromagnetic wave, if the electric field oscillates in magnitude along a single axis, then the wave is said to be of a linearly polarized wave. At a given point, if the axis is perpendicular to the earth's surface, then this type of linear polarization is called vertical polarization. It is called horizontal polarization if the axis is parallel to the earth's surface at that point.

3.9.2. Circular Polarization

When the electric field of a propagating electromagnetic wave has two orthogonal components with equal magnitude and 90 degrees out of phase, then the wave is called a circularly polarized wave. A circularly polarized wave's electric field rotates in a circle. If the rotation is counter clockwise then it is called right hand circularly polarized wave. If the rotation is clockwise, then it is called a left hand circularly polarized wave.

3.9.3. Elliptical Polarization

For an elliptically polarized wave, the electric field has two orthogonal components which are 90 degrees out of phase but the magnitudes of these components are not equal. Similar to the circular polarization, elliptical polarization can also be divided into two classes: (i) right hand elliptically polarized where the rotation of electric field is in counter clockwise direction and (ii) left hand elliptically polarized where the rotation of electric field is in a clockwise direction.

3.9.4. Polarization Mismatch Factor

Polarization is a very important factor for a communication sub-system. Specifically, for channels employing line-of-sight communications, having identically polarized antennas at both ends is crucial to achieve maximum signal strength. Theoretically, a polarization mismatch of 90 degrees between the transmitting and receiving antennas would result in zero voltage response in the receiving antenna. However, in practice, if the two antennas are linearly polarized, a polarization mismatch between the two antennas of 45 and 90 degrees will cause signal degradation of approximately 3 dB and 26 dB, respectively. For circular polarization, if one antenna is left hand circularly polarized and another one is right hand circularly polarized, then signal degradation can be up to more than 20 dB.

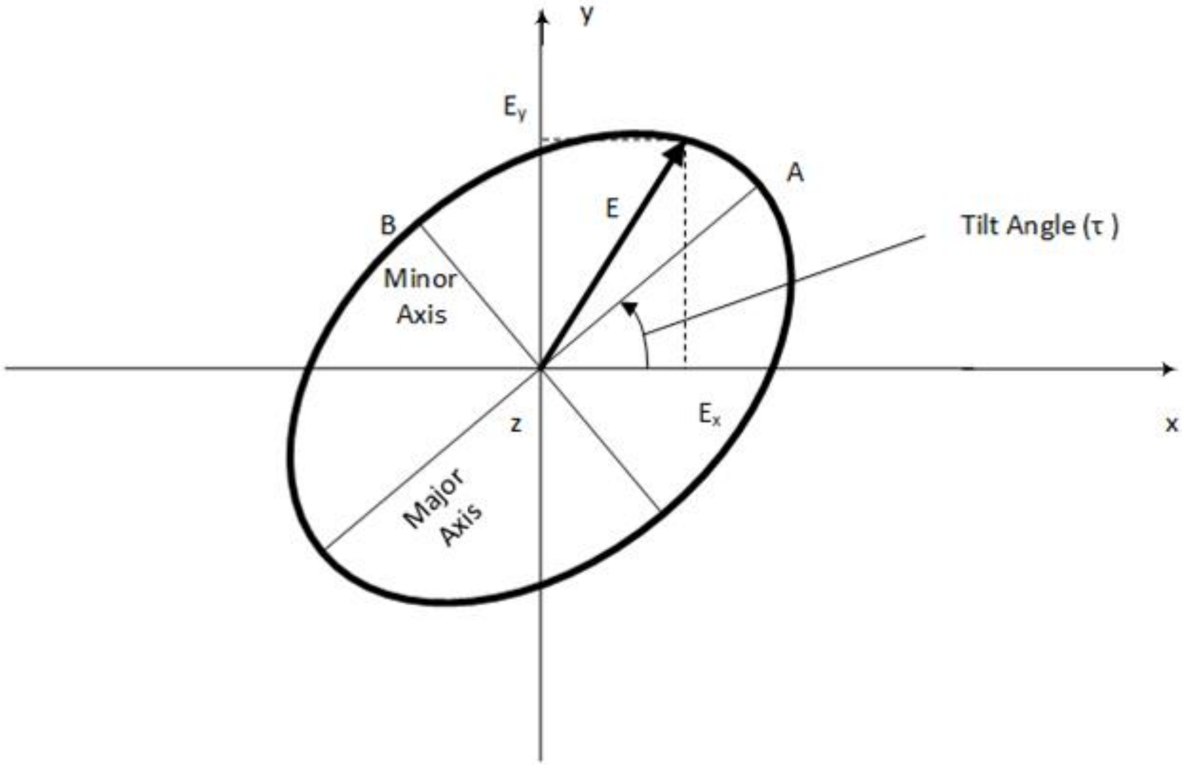

Fig. 3.7: Polarization ellipse.

For a linearly polarized electromagnetic wave, the electric field (oscillating along the y direction) can be given by [Mhed07]

$$E_y = E_2 \sin(\omega t - \beta z) \tag{3.20}$$

The electric field of an elliptically polarized wave rotates in an elliptical shape on the plane, the tip of the vector creating an ellipse. This is called the **polarization ellipse**. Figure 3.7 shows a polarization ellipse. This ellipse has a major and minor axis. The ratio of this major to minor axis is called the **Axial Ratio.** It can be said that circular and linear polarization are two extreme cases of elliptical polarization. Therefore, an elliptically polarized wave can be represented by two linearly polarized components. Among these two, one component is in the x direction where the other is in the y direction. Then the electric field components along those axes can be given by [Mhed07]

$$E_x = E_1 \sin(\omega t - \beta z) \tag{3.21}$$

$$E_y = E_2 \sin(\omega t - \beta z + \delta) \tag{3.22}$$

where, E_1 is the amplitude of wave linearly polarized in x direction, E_2 is the amplitude of wave linearly polarized in y direction, and δ is the time-phase angle. If we combine these two equations, we can get the instantaneous total vector field E which is given by [Mhed07]

$$E = \hat{x} E_1 \sin(\omega t - \beta z) + \hat{y} E_2 \sin(\omega t - \beta z + \delta) \tag{3.23}$$

From Fig. 3.7 which shows a polarization ellipse, we can see that OA and OB are the semi-major and semi-minor axes. The tilt angle of this ellipse is given by τ. For this elliptical wave, the axial ratio can be given by [Mhed07],

$$Axial\ Ratio = \frac{OA}{OB} \quad (1 \leq Axial\ Ratio \leq \infty) \tag{3.24}$$

The polarization of a wave can also be represented by Poincare sphere. In this case, there is a point on the sphere where the latitude and longitude of the point are related to the parameters of the polarization ellipse as [Mhed07]

$$Longitude = 2\tau \tag{3.25}$$

$$Latitude = 2\varepsilon \tag{3.26}$$

where, τ is the tilt angle of the polarization ellipse and $\varepsilon = tan^{-1}(\frac{1}{Axial\ Ratio})$. Moreover, there are boundary conditions for these values where $0° \leq \tau \leq 180°$ and $-45° \leq \varepsilon \leq 45°$.

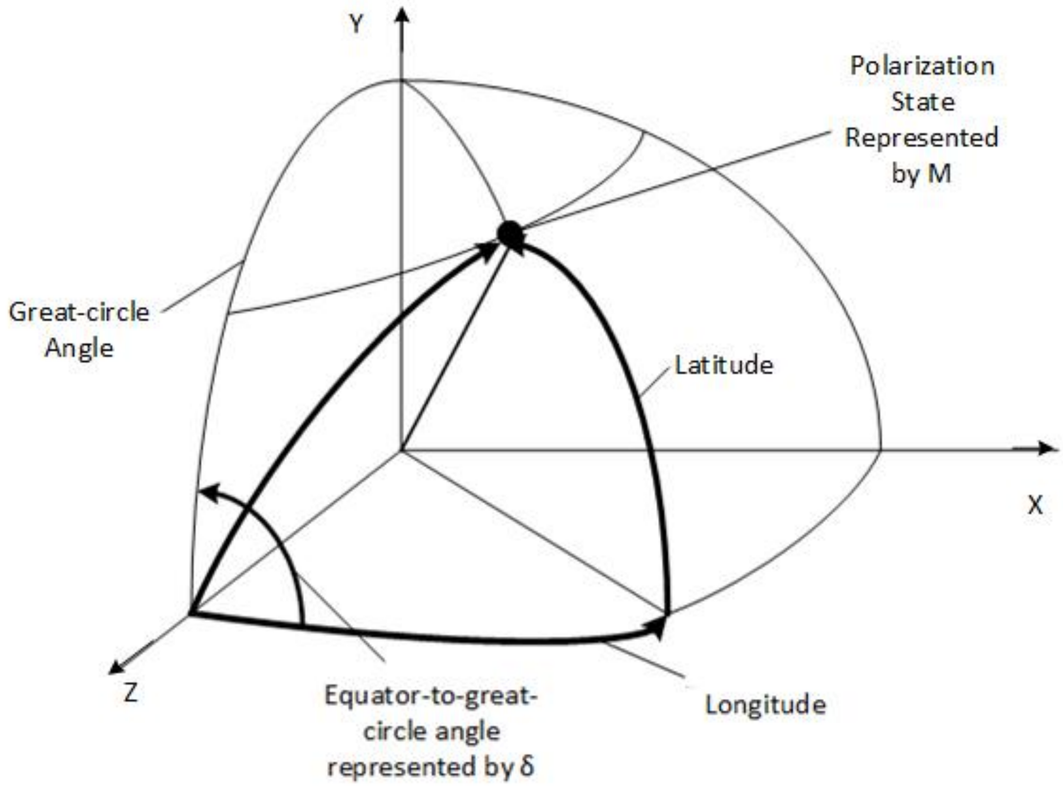

Fig. 3.8: Great circle angle of a polarization ellipse.

From Fig. 3.8, we can see that the angle subtended by the great circle drawn from a reference point on the equator can be given by 2γ [Mhed07]. The angle between the great circle and the equator can also be given by δ [Mhed07]. These two angles can also successfully express the polarization state described by a point on a sphere. From Fig. 3.8, we can get the following parameters which were given in [Mhed07]. The great circle angle is represented by 2γ, the equator to great circle angle is represented by δ,

$$\gamma = tan^{-1}\left({}^{E_2}/_{E_1}\right) \quad [0° \leq \gamma \leq 90°], \tag{3.27}$$

and δ is the phase difference between E_y and E_x where $[-180° \leq \delta \leq 180°]$.

Now, the polarization state can either be described by the angles (ε, τ) or (γ, δ). If the polarization state is expressed by $M(\varepsilon, \tau)$and when it is a function of the angle $(\varepsilon\ and\ \tau)$, and the polarization state $P(\gamma, \delta)$ described by the angles (γ, δ), then we get the following Fig. 3.9, which shows the polarization ellipse with the relation of angles $\varepsilon, \gamma\ and\ \tau$.

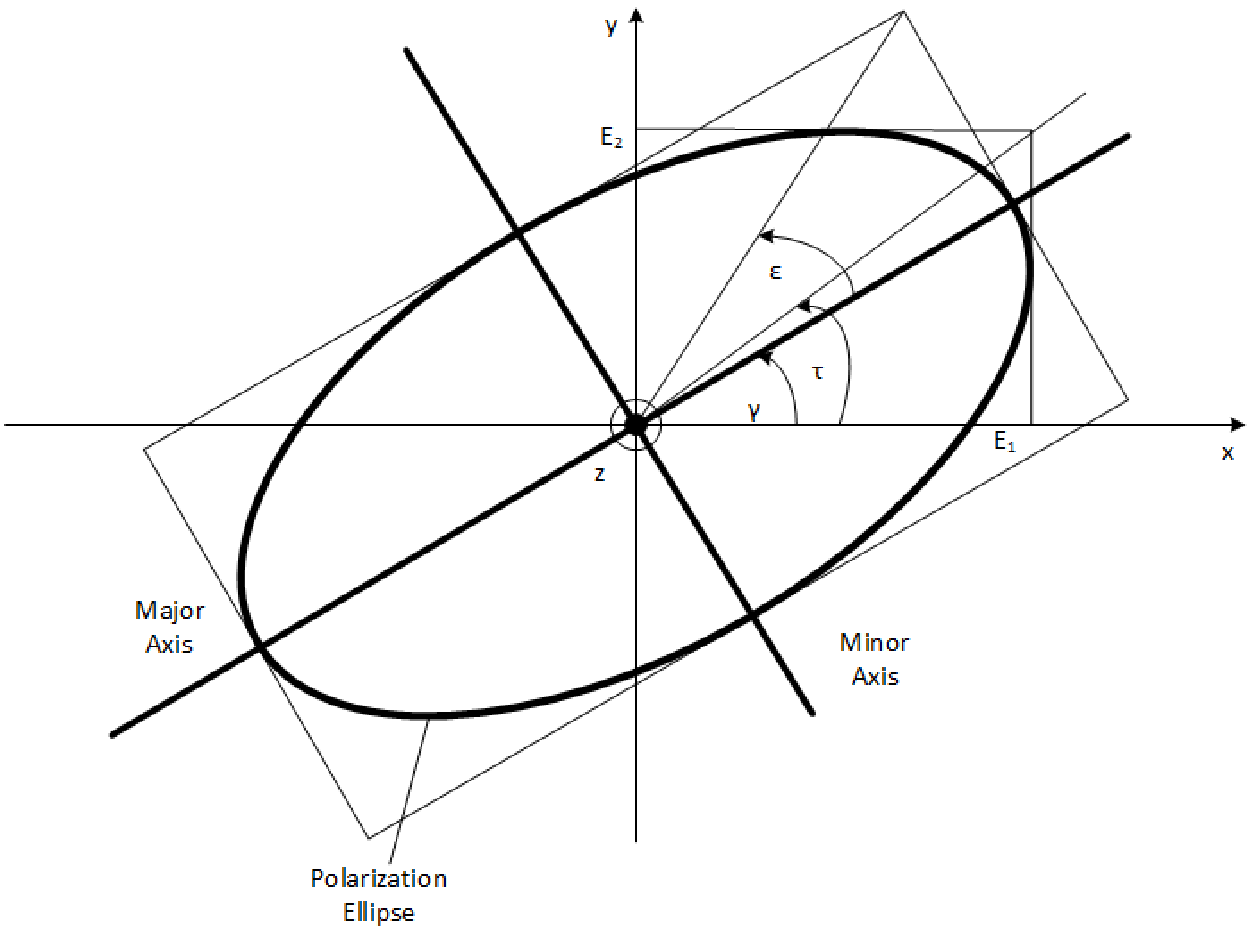

Fig. 3.9: The relation of angles in the polarization ellipse.

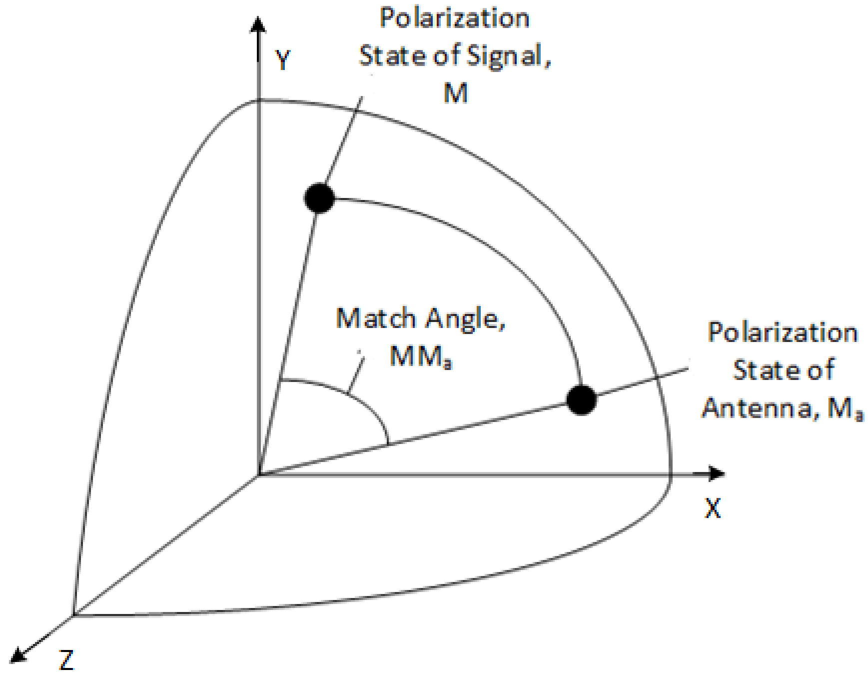

Fig. 3.10: Poincare sphere representation of polarization state

Figure 3.10 is an application of Poincare sphere representation which provides some of the more concrete physical parameters for an antenna which is receiving a wave of arbitrary polarization. Here, the voltage response of the antenna can be given by [Mhed07]

$$V = k\ cos\frac{MM_a}{2} \tag{3.28}$$

where, MM_a is the angle subtended by great circle line from polarization state of wave M to the polarization state of the antenna M_a, and k is a constant.

The transmitting antenna radiates the electromagnetic waves with a certain polarization state when the waves leave the antenna. This polarization is called the polarization state of the transmitting antenna. From Eq. (3.28), we can see that the constant k is dependent on the field strength of the wave and the size of the antenna. Therefore, the voltage response of a receiving antenna depends on the size of the antenna, field strength of the wave and the polarization states of the wave and antenna. So, when the polarization state of the antenna is matched with the polarization state of the electromagnetic wave, we get $MM_a = 0$. Maximum amount of voltage response can be achieved in the receiving antenna in this case. This is called polarization matching. However, the antenna will have zero voltage response after receiving the wave when the angle subtended by the great circle line from M to M_a is 180°. This is called polarization mismatch. For example, if the receiving antenna's polarization is linear in the y direction and the incoming wave's polarization is linear in the x direction, then no voltage response will be felt in the antenna.

The polarization mismatch factor can be given by [Mhed07]

$$F = cos^2 \frac{MM_a}{2} \tag{3.29}$$

From Eq. (3.29), we can see that when $MM_a = 0$ and the antenna is perfectly matched with the polarization of the wave, the polarization mismatch factor is 1. This shows a perfect match. The polarization mismatch factor is 0 when $MM_a = 180°$ which means there is a complete mismatch between the polarization states of the antenna and the wave. In [Mhed07], it had been shown that for linear polarization, $MM_a/2 = \Delta\tau$. Here, $\Delta\tau$ is the difference between the tilt angles of wave and antenna. So, we get

$$F = cos^2 \Delta\tau \tag{3.30}$$

3.10 Yagi Antenna

A Yagi-Uda antenna is a directional antenna with multiple elements. It is basically constructed from an array of linear dipole antennas. A Yagi antenna has three main components: (i) reflector element, (ii) driven element and (iii) a number of director elements.

Here, the reflector and the directors are parasitic elements which radiate passively. These elements induce current by mutual coupling. However, the driven element is connected to a transmission line. This transmission line feeds the energy to the driven element for radiation by the antenna.

The construction of the Yagi antenna consists of placing the three elements with different design specifications for different outputs from the antenna. Typically, the driven element is placed between the reflector and directors. It is a half wave dipole and is shorter than the reflector element in length. The director elements are shorter than the driven element and their design specifications vary greatly depending on the output of the antenna. Among them, the length, diameter and spacing between the director elements are important. Moreover, the spacing between the reflector and the driven element is also an important design choice.

The Yagi antennas are highly directional antennas. Highly directional Yagis have their radiation pattern act like a flashlight beam. The gain of this directional antenna is thus dependent upon the angle the antenna is facing.

The reflector and the directors of the antenna are parasitic elements, which mean they are not actually connected to the feeder. They simply re-radiate the signals which are radiated by the driven element. But in this case, the phases of these signals are a bit different from the waves radiated by the driven element. Because of this phase difference, some signals are cancelled out and some are reinforced. The main design goal of the Yagi antenna is to cancel out the signals in other directions and reinforce the signal in the desired direction. Therefore, it is these parasitic elements which are responsible for the directional capabilities of the Yagi antenna. As they are not directly connected to the power, the amplitude and phase of the current that is induced by the waves radiated by the driven element, cannot be controlled completely. But it can be altered by tuning the length of these elements and the spacing between them and the driven element. By these phase changes, the Yagi antenna tries to cancel out the waves in the undesired direction and reinforce the waves in the desired direction. However, a complete cancellation cannot be achieved, although the Yagi provides very good directivity and front to back ratio.

To provide further details on the principle of Yagi antennas, the inductive and capacitive nature of the reflectors and directors are discussed briefly in this section. Typically, the reflector element is made inductive to obtain the phase shift of the radiated wave. The main reason behind this is that, when current is induced in a parasitic element which is inductive, the phase of the induced current is in such way that it pushes the power away from this element in the opposite direction. This helps the reflector element to “reflect” power in the desired direction of propagation. The reflector is made inductive by tuning it below resonant which is typically done by adding an inductive component or, increasing the length. The director elements are made capacitive, by tuning it above resonant. This is done by physically adding capacitive elements or reducing the length of the element below resonant. The capacitive nature of the directors cause the phase of the current induced in them to move the radiation towards them. Hence, the directors help to radiate the waves in the desired direction. The number of directors determines the gain, directivity and beamwidth of a Yagi antenna. With more directors, the gain and directivity of the antenna increases, reducing the beamwidth.

Yagi antennas can provide a high amount of gain in a desired direction which makes it very attractive for long range communication. With a higher gain, the beamwidth decreases and the antenna directs all the transmitted power in the precise direction of the receiver. When a Yagi is used in the receiving end, it provides the same gain for the reception of the signal in the area, increasing the communication range drastically. Figs 3.11 and 3.12 show the radiation patterns of a 7 element Yagi antenna. Figure 3.13 shows a 3D representation of the radiation pattern.

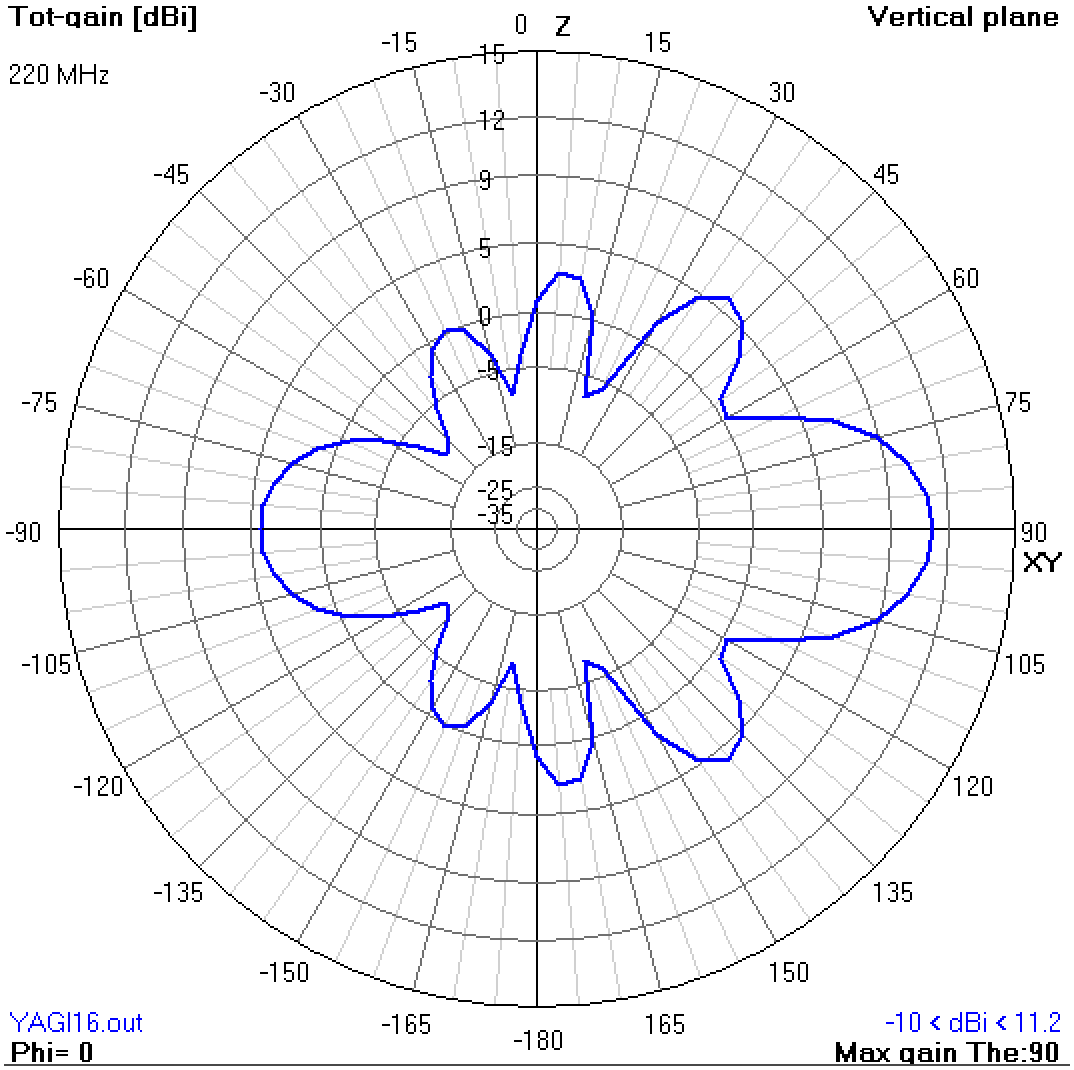

Fig. 3.11: Vertical radiation pattern of Yagi antenna.

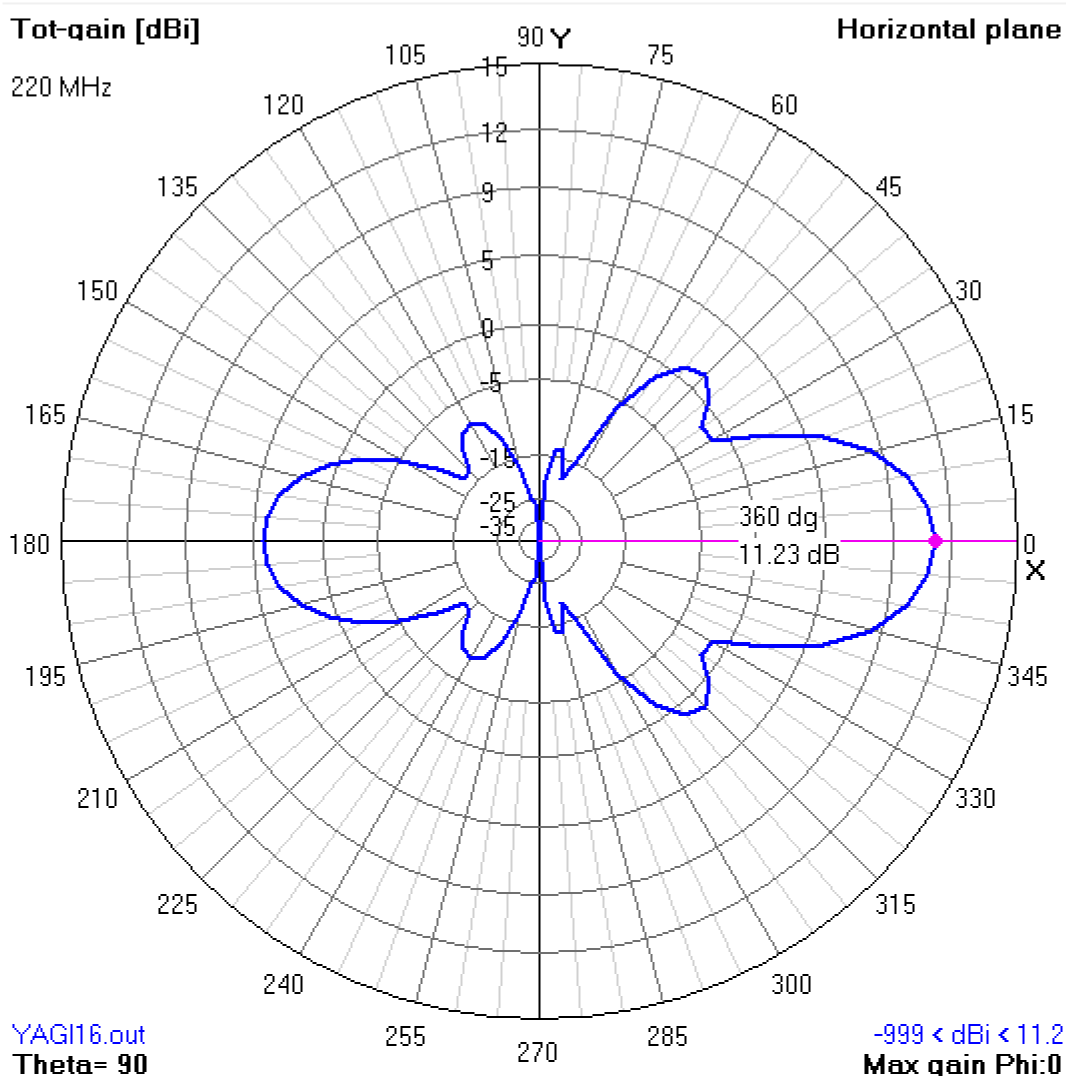

Fig. 3.12: Horizontal radiation pattern of Yagi antenna.

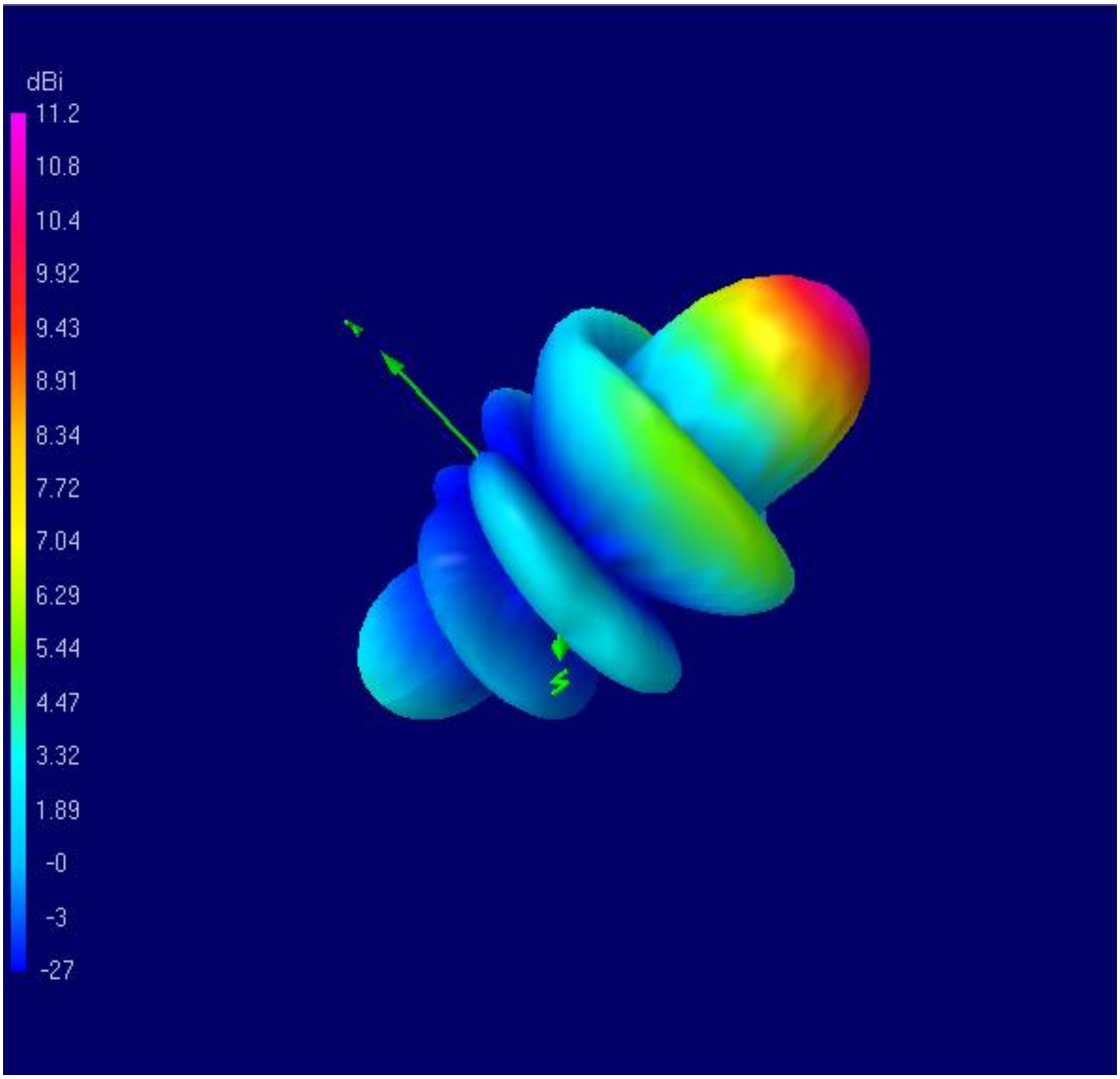

Fig. 3.13: 3D radiation pattern of Yagi antenna.

From these figures we can see that the gain of Yagi antenna depends on the azimuth and elevation angle the antenna is directed towards, with a high level of directivity. To calculate this gain in that specific direction, the author in [Myli07] approximated the Yagi antenna as an array of half wave dipole elements. Linear array theory [Myli07] was applied to find the array factor for those half wave dipoles. The array factor was calculated by

$$AF = I_0 + I_1 e^{j\beta d_1 cos\theta} + I_2 e^{j\beta (d_1+d_2) cos\theta} \tag{3.31}$$

where, I_0, I_1 and I_2 are the current excitations at the element centers which was found by simulating them in an antenna modeling software. The pattern of the whole Yagi antenna will be represented by the array of half wave dipole antennas as shown in the figures. The radiation pattern of this x directed dipole can be found by an analogy to an antenna which is equivalent to the previous one but oriented along the z axis. The radiation pattern of this antenna can be given by [Myli07]

$$F(\theta,\varphi) = \frac{\cos(\frac{\pi}{2}cos\theta)}{sin\theta} \tag{3.32}$$

For an angle which is defined along the x-axis, its spherical angle representations can be given by

$$cos\gamma = sin\theta cos\varphi \tag{3.33}$$

$$sin\gamma = \sqrt{1 - sin^2\theta cos^2\varphi} \tag{3.34}$$

The x directed dipole makes an angle γ with the incident wave and the z directed dipole make an angle θ. These two angles are equivalent of each other. From this we can get from [Myli07]

$$F(\theta,\varphi) = \frac{\cos(\frac{\pi}{2}sin\theta cos\varphi)}{\sqrt{1-sin^2\theta cos^2\varphi}} \tag{3.35}$$

The directivity is given by [Myli07]

$$D_{yagi}(\theta,\varphi) = D\left|F_{yagi}(\theta,\varphi)\right|^2 \tag{3.36}$$

where, $F_{yagi}$is the normalized radiation pattern of the antenna and D is the peak value of directivity. The gain is also given by [Myli07]

$$G_{yagi}(\theta,\varphi) = e_{cd}D_{yagi}(\theta,\varphi) = G\left|F_{yagi}(\theta,\varphi)\right|^2 \tag{3.37}$$

where, $G = e_{cd}D$ is the maximum gain.

3.11 Antenna Modeling

Antennas operate by transmitting and receiving electromagnetic waves. These electromagnetic waves are mysterious in a sense that they do not have any auditory or visual representation. In plain words, we cannot see or smell them. However, these waves propagate along the actual physical environment and are influenced by the physical objects in its path. As we cannot see the waves' propagation, its radiation pattern and propagation characteristics are used to model its path. Moreover, antenna designing is a complicated process with an iterative trial and error design cycle. Computer aided antenna modeling tools are a popular way to model the radiation pattern and propagating characteristics of a wave radiated by an antenna. Most of these modeling tools use numerical electromagnetics codes (NEC) to model the electromagnetics concerning the antenna.

3.11.1 Numerical Electromagnetic Codes

Numerical electromagnetics code is a software package that was written by Gerald J. Burke and Andrew J. Poggio [Wiki15]. This software package is widely used to model different types of wire and surface antennas. It is very popular among antenna designers and amateur radio operators worldwide. The code uses algorithms which employ electric field integral equations for modeling the electric field's response of these wires. For closed and conducting surfaces, the algorithm uses the magnetic field integral equations. These equations are solved using the method of moments [Wiki15] solutions. The NEC code can be applied to calculate or model a wide variety of antenna systems from large arrays to very small, complex antenna structures, wires underground, insulated wires, impedance loads, Yagi antennas and patch antennas.

In the next sections, some of the antenna modeling software that use NEC codes are discussed.

3.11.1.1. EZNEC

EZNEC and EZNEC+ are two of the most popular antenna modeling software that is commercially available [Lewa09]. It is able to design and simulate almost every kind of antenna out there. It can calculate many important parameters of the antenna such as their gain, radiation patterns in azimuth and elevation planes, feedpoint impedance, beamwidths, 3-dB beamwidth, and front to back ratio. The design of any antenna structure can be done by describing the antenna as a group of conductors. Various physical parameters of these conductors can be changed and modified such as length, diameter, and orientation. Moreover, feed points can be added to a source e.g. transmission line. The antenna can also be modeled as connected to a ground or any other metal structure. It is one of the best tools to model antennas currently available today.

3.11.1.2. 4NEC2

4NEC2 is a very popular antenna modeling tool which is free to use. It provides almost all the functionality that was discussed above for EZNEC. One of the most useful features of this software is the sweeper tool which lets the user to see a graphical representation of the effects of antenna performances upon changing its design parameters. 4NEC2 provides a graphical 3D geometry editor, NEC editor, gradient style editors to cater to the needs of different levels of antenna designers. There are genetic algorithm based optimizers which can be used to optimize the design parameters of the antenna.

The different characteristics of a directional antenna, its gain and directivity, and radiation patterns are discussed in the sections above. The next sections provide some theoretical background on the optimization algorithm that is employed in this research assignment to optimize the fading prediction model.

3.12. Particle Swarm Optimization

3.12.1. Multi Objective Optimization

Optimization refers to the technique of choosing the best elements from a set of choices that are available. It is also sometimes referred to as mathematical programming. A lot of real world problems consist of a stage where a mathematical function needs to be maximized or minimized in order to find the best possible solution to the problem. An optimization procedure selects the inputs to that mathematical function from an available set in a way so that the output of the function is either maximized or minimized. In other words, an optimization procedure takes into account the constraints and finds the best possible input values to a mathematical function that would maximize or minimize its output. In many of these problems, the function that needs to be maximized (or minimized) can be more than one. These problems are called multi-objective optimization problems. These objective functions usually conflict with each other. Therefore, any single solution does not exist that satisfies the maximum value for all these functions. For these cases, the main goal is to find a trade-off between the objective functions' outputs to get an acceptable outcome.

3.12.2. Particle Swarm Optimization Technique

Particle swarm optimization (PSO) is a population based search algorithm that simulates a bird flock and the behavior of birds when searching for food. It was first proposed by James Kennedy and Russel Eberhert. PSO conducts its search based on heuristics and is often referred to as an evolutionary algorithm. It is a very simple optimization technique which was originally designed to balance weight in a neural network. But the simplicity of the algorithm made it popular as a global optimization tool. The simple implementation, less computational complexity of this algorithm and population based search technique makes it a natural candidate to solve multi-objective optimization problems. Since its first proposal, the PSO has seen different variations to solve different kinds of optimization problems [ReCo06].

3.12.2.1. Main Algorithm

PSO simulates a flock of bird flying through the search space with the main goal to find food. In this algorithm, the **swarm** refers to the total population of the flock. The **particle** refers to the individual member of the swarm. These particles are the solutions to the optimization function the algorithm is trying to optimize. The position of these particles in the search space is also determined by their solution. The term **pbest** or **personal best** refers to the best position of a particle that has been achieved by the algorithm. By best position, it is meant that the particle's position in the search space that provided the best solution to the optimization function. The term **lbest** or **local best** is the position of the best particle member of the neighborhood. **Gbest** or, **global best** is the position of the best particle in the entire population. The **leader** particles are the particles which guides or, directs other particles under their influence to the better part of the search space. The **velocity** vector is an important parameter for the PSO algorithm as it dictates the direction in which a particle should commence for a better optimization value. The **inertia** weight parameter determines the effect the previous velocities might have on the current velocity of the particles. There are also two constant learning factors in the algorithm. They are represented as C_1 and C_2. C_1 is called the cognitive learning factor and determines the attraction towards the particle's own success. C_2 is called the social learning factor which determines the attraction of the particle's neighbor's success. The structure of the population or, the swarm of PSO is also varied according to its application. These are called neighborhood topologies.

In the algorithm, first, the particles are created randomly which represents the solution to the optimization function. Then these particles fly through the hyper-dimensional search space simulating a flock of bird flying with the aim of finding food. The particles change their position at each iteration of the algorithm. The change is based on the particle's tendency to be influenced by its own success or, the success of its neighborhood particles. If particle p_i has a position of $\vec{x_i}(t)$ at time t, then the new position of that particle will be found by adding a velocity term $\vec{v_i}(t)$. This can be shown mathematically by [ReCo06]

$$\vec{x_i}(t) = \vec{x_i}(t-1) + \vec{v_i}(t) \tag{3.38}$$

The velocity vector can be given by,

$$\vec{v_i}(t) = W\vec{v_i}(t-1) + c_1 r_1 \left(\overrightarrow{x_{pbest_i}} - \vec{x_i}(t)\right) + \left(\overrightarrow{x_{leader}} - \vec{x_i}(t)\right) \tag{3.39}$$

where r_1 and r_2 are two random components that bring a stochastic nature to the algorithm. They can be from 0 to 1.

Figure 3.14, shows the pseudo code for the main algorithm of particle swarm optimization.

Particle Swarm Optimization
Pseudocode

```
Begin
    Initialize Swarm
    Locate Leader
    g=0
    While g<gmax
            For each particle
                Update position (flight)
                Evaluation
                Update pbest
            End For
            Update Leader
            g++
    End while
End

                End of code
```

Fig. 3.14: Pseudocode for general Particle Swarm Optimization.

3.12.3. Strengths of Particle Swarm Optimization

The PSO algorithm is a simple algorithm to implement. Its simplicity is one of the key reasons for its widespread usage. The basic PSO algorithm adopts only one operator for creating new solutions [ReCo06]. The majority of evolutionary algorithms do not do so with just one operator.

The computational complexity of this algorithm is relatively low which makes it ideal for fast optimization applications. The usage of PSO in these applications provides very good results in a reasonable amount of time.

3.12.4. Differences Between PSO and Evolutionary Algorithms

There are some major differences between PSO and evolutionary algorithms. Evolutionary algorithms employ offspring generation for optimization. PSO does not have any notion of offspring generation. Evolutionary algorithms have the workflow of representing the parents, selecting the individuals, and tuning the parameters for optimization. However, the PSO has only two steps with particle formation and parameter tuning. Moreover, the PSO employs a leader based search strategy where leaders influence the search space of particles. This compensates for the lack of selection parameters for PSO [ReCo06]. Another major difference between PSO and evolutionary algorithms are the techniques they use to manipulate the particles in the population. In PSO, a velocity operator is used to set the velocity of particles that are flying through the search space. There is also an inertia operator which controls the area of search for the particles. These operators affect the flight path of the particles which is similar to the change in direction of mutation in evolutionary algorithms. In PSO, the change in direction of the particles is influenced by the particle's and the entire population's best performances. These are the personal best and global best values of the algorithm. The change of exploration for the particles is another parameter that the PSO controls. If the deviation between the direction of personal best and global best is high, then the range of exploration will be higher. For a smaller deviation, the range of exploration will be shorter. However, for evolutionary algorithms, there exists a mutation operator that has the power to set the direction of mutation in any direction.

3.12.5. Neighborhood Topology

The particles of the swarm in the PSO algorithm are connected with each other. Depending on the connection, the neighborhood of the algorithm can be classified in different groups. Some of the widely used neighborhood graphs are listed and described below.

An **empty graph** is the kind of topology where the particles are not connected to any other particles in the swarm. In this configuration, the particles do not compare their best positions with any other neighboring particles. It only compares its position with its previous best positions it found so far. Another popular topology is the **local best** connection. In this configuration, the particles are connected with its k immediate neighbors. With these neighbors, a local neighborhood is created within which the particle compares its best position. The best position of the neighborhood is called the local best, with the particle's own best as personal best. The **star topology** is also one of the most popular configurations for PSO in which, all the particles are connected to each other. This enables all the particles to compare their own best positions with the best position achieved by the entire swarm. This configuration is one of the most widely used implementations because of their simplicity and effectiveness. The **wheel topology** provides a configuration where one particle is connected to all the other particles. In this case, this particle acts as a sink and no other particles are connected with each other. The particles which act as a sink are called focal particles. As all the particles are disconnected with each other, the focal particle is the only way to exchange information. All the information about the best position of all particles is provided to the focal particle. This particle is then responsible to compare all the particle's positions and choose the best performing particle. It then directs the particles to that part of the search space for further exploration. The information is also supplied to all the particles for updating their databases. The **tree network** is also one of the popular configurations of PSO algorithms in use today. For this configuration, the particles are connected in a tree like fashion. However, in this setting, the particle do not compare its best position with the best position of the entire swarm, but just the best position of the particle that is directly above that particle. In this case the particle just takes into consideration the best position of the parent's best position. If the best position of the particles is better than the best position of the parent particles', then the particles exchange their position. Thus, this configuration always ensures a dynamic neighborhood of particles.

In the sections given above, theoretical information is provided for different principles and ideas used in this thesis. The fundamental factors of wireless communication along with the impacting factors of a time-variant wireless channel ware discussed. Some of the basic principles of antennas and their impacting characteristics on a wireless channel are also talked about. Moreover, the fundamentals of particle swarm optimization and their neighborhood topology are discussed in detail. In the sub-sequent sections, some of the research works from the literature are discussed where similar ideas are implemented using these theories.

The authors in [BoYo11], applied cognitive radio technology to improve coordinated unmanned aerial vehicle missions. The project was conducted in Virginia Polytechnic Institute and State University. The main objective of this project was to develop cognitive radios in UAVs to overcome a lot of issues regarding cooperative communications. In this context, the term cooperative communication means a system where "users share and coordinate their resources to enhance the transmission quality" [BoYo11]. Cooperative communications is increasingly getting popular among UAV communication strategies. A lot of research is being undertaken that increases the range and quality of inter UAV communications employing cooperative communication. For this, the authors in this research employed cognitive radios. In their research, they defined the cognitive radio as "a frequency and waveform agile software defined radio that is aware of (a) its environment, (b) its user's needs and prerogatives, (c) its own capabilities, and (d) the rules governing its operation and able to take action based on that awareness to accomplish its missions" [BoYo11]. Cognitive radios are supposed to be intelligent, able to learn about its environment and adapt to its changes. During their research, the authors find that while the UAV is operating under its normal flight plan, the signal sometimes fades or drops out. This fading of the signal is related to the combination of aircraft position vector, heading vector, orientation vector which includes the roll, pitch and yaw angles of the UAV. Their research was about developing smart radios that will be able to take into account these signal degrading components and take some measures to prevent signal fading.

In [WaRS09], the authors study the impact of antenna orientation on the received signal strength of wireless sensor network devices. Although, this is different from an aircraft system, the wireless sensor nodes also share the same characteristics for wireless communications as the UAV systems. The authors mainly studied the effect of orientation change of the antenna to the quality of data transmission. They conducted indoor and outdoor experiments with the wireless sensor nodes with different antenna orientations. They conclude from the experiments that the antenna orientation has a significant impact on the performance of the wireless channel. They state in their paper that the antenna orientation is one of the most overlooked factors that affect the wireless channel performance.

After different experiments and simulations reported in [WaRS09], the authors claim that the wireless sensor nodes suffer from decrease in accuracy due to the orientation mismatch of antennas. However, research has been undertaken where the type and range of antennas was taken into consideration to gauge their impact on the wireless channel [BAFB06], [JoFH06]. In these research assignments, the authors found that along with the type and range, the variation of orientation of the antenna causes major changes in the received signal. In [LyLS06], the authors also studied the orientation change of an antenna and its impact on the signal strength. However, the authors conclude that the variation of antenna does not affect the performance of the communication when both the receiver and transmitter are at the same altitude. Authors in [LZZG06] show that there is a significant relationship between the Received Signal Strength Indicator (RSSI) and the Packet Reception Ratio (PRR). This further confirms the validity of using RSSI as a proper metric to evaluate the performance of the wireless channel.

In our research assignment, the impact of antenna orientation is of paramount importance. The wireless channel between the ground control station and the UAV will suffer from degradation due to antenna orientation mismatch as their altitudes will vary. Moreover, although the orientation change and its effects were studied in the literature, the overall effect of this on the fading channel was not done before according to the best of our knowledge. One of the main motivations of this research assignment is to study the impact of antenna orientation among other factors, on the fading parameter of the wireless channel.

In a similar research assignment conducted by the authors in [WaZh08], the joint effects of node mobility and channel impediments on the wireless channel were investigated. The channel variability and node mobility were measured using two metrics named as the *Effective Transmission Range* (ETR) and node-pair distance. In this paper, the authors captured the effects of path loss, shadowing and multipath fading in one single metric, the ETR. The metric node pair distance was a measure of how smooth the node mobility is. The authors studied the link lifetime characteristics of the wireless links and the effects of the above mentioned two metrics have on it. They were able to show that link lifetime distribution can be given by an exponential distribution whose parameters can be obtained from the effective transmission range metric. For mobile nodes with slower speeds, the average link lifetime depends heavily on the wireless channel characteristics. However, for faster mobile nodes, the link lifetime is dependent on the mobility of the nodes. Correspondingly, the authors in [KJTT08] also prove that the transmitter and the receiver's relative movement can cause severe degradation to the wireless channel due to its multipath propagation, mobility and multiuser interface. These research findings further establish the fact that the mobility of UAVs plays a huge role in determining the performance of wireless communication along with the channel impediments.

In [Sain11], the authors modelled and characterized the wireless channel between wireless nodes set up in harsh environments. The primary goal was to characterize the wireless channel in harsh, industrial environments. The author conducted experiments that measured the *Received Signal Strength Indicator* (RSSI) and *Packet Error Rate* (PER) for radio components using the 2.4 GHz frequency band. They transmitted and received 10,000 packets and for those packets, the RSSI and PER were measured. They concluded the Rician K factor as a measure of the link quality which is given by the power difference between the LOS component and multipath components. With the data gathered from the experiments, the author reports that the relationship between the signal attenuation and distance between transmitter and receiver is not linear. In other words, the RSSI and PER of the nodes situated in the same distance from the transmitter will not necessarily be the same. The author concludes that path distance between the transmitter and receiver is not the only factor that can impact the signal attenuation in a real world wireless channel. This attenuation also has complex relationship with the multipath effects and line of sight from the surrounding objects in the environment.

So we can see that the channel impediments and the mobility of the UAV both will impact the fading channel. In order to fully utilize the wireless channel between the ground control station and the UAV, these fading out of the signal should be predicted beforehand so that different measures can be taken to mitigate the signal degradation. In [DuHH00], the authors developed an algorithm to predict the fading coefficients of a time-varying wireless channel. The authors use this prediction algorithm to use adaptive transmission techniques in case of performance degradation of the rapidly changing wireless channel. The prediction algorithm considers the past observation of the channel to predict the future fading coefficients' *minimum mean squared error* (MMSE) estimates. However, for a micro UAV channel between a ground control station and a UAV, the propagation environment changes rapidly, especially in an urban environment. Moreover, the UAV is subject to constant change of its altitude and orientation due to complex flight maneuvers. For this case, the prediction algorithms must take into consideration the most impacting factors of the channel such as the distance, antenna orientation, and polarization mismatch of antennas. In our research assignment, we devise a particle swarm optimization based algorithm that takes into account the above mentioned factors and provides the estimation of fading coefficients which can be used to determine how the channel will behave.

Thus, we can see the importance of predicting how the channel will behave in terms of different propagating environment, different multipath components scattering the transmitted signals, and different orientation of the aircraft antennas. The determination of the wireless channel model in the characterization of the channel is thus very important. Different researchers adopted several channel models to represent the propagating environment and its effects on the wireless channel. In [PILS06], the authors modeled the wireless channel between a satellite and a ground based receiver with the Nakagami fading channel and fading parameter m. The reason for choosing the Nakagami fading model was due to its ability to model a wider range of fading severity. Moreover, the fading parameter m can be used to express the severity of fading existing in the channel. The authors conducted a number of experiments with the U-NAV Microelectronics in Finland. They evaluated both an outdoor channel and an indoor channel by receiving a satellite signal from one GPS receiver connected to an outdoor antenna and another GPS receiver which is situated indoors. Based on the measurement data, they concluded that the Nakagami m distribution performs very well in modelling the indoor and outdoor satellite channels. In [LLSR05] and [LaLS05], the authors too, demonstrates from experimental data that the Nakagami m distribution is the best performing model to characterize the indoor and outdoor wireless channels. Here they showed that the m parameter successfully represented the fading that is existent in the channel. Moreover, authors in [LaLo05] showed that the Nakagami m distribution is also able to model the CDMA interference and [LaLR04] reported that Nakagami-m distribution was successful in characterizing WCDMA wireless channels in dense urban propagation environments. In [SOSL94], the authors include another conclusion that is very important in ground to air wireless links. They conclude that Nakagami-m distribution is also able to model the scintillating ionospheric effects on radio signals. This is an important factor for a ground station-to-UAV channel since the UAV might reach high altitude during the course of its flight. In our research, the fading channel between the ground control station and the UAV is also modeled using the Nakagami-m distribution due to the above mentioned reasons. The fading parameter m is used to represent the fading of the channel. Moreover, the impacting factor's effects on this fading parameter ware also investigated using regression analysis and real world experiment data.

However, a quick study of the literature reveals the fact that a lot of research assignments employed the Rayleigh and Rician models to characterize the fading channel between mobile radios. The reason for choosing the Nakagami fading model over these two popular channel models can be found in [TaHo03]. In this work, the authors state that in the case of a mobile radio operating in a dense urban environment with line of sight and non line of sight propagation, the signal received by the receiver will consist of a significant number of multipath components along with the line of sight component. This occurs due to reflections, refractions and scattering of electromagnetic waves from the surrounding obstacles. The phase, amplitude and angle of arrivals of these multipath components will vary greatly and recombine in the received signal. This in turn will cause the fading of the received signal. It has been reported in the literature that when there is no line of sight between the transmitter and receiver, the fading of the received signal will follow a Rayleigh distribution. In this case, the received signal will not carry any line of sight components and will only consist of multipath random components. This creates severe fading of the signal. If there is line of sight between the transmitter and receiver, the received signal will follow a Rician distribution. The authors in [TaHo03], state that the Rayleigh distribution is not capable of modeling the full range of fading for long distance propagation environments because of the fact that it does not consider any line of sight component present in the received signal. Nakagami developed a parametric gamma distribution based density function that was able to model the real world experimental data for transmitted and received signal. His model, widely known as the Nakagami model mitigated the limitations of Rayleigh model by being able to model both the line of sight and non line of sight components. In our research, the UAV is assumed to operate in different urban environments communicating with a portable ground control station. In this scenario, the complex maneuvers of the aircraft can include both line of sight and non line of sight communications. Especially, in a densely packed urban environment with a number of high rise structures, and the limited height of the portable ground control station, it is very difficult to assume, or predict if the channel will have a line of sight or non line of sight component. Therefore, the Nakagami fading model is the best available option to model the time variant wireless channel between the UAV and the ground control station.

This realistic channel model, which closely resembles the wireless channel between the ground control station and the UAV, provides a varied performance which depends on a few impacting factors. One of them is the antenna orientation on board the UAV. Because of the complex aerial maneuvers the UAVs usually conduct during its flight operation, the orientation of the antenna onboard the UAVs is constantly changing. This is an important area of research for communication between UAVs and much research work can be found in the literature. In [BADD04], the authors conducted experiments to measure the throughput, connectivity and range of airborne UAVs who are connected in a mesh network. They use 802.11b radios for inter-UAV communications. In [AHPP07], the authors use 802.15.4 compliant radios to test the wireless performance of air-to-air and air-to-ground communications. The authors in [CHKV06], used a fixed wing UAV integrated with a 802.11a radio to test the wireless performance for a linear flight path of the aircraft. Authors in [FMTN06] used the ray tracing technique to develop path loss models for communication between UAVs and ground control stations. However, these studies do not include the effects of antenna orientation mismatch on the performance of the channel. Other impacting factors such as polarization mismatch factor, directional gain (for directional antennas) are also not considered in these research assignments. In [YaKB11], the authors focused on the impact of antenna orientation on small quad-rotor UAVs fitted with 802.11a based radios. The link between the UAV and a ground control station was analyzed using two sets of onboard antennas both on the UAV and ground control station. Two different antenna orientations were used in the experiments. The first orientation consists of one antenna being horizontal and the other in a vertical position. On the second orientation, both of the antennas were mounted horizontally. In this case, the antennas are faced perpendicular to each other. The authors conducted experiments to investigate the impact of altitude and yaw of the UAV on the received signal strength and throughput. The flight environment of the UAV consisted of an open field and university campus area. The data communications between the UAV and ground control station was also characterized by estimating the path loss exponent of the propagation model. The ground control station consisted of a Netgear WNDR3700 version 2 which had an Atheros AR7161 chipset. The wireless cards were also Atheros AR9280 operating on 802.11an and 802.11bgn protocols. The antennas used in the ground control station were WiMo 18720.11 omnidirectional antennas. The ground station was operated with a Linux based Open WRT Backfire 10.03.1-RC5 operating system. The UAV used in the experiments was an ASCTEC Pelican with a wireless network card from SparkLan which is 802.11abgn compliant. The antennas were identical to the ground control station. The UAV was operated by Ubuntu Linux 10.04 operating system. The received signal strength of the received signal was measured by the built in network monitor interface in Linux. From the experimental data, the authors conclude that the adverse effects of the antenna orientation change during aircraft flight can be mitigated using one horizontal and one vertically mounted antenna. Their results also show that the wireless channel behaves differently in the hovering and moving phases of the UAV. Moreover, their work demonstrates the severe degradation of signal strength due to the tilting of the quadrotor UAVs and significant measures need to be taken to mitigate these adverse effects.

Although this research work puts an emphasis on the effects of antenna orientation change and successfully characterize the channel response, there are some limitations or, areas of possible extensions. The paper investigates the effects of the orientation change only on the received signal strength and throughput. However, in our research we combine the adverse effects of the orientation change and other impacting factors to the long term fading process of the channel. According to this fading model, the fading parameter can be estimated given the conditions of the propagation environment. In the experiments conducted in this paper, the authors tested the RSSI only for two antenna orientations. In our research, along with other factors, the orientation of the antenna is varied from vertical to horizontal by 0°, 23°, 45°, 68° and 80° degrees. For each of these angle mismatches, the polarization loss factor is calculated and used in the regression analysis to investigate their effects. This research assignment employs omnidirectional antennas in both the UAV and ground control station. However, having omnidirectional antennas on both ends introduces a big limitation on the range of this point-to-point link. In our research, the ground control station is equipped with a directional Yagi antenna and the UAV is equipped with an omnidirectional antenna. This drastically increases the range of the wireless link between the UAV and ground control station. However, directional antennas have their own share of limitations. Although the range is increased, the beamwidth and directivity of antenna limits the gain to a limited area of coverage. This directive gain is also taken into consideration in our research as an impacting factor and effects of its deviation is also investigated. The research in [YaKB11] employs the Log Normal Shadowing path loss model to model the wireless channel. In our research, the wireless channel is modeled with both the log normal shadowing and the dual slope piecewise linear model. The model that best fits the experimental data is chosen for further analysis. The authors in [YaKB11] monitored the received signal strength, transmission rate and other throughput data from the frame data of the 802.11 packets. This was done by a built in function called Linux network monitor in the Linux operating system. However, in our research experiments, a spectrum analyzer is connected to the ground control station antenna to measure the received signal strength, signal amplitude and other measurements. The employment of the spectrum analyzer to obtain measurements has some advantages over the network monitor software. With the spectrum analyzer, it is possible to tune into one specific center frequency and analyze the transmission in that frequency. In our research, we use frequency hopping spread spectrum radios which transmits in different frequency bands. The spectrum analyzer is able to scan the full spectrum or, tune into one specific transmission frequency to analyze the wireless signal. Also, any shift in transmission frequency can also be investigated by the spectrum analyzer for a frequency hopping system. The resolution bandwidth of the spectrum analyzer used in our thesis also plays a huge role in the measurements of the received signals. It is a bandpass filter that is situated before the detector in the configuration of the spectrum analyzer. The main purpose of this bandpass filter is to measure the noise floor and to determine the closeness of two signals which can be separated out in the spectrum analyzer. Lower resolution bandwidth decreases the measured noise floor because the filter will pass lower frequency components to the detector. Similarly, higher resolution bandwidth causes the measured noise floor to be higher. In our experiments, the resolution bandwidth is set to 1 MHz. This ensured that the noise floor would be measured correctly and the signal will be detected with a good resolution. Moreover, any interfering signal can be detected as well.

The video bandwidth is another important parameter for the measurement of signals with a spectrum analyzer. This is a low pass filter which is situated after the envelope detector in the spectrum analyzer. This determines how the analyzer records the sample of the analyzed signals. The main function of this filter is to differentiate the power level between two signals. Therefore, it is very important in our measurement where the received signal's power will be measured to detect the fading. Moreover, the spectrum analyzer used in our research has a very low sweep time of minimum 1μs. The sweep time determines the amount of time the analyzer sweeps the frequency bandwidth. In our experiments, the sweep time is set to 1ms which forces the spectrum analyzer to scan the frequency every 1 ms to capture the received signal amplitude.

The spectrum analyzer also has one important function that provides great advantage in the measurement of signals. The detection can be sample detection, peak detection and average detection, among other choices. In our research, we use the peak detection for the detector so that the analyzer can detect the peak signal that is being received by the ground control station antenna. This enables us to get a very high resolution image of the spectrum and to detect the fading of the signal.

In [YaKB11], the authors conducted their experiments with radios which operated on 2.4 GHz and 5 GHz frequency bands. However, the 900 MHz frequency band provides some advantages over the 2.4 and 5 GHz bands for point-to-point communication. As the attenuation suffered by radio waves operating in a lower frequency is much lower than its high frequency counterparts [Comm14], the 900 MHz frequency band performs better than 2.4 GHz frequency waves. Therefore, the path loss suffered by 900 MHz radio waves is lower. However, for the same size and dimensions of antennas, the 2.4 GHz band has a higher gain and the bandwidth is able to carry much more information than the 900 MHz radio waves.

In our research, significant attention is provided to the atmospheric attenuation of the waves by water vapor and other atmospheric gases. For 2.4 GHz, these attenuations are higher than the 900 MHz radio waves. Moreover, obstacles situated in the line of sight of radio wave propagation attenuate a 2.4 GHz radio wave more than the 900 MHz wave. In our research, this is an important consideration as the operating environment is assumed to be a densely packed urban environment with trees, buildings, cars and other structures obstructing the line of sight for the radios. Due to these limitations of the 2.4 GHz frequency band, the radios used in our experiments used the 900 MHz frequency radio waves. Moreover, the researchers in [YaKB11] investigated the effects of antenna orientation on the received signal strength only. Our research is a logical extension of this work which takes the propagating distance, directive gain of directional antenna, the polarization mismatch factor of the two antennas and investigates their overall effect on the fading distribution of the wireless channel. It also provides as indicator of the severity of fading by the fading parameter m, which is used to construct the model for prediction of fading using a particle swarm optimization based algorithm.

3.13. Summary

This chapter provides detailed theoretical information about some of the fundamental components for point-to-point communication between a UAV and a ground control station. A widely used optimization algorithm named particle swarm optimization is also discussed in this chapter. In addition, some of the recent research concerning the communication channel for a ground station-UAV link is discussed in detail with some of their limitations and possible areas of extension. These limitations and extensions are the key motivations of this thesis. In the next chapter, the design and implementation of the communication sub-system for the ground control station and the UAV module are discussed in detail.

This page intentionally left blank

CHAPTER 4

SYSTEM DESIGN & IMPLEMENTATION

This chapter provides the detailed discussion on the design and implementation of the communication subsystem for the unmanned aerial system used in this thesis. This project is completed to fulfil the requirements of a Mitacs Accelerate research internship conducted in a joint venture between University of Manitoba (Delta Research Group) and Buoyant Aircraft System International (BASI). The communication subsystem is designed and implemented to provide a long range communication backbone for a new class of UAVs being designed by BASI. This chapter discusses about the ground control station and UAV module hardware, ground control station user interface and UAV module server software along with other implementation details.

4.1. Hardware Design and Implementation

The hardware design and implementation for the communication sub-system for the unmanned aerial system consists of two parts: ground control station and UAV module. The ground control station is designed to be portable and lightweight. The UAV module is designed to be as light as possible to limit the overall weight of the UAV. The block diagram of the entire communication sub-system is provided in Fig. 4.1.

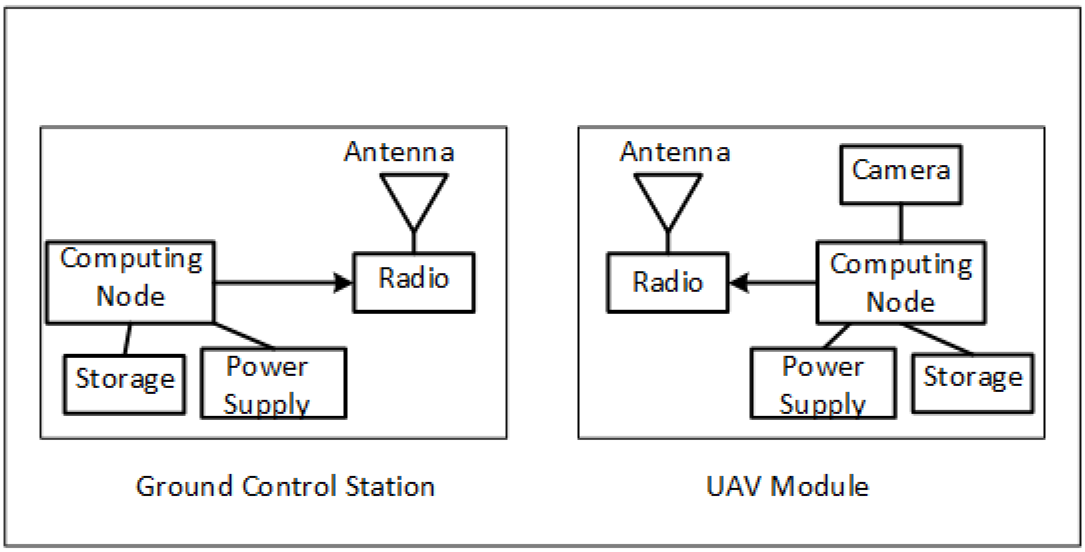

Fig. 4.1: Hardware block diagram of ground control station and UAV module for the communication sub-system.

In the subsequent sections, detailed information on the individual modules as well as their descriptions are provided. Further information about the hardware components is provided in the appendix section.

4.1.1. Ground Control Station (GCS)

The ground control station for the unmanned aerial system consists of the transceiver module, a microcontroller, an antenna, power supply and a display module. One of the design goals for this module is to make it portable and lightweight. Portability is an important factor for the ground control station as it provides flexibility in transportation, set up and operation of the GCS in different environments.

The following sections provide more information on the hardware components used in the ground control station for the unmanned aerial system.

4.1.1.1. DNT900 Radio Transceiver Module

One of the main components of the ground control station is the radio transceiver which is used to transmit and receive wireless data. In this research work, we choose the DNT900 radio transceiver as the transceiver for the communication subsystem to create a wireless point-to-point link between the GCS and the UAV.

The DNT900 is a 900 MHz spread spectrum wireless transceiver designed by RFM [Mura10]. It provides support for wireless communication for point-to-point, point-to-multipoint, peer-to-peer and tree-routing networks. The transceiver employs *Frequency Hopping Spread Spectrum* (FHSS) technology for mitigating fading effects and interference. It operates in 900 MHz ISM band and enables license free use in many countries including Canada. One of the strengths of this transceiver is its built-in data buffering ability and error-correction protocol to provide a stable data flow between the transmitter and the receiver. The transceiver along its development board is shown in the Fig. 4.2.

Fig. 4.2: DNT900 radio development board [Mura10].

The DNT900 radio transceiver divides the 902-928 MHz frequency band into 50 frequency channels and transmits in each channel with a pseudo-random sequence. This frequency hopping spread spectrum technique compensates for multipath fading and eavesdropping. It provides support for point-to-multipoint links and one of the future implementations of the designed system is to create a network of ground control stations with a UAV using point-to-multipoint links. The transceivers provide good communication range of over 40 mile with omnidirectional antennas. The development board is equipped with analog and digital I/O ports for ease of interfacing with sensors and microcontrollers. It has built-in *Advanced Encryption Standard* (AES) encryption for data integrity and security.

One of the design goals of this research project is to design a transmission power control scheme for optimal communication between the GCS and the UAV. The DNT900 radio transceivers offer a variable transmission power option with 1, 10, 100, 250, 500 and 1000 mW of transmission power. It provides a high data rate of 500 kb/s for a point-to-point wireless link. The maximum serial data rate for communication with host device is 460.8 kb/s. Further technical information about the DNT900 radio transceiver is provided in the appendix section.

The DNT900 radio offers flexibility for its small form factor. It is a low cost solution with a good wireless performance in terms of range and data rate. Due to these reasons, this transceiver is chosen as the transceiver module for the communication subsystem.

4.1.1.2. Computing Module

The heart of the ground control station is a Raspberry pi single board computer. This computing module provides all the computing functionality to the GCS and acts as the brain of the system. It is interfaced with the DNT900 transceiver for a seamless operation of the ground control station for optimal data communication with the UAV. The designed communication protocol is implemented with this module. Moreover, it runs the GCS command line user interface on top of a Linux based operating system.

The Raspberry Pi is a credit card sized computer which is designed and developed by Raspberry Pi Foundation, UK [Wiki09]. It houses a Broadcom BCM2835 system on a chip (SoC) and includes an ARM1176JZF-S microprocessor. The microprocessor runs at a clock speed of 700 MHz. It includes a dedicated VideoCore Graphics Processing Unit (GPU) for dedicated image and video processing capabilities. The on-board memory is 512 MB and it uses an 8 GB flash disk for data storage. Figure 4.3 shows the Raspberry Pi model B used in this project.

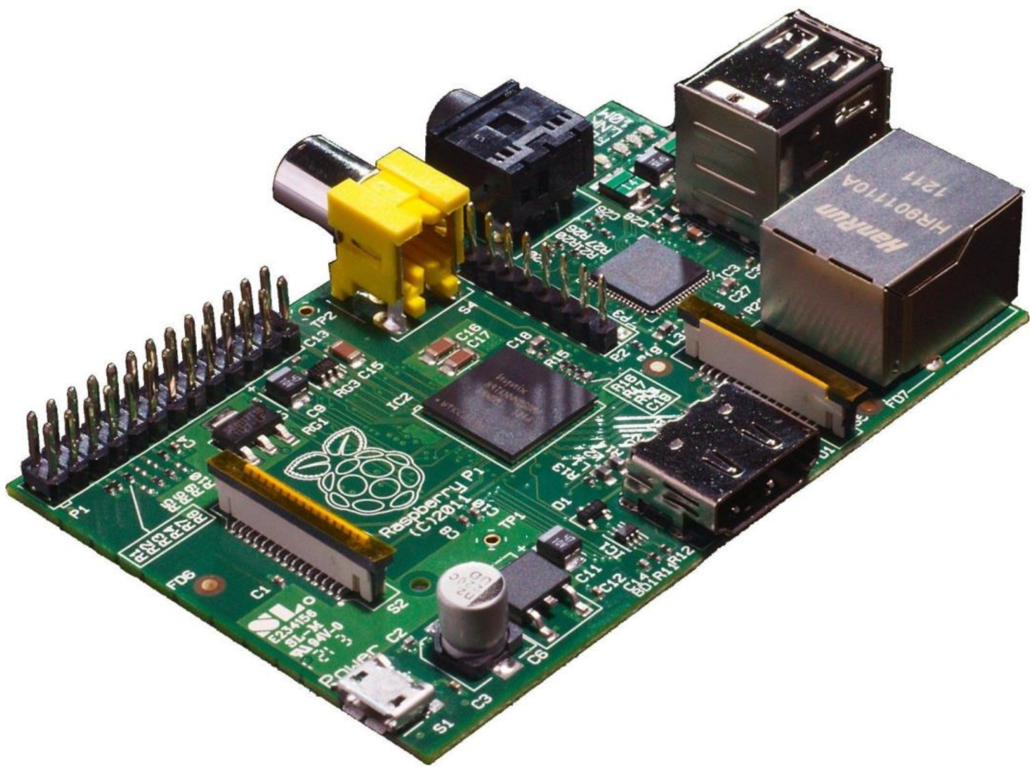

Fig. 4.3: Raspberry Pi model B [Wiki09].

The processor employs a level 2 cache memory of 128KB for faster processing of instructions. The SoC provides a real world performance of approximately 0.041 GFLOPS. However, the Raspberry Pi SoC provides options for overclocking the 700 MHz processor to a maximum of 1GHz, but for native clock speed, no heat sink or cooling is required. Figures 4.4 and 4.5 show the PCB design and block diagram of the Raspberry Pi single board computer respectively. The dedicated GPU runs at a clock speed of 250 MHz. The memory of 512 MB is shared by the GPU and the *Central Processing Unit* (CPU). The Raspberry Pi computer is also equipped with 8 General Purpose Input/Output (GPIO) pins, UART, I^2C bus, SPI bus, I^2S audio, 3.3V, 5V and a ground connection.

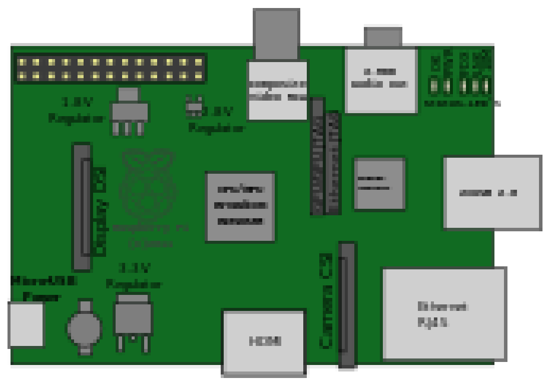

Fig. 4.4: PCB design of major ICs and connectors of Raspberry Pi [Wiki09].

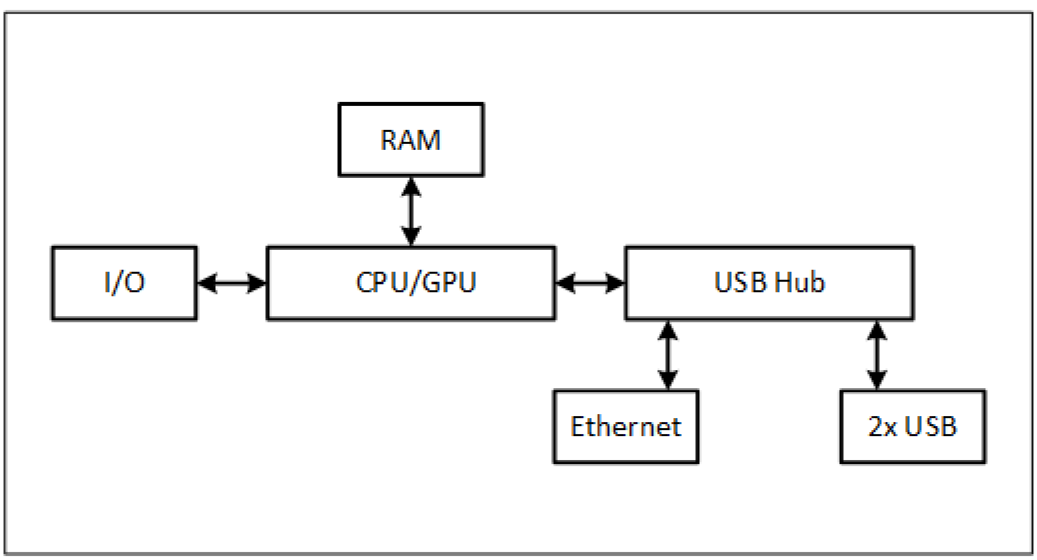

Fig. 4.5: Block diagram of Raspberry Pi model B.

4.1.1.2.1. GPU/CPU Memory Split

One of the main motivations behind using Raspberry Pi as the computing node in this system is its ability to perform complex image and video processing due to its dedicated GPU. The main memory for the single board computer is 512 MB which is shared between the CPU and GPU with a certain ratio. In order to perform high definition image and video processing required in this research project, the GPU needs a larger memory. The Raspberry Pi model B comes with a default setting of memory split with the GPU getting only 64 MB. One of the design goals of this research project is to transmit high definition image and video files from the UAV to the ground control station for monitoring and image processing purpose. For this reason an increase in the shared memory of the GPU is needed. The GPU memory is increased to 256 MB by modifying the startup configuration file for the Raspberry Pi.

4.1.1.2.2. Kernel Modification

The DNT900 radio can operate at a maximum data rate of 460.8kb/s for its serial connection to the host device. For the Raspberry Pi model B, the maximum serial data rate is 115.2 kb/s. The stock Linux kernel for the Raspberry Pi employs this hard coded serial data rate. In order to maximize the serial data rate between the computing node and the radio transceiver, the Linux kernel is modified to work with maximum data rate of 460.8 kb/s matching the radio transceiver's data rate.

4.1.1.3. FTDI USB to Serial UART Interface Integrated Circuit

The interfacing of the DNT900 radio transceiver with the Raspberry Pi computer is achieved by a Universal Serial Bus (USB) to serial UART interface Integrated Circuit (IC). The

IC is a FT232R chip developed by FTDI [Ftdi14]. A USB to serial cable is used to connect the radio transceiver to the Raspberry Pi's USB interface. The development board for the DNT900 radio provides the serial interface. The FT232R provides a clock generator output with asynchronous and synchronous bit bang interface modes. The chip itself contains an EEPROM, clock circuits and USB resistors. One of the main reasons to choose this USB to serial converter is the built-in clock generator on the chip. As the Raspberry Pi does not have an external clock, this clock generator can be used to drive the Raspberry Pi. The FT232R IC used in the project can be seen in the Fig. 4.6. Further technical information on the IC is provided in the appendix section.

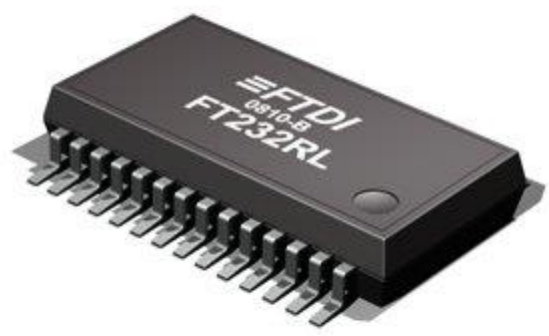

Fig. 4.6: The FTDI232RL integrated circuit [Ftdi14].

4.1.2. Antenna

Antennas are one of the key components in any wireless system design. Antennas take the oscillating electric current supplied by the radio transmitter and radiate the energy from the current as electromagnetic waves [Ante08]. In our communication subsystem, we use a Yagi directional antenna as the antenna for the ground control station. Figure 4.7 shows the Yagi antenna used in our system.

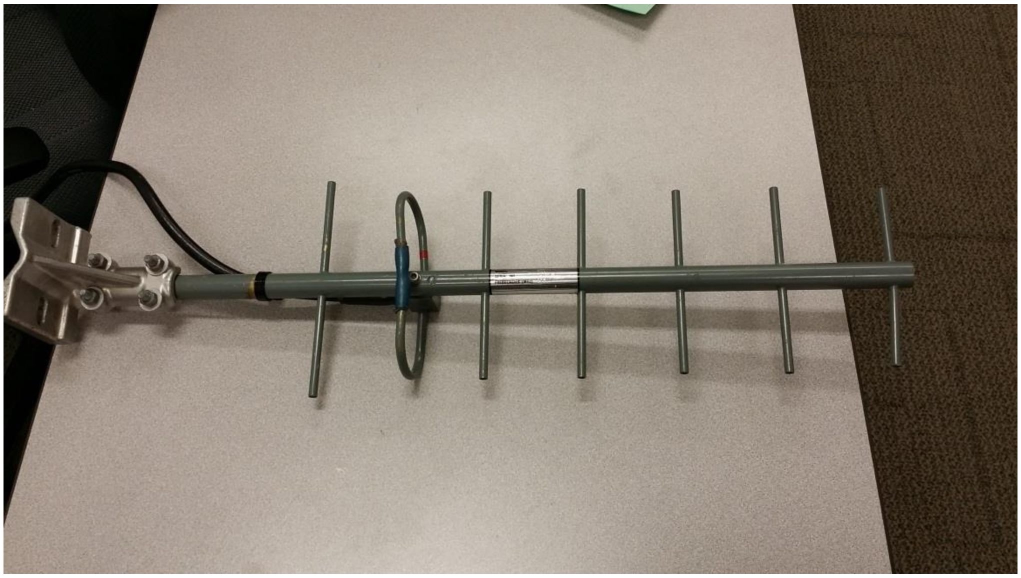

Fig. 4.7: The Yagi 12.1 dBi 900 MHz antenna.

Yagi antennas were designed by two famous Japanese antenna experts Yagi and Uda. The antennas are also referred as Yagi-Uda antenna in the literature. Yagi antennas work on the principles of modifying the radio frequency (RF) pattern of a dipole antenna by adding elements of various lengths and spacing in front and the back [Hamu00]. This results in a more focused beam in one direction which causes the directionality of the antenna. This also results in much stronger receive and transmit signals in that direction. Yagi antennas have a resonant fed dipole which acts as the driven element. The parasitic elements are of two types: (i) reflectors and (ii) directors. Reflectors are responsible for redirecting the electromagnetic waves to a particular direction and are usually placed behind the driven element. The director elements are responsible for the directionality of the waves. The horizontal spacing between the elements is called the boom of the antenna.

The particular Yagi antenna we are using in this project is designed by Sinclair Technologies. It is a 7 element Yagi antenna with a gain of 12.1 dBi. The operating frequency range is 806-870 MHz with the frequency bandwidth as 64 MHz. The Voltage Standing Wave

Ratio (VSWR) is 1.5:1. The front to back ratio is 20 dB. The antenna is impedance matched at 50 Ohms. Maximum input power that can be fed into this antenna is 125 W. The overall length of the antenna is 24 inches and the total weight is 1.06 lbs. It uses an N-female connector to connect to the transceiver. It can withstand a maximum wind velocity of 150 MPH. The datasheet of this antenna produced by the manufacturer is provided in the appendix section.

The radiation pattern of an antenna provides the concentration of RF energy in all directions in the plane perpendicular to the antenna [Ante08]. From a radiation plot, system designers are able to specify which regions will have the maximum amount of RF energy for that specific antenna configuration. In this project, one of the main motivations behind using a directional antenna is to create a long range wireless link between a UAV and the ground control station. Directional antennas such as Yagi provide a high gain (12.1 dBi in this case) which is highly directional and can create long range wireless link with the airborne UAV.

One of the research questions that this thesis addresses is the characterization of the wireless channel between a low altitude UAV and a portable ground control station equipped with linearly polarized antennas. Although, equipping the ground control station with circularly polarized antennas with the UAV node equipped with linear, overcomes the orientation mismatch problems for these systems. However, analysis of a linearly polarized link in this scenario was conducted as a first step, which will lead to a full investigation of other polarization configurations in future studies. Moreover, employing directional antennas in the ground control station increases the range of this UAV-GCS link considerably than omnidirectional antennas. This thesis analyzes some of the impacting factors that the directional antenna configuration introduces, which might have a negative impact on this highly mobile channel.

4.1.3. Antenna Connectors

Antenna connectors or, RF connectors are electrical connectors which work at radio frequencies and connect the transmitter to the antenna terminal [Wiki14]. They are used with coaxial cables and are impedance matched to minimize change in impedance in transmission lines.

4.1.3.1. RP-SMA Antenna Connector

In this research, the DNT900 transceiver uses a *reversed polarized subminiature version A* (RP-SMA) antenna connector. These are semi-precision coaxial RF connectors with a screw type coupling mechanism [Smac14]. These connectors employ 50 ohm impedance for the transmission line. Figure A.8 in the appendix section A9 depicts a standard male SMA connector.

A variant of these SMA connectors is the reverse polarity SMA connectors which changes gender of the interface. For example, a standard reverse polarity SMA female connector will have a male pin as the center receptacle. The RP-SMA male connector used by the DNT900 is shown in Fig. A.9 in appendix section A9.

4.1.3.2. N-Female Antenna Connector

The Yagi antenna uses an N-female antenna connector at the antenna terminal. The N-connectors are threaded, weatherproof and is joined by a co-axial cable [Ncon14]. These connectors can handle frequencies up to 11 GHz. The N-female antenna connector used in this research can be seen in Fig. A.10 in appendix section A9.

4.1.3.3. Transmission Line

The transmission line between the transmitter and the Yagi antenna used for the ground control station is chosen as a co-axial cable with an impedance of 50 ohms. It uses a RP-SMA male connector on one end to connect with the RP-SMA female connector from the transmitter. On the other end, it uses an N-male connector to connect with the N-female connector of the Yagi antenna. The transmission cable is weatherproof and can be seen in Fig. A.11 in the appendix section A9.

4.1.4. Antenna Tripod

The antenna tripod used to hold the Yagi antenna for the ground control station is a preassembled tripod mount from TipTop Electronics [Elec14]. The tripod legs include holes for fastening to a surface for ease of use. It can be folded into a smaller form factor for carrying and transportation purposes and is ideal for a portable ground control station. The tripod used for the ground control station can be seen in Fig. A.12 in appendix section A9.

4.1.5. Power Supply

One of the key components of the ground control station is the power supply used to power all the components. One of the most important design goals of this project is to design and implement a portable ground control station. In order to do so, the power supply has to be portable, lightweight and also carry enough power for a long range of operation. During the design phase, a lot of consideration is put into the low power consumption for each component. However, to provide power for the computing node, the transceiver and the display module, we needed a good amount of power.

The power supply chosen for the ground control station is a USB battery pack with 10000 mAh [Adaf14]. It provides 2 USB interface with 5 V and maximum current draw of 2A. It is a rechargeable battery pack with small form factor and lightweight. It employs a lithium ion battery with 10000 mAh. Two boost converters provide the 5 V DC voltage with a maximum current draw of 2A for each USB interface. There is a Light Emitting Diode (LED) display which indicates the charge on the battery and provides an on-off switch. The battery pack can be seen in Fig. A.13 in appendix section A9.

4.1.6. Storage

The storage device to store the operating system, the ground control station user interface, flight data and high definition image and video files transmitted from the UAV used in the system is a 8 GB Secure Digital (SD) nonvolatile memory card. This memory card is a common storage device for mobile phones and digital cameras. The Raspberry Pi provides an interface for this storage device and all the data are saved in this memory location. This also acts as a black box for the unmanned aerial system as it records all the data that is transmitted from the UAV in separate files. The SD card used in this project can be seen in Fig. A.14 in appendix section A9.

4.1.7. Display Module

As a display module and to hold all the components, we use a portable briefcase which is designed for FPV flying or aerial photography. The components are fitted inside the casing with ample room for operation. The briefcase has a 7 inch LCD monitor which is used as the display module for the ground control station to display various data and act as a user interface. A keyboard is connected with the case to provide user interface as well. There is a sun hood available at the top of the display screen to help operate in glaring sun light. The video inputs are integrated with the Raspberry Pi composite audio video interface. A dedicated 12 V battery with a barrel connector is used to power the display module. There is also a voltage indicator of the power supply available to let users know about the voltage level of the power supply used. The briefcase provides additional functionalities such as integration with a tripod, portability, weatherproofing and ruggedness. The briefcase ground station used in this project can be seen in Figs A.15 and A.16 in the appendix section A9.

4.2. UAV Module

The UAV module of the communication sub-system is responsible for receiving data from ground control station, transmitting flight data to the ground control station, capturing high definition image and video files and transmitting them back to the ground control station. The UAV module is also integrated with a computing node which is a Raspberry Pi, a radio transceiver which is a DNT900 radio module, FTDI USB to serial interface, a high definition camera module, an omnidirectional antenna and a power supply. All the components except the antenna and the camera module has been described in the previous sections. We provide detailed information about these components in the sub-sequent sections.

4.2.1. High Definition Camera Module

The UAV module for the communication sub-system employs a high definition camera module to capture high definition image and video files. The module has a five megapixel fixed focus camera that is able to record videos at a resolution of 1080p at 30 frames per second (fps), 720p with 60 fps and VGA with 90 fps [Adaf13]. The camera module is interfaced with the

Raspberry Pi single board computer with a 15 cm ribbon cable at the CSI port. It is accessed by the MMAL application programming interface (API) through the shell script of Linux. The camera module used in this project can be seen in the following Fig. 4.8.

Fig. 4.8: Camera module [Adaf13].

The CSI port that is used to interface the camera module is capable of high data rates and designed to carry pixel data exclusively [Adaf13]. The module is extremely small and lightweight with dimensions of 25mm x 20mm x 9mm and weight of 3 grams. The BCM2835 SoC is connected to the module via the CSI bus. The Omnivision 5647 sensor employed in the camera module has a fixed focus lens which can capture still image with a very high resolution of 2592 x 1944.

4.2.2. Omnidirectional Antenna

The antenna used in the UAV module is an omnidirectional quarter-wave monopole with a gain of 2.1 dBi. It is designed to operate in the frequency range of 902 - 928 MHz. The antenna is chosen due to its small form factor and lightweight. The maximum range for this antenna is 3000 feet. The antenna used on the UAV module can be seen in the Fig. 4.9.

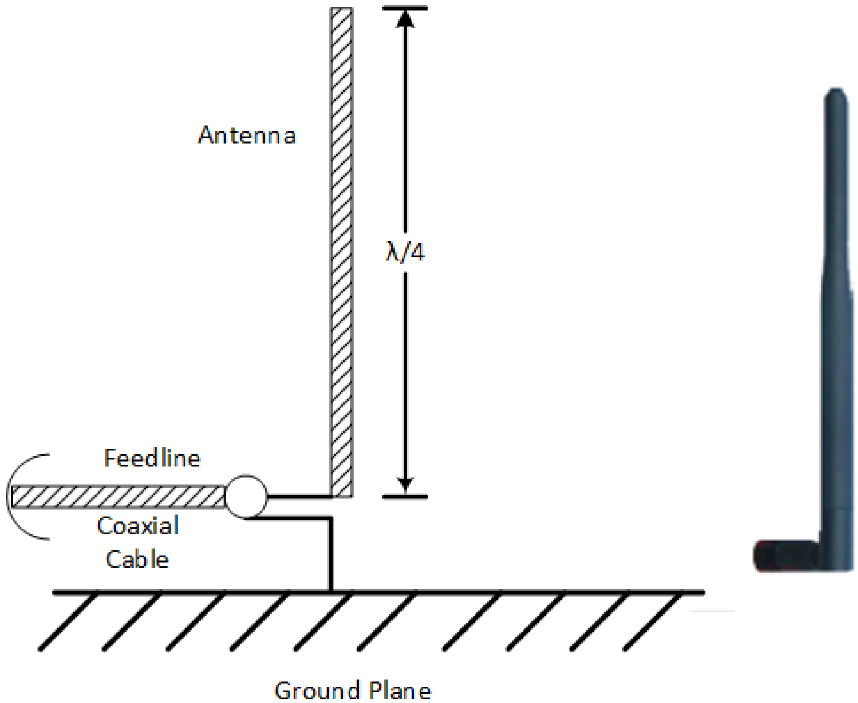

Fig. 4.9: 2.1 dBi omnidirectional antenna.

The radiation pattern of this antenna is a horizontal doughnut [Wilk12]. Although this antenna provides less gain than a directional Yagi, studies have shown that for aerial systems, omnidirectional antennas provide a better coverage due to their fast movement and orientation change [CHKV06]. These antennas are usually used at the control end of a polling system and provide a good range. There is a swivel mechanism with the build configuration of the antenna that allows it to change its orientation relative to the base. It has a VSWR of less than 2:1 and is impedance matched at 50 ohms. The antenna connector is a RP-SMA male that connects with the DNT900 transceiver's RP-SMA female connector. The connector is mainly made of brass with nickel and gold plating. The length of the antenna is 7 inches with a diameter of 0.5 which includes the polyurethane whip.

4.3. Software Design and Implementation

To implement an optimal communication subsystem for the unmanned aerial system, a command line user interface for the ground control station and the UAV module are designed and implemented. The user interfaces are written in C++ programming language. Detailed information about the user interfaces, operating system environment, implemented functions and classes are provided in the sub-sequent sections.

4.3.1. Operating System

The ground control station and the UAV module run Arch Linux as its main operating system. It is a distribution of the widely popular Linux operating system which is free and open source. This distribution is mainly targeted towards i686 and x86-64 computers [Arch11]. Arch Linux has a dedicate package manager called Pacman for installation and removal of software packages.

Arch Linux is widely used for different embedded system applications due to its simplicity of design and re-configurability. There is no graphical front end that is provided with the operating system. The command line interface and the Shell provide a powerful mechanism to access, edit and configure system configuration files. This gives the developer the ability to re-configure the operating system by modifying the kernel according to the needs of the application.

One of the main reasons behind choosing this operating system for our communication subsystem is also the minimalistic and simplistic design approach. This is one of the most lightweight distributions of Linux and is not resource hungry. That makes it an ideal choice for low power computing platforms such as a Raspberry Pi. Moreover, the lightweight applications designed for Arch Linux consumes less CPU resources which provide more resources to the dedicated embedded application. This type of development and operating environment is ideal for our communication subsystem where system portability and limited battery power are two of the most important design constraints. Arch Linux also uses rolling releases to update its operating systems to the latest version and makes system update faster and easier for dedicated embedded applications.

4.3.2. Ground Control Station User Interface

The command line user interface for the ground control station is named orbo_gcs_1.6.exe file and resides in the Raspberry Pi computer. It is a user friendly command line interface and provides a lot of functionality for data transmission, reception, wireless channel characteristics, and commands for capturing and receiving high definition image and video files. Figure A.17 in the appendix section A9 shows the main menu of the command line user interface.

In the sub-sequent sections, detail information about each functions and sub-functions are provided.

4.3.2.1. Function CONNECT()

This is the first item on the main menu of the ground control station user interface. This function creates a wireless bridge between the ground control station and the UAV. In the first stage, the software attaches the line discipline of the Linux code to operate the radio to its ttyUSB0 port. A batch of Request To Send (RTS) and Clear To Send (CTS) is communicated between the ground control station and the UAV module which is always in a listening state.

After the initial RTS/CTS signaling, the UAV module acknowledges the communication status by an acknowledgement packet and communication is established between the two modules. If there is no acknowledgement from the UAV module, or the connection request could not be sent for some reason, the software produces an error message for the user and gets back to the main menu. Figure A.18 in the appendix section A9, shows the RTS/CTS signaling and acknowledgement reception for the CONNECT () function.

4.3.2.2. Function MONITOR_ORBO()

This function is responsible for monitoring the UAV system. Critical flight and sensor data gathered from the UAV are transmitted back to the ground control station in real time. The data are recorded in the storage device on the UAV module and as well as in the storage device in the GCS. This function also employs two batches of RTS/CTS signaling for medium access control (MAC) purposes. The first round of RTS/CTS establishes the connection and prepares the stage for data communication. The second round acknowledges the end of communication. After successful completion of data transfer, the data are displayed to the user and a report is generated consisting of total packets received, total bytes received and total packets discarded. Figure A.20 in appendix section A9, depicts a screen shot of the report generated after each file transfer. The data are also saved in a file which resides in the flash memory of the Raspberry Pi and the file name is provided to the user. A screen shot of the function in process is provided in Fig. A.19 in appendix section A9.

4.3.2.2.1. Data Encapsulation and Packetization

All the data sent from the UAV and the ground control station has similar structure. The packets are 256 bytes in size. There are 6 bytes of header information and 250 bytes of data information in each packet. The header information consists of 2 bytes of packet index which represent the index number of that packet. The next byte of header information is the packet type which represents if that packet is a data packet or a control packet. The next byte consists of last packet header information. This is a Boolean variable and indicates if this is the last packet of the transmission. The last two remaining bytes represent the checksum value of the packet which is employed for data integrity and error checking. The following Fig. 4.10 provides the structure of the data packets as mentioned above.

Frame				
Packet Header				Packet Data
Index 2 Bytes	Type 1 Byte	Last 1 Byte	Checksum 2 Bytes	Data 250 Bytes

Fig. 4.10: Packet format.

4.3.2.2.2. Checksum

There is a checksum algorithm designed and implemented to maintain the data integrity of the system. The algorithm is based on a sum-of-bytes checksum technique. The checksum value is calculated from the sender and provided in the header information of the data packet. The receiver receives the packet, extracts the checksum value from the header information and then counts the checksum value of the received packet. If the checksum values matches, then it is believed that the packets arrived successfully without any alteration to the data. If not, the data packet is discarded and this information is provided to the user. However, retransmission of corrupt data packets by the transmitter is not implemented in our system. In the future iterations, forward error correcting codes will be implemented to detect and correct errors in received data packets without the need for retransmission.

4.3.2.3. Function MONITOR_COMMUNICATION_LINK ()

This function provides the user with important characteristics of the wireless channel in real time to monitor the quality of the communication link. It also employs RTS/CTS signaling for MAC purposes and displays current transmitting frequency, current transmission power, instantaneous received signal strength indicator, receiver distance and current data rate with the help of a polling mechanism. This information too, is saved in file which resides in the flash memory of the system for later analysis. Figure A.21 in appendix section A9, shows a screen shot of the real time communication link monitoring.

4.3.2.4. Function ORBO_LIVE ()

This function is responsible for sending command to the UAV module to capture high definition image and video information by the camera module and transmit it back to the ground control station for aerial monitoring and computer vision purposes. There is also a round of RTS/CTS signaling in this function for media access control. After that, the camera module in the UAV module captures image or video files and stores it in the flash memory of its computing node. It then transmits the binary image/video file to the ground control station. The ground control station receives the binary image/video file and stores it in its flash memory. It then outputs the image/video file to the user.

4.3.2.5. Other Functions

There are some other functions which are designed for the command line user interface for the ground control station. For this research, these are not implemented yet and are suggested as future extensions of the research. The MONITOR_BATTERY_HEALTH () function will be able to monitor the battery health information on both the ground control station and the UAV which is crucial for a successful operation of this long range communication module. The SEND_COMMAND () function will be able to send emergency flight commands to the UAV for emergency landing and other critical maneuvers. The HELP () function provides the user with information about the usage of the command line user interface. The EXIT () function asks confirmation from the user if they really want to quit the ground control station user interface and if so, terminates the program. Figures A.22 and A.23 in appendix section A9, show some screen shots of these functions.

4.3.3. UAV Module Server Software

The UAV module software acts as a server to the communication subsystem. After the initialization of the program, it always stays in a listening mode for connection requests from the ground control station. It uses the RTS/CTS signaling to establish a wireless bridge with the ground control station upon a connection request from the GCS. It then serves different request from the ground control station software such as sending flight data, sending communication link parameters, capturing high definition image and video files and then transmitting them. After completing each request, it goes back to the listening mode for listening to new requests from the ground control station software. Figure A.24 in appendix section A9, depicts the RTS/CTS signaling, acknowledgement reception and report generation of the UAV module.

4.4. Summary

This chapter provides a detailed discussion on the design and implementation of the communication sub-system for the unmanned aerial system employed in this thesis. The hardware components along with the software components are briefly talked about. Moreover, implementation details and some of the technical challenges faced are also elaborated. The next chapter provides detailed information on the design of experiments conducted for this research assignment. In addition, the model scenario for the experiments, assumptions made, choice and justifications of experimental parameters and experiment procedures are discussed.

CHAPTER 5

DESIGN OF EXPERIMENTS

This chapter provides detailed information on the experiments conducted for this research. In the beginning of this chapter, the model scenario of the experiments is talked about. Any assumptions made which are critical and specific to this thesis are also discussed in this section. The hardware used for the set of experiments are also talked about. The detailed design of the ground control station and UAV platforms used to measure the wireless link are also provided. Lastly, the methodology of the experiments is provided at the end of this chapter.

5.1. Model Scenario and Assumptions

In this thesis, the propagating environment is assumed to be an urban scenario. A UAV and a portable ground control station communicating in this scenario. A point-to-point wireless link is used in this communication system. This scenario can be easily realized in surveillance, monitoring applications of unmanned aerial vehicles. Widespread use of micro-UAVs will make it an attractive option for law enforcement agencies to monitor densely packed urban areas. However, scenarios like these bring their own sets of technical challenges with the unknown fading effects due to buildings, cars, roads, and trees. Moreover, the use of a portable ground control station adds up to the challenges with its directional antennas. A very challenging scenario is chosen to measure the worst case results of the performance of the wireless channel. However, we only consider a point-to-point link between the UAV and ground control station, without considering multipoint links or their performances.

In our model scenario, the UAV is equipped with a single omnidirectional antenna. Although usage of directional antennas increases the range of communication, deploying them on-board a UAV is not practical. Complex aerial maneuvers, coupled with the small size and form factor of the UAVs, do not allow easy integration of directional antennas with them. Most micro-UAVs in practical use today employ an omnidirectional antenna. Therefore, in our experiments, the UAV is assumed to be fitted with an omnidirectional antenna. The portable ground station is designed to be fitted with a directional Yagi antenna. The size of the Yagi antenna is kept small because of the portability of the ground control station. Employing a directional antenna with the ground control station increases the range of communication drastically. In addition, a lot of commercially available micro-UAV systems employ ground control stations fitted with directional antennas.

This research ignores the effects of Doppler shift that impacts the wireless channel's performance. The reason for doing so was discussed in detail in the theoretical background chapter. The antennas used in this study are impedance matched to 50 Ω. The negligible impedance mismatch between the antenna terminals are ignored, limiting the scope to propagation channel characteristics and fading variation analysis. Moreover, implementation of electrically steerable phased array antennas, either flush-mounted on aircraft fuselage or integrated with ground control station is not included in this study. Figure 5.1 depicts the propagating environment and model scenario assumed in this research.

Fig. 5.1: Model scenario and propagation environment.

5.2. Spectrum Analyzer

The spectrum analyzer used in the experiments is an Anritsu VNA Master MS2036A portable spectrum analyzer. It is a powerful, handheld device with dual functionality as a 2 port vector network analyzer from 2 MHz to 6 GHz, and a spectrum analyzer for 9 KHz to 7.1 GHz. There is also a power meter integrated which is able to measure the signal power in the above mentioned frequencies [Comp08]. This spectrum analyzer is ideal in measuring different parameters of the spectrum used in microwave communication systems. In addition to spectrum monitoring, this device is also useful in identifying any interference that might affect the wireless channel in our UAV-to-ground control station link.

The biggest advantage of this device in our experiments is its portability. As it is handheld and operated with battery power, field measurements of the ground control station's received signal is able to be obtained with a high level of accuracy. Real world tests are conducted in different parts of the university campus with varying distance between the ground control station and the UAV, which provides meaningful and important data for analysis. The spectrum analyzer component has various built in functions that are crucial in testing the characteristics of the time variant wireless channel between the UAV and the portable ground control station. Field strength of the received signal, bandwidth, power, adjacent channel power ratio and carrier to interference ratio are some of the measurement capabilities that the spectrum analyzer has. The interference analyzer is also heavily used during our experiments to identify and isolate any interfering signals.

Fig. 5.2: Front panel view of Anritsu MS2036A spectrum analyzer.

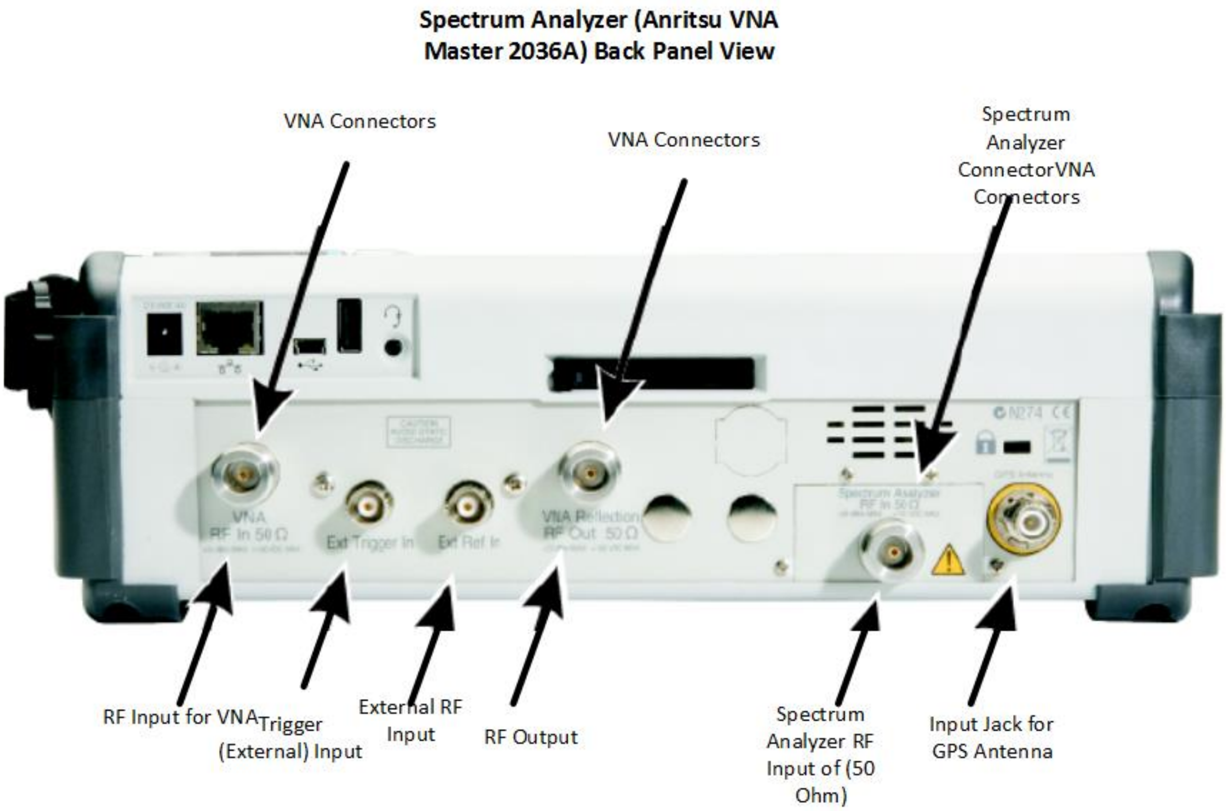

Fig. 5.3: Back panel view of Anritsu MS2036A spectrum analyzer.

Fig. 5.4: Spectrum analyzer integrated with ground control station platform.

In Figs 5.2, 5.3 and 5.4 we can see the front panel view, back panel view and ground control station integration view for the spectrum analyzer. The MS2036A device is operated in the spectrum analyzer mode during the experiments to measure the received signal's amplitude in order to analyze the fading. The device is connected to the ground control station's Yagi antenna with a RF cable which was impedance matched to 50 ohms. This is done via the RF input port situated in the back panel of the spectrum analyzer (Fig. 5.3). The spectrum analyzer is placed in a portable cart by the ground control station platform for ease of measurement during the experiment period. As the radios operate in a frequency hopping mode, the spectrum analyzer focuses on one single frequency to analyze the received signal's amplitude variation. This is achieved by setting the center frequency of the spectrum analyzer to 912.00 MHz and a span of zero. This ensures that the spectrum analyzer is scanning the 912.00 MHz frequency band only. To measure the amplitude of the received signal, the reference level is set to 0.0 dBm to get a good, clear reading of the variation of the signal amplitude. To capture the instantaneous amplitude measurement of the signal, the trace mode of the spectrum analyzer is set to maximum hold. This ensures that the spectrum analyzer captures the best performing received signal transmitted from the UAV node. The input attenuation is set to a default value of 20 dB. This is set to auto mode which ensures that the value of the spectrum analyzer's input attenuator would increase as the reference level is increased to mitigate any discrepancies in data acquisition. The resolution bandwidth is set to 1 MHz with the sweep time of 1 ms. The data for each reading is captured as a JPEG file which captures the screenshot of the spectrum analyzer display and a SPA file which captures the detailed amplitude values in a plain text format. They are saved in an external flash drive connected to the spectrum analyzer and later transferred to a desktop computer for further analysis. Figure 5.5 shows an amplitude read out of the spectrum analyzer during experimentation.

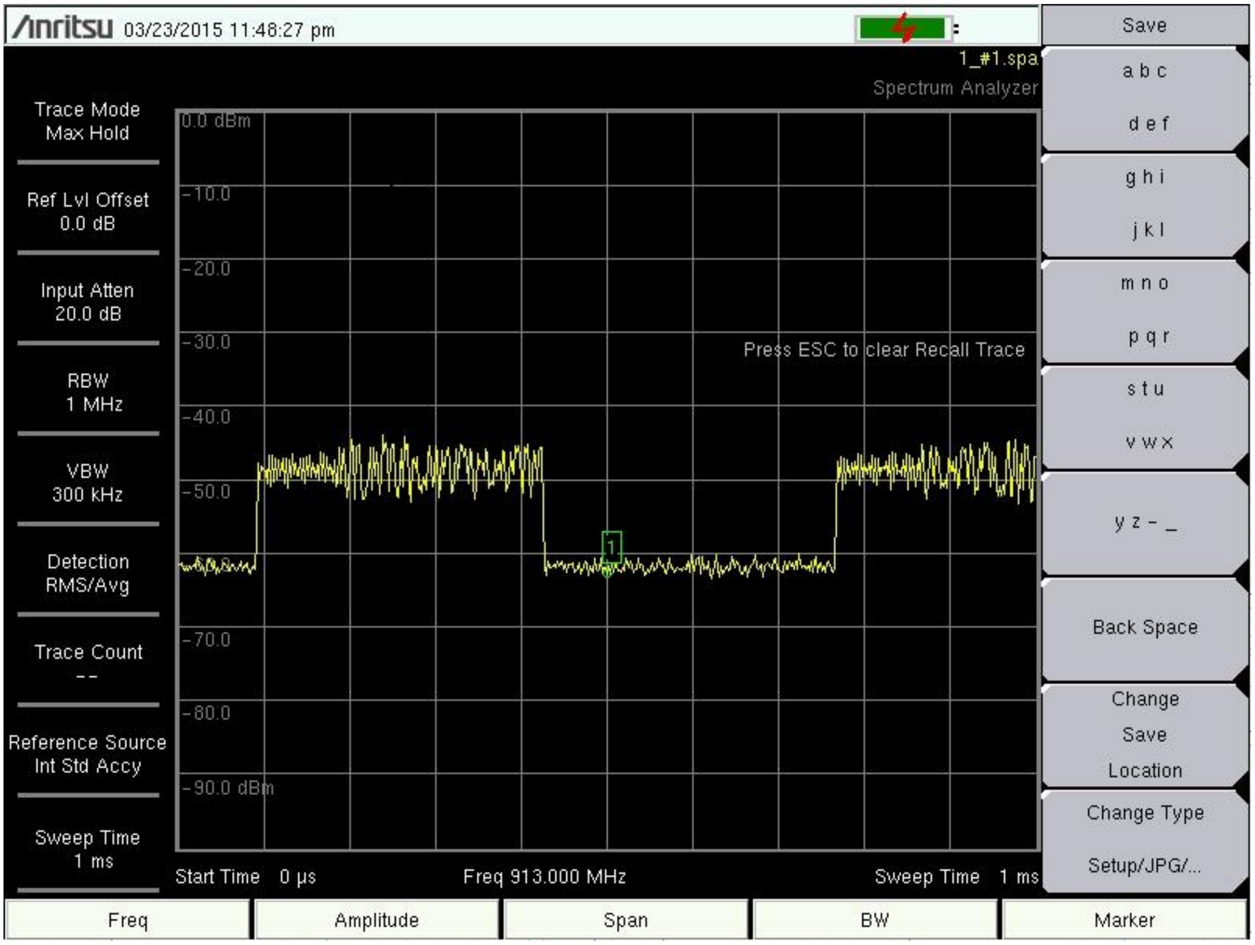

Fig. 5.5: Received signal amplitude data from spectrum analyzer.

5.3. Ground Control Station Platform

The ground control station consists of the radio node, Raspberry Pi microcontroller system, a display module, battery power supply, a physical user interface, a command line interface for operation, a directional Yagi antenna and a mechanical platform for tracking and housing the antenna. All of these components are discussed in detail in the previous chapter. The next section describes the mechanical platform that is designed and implemented to track the

UAV node during flight and to vary the directional antenna's directive gain and polarization to measure the fading.

Fig. 5.6: Ground control station structure.

In Fig. 5.6, we can see the complete structure of the portable ground control station designed and implemented for this research. The first structure (1) is a commercially available portable antenna tripod. This tripod provides a strong base support for the antenna in different terrains and can withstand a variety of antenna weight and structures. The second part (2) is a secondary base for the antenna which provides additional support for the antenna, flexibility to adjust the height of antenna and connects to the third sub-structure of the platform. It is constructed from polyvinyl chloride (PVC) material of schedule 40. The third substructure (3) is also constructed from PVC material and provides a 360° degree field of view in azimuth direction. The fourth sub-structure (4) provides a 90° degree of view for the elevation angle. These two sub-structures are crucial for manual tracking of a UAV in flight and providing variation in the azimuth, elevation and polarization mismatch factor for the communication system measurements. The fourth sub-structure is attached to the directional Yagi antenna which receives the signal to be measured. The antenna is positioned at a height of 3.5 feet from the ground during the measurement period.

5.4. UAV Node Platform

The UAV node platform consists of a radio module for transmitting and receiving data, a Raspberry Pi microcontroller as the heart of the system, an omnidirectional antenna for wireless transmission, and a mechanical platform to emulate a UAV in flight. The main components of the UAV node platform, along with the block diagram of entire system are provided earlier in the previous chapter. The sub-sequent sections provide a detailed description of the mechanical structure of the UAV node along with the justification of its usage.

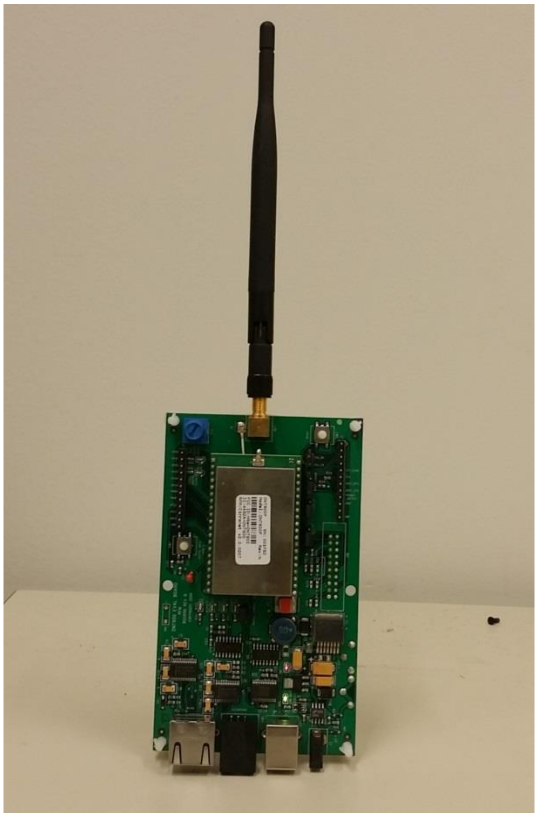

Fig. 5.7: The UAV transmitter node with omnidirectional antenna.

In Fig. 5.7, the UAV transmitter node with the omnidirectional antenna during the experiments is depicted. The radio, microcontroller and the battery are housed in a small box made out of heat shielding material. The box provides protection from physical damage as well as shielding from excessive cold and rain. The omnidirectional antenna is connected to the radio node and protrudes outwards from the box through a small incision. The box containing the node is attached to a mechanical platform and placed on the roof of the engineering building of University of Manitoba, Fort Garry campus. Figure 5.8 shows the mechanical structure seen from a room which is situated at the roof of the building.

Fig. 5.8: The UAV node structure seen from the UMARS (rooftop) room.

The reasons for simulating the UAV node through a mechanical structure are two-fold. Firstly, we did not have access to an unmanned aerial vehicle to have a real flight test to measure the variation of signal amplitude in-flight. Secondly, and more importantly, a real flight test with a UAV over a densely populated campus area requires advanced expertise in flying UAVs with some risk factor which we wanted to avoid. Moreover, recent regulation changes made by Transport Canada restrict flying of UAVs over populated and public places without proper authorization which adds further complications to the matter. Therefore, after careful consideration, the UAV node is simulated by placing the mechanical platform on the roof of the engineering building with an altitude of 50 feet from the ground.

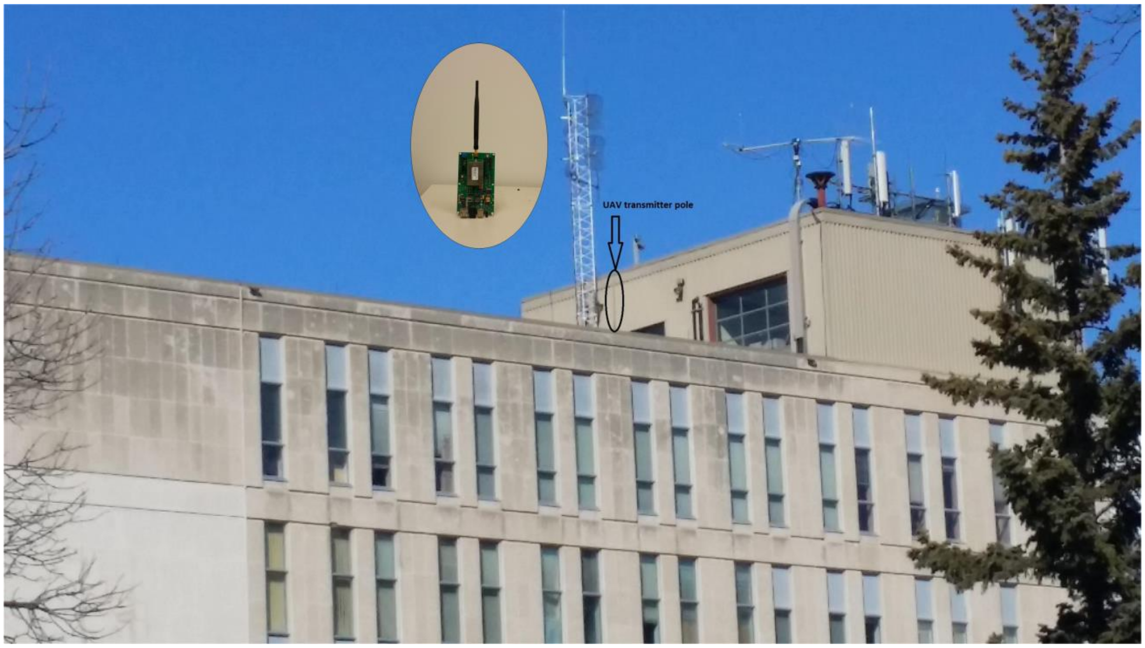

Fig. 5.9: The position of UAV transmitter node on engineering building rooftop (the UAV transmitter node attached to the transmitter pole can be seen in inset).

However, this simulation of a UAV node in flight has some added advantages for our experiments. The position of the UAV node on the roof is carefully chosen so that there will be sufficient number of buildings/rooftop edges in the propagation path of the signal to the ground control station. From Fig. 5.9 we can see that edges of rooftops are in the way of the transmission path. This creates a real world urban scenario where the radio wave's propagation path might be obstructed by buildings, billboards and other urban structures. This would definitely increase the multipath fading of the signal, which cannot be realized if we employ a clear line of sight from the ground station to the UAV. This ensures that the experiments conducted in this configuration provide a real world urban propagation environment with maximum multipath fading. Moreover, by careful selection of the ground control station's positions, the effects of signal scattering due to building edges constructed from different materials can be analyzed closely.

From Fig. 5.9, we can see that the rooftop of the engineering building houses multiple antennas for different communication systems. There are antennas that provide connectivity to mobile phones on campus along with a satellite tracking antenna that receives data from satellites. There are significant amount of interference from all these communication devices situated in the vicinity of our UAV node. This also provides a real world urban scenario as these high powered base station antennas are almost everywhere in most modern cities. Any simulation of a real world urban wireless communication system would be incomplete without considering the interference from these systems. One of the major goals of this research is to identify and analyze the effects of these interfering signals in a point-to-point link between a UAV and a ground control station. Therefore, this configuration provides the perfect setting for this analysis. Identification and isolation of these interfering signals are achieved by first scanning the spectrum with the spectrum analyzer to measure the level of interference being present in our communication channel.

The placement of the UAV node platform is beneficial for the variation of propagation distance between the ground control station and UAV. The engineering building is one of the tallest structures in the campus. Careful observation of the map of the campus reveals the fact that a clear line of sight can be achieved from different parts of the campus to its rooftop. This is of importance in our experiments as it allows the measurement of received signal amplitude from a wide range of distance. A maximum propagation distance of 800 meters is achieved during the experiments.

The UAV node simulation through the mechanical structure provides an added benefit of creating a controlled environment for the experiments. The complex flight maneuvers of a quadcopter employ constant shifting of its orientation to achieve stability. In order to test a reconnaissance UAV sending surveillance data to a nearby ground control station using an actual UAV in-flight, would suffer from these constant change of orientation from the UAV antenna. This would have an impact on the performance of the wireless channel and it would be very complicated to compensate for these shifts. In a real world test site, this would be almost impossible without the employment of high precision electronic sensor equipment. The mechanical platform thus provides a more controlled environment as the structure is fairly stable which made the transmission possible from a stable platform without any shift in its orientation. This ensures the data we collected during the experiments are fairly accurate. However, minor changes in the position of the structure occurred during measurement due to wind, but was kept at a negligible value by fixing the structure to the wall with structures made from Styrofoam material. The usage of Styrofoam materials ensures that these structures do not impact the wireless radio waves during transmission or reception. Moreover, placing the mechanical structure on the rooftop through the window of the room ensures easy access to the test equipment in all weather conditions.

5.5. Experiment Procedure

In the sections above, detailed information about the hardware components used in the experiments is provided. In addition, the model scenario and critical assumptions made are talked about. In this section, the detailed methodology of the experiments is provided. This section is critical in the conceptualization of the experiment procedures and correct evaluation of the measurement data obtained. The step by step explanation of the experiment procedure is given below.

(i) The transmitter node (UAV node) is positioned on the rooftop of the engineering building through a mechanical platform that simulates a UAV in flight. A custom program written in C++ programing language is preinstalled in the Raspberry Pi microcontroller's operating system (Arch Linux ARM). This program's function is to transmit a UDP packet of 256 bytes every 1ms through the transmitting radio node. The transmission power of the radios is pre-configured at 1W. The data rate is set to a maximum of 500kb/s. The radio is connected to the microcontroller system through the serial interface. The baudrate of this serial connection is set to 9.6kb/s. No parity is configured for this serial channel. There is 1 stop bit that signals the end of packet. The transmitter node is being operated as the base radio mode while the ground control station radio is being operated in the remote mode. The hop duration is set to 0.05ms/count which is a 12-bit value. This sets the duration of the hop frame. An AES (Advanced Encryption Service) based security key is also configured to provide additional security in data transmission. The transmitter node is configured to send heartbit messages to the remote radio at a certain time interval. These heartbit status messages contain the node's base node network ID, routing address (if routing is enabled) and other parameters that measure the performance of the wireless channel. The heartbit status message interval is set to 20 seconds in our experiments. The frequency band of the radio is set to a hopping pattern between 902 MHz and 928 MHz with up to 50 frequency channels. The transmitting radio is also configured to provide the following parameters in a status report after each successful transmission. These parameters are critical in analyzing the status of the channel and success rate of packet transmission.

- MAC address of transmitter and receiver node
- Current frequency band
- Current range delay
- RSSI last
- Current RF data rate
- Current transmission power
- Link status
- Average packet success rate

The DNT900 radios have built in protocol mode operation support. However, to reduce additional complexities, the protocol mode is disabled and the radios operate in the transparent mode. The operating mode for both the radios is selected as point-to-point. With these above mentioned configurations, the UAV node transmits data packets to the ground control station node every 1ms.

(ii) The portable ground control station is positioned at different places on campus with the distance between the UAV and ground control station varying from 100m to 800m. The positions of the ground control station along with the position of the transmitting node are shown in Fig. 5.10.

Fig. 5.10: Positions of ground control stations and UAV node on campus.

For each of these positions, the directional Yagi antenna is manually aimed towards the UAV node through the mechanical tracking platform. The received signal amplitude is captured by the spectrum analyzer and the measurement data are saved.

(iii) For each position, the azimuth angle of the directional antenna is varied by 15 degrees in both direction and the received signal's amplitude is recorded by the spectrum analyzer. Figure 5.11 shows the variation in the azimuth angle for the directional Yagi antenna.

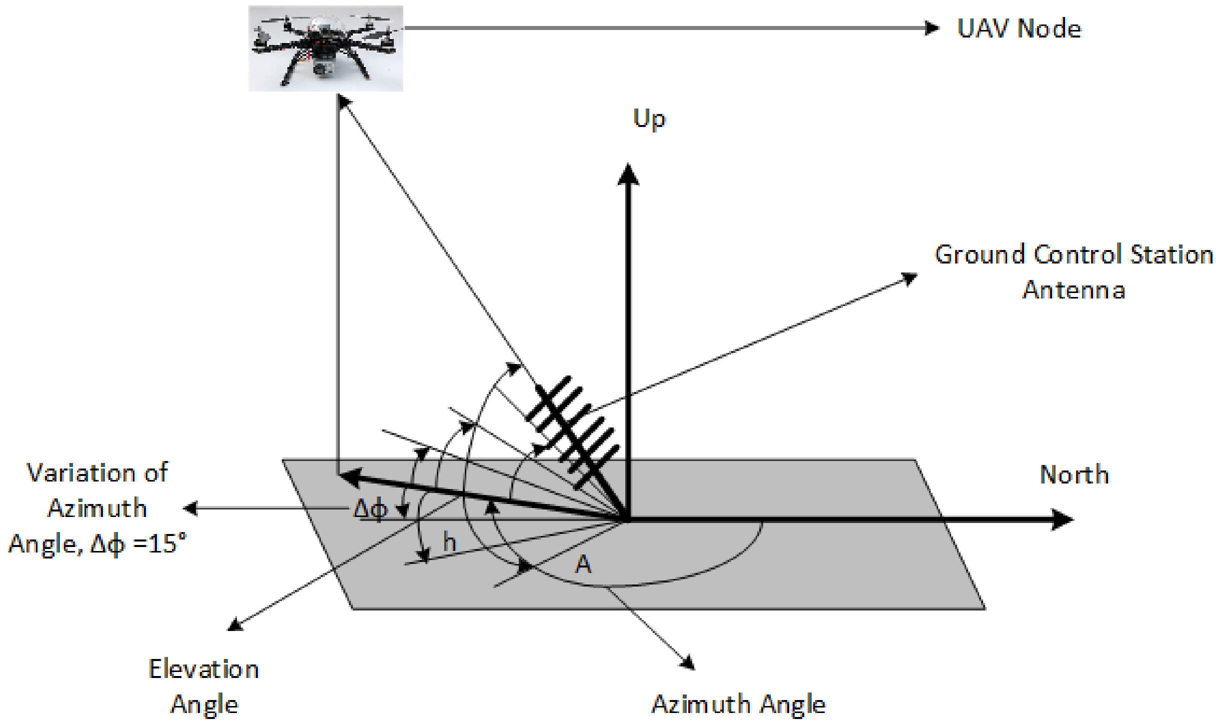

Fig. 5.11: Azimuth angle variation of the ground control station antenna.

(iv) For each azimuth angle deviation, the elevation angle of the antenna is varied by 15 degrees in both direction and the amplitude is recorded. Figure 5.12 shows the elevation angle variation.

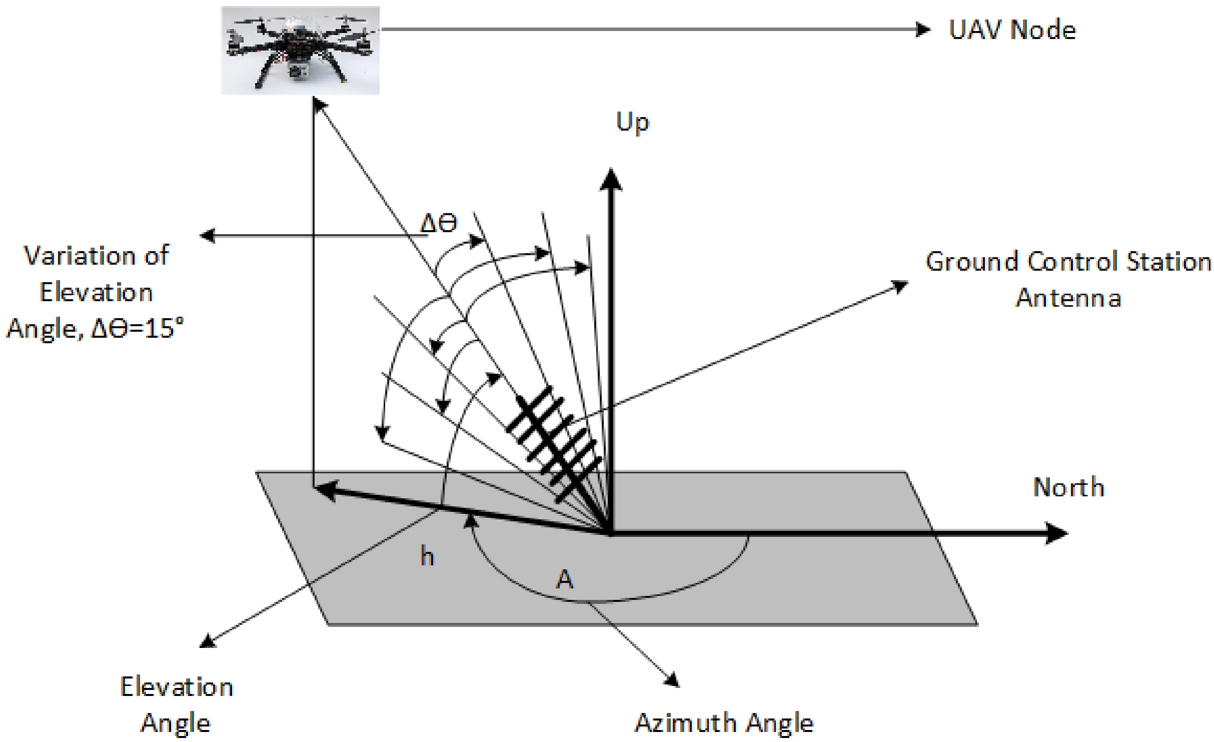

Fig. 5.12: Elevation angle variation of the ground control station antenna.

In these experiments, the variation of the elevation and azimuth angle is done by 15 degree steps in both directions from the direction of reception. The angles are varied from 0° to 45° degrees in both directions. The reasons for taking the variation in 15 degrees steps are related to the antenna aperture, gain, directivity, radiation pattern and beamwidth of the antenna. An antenna aperture provides a measurement on the effectiveness of an antenna in receiving the radio wave's power that is incident on it. It is the area that is responsible for the interception of the power of the receiving radio signal, converting it to electrical power and sending to the load connected to its out terminals [Wiki09]. The antenna aperture can be given by

$$A_{eff} = \frac{P_0}{PFD} \tag{5.1}$$

where P_0 is the power transferred to the load of the antenna during signal reception, and PFD is the power flux density of the incoming radio waves.

The ability to receive power from an incoming radio wave by antenna is directly proportional to its antenna aperture. The higher the aperture, the higher the power reception is. However, the incoming radio signal's direction relative to the receiving antenna's orientation directly impacts the antenna aperture as it can be stated as a function of these two parameters. This is due to the fact that the gain of a directional antenna depends on its radiation pattern. The directivity parameter of a directional antenna is responsible for the variation of this gain in different azimuth and elevation angles. Moreover, the beamwidth and major lobe of an antenna dictates the area that will receive the highest power of the incident radio wave. From [Wiki09], it can be seen that an isotropic antenna's aperture can be given by

$$A_{eff} = \frac{\lambda^2}{4\pi} \tag{5.2}$$

where, λ is the wavelength of the radio wave. From a change of variable and the definition of antenna gain we can show that gain

$$G = \frac{4\pi A_{eff}}{\lambda^2} \tag{5.3}$$

This shows that the antenna aperture is proportional to the antenna's gain. In our ground control station, we employ a high gain Yagi antenna of 12.1 dBi. So, the aperture of this antenna is also high. This high aperture produces small angular beamwidths of the antenna. This can be seen from its radiation patterns (Fig. 3.11

and Fig. 3.12). These highly directional antennas direct their radio waves in a narrow beam in one direction. From reciprocity, they also receive the majority of power from the incident waves in this narrow direction. So, the gain and aperture of a directional antenna is mostly dependent on the direction of the main lobe.

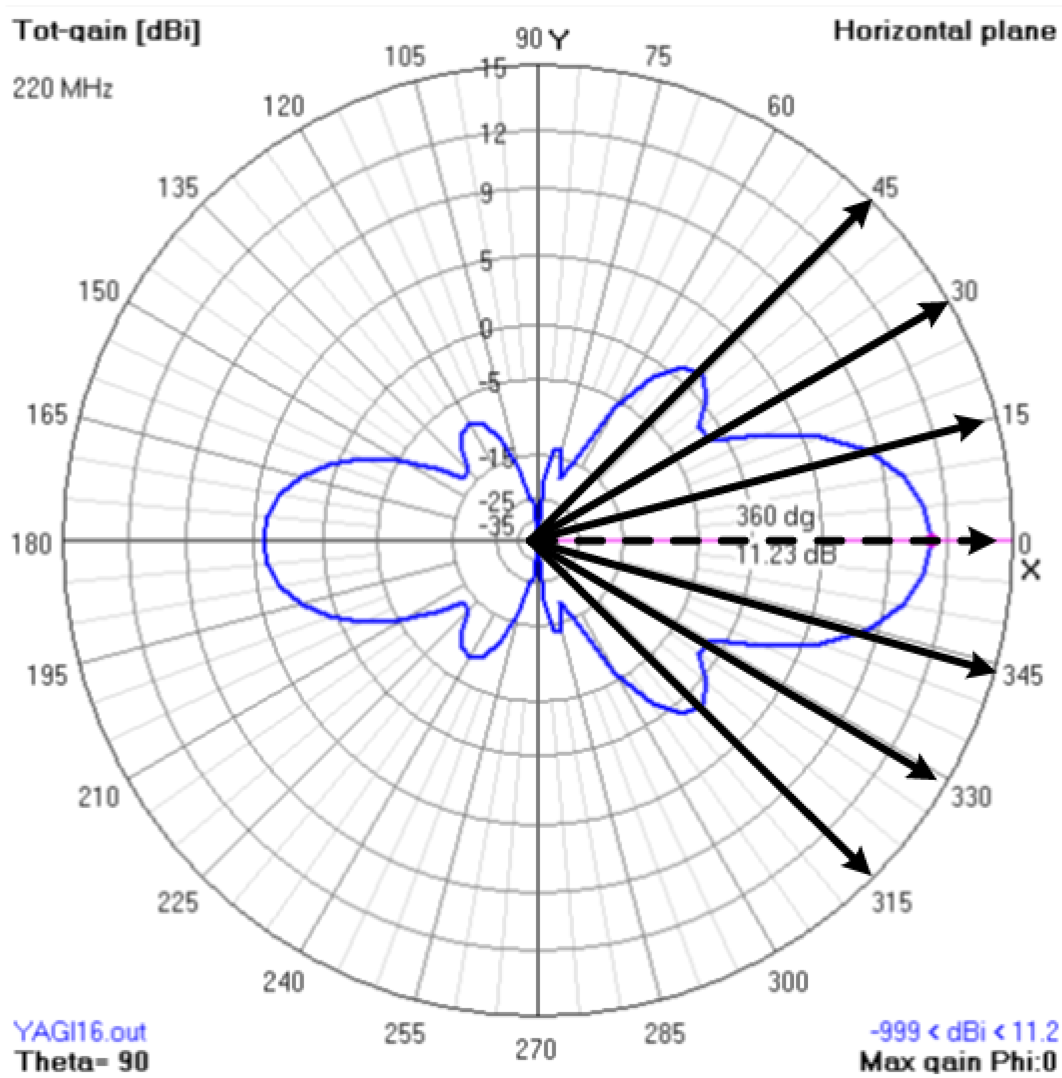

Fig. 5.13: Azimuth angle variation of Yagi antenna and its radiation pattern on horizontal plane.

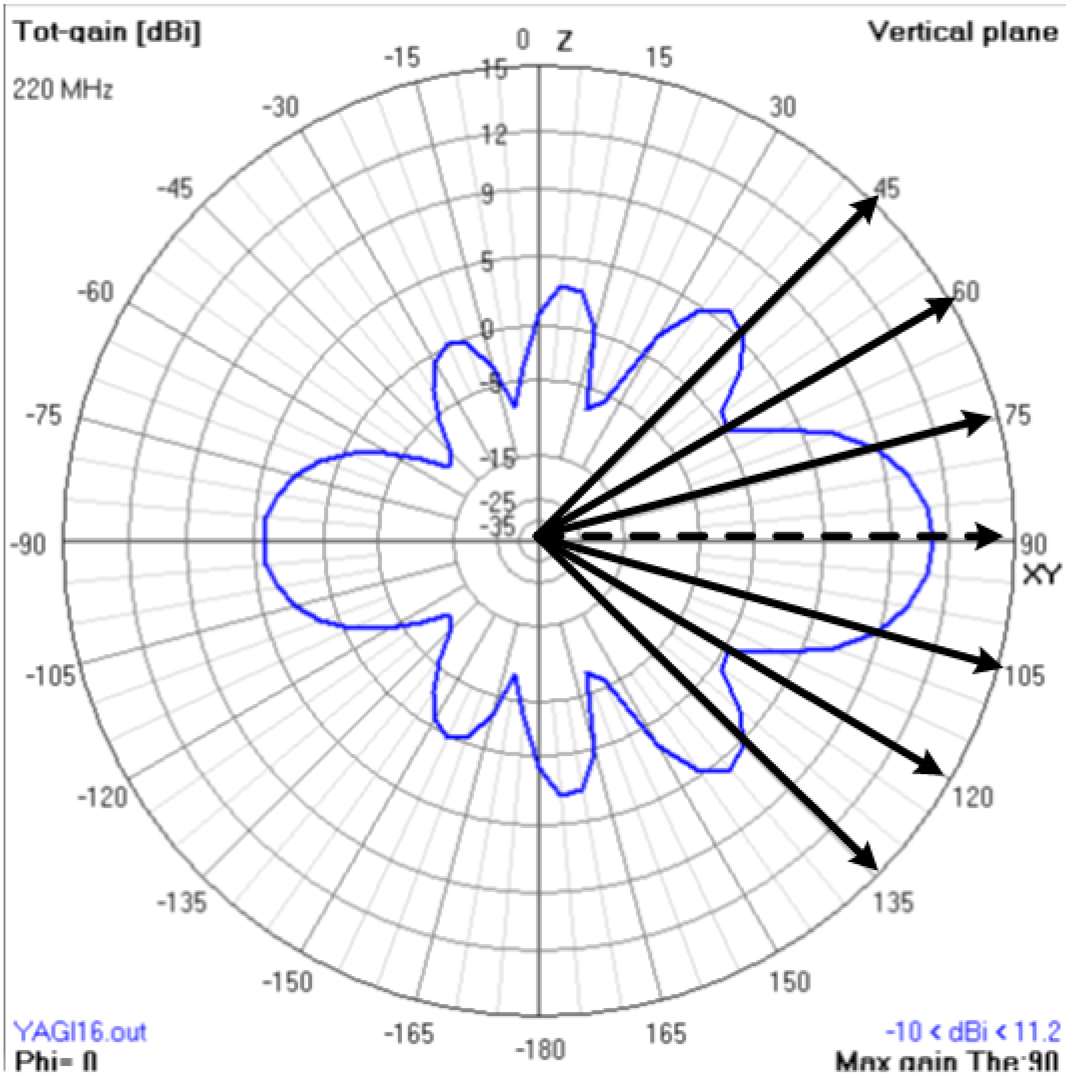

Fig. 5.14: Elevation angle variation of Yagi antenna and its radiation pattern in vertical plane.

From Figs 5.13 and 5.14, we can see that a total variation of 45° degrees from the highest direction of radiation covers the major lobe of the directional Yagi antenna. The direction below that angle only covers the side lobes of the antenna. As stated above, for the high directional Yagi antennas, the majority of the received signal is concentrated to the major lobe of the antenna. Therefore, it is safe to assume that the coverage of the major lobe is sufficient to analyze the received signal's amplitude variation.

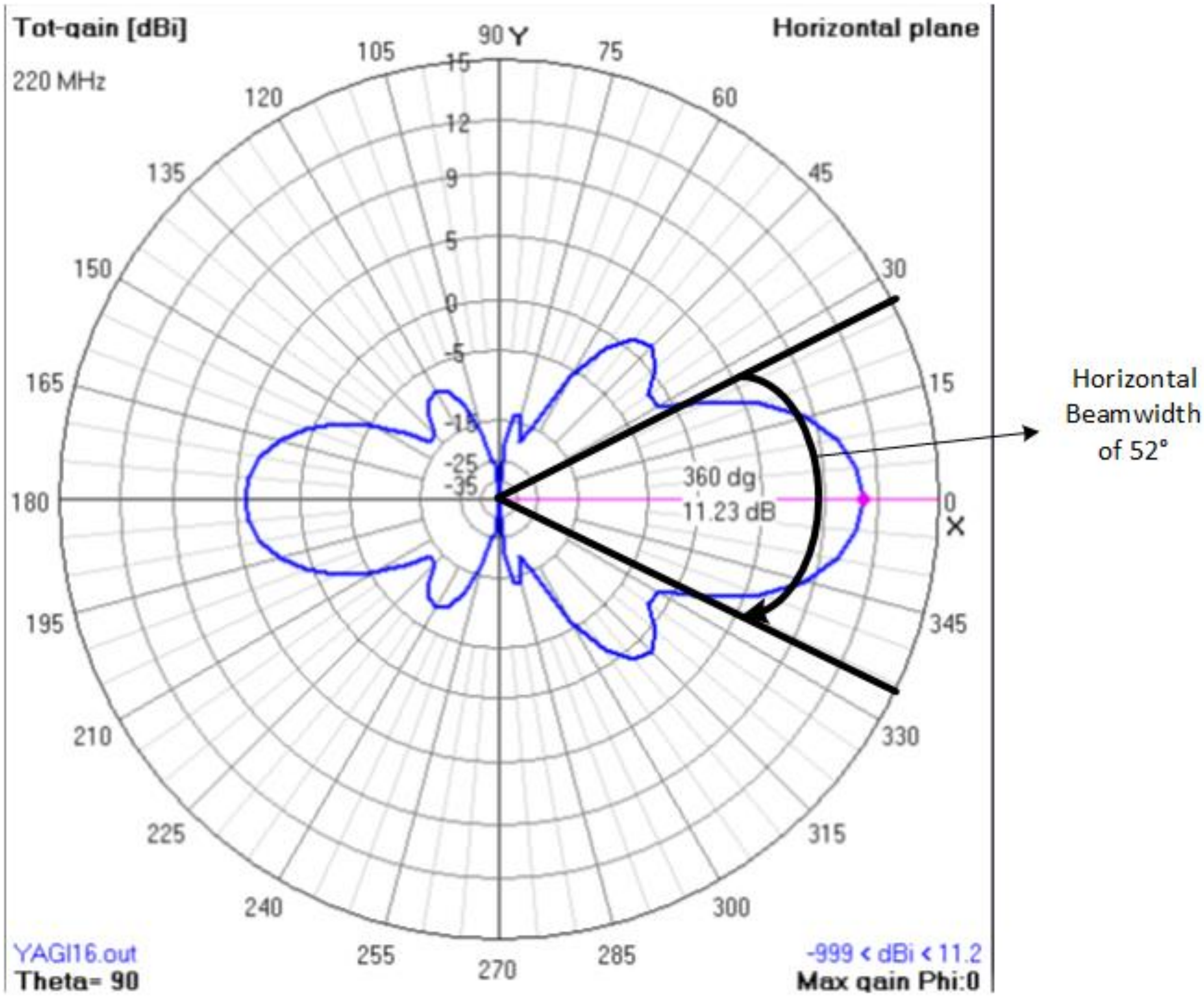

Fig. 5.15: Horizontal beamwidth of the Yagi antenna.

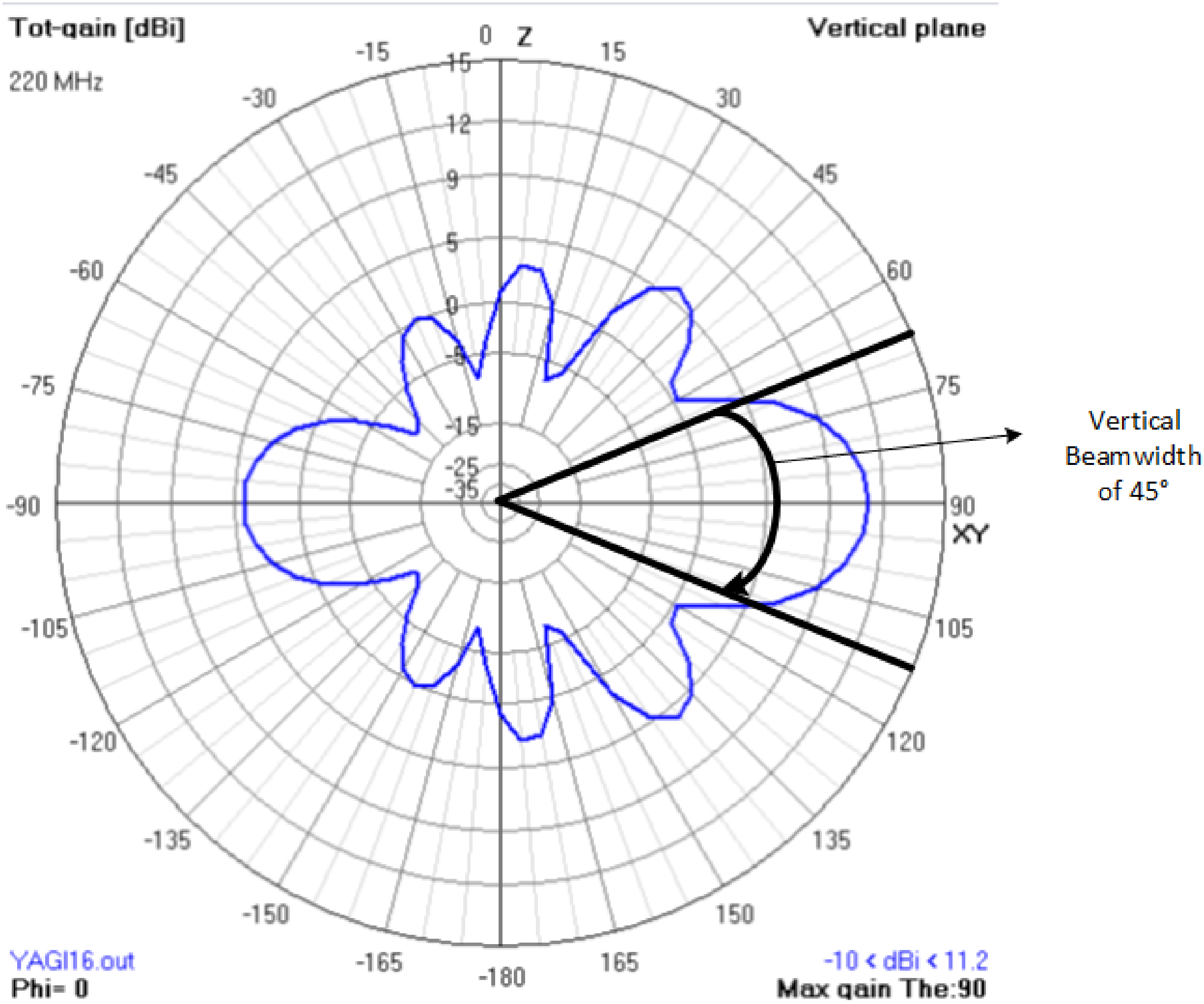

Fig. 5.16: Vertical beamwidth of the Yagi antenna.

In addition, Figs 5.15 and 5.16 provide the angular beamwidth for this Yagi antenna in the azimuth and elevation plane. Similarly, we can see that our variation of 45° degrees covers the angular beamwidth in both planes. Anything below this angle experiences a major drop in the received signal amplitude and by the nature of directional antenna operation, should not be occurring. This is due to the fact that the UAV node will be tracked by the ground control station antenna by some sort of tracking mechanism. Moreover, achieving a higher resolution in the variation of azimuth and elevation (steps less than 15°) has its practical limitations. Achieving this kind of high resolution in a real world experiment environment is complicated and requires the use of high precision sensor equipment. This adds additional complexities to the experiments and measurement data. For these reasons, $15°$ degree steps are a preferable design choice that is obtained. However, future extensions of this research will demand a higher resolution in the variation of azimuth and elevation angles of the directional antenna.

(v) For each azimuth-elevation angle pair, the orientation of the Yagi antenna is varied from vertical to horizontal with the increments of $0°, 23°, 45°, 68°\ and\ 80°$. Figure 5.17 shows the variation in antenna orientation.

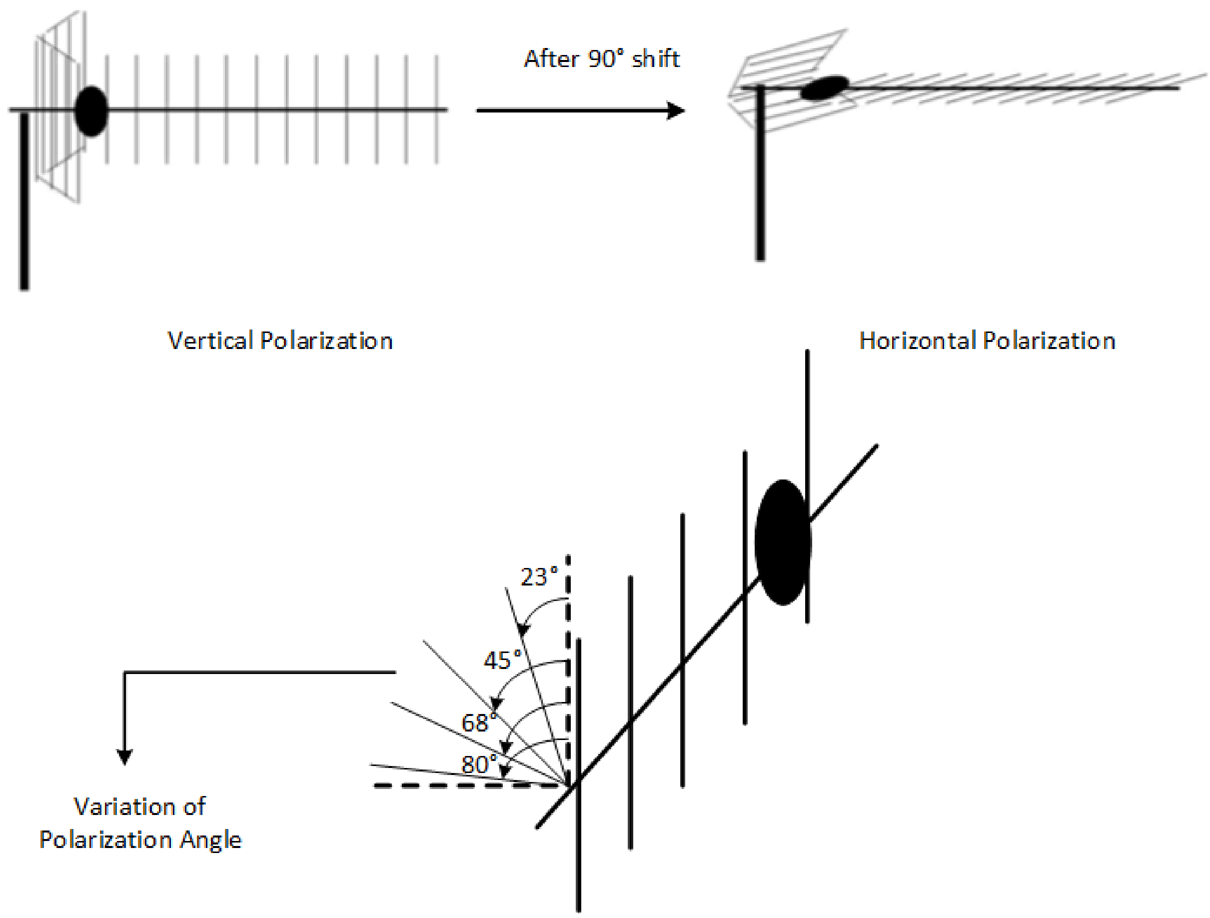

Fig. 5.17: Variation in polarization (vertical to horizontal) of the Yagi antenna.

(vi) Steps (iii), (iv) and (v) are repeated for each position of the ground control station and the amplitude data are collected.

(vii) 5 sets of data are collected over the course of 5 different days using the above mentioned procedure. One of the preliminary objectives of this research is to test if the wireless channel between a UAV and a ground control station is affected by the humidity of the environment. Moreover, ice formation in the melting layer region of the ionosphere is known to cause further attenuation of radio waves as stated in the literature review chapter. Therefore, the data link between a high altitude UAV and a ground control station would be an interesting area of study to measure its impact. This is the reason behind recording measurements in five different days. However, the humidity did not vary that much during the course of experiments to test its correlation with the performance of the channel. Moreover, a high altitude UAV was not available to us to conduct the experiments. This can also be a possible extension of this research assignment in the future.

5.6. Summary

In this chapter, a description of the test apparatus and the experiment procedure are provided. The next chapter provides a detailed discussion on the results of these experiments conducted. Moreover, some of the key research questions are answered along with a discussion on some critical observations made during the analysis of the experiment data.

CHAPTER 6

RESULTS & DISCUSSIONS

The previous chapter provided the details of the hardware used in the experiments, procedure of experiments conducted and their technical details. This chapter provides an in-depth discussion on the results and analysis of these experiments. The correlation of link quality with propagation distance between a ground control station and a UAV is investigated. For this point-to-point link, the large scale fading is analyzed and compared with existing channel models. The small scale fading or, multipath fading is also analyzed for this link and compared. In addition, the large scale fading is modeled with a piecewise linear model and the small scale fading is modeled with Nakagami model. The shape parameter of the Nakagami fading model is analyzed for a Yagi-to-omnidirectional and omnidirectional-to-omnidirectional link. The relationship of the shape parameter m is investigated with different impacting factors to the wireless link. Individual linear regression models are developed and examined based on the correlation of shape parameter with these factors. A multiple regression model is developed that fully characterizes the overall effects of these factors on the shape parameter of the Nakagami fading model. This regression model is supported by various statistical analyses. Moreover, based on this multiple regression model, a particle swarm optimization based algorithm is developed and tested that is able to predict the underlying parameters of the fading model for a proper estimation of the wireless link.

This chapter is a critical element of this thesis as it provides the reader with an analysis of the experimental data that supports the theoretical models developed for point-to-point wireless communication between a UAV and a ground control station. Detailed discussion on the experimental procedure and results play an important role in establishing the connection between the theoretical assumptions and practical implementations. Moreover, attempts have been made to answer some of the key research questions posed in this research.

6.1. Correlation of Radio Link Quality with Distance

The main goal of this experiment is to investigate the relationship of the point-to-point link's quality, with the propagation distance between the ground control station and the UAV. In a densely populated area, the distance between a low altitude UAV and a portable ground control station plays an important role in the performance of the wireless communication. This section investigates the role of the propagation distance in affecting the performance of this link employing both directional and omnidirectional antennas.

During this experiment, the UAV is positioned on the roof of the engineering building of University of Manitoba to simulate a UAV in flight. The ground control station's position relative to the UAV node is varied from 0-800 meters by setting them up in different places on campus. The positions of the ground control station are carefully chosen in a way that includes both a clear line-of-sight and an obstructed line-of-sight between the UAV node antenna and the ground control station's antenna. The positions of the UAV node and the ground control station node in different places on campus can be seen in Fig. 5.10. With each position, data are transmitted from the UAV node to the ground control station node and the received signal's amplitude is recorded with a spectrum analyzer. The signal amplitude is measured in dBm. Five sets of data are collected in a course of 5 different days.

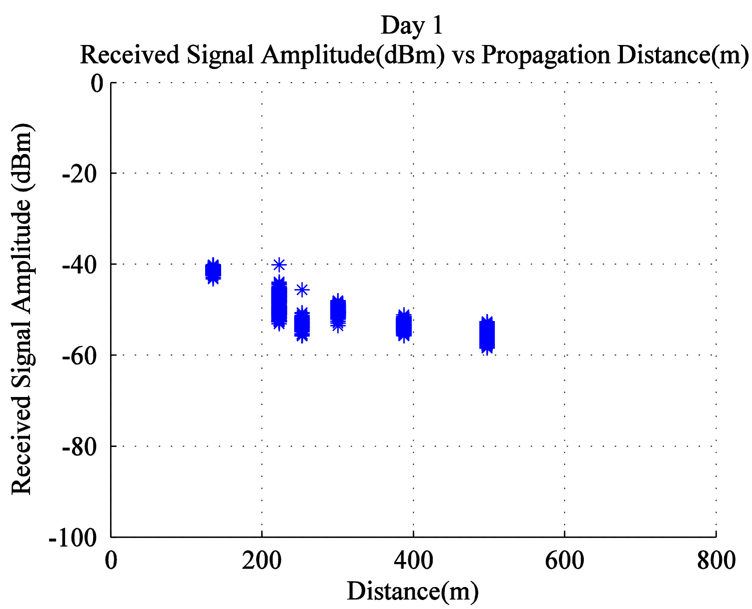

Fig. 6.1: Received signal amplitude against propagation distance for day 1 measurements.

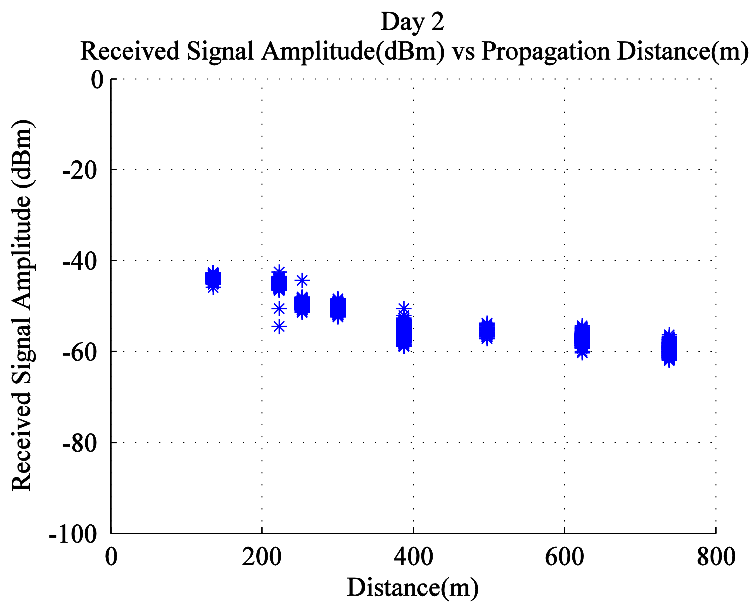

Fig. 6.2: Received signal amplitude against propagation distance for day 2 measurements.

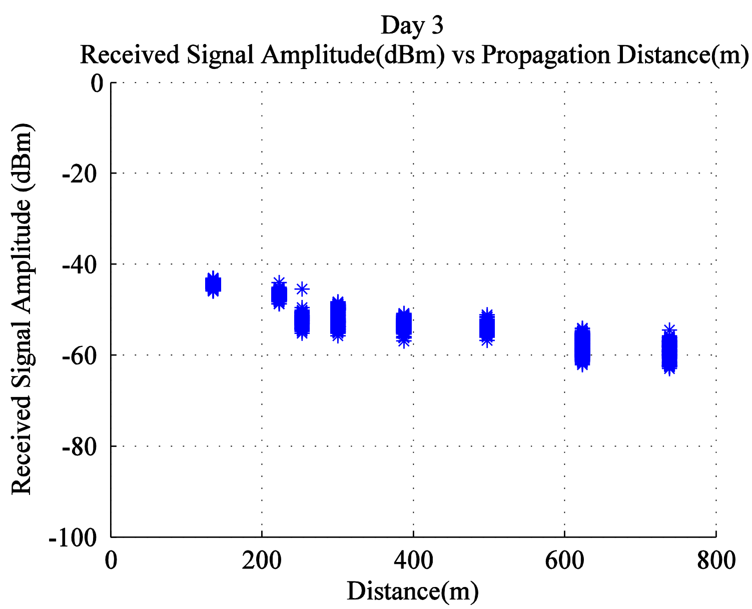

Fig. 6.3: Received signal amplitude against propagation distance for day 3 measurements.

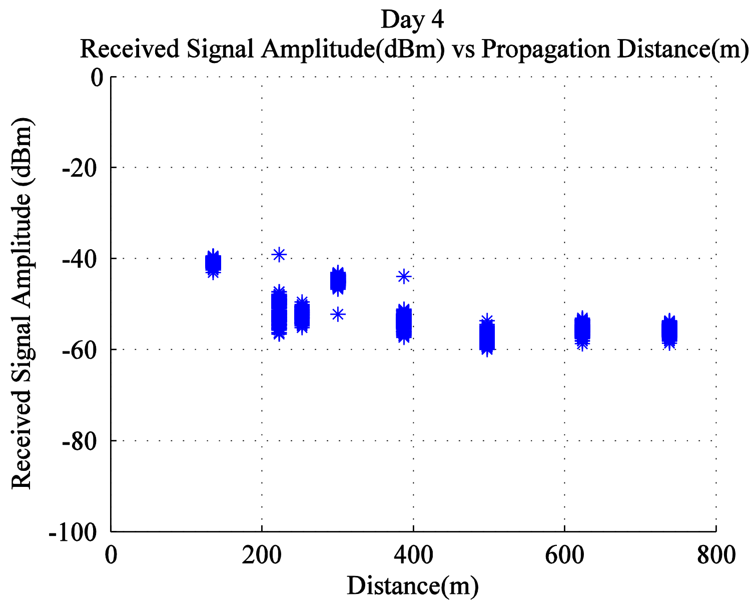

Fig. 6.4: Received signal amplitude against propagation distance for day 4 measurements.

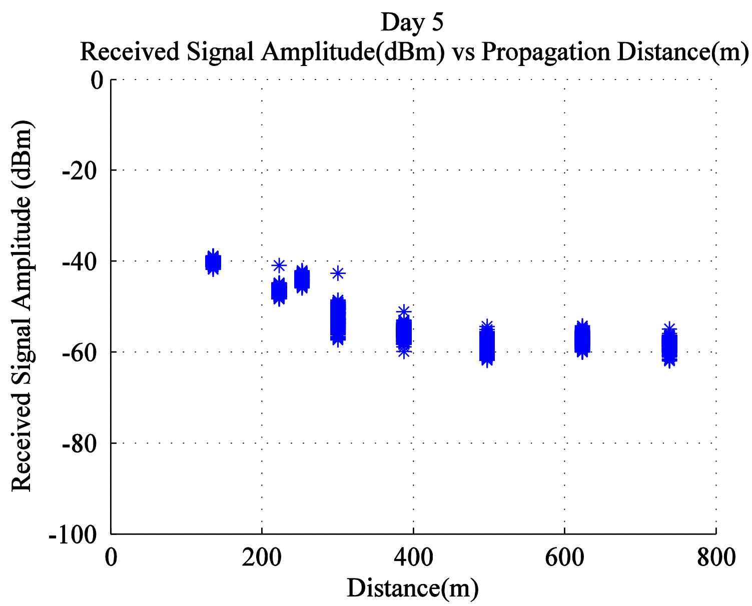

Fig. 6.5: Received signal amplitude against propagation distance for day 5 measurements.

Figures 6.1 to 6.5 show the received signal amplitude against the distance between the ground control station and the UAV measured in five days. For day 1, the received signal amplitude is measured against a propagation distance varying from 0-500 meters. Day 2 to day 5 measurements consists of signal measurement against a propagation distance varying from 0-800 meters. From these figures, we can see that the signal amplitude in the ground control station decreases as the propagation distance increases. This phenomenon has been explained in the theoretical background chapter which states that the electromagnetic signal will suffer from attenuation as the signal propagates along the wireless channel. However, careful observation of Figs 6.1-6.5 shows that this attenuation of signal is not linear as some of the path loss model suggest, for a densely populated propagation environment employing a directional antenna on the receiver end and an omnidirectional antenna on the transmitting end. The path loss of this wireless signal follows the piecewise linear model for propagation. Although it can be seen that the signal's amplitude gradually decreases, propagation distance of 253 meters shows higher degradation of signal amplitude than the trend. This is due to the fact that the ground control station's position in that distance is in such a way that it's antenna has a partially obstructed line-of-sight with the UAV node's antenna. This obstructed propagation path consists of multiple edges of rooftops which contributes to the scattering of the signal more than the other paths. This sudden drop of signal amplitude proves that the wireless link suffers significant attenuation due to scattering from building edges in an urban propagation environment. The height difference between the ground control station antenna and the UAV antenna also plays an important role in this signal attenuation. However, this requires further research for a proper investigation of its effects on the signal attenuation of this channel.

Another interesting observation that can be made from these plots is the dual slope linearity of the received signal's amplitude. We can see that the received signal amplitude resembles the dual slope piecewise linear channel model with N=2 segments. There is one breakpoint (N-1) which is determined through regression analysis. From the figures we can see that from propagation distances 0-253 meters, the power falls off with a certain path loss exponent. After 253 meters, the power falls off with a different path loss exponent. These two path loss exponents can be calculated from the slopes of the piecewise linear segments and are discussed in the later sections of this chapter.

These results strongly suggest that the wireless signal's amplitude does not follow a straight line in attenuation for a wireless link that employs partially obstructed line-of-sight communication between transmitting and receiving antennas. Moreover, the performance of a wireless link employing directional and omnidirectional antennas is strongly related to the propagating distance. However, this relation has strong dependencies to the propagation environment as the signal propagation is highly effected by scattering and multipath propagation due to building edges, cars, roads and other obstructions.

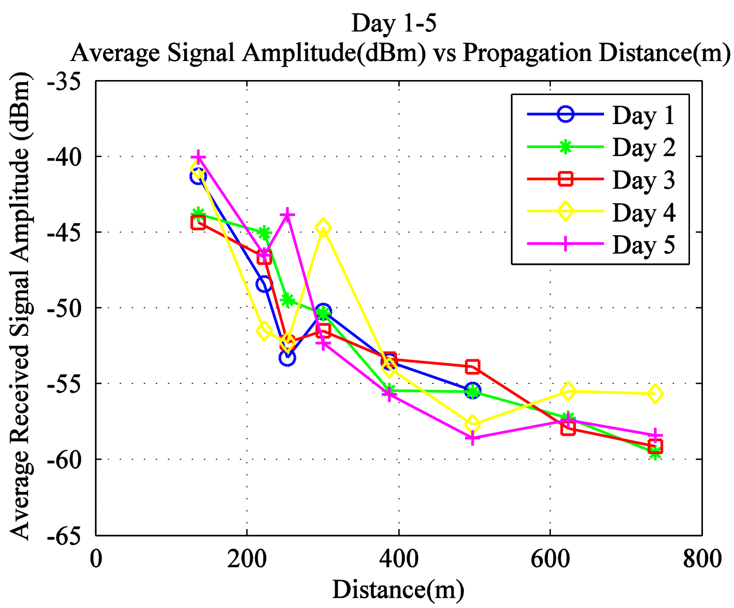

Fig. 6.6: Average of received signal amplitude against propagation distance for 5 measurements.

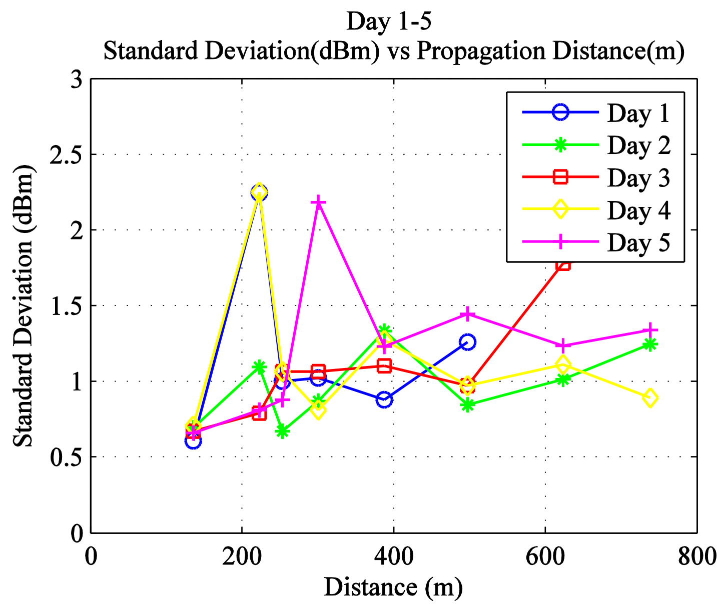

Fig. 6.7: Standard deviations of received signal amplitude against propagation distance for 5 measurements.

Figure 6.6 shows the average of the received signal amplitude against the propagation distance between the ground control station and the UAV. It can be seen that the average value of the amplitude gradually decreases as the distance increases. The drop on the average amplitude value for a distance of 253 meters reaffirms the fact that partial obstruction of the propagation path has a significant effect on the signal attenuation. However, from the dataset of day 4 and 5 (showed in yellow and magenta), we can see a sharp increase in the signal amplitude's average value. This confirms that when the propagation path is partially obstructed by building edges, the amplitude of the signal behaves in an unpredictable way due to the scattering and multipath propagation. As stated in the literature review section, the multipath components resulting from scattering, reflection or refraction, can add constructively or destructively on the receiving antenna which causes the amplitude variation. This fact can be clearly seen in this plot as the same position of the ground control station antenna will receive a different level of signal amplitude. Moreover, from a propagation distance of 0-253 meters, the amplitude variation is significantly higher than from distances 301-800 meters, which shows a gradual decrease in the average signal amplitude. This is due to the fact that the positions of the ground control station had a less obstructed line-of-sight for distances 301-800 meters than the former. This strongly suggests that the variation of signal amplitude significantly depends on the nature of line-of-sight propagation path between a ground control station and a UAV.

Figure 6.7 shows the standard deviation of received signal amplitude against the propagation distance between the ground control station and the UAV. It can be seen that the standard deviation gradually increases as the propagation distance increases. This shows a higher variation in the signal amplitude with higher propagation distance. As the distance between the transmitter and receiver increases, the wireless signal has to cover a larger distance to reach the receiver. In an urban environment, this means that the signal passes through a larger number of buildings, cars, roads and other obstructing materials. This in turn, creates more multipath propagation due to scattering, reflection and refraction. Thus the signal amplitude suffers from higher variation as the propagating distance increases. However, from Fig. 6.7 it can be seen that some data sets suggest a higher deviation in signal amplitude (for distances of 223 and 301 meters) than the rest. As stated before, the positions from 0-253 meters had partially obstructed line-of-sight between the transmitter and receiver antenna which significantly affects the amplitude variation. Thus, the standard deviations for these two positions suffer from a high variation of amplitude of more than 2 dB.

The above mentioned results also draw an interesting observation regarding the wireless communication between a ground control station with a directional antenna and a UAV with an omnidirectional antenna. As the propagation distance increases between these two antennas, the signal amplitude decreases gradually from approximately -40dBm to -60dBm. However, the dual slope nature of the linear curve suggests that the propagating path partially obstructed by objects (from distances 0 to 253 meters), suffers from a higher amount of signal variation. The later positions (301 to 800 meters) employs a clearer line-of-sight between the transmitter and receiver and thus the power falls off more smoothly according to the propagation distance. This suggests that the employment of directional antenna on the ground control station has its advantage of higher gain in larger propagating distance. The signal can be received with higher amplitude in further distances due to the antenna's directive gain and the signal degradation is smoother as the distance increases. However, one of the drawbacks of this configuration is the multipath propagation effects in lower distances. Even though the propagation distance is lower, the received signal amplitude suffers from high attenuation in distances from 0-253 meters due to signal scattering, reflection and refraction from a partially obstructed propagation path. The lower angular beamwidth, higher directivity and directional properties of directional antenna are the main reasons for this phenomenon.

Another experiment is conducted by varying the propagation distance between the ground control station and the UAV node with a different antenna configuration. In this configuration, both the UAV node and the ground control station node are equipped with identical omnidirectional antennas. Figures 6.8, 6.9 and 6.10 show the received signal amplitude in dBm, average value of received signal amplitude and standard deviation of amplitude against different propagation distances correspondingly.

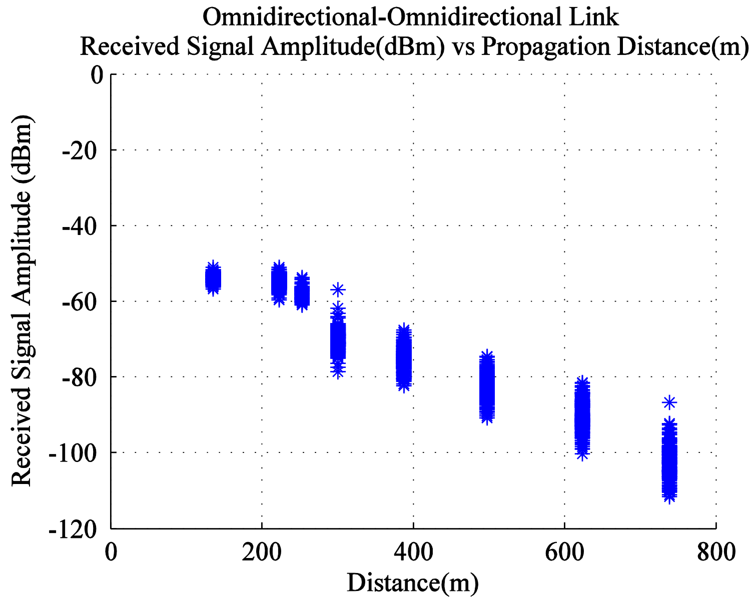

Fig. 6.8: Received signal amplitude against propagation distance with omnidirectional-omnidirectional link.

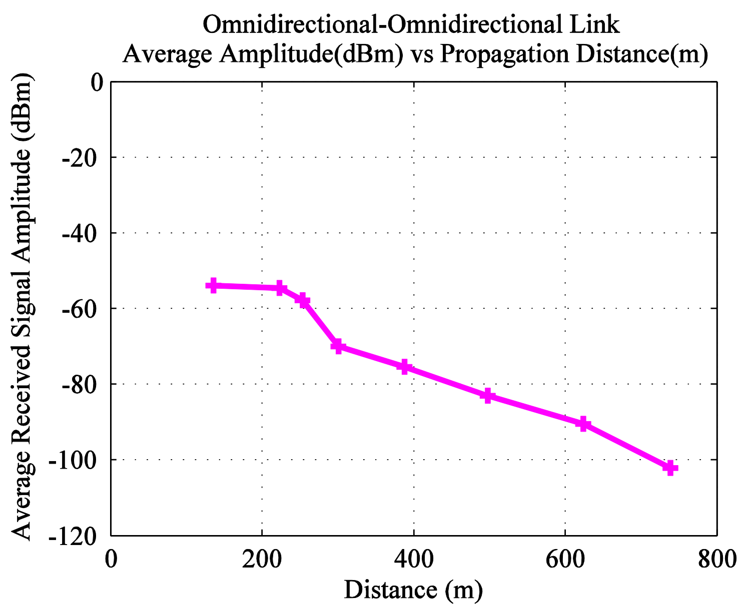

Fig. 6.9: Average of received signal amplitude against propagation distance with omnidirectional-omnidirectional link.

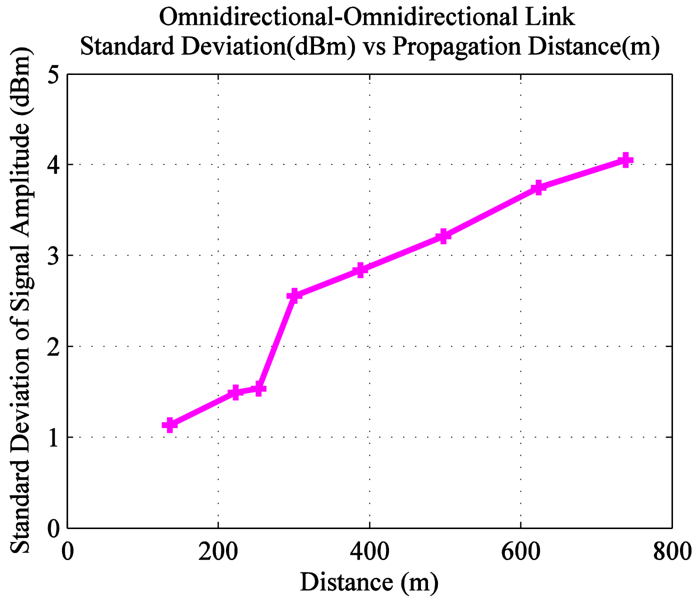

Fig. 6.10: Standard deviation of received signal amplitude against propagation distance with omnidirectional-omnidirectional link.

From Fig. 6.8, it can be seen that as the propagation distance between the ground control station and the UAV increases, the received signal amplitude decreases drastically. The signal degradation ranges from a value of approximately -55dBm to less than -110dBm. This huge reduction in received signal amplitude is due to the fact that omnidirectional antennas have lower gain than the directional antennas. It can also be realized from this figure that the propagation follows a dual slope piecewise linear model for signal attenuation. This model has identical properties as the directional-omnidirectional link with N=2 segments and a critical distance of 253 meters. Two different slopes can be found from these two piecewise linear segments. From distances 0-253 meters, the signal falls off with a certain path loss exponent which is significantly lower than the path loss exponents for distances 301-800 meters. This implies that for lower propagating distances, even though the propagation path is partially obstructed by building edges, the path loss exponent is lower for an omnidirectional antenna at the ground control station. However, as distance exceeds the critical distance of 253 meters, even though the propagation path has a clearer line-of-sight, higher attenuation is suffered by the signal. This can be reaffirmed by Fig. 6.9 which shows the average of received signal amplitude by the ground control station against the propagation distance. We can clearly see that the average signal amplitude drops significantly after the critical distance of 253 meters. Figure 6.10 shows the standard deviation of the received signal amplitude against the propagating distance between the ground control station and the UAV. Another interesting observation can be made from this variation of standard deviation for this omnidirectional-to-omnidirectional link. From the critical distance of 253 meters, there is a sharp rise in the standard deviation of the received signal amplitude. The standard deviation changes drastically from approximately 1.2 dB in 153 meters to more than 4dB in 739 meters. This strongly suggests that the wireless signal transmitted from the UAV suffers from significant amplitude variation as the propagating distance increases. These phenomena can be explained by a distinct property of omnidirectional antennas. Omnidirectional antennas radiate equally in all direction in the plane perpendicular to the antenna, amidst its limited range. For lower propagating distances (0-253 meters) the positions of the ground control station had partially obstructed line-of-sight between the ground control station and the UAV antenna. The transmitted signal was scattered, reflected and refracted from building edges and roads. However, as omnidirectional antennas radiate equally in the perpendicular plane, the scattered and reflected signal components were picked up with equal power by the ground control station antenna. Thus, these positions demonstrated better performance in picking up signals transmitted from the UAV node. When the propagating distance became larger (301-800 meters), the signal suffered more shadowing, scattering, reflection, refraction from the surrounding objects and had to travel a further distance in order to reach the receiving antenna. This caused further attenuation of the signal and the received signal amplitude fell off significantly despite the transmitter and receiver being in each other's communication range. These results suggest that the omnidirectional antenna is less prone to signal degradation due to scattering, reflection and refraction from surrounding objects than their directional counterparts in lower propagation distances. However, the directional antenna performs significantly better in larger distances where there is a clearer line-of-sight between the ground control station and UAV nodes.

6.2. Fading Analysis of the Wireless Link

The previous section provided detailed discussion on the correlation of wireless link quality with propagating distance employing different antenna configurations. In this section, the fading of this wireless link between the UAV and portable ground control station is analyzed. The large scale and small scale fading components are first identified and then compared with existing fading models. Critical parameters of these models are calculated through regression analysis and discussed. The experiments conducted for both omnidirectional-to-omnidirectional and directional-to-omnidirectional antenna configurations.

6.2.1. Large Scale Fading Analysis

This section provides detailed discussion on the large scale fading analysis of the wireless channel between the UAV and portable ground control station. As stated in the theoretical background chapter, large scale fading of a wireless channel involves path loss and shadowing of the electromagnetic signal during its propagation from transmitter to receiver. In this section, the large scale fading component is identified from the experiment data and compared with existing channel models. Moreover, critical parameters for these models are calculated from the data through regression analysis, compared and discussed.

6.2.1.1. Comparison of Existing Channel Models

The Free Space Path Loss (FSPL) model is a widely used model for wireless signal propagation in a point-to-point link. This model is simulated in MATLAB to compare with our experiment data. The theoretical background chapter provides detailed discussion on this channel model and its parameters. The parameters used to simulate this model in MATLAB are given below.

- Transmit power = 30dBm
- Antenna gain = 1 (for omnidirectional antenna)
- Frequency = 900 MHz

The FSPL model is given by

$$\frac{P_r}{P_t} = \left[\frac{\sqrt{G_l}\lambda}{4\pi d}\right]^2 \tag{6.1}$$

$$P_r(dBm) = P_t(dBm) + 10log_{10}(G_l) + 20log_{10}(\lambda) - 20log_{10}(4\pi) - 20log_{10}(d) \tag{6.2}$$

The received power in the simulations conducted in MATLAB and ratio of received power to transmit power can be seen in Figs 6.11 and 6.12.

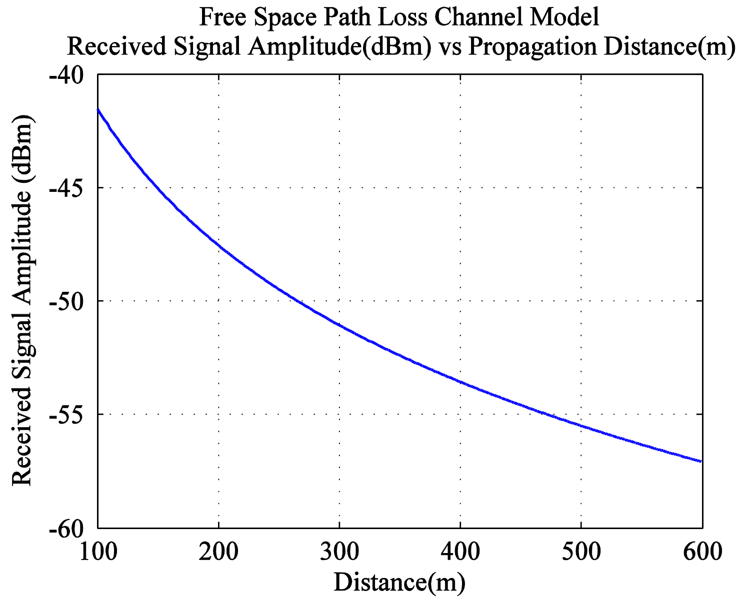

Fig. 6.11: Received signal amplitude against propagation distance for Free Space Path Loss Channel Model.

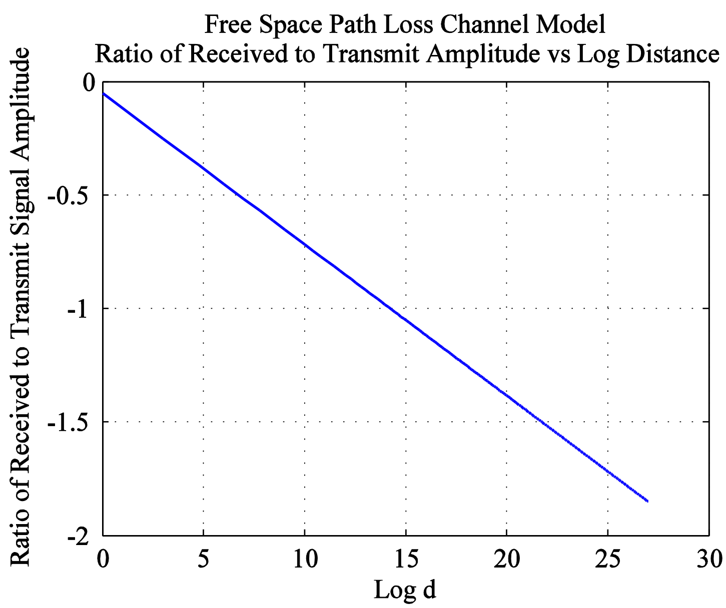

Fig. 6.12: Ratio of received to transmit signal amplitude against propagation distance for Free Space Path Loss Channel Model.

The Dual Slope Piecewise Linear (DSPL) model is widely employed in the literature for modeling signal propagation in vehicular networks. It provides a more robust and realistic channel propagation model for wireless signal propagation in harsh environments. This model is simulated in MATLAB as well to analyze our experiment data. The parameters used in the simulation are provided below.

- Constant path loss factor = -31.54
- Path loss exponent = 2
- Reference distance = 100 meters
- Critical distance = 400 meters
- Path loss exponent after the critical distance = 4

The model can be given by

$$P_r(dB) = \begin{cases} P_t + K - 10\gamma_1 log_{10}\left(\frac{d}{d_0}\right) & d_0 \le d \le d_c \\ P_t + K - 10\gamma_1 log_{10}\left(\frac{d}{d_0}\right) - 10\gamma_2 log_{10}\left(\frac{d}{d_c}\right) & d > d_c \end{cases} \quad (6.3)$$

Figure 6.13 shows the simulated received power in dBm for the DSPL model in MATLAB.

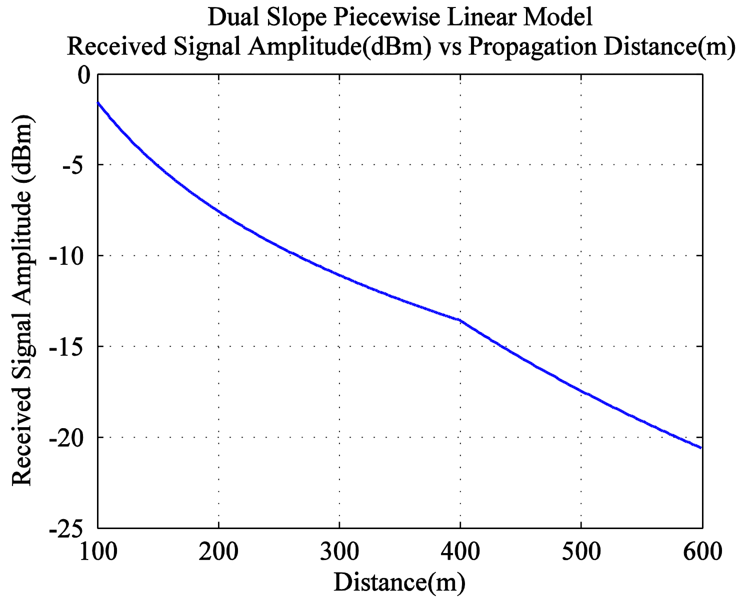

Fig. 6.13: Received signal amplitude against propagation distance for Dual Slope Piecewise Linear channel model.

The Log Normal Shadowing model is also simulated in MATLAB to analyze our experiment data. The model parameters are given below.

- Received power at a reference distance = -41.5266dBm
- Path loss exponent = 2.75
- Reference distance = 100 meters

The model can be given by

$$P_r = P_r(d0) + 10\gamma log_{10}\frac{d}{d0} + X_\sigma \qquad (6.4)$$

Figure 6.14 shows the simulated received power for the log normal shadowing model in MATLAB.

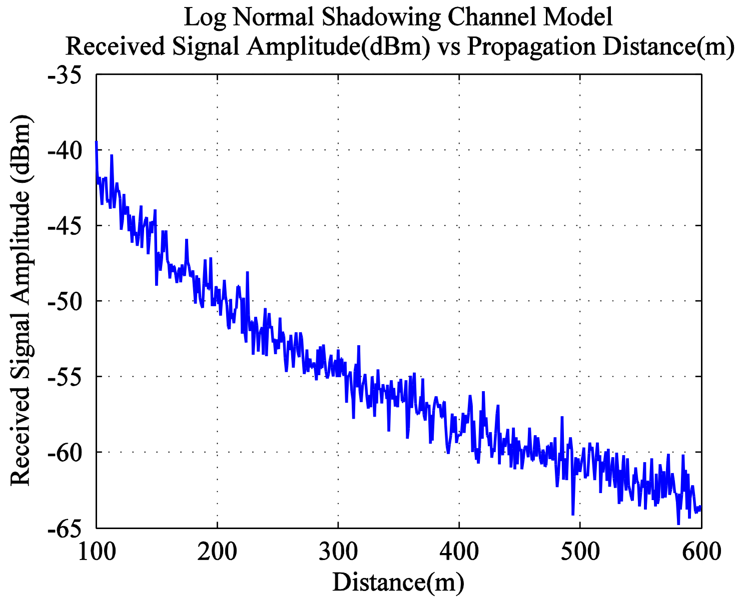

Fig. 6.14: Received signal amplitude against propagation distance for Log Normal Shadowing channel model.

Through visual inspection of the three simulated channel models, we can see that the DSPL model and the Log Normal Shadowing model show similar propagation characteristics to our experiment data. Although the FSPL model is widely used in modeling signal propagation, it is more suitable for a link that has an unobstructed line-of-sight between the transmitter and receiver. In our scenario, we investigate the wireless channel between a low altitude UAV and a portable ground control station in an urban scenario. The probability of having a clear line-of-sight between the two antennas is very low in this kind of propagation environment due to buildings, cars, trees, and roads. For this scenario, the DSPL and Log Normal Shadowing model is more suitable. Therefore, these two models are further analyzed with the experiment data. Moreover, the performance of these two models are compared and analyzed for two different antenna configurations.

6.2.1.2. Regression Analysis of Dual Slope Piecewise Linear Model with Experiment Data

The simulated DSPL model is fitted with the experiment data in MATLAB for two antenna configurations. The first configuration consists of an omnidirectional antenna on the UAV node and a directional Yagi antenna on the ground control station node. The second configuration consists omnidirectional antennas on both nodes. The path loss exponents and critical distance are calculated through regression analysis. The Goodness of Fit parameters are also computed by MATLAB and provided.

For the first configuration, the fitted experiment data on the DSPL model can be seen in Fig. 6.15.

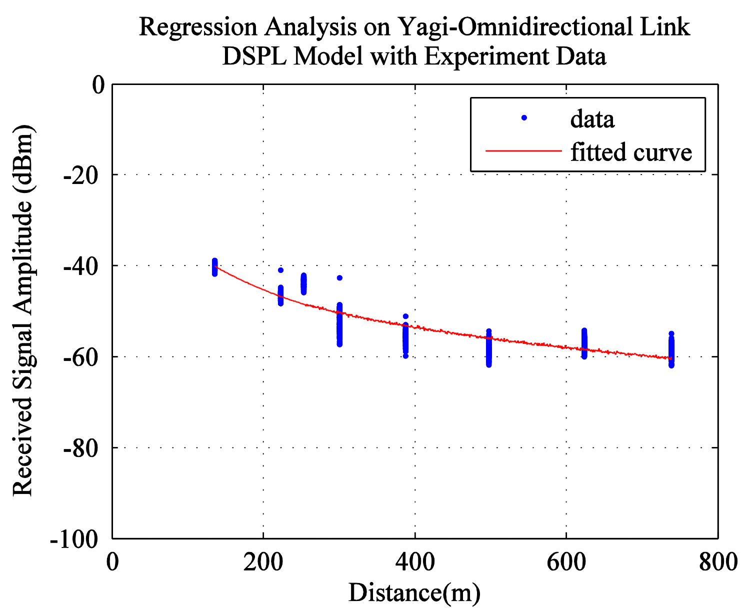

Fig. 6.15: Regression analysis on experiment data with DSPL channel model (Yagi-Omnidirectional configuration).

The estimated coefficients are given below.

- Path loss exponent, γ_1 = 3.111

- Path loss exponent, γ_2 = 2.559
- Critical distance, d_c = 253 m

The Goodness of Fit parameters for the fitted data are provided below.

- $rmse$: 2.5913
- $adjrsquare$: 0.8568
- dfe: 1432
- $rsquare$: 0.8572
- sse: $9.6156e + 03$

For the second configuration, the fitted experiment data on the DSPL model can be seen in Fig. 6.16.

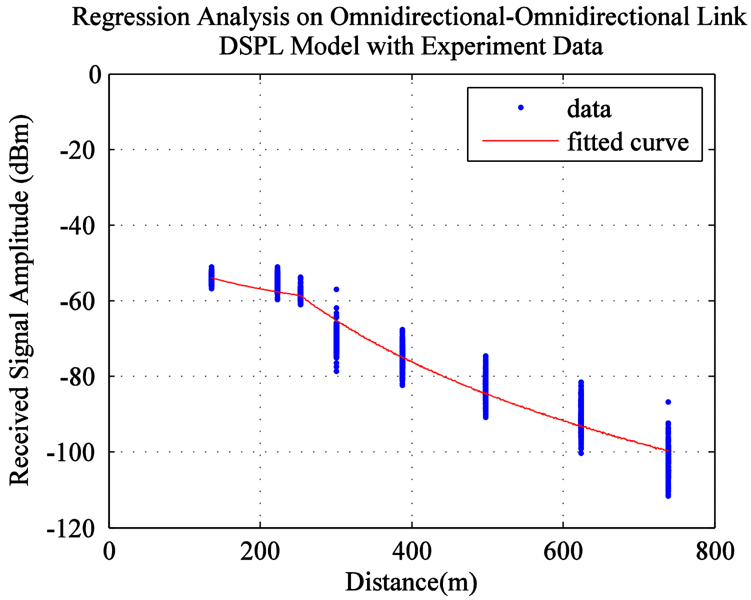

Fig. 6.16: Regression analysis on experiment data with DSPL channel model (omnidirectional-omnidirectional configuration).

The estimated coefficients are given below.

- Path loss exponent, $\gamma_1 = 1.727$
- Path loss exponent, $\gamma_2 = 8.819$
- Critical distance, d_c = 253 m

The Goodness of Fit parameters are given below.

- $rmse$: 3.9677
- $adjrsquare$: 0.9430
- dfe: 1311
- $rsquare$: 0.9432

- sse: $2.0638e + 04$

Many interesting observations can be made from this data. Both the models give a critical distance of 253 meters. This reaffirms the fact that the wireless signal's propagation path was partially obstructed by building edges in these positions of ground control station. For distances greater than 253 meters, the propagation path had a clearer line-of-sight. This confirms that the wireless signal propagates with a certain path loss exponent until distance 253 meters which is highly dependent on the propagation environment. After that critical distance, the signal suffers from less attenuation due to a clearer line of sight propagation path. This can be further confirmed by the path loss exponents γ_1 and γ_2 for the first configuration. We can see that when the ground control station is equipped with a directional Yagi antenna, the path loss exponent until the critical distance of 253 meters is 3.111. However, after the critical distance, the path loss exponent reduces to 2.559. This finding is critical to the DSPL model which approximates that the signal suffers more attenuation after the critical distance. The reduction of path loss exponent after the critical distance can be fully credited to the directional nature of Yagi antennas, as stated before. As the directional antenna is more prone to signal scattering from building edges due to partially obstructed line-of-sight, these positions of the ground control station suffered from further attenuation and had a higher path loss exponent. However, as the distance increased, the line-of-sight between the receiver and the transmitter antenna became less obstructed and the signal suffered less attenuation causing a reduction in the path loss exponent.

Another important reason for this behavior of directional antennas is the angular beamwidth. As stated in the theoretical background chapter, the angular beamwidth of directional antennas expands as the distance increases. From Fig. 5.15, it is apparent that the main lobe of the directional antenna has a lower beamwidth in lower distances. The angular beamwidth increases as the length of the main lobe increases, also increasing the coverage area of the antenna. This implies that in further distances, the directional antenna is able to cover larger angular distances when receiving electromagnetic waves from a transmitter. Therefore, when the separation distance between the ground control station and the UAV is low, the directional antenna's beamwidth becomes narrower and is more susceptible to building edges which obstructs its line-of-sight. However, as the distance increases, the beamwidth becomes wider and increases the coverage. This makes the beamwidth of the receiving antenna less susceptible to building edges and improves the level of reception of wireless signals.

The Goodness of Fit provides the adjusted r squared parameter with a value of 0.8568, r squared parameter with a value of 0.8572 and a root mean squared error parameter with a value of 2.5913. These values show that the model was a good fit to the experiment data.

For the second configuration, the path loss exponents are given as γ_1 = 1.727 and γ_2 = 8.819. This shows that fitting the ground control station with an omnidirectional antenna provides a better performance until the critical distance with a lower path loss exponent than the directional antenna. This is due to the fact that omnidirectional antennas radiate/receive equally in all direction on a plane. Thus, the scattering of waves due to building edges does not affect the communication channel in lower distances. However, as the distance increases, the lower gain of omnidirectional antennas forces them to receive lower amplitude of the received signals due to signal attenuation from path loss, shadowing and multipath effects. This results in a lower performance than the directional antennas. The goodness of fit parameters confirms that the model is a good fit to the experiment data.

6.2.1.3. Regression Analysis of Log Normal Shadowing Model with Experiment Data

The Log Normal Shadowing model is fitted with the experiment data with MATLAB and the path loss exponent is calculated through regression analysis. This is also done for the two antenna configurations as stated in the previous section.

For the first configuration, where the ground control station is equipped with a directional Yagi antenna, the fitted data with the model can be seen in Fig. 6.17.

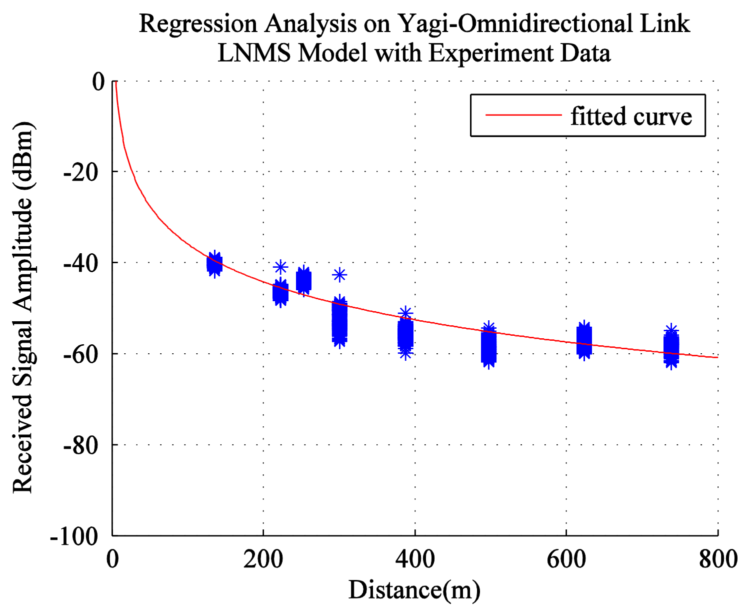

Fig. 6.17: Regression analysis on experiment data with the Log Normal Shadowing channel model (Yagi-Omnidirectional antenna configuration).

The estimated coefficient is provided below.

- Path loss exponent, γ = 2.346

The goodness of fit parameters for the fit is provided below.

- $rmse$: 2.7728

- $adjrsquare$: 0.8360

- dfe: 1435

- $rsquare$: 0.8361

- sse: $1.1032e + 04$

For the second configuration with omnidirectional antennas on both UAV and ground control station, the fitted data with the log normal shadowing model can be seen in Fig. 6.18.

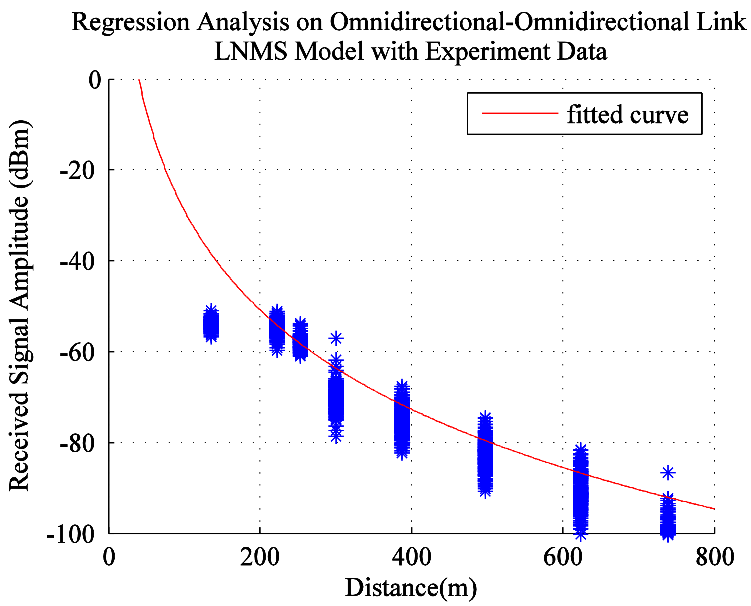

Fig. 6.18: Regression analysis on experiment data with the Log Normal Shadowing channel model (Omnidirectional-Omnidirectional antenna configuration).

The estimated coefficient is given below.

- Path loss exponent, γ = 5.293

The goodness of fit parameters are provided below.

- $rmse$: 7.1109

- $adjrsquare$: 0.8170
- dfe: 1314
- $rsquare$: 0.8172
- sse: $6.6443e + 04$

From these data, it can be seen that the directional antenna (γ = 2.346) outperforms the omnidirectional antenna (γ = 5.293) configuration. This is mainly due to the fact that the directional antennas suffer from less attenuation in further distances than their omnidirectional counterparts. However, after careful inspection of the goodness of fit parameters of the two models, it can be seen that the DSPL model provides a better fit to our experiment data than the Log Normal Shadowing model. This is a critical observation in our thesis which confirms the fact that for a wireless communication link employing a low altitude UAV and a portable ground control station operating in a densely populated urban scenario, the signal propagation closely follows the Dual Slope Piecewise Linear model. The adjusted r squared parameter, which provides how well the variation in data can be explained by the model, provides a good measure to the fit. The DSPL model had adjusted r squared value of 0.8568 (directional Yagi) and 0.9430 (omnidirectional antenna) where, the Log Normal Shadowing model had adjusted r squared value of 0.8360 (directional Yagi) and 0.8170 (omnidirectional antenna). It can be concluded from these results that the DSPL model is able to better represent the actual propagation environment for this wireless link between a UAV and ground control station and thus is used in the Nakagami fading analysis of the channel.

6.2.2. Small Scale Fading Analysis

The small scale fading involves multipath propagation of the wireless signal due to objects in its propagation path from transmitter to receiver. This is also known as multipath fading. In literature, this small scale fading is widely represented by Gaussian, Rayleigh and Rician distributions. The Nakagami distribution can model both Rayleigh and Rician fading and provides a fading parameter m that can be used to characterize the severity of fading within the wireless channel. In this section, the small scale fading is superimposed on Dual Slope Piecewise Linear model and Log Normal Shadowing model by Gaussian and Nakagami distributions to analyze the small scale fading.

6.2.2.1. Gaussian Fading Analysis

The Gaussian distribution is superimposed on the DSPL large scale fading model to represent the small scale fading as

$$P_r(d) = \begin{cases} P_r(d_0) - 10\gamma_1 log_{10}\left(\frac{d}{d_0}\right) + X_{\sigma_1} & d_0 \leq d \leq d_c \\ P_r(d_0) - 10\gamma_1 log_{10}\left(\frac{d_c}{d_0}\right) - 10\gamma_2 log_{10}\left(\frac{d}{d_c}\right) + X_{\sigma_2} & d > d_c \end{cases} \quad (6.5)$$

where, X is a zero mean Gaussian random variable with standard deviation of σ_1 and σ_2. The model is simulated in MATLAB and the received power against propagation distance can be seen in Fig. 6.19. Here, the standard deviations are valued as σ_1= 2.6 and σ_2 = 4.4.

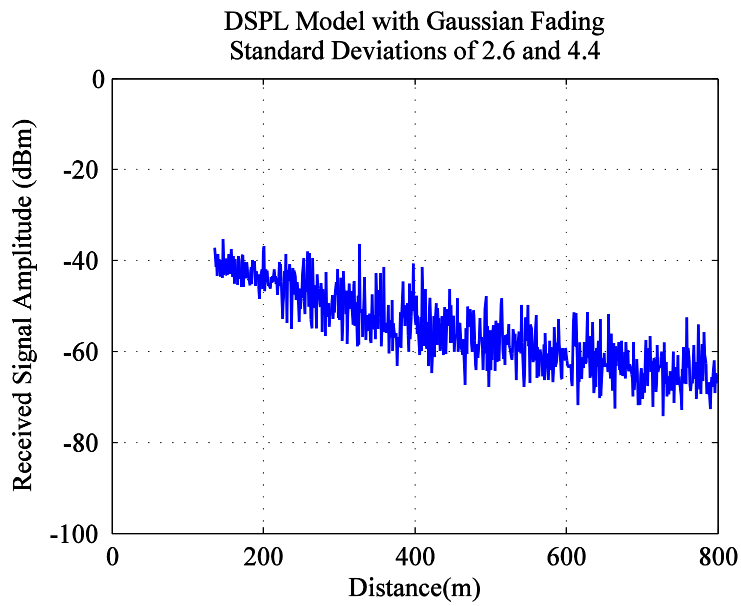

Fig. 6.19: Gaussian fading with Dual Slope Piecewise Linear channel model.

The Gaussian distribution is then superimposed on the Log Normal Shadowing large scale fading model as

$$P_r = P_r(d0) + 10\gamma log_{10}\frac{d}{d0} + X_\sigma \qquad (6.6)$$

where, X is a zero mean Gaussian random variable with standard deviation of σ. The model is simulated in MATLAB and the received power against propagation distance can be seen in Fig. 6.20. Here, the standard deviation is valued as σ = 3.65.

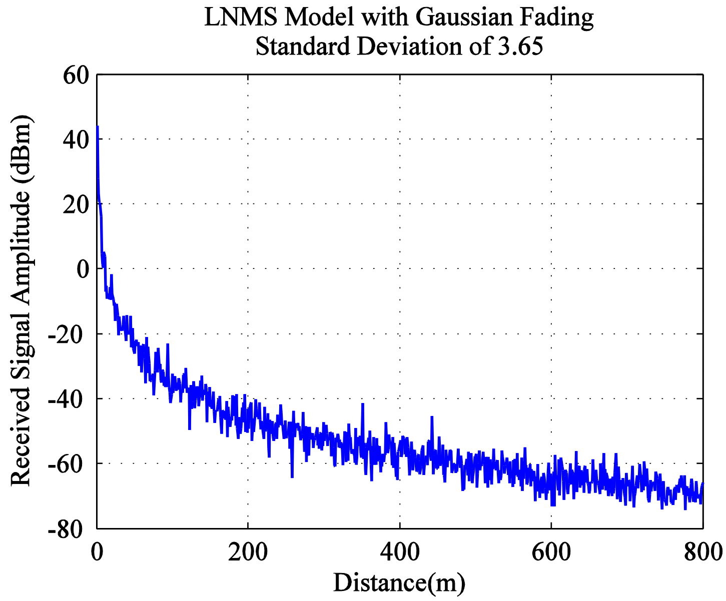

Fig. 6.20: Gaussian fading with Log Normal Shadowing channel model.

These two models are fitted with the experiment data and the standard deviations are calculated through regression analysis. The calculations are done for both antenna configurations. The results of the regression analysis are provided in the tables below.

Table 6.1: Standard deviations of dual slope piecewise linear channel model for yagi-omnidirectional and omnidirectional-omnidirectional links.

Standard Deviation	Directional – Omnidirectional [dB]	Omnidirectional-Omnidirectional [dB]
σ_1	0.3159	1.826
σ_2	0.5121	2.569

Table 6.2: Standard deviation of log normal shadowing channel model for yagi-omnidirectional and omnidirectional-omnidirectional links.

Standard Deviation	**Directional – Omnidirectional [dB]**	**Omnidirectional-Omnidirectional [dB]**
σ	3.854	7.189

Table 6.1 provides the standard deviations for the Gaussian distribution in DSPL model for both the antenna configurations. It can be seen that the directional-to-omnidirectional antenna configuration outperforms its omnidirectional counterpart. The antenna configuration employing a directional antenna on the ground control station suffers much less signal variation due to multipath propagation. This can be explained by some distinct properties of the directional antenna. Directional antennas have lower angular beamwidth with high gain. This higher gain adds to the system gain of the receiving antenna and increases the received signal amplitude. This in turn improves the signal to noise ratio (SNR) and can improve the quality of received signal. Moreover, directional antennas focus the radiation energy in one specific direction with a narrow angular beamwidth. When distance is low between the ground control station and the UAV, the beamwidth of the antenna is also narrower. The probability of scattered, reflected and refracted signals from different objects falling in this narrow beamwidth and increasing the number of multipath components is lower. Therefore, we can see a lower variation or, fading in directional antennas when the propagation distance is low. However, as the distance increases, the beamwidth becomes wider, giving rise to the probability of scattered signal falling into the beamwidth and affecting the multipath components. Thus, in larger distances, the signal suffers

from more multipath fading. We can also see a significant increase in multipath fading as the propagation distance increases for both antenna configurations. This is due to the fact that as distance increases, the number of objects in the environment also increases. These objects scatter, reflect and refract the signal and as more distance is traveled by the signal, the more multipath propagation occurs. Therefore, for larger distances, both the configurations show an increase in multipath fading. The same facts can be observed in table 6.2 which gives the standard deviation for directional-to-omnidirectional link and omnidirectional-to-omnidirectional link with the Log Normal Shadowing channel model.

6.2.2.2. Nakagami Fading Analysis

The previous section demonstrated the variation in received signal caused by multipath propagation for a point-to-point link between a UAV and a ground control station. To represent the fading, Gaussian distribution is superimposed on both large scale fading models. Both antenna configurations suffer from significant multipath fading. This fading increases as the propagation distance increases. To further analyze this fading and to represent its severity, Nakagami distribution is superimposed on the Dual Slope Piecewise Linear model and through regression analysis with the experiment data, the Nakagami shape parameter (m) is calculated. This is done for both antenna configurations to investigate the effects of fading as propagation distance increases. The procedure for Nakagami fading analysis is provided below.

(i) Received signal amplitude versus separation data are smoothed with a sliding average to identify large scale components of variations

(ii) Large scale component is used to normalize the raw data

(iii) Separation distance is divided into several bins with each distance bin forming empirical distributions to be fit with a Nakagami distribution

$$f(x; \mu, \omega) = \frac{2\mu^{\mu} x^{2\mu-1}}{\omega^{\mu}\Gamma(\mu)} e^{\frac{-\mu x^2}{\omega}} \tag{6.7}$$

(iv) Maximum likelihood estimation is performed for each distance bin to optimize the shape parameter for Nakagami distribution

The result from this Nakagami fading analysis is provided in tables 6.3 and 6.4.

Table 6.3: Variation of nakagami fading parameter m against propagation distance for yagi-omnidirectional antenna configuration.

Distance Bin [m]	**Fading Parameter**
136	10.78510
223	8.08841
253	4.56587
301	1.54508
388	4.22228
498	5.11729
624	1.76059
739	1.62976

Table 6.4: Variation of nakagami fading parameter m against propagation distance with omnidirectional-omnidirectional antenna configuration.

Distance Bin [m]	Fading Parameter
136	3.96352
223	2.51155
253	2.07969
301	0.831046
388	0.703678
498	0.574579
624	0.483032
739	0.398284

From table 6.3, we can see that the fading parameter gradually decreases as the propagation distance increases with a directional-to-omnidirectional antenna configuration. However, the distance bin of 301 meters shows a sudden drop of fading parameter which implies severe fading in that position. As stated before, this position of the ground control station has a line-of-sight with the UAV node antenna which is partially obstructed by multiple building edges in its path. According to the theory, scattering of electromagnetic waves by building edges causes a significant amount of multipath propagation. Thus, this position suffers from significant amount of multipath fading because of these edges in the line-of-sight of propagation.

Table 6.4 provides the fading parameters computed for several distance bins for the ground control station equipped with an omnidirectional antenna. Similarly, the fading parameter decreases gradually as the propagation distance increases, as expected. However, the severity of fading is much lower in the directional antenna configuration than the omnidirectional antenna configuration for the reasons stated above. Figure 6.21 shows the change in Nakagami shape parameter as the propagation distance increases for the two antenna configurations. It can be clearly seen that the directional antenna achieves a better performance than its omnidirectional counterpart for distances 0-800 meters.

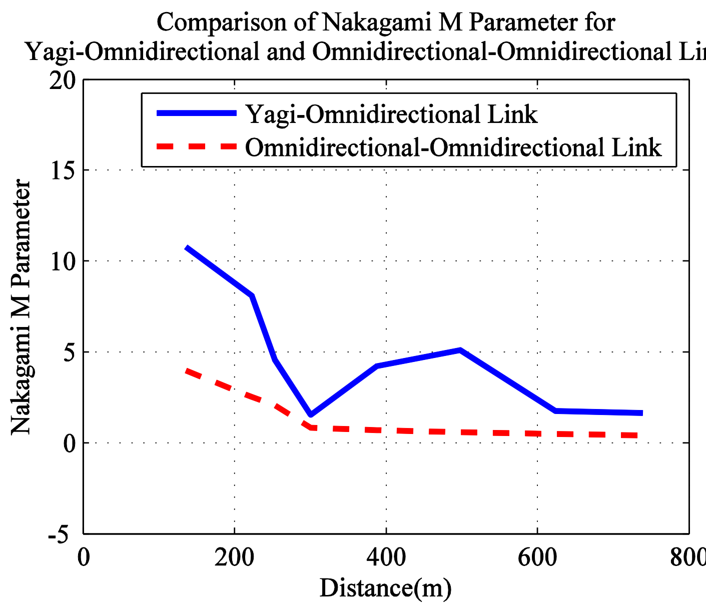

Fig. 6.21: Comparison of Nakagami m parameter variation for Yagi-omnidirectional and omnidirectional-omnidirectional antenna configurations.

6.3. Relationship of Nakagami Shape Parameter with Different Factors

In the previous sections, we have seen that the Nakagami shape parameter representing the severity of small scale fading varies significantly according to the propagation distance. Among the two considered antenna configurations, the directional-to-omnidirectional antenna configuration performs superiorly. In this section, the correlation of this m parameter with three delimiting factors is investigated, with the ground control station equipped with a directional Yagi antenna. As stated in the theoretical background chapter, three factors have a major impact in wireless communication involving a directional antenna: (i) directional gain of antennas in a specific spherical angle, (ii) polarization loss factor between transmit and receive antennas and (iii) multipath propagation due to buildings, cars, roads, and trees. First, individual relationships between the m parameter and these above mentioned factors are derived. Then, the overall effects of these factors on the fading parameter are investigated and modeled through multiple regression analysis. In addition, this multiple regression model is evaluated through various statistical measures to test how the variation in experiment data can be explained by this model.

6.3.1. Modeling and Simulation of Transmit and Receive Antennas with 4NEC2

In order to calculate the gain of the directional antenna in specific spherical angles, the directional Yagi antenna needs to be modeled and simulated. A directional antenna provides a narrow angular beamwidth in the direction it is facing. This beamwidth depends on the type and structure of the directional antenna. The Yagi antenna of the ground control station needs to be facing the UAV node antenna in specific azimuth and elevation angles to achieve the best possible communication. This section simulates the Yagi antenna employed in the ground control station to calculate the directive gain it achieves. Moreover, the reduction in the directive gain due to any deviations in the spherical angles can also be calculated. The Yagi and omnidirectional dipole antennas are simulated with 4NEC2 antenna simulation software.

6.3.1.1. Modelling and Simulation of Yagi Antenna

The seven element Yagi antenna is simulated in 4NEC2. The 3D view of the Yagi model is shown in Fig. 6.22. After the model is created, the antenna is simulated in 4NEC2 to provide the gain of this antenna in certain spherical angles. The total gain of the antenna, transparent view of gain, 2D slice view, vertical and horizontal radiation patterns are shown in Figs 6.23 to 6.27.

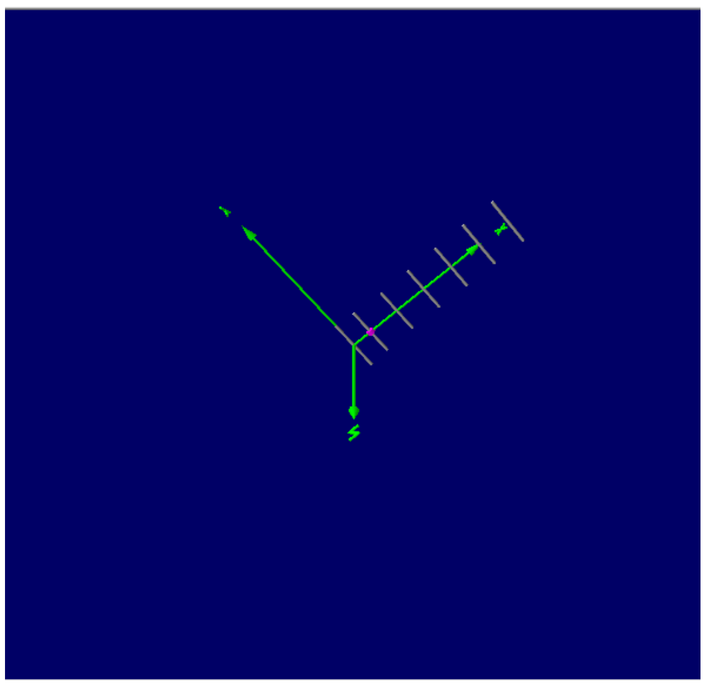

Fig. 6.22: 3D view of Yagi antenna modelled with 4NEC2.

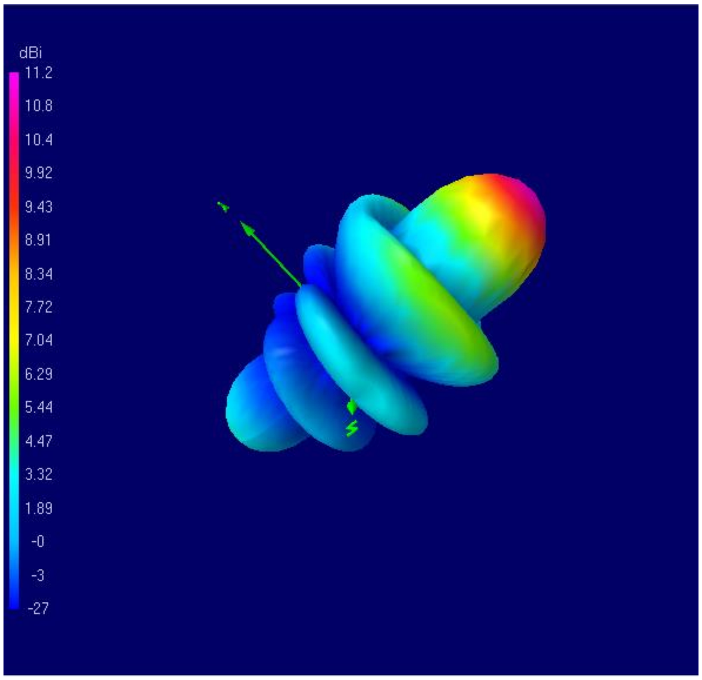

Fig. 6.23: Total gain of Yagi antenna modelled with 4NEC2.

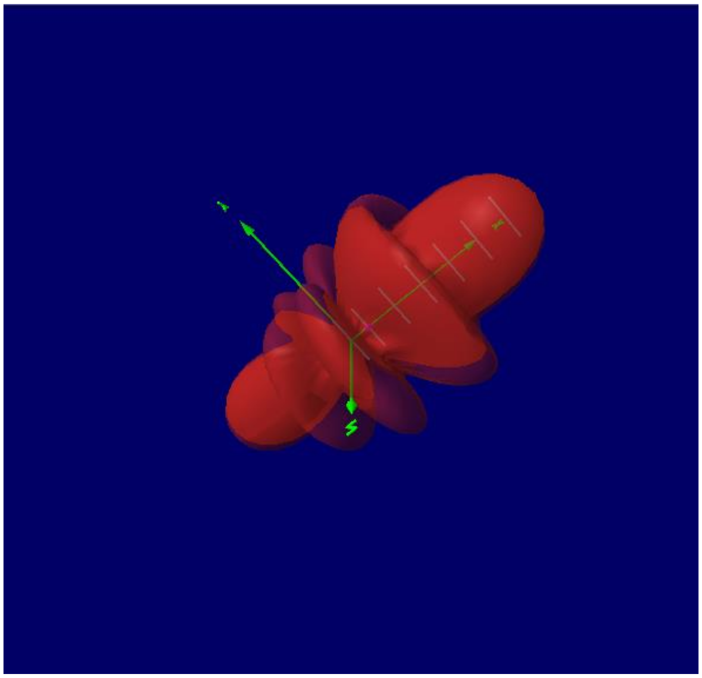

Fig. 6.24: Total gain (transparent view) of Yagi antenna modelled with 4NEC2.

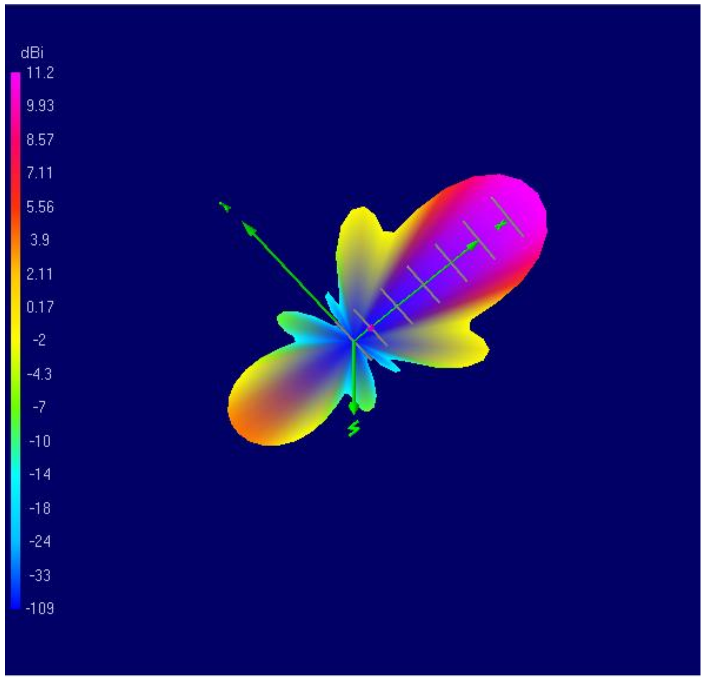

Fig. 6.25: Total gain (2D slice view) of Yagi antenna modelled with 4NEC2.

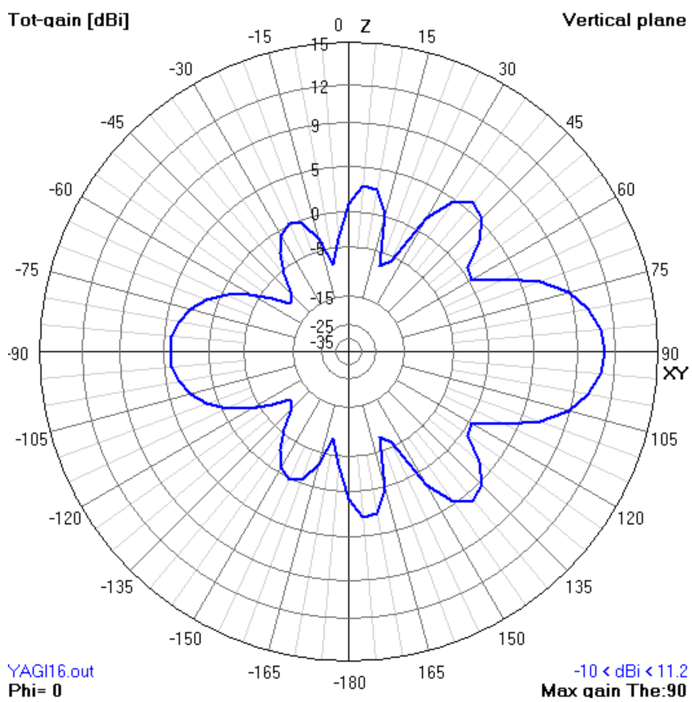

Fig. 6.26: Vertical gain of Yagi antenna modelled with 4NEC2.

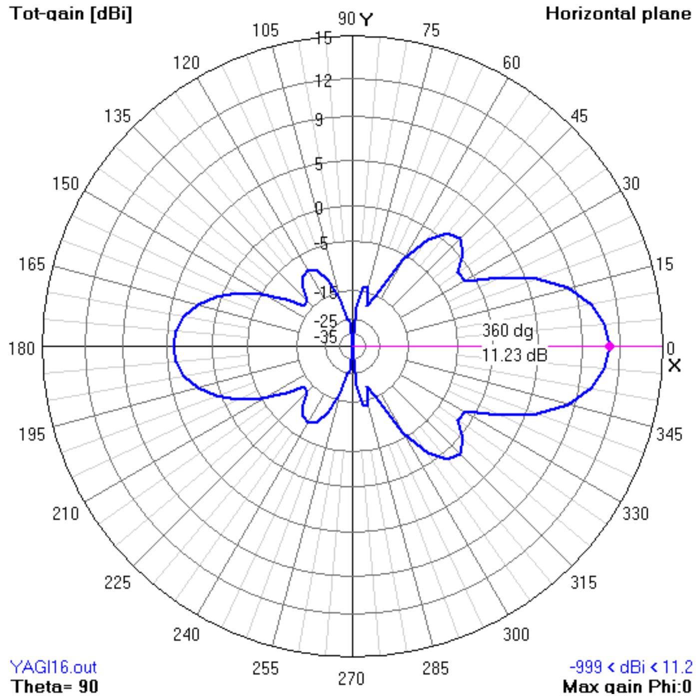

Fig. 6.27: Horizontal gain of Yagi antenna modelled with 4NEC2.

The omnidirectional dipole antenna is also modelled in 4NEC2 to calculate its omnidirectional gain. It is simulated in the same simulation environment. Figures 6.28 to 6.33 show the antenna model, total gain, transparent view of gain, 2D slice view, vertical and horizontal radiation patterns of the omnidirectional antenna.

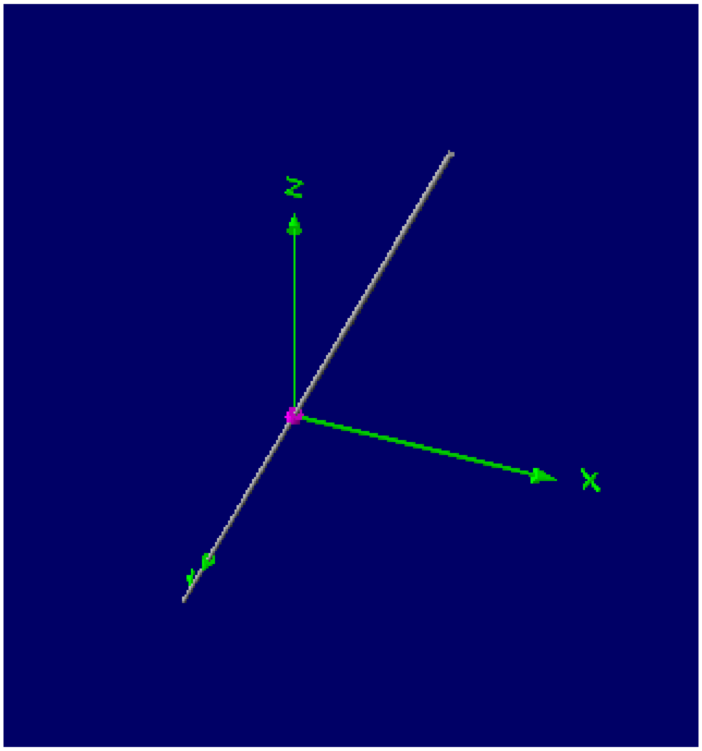

Fig. 6.28: 3D view of omnidirectional antenna modelled with 4NEC2.

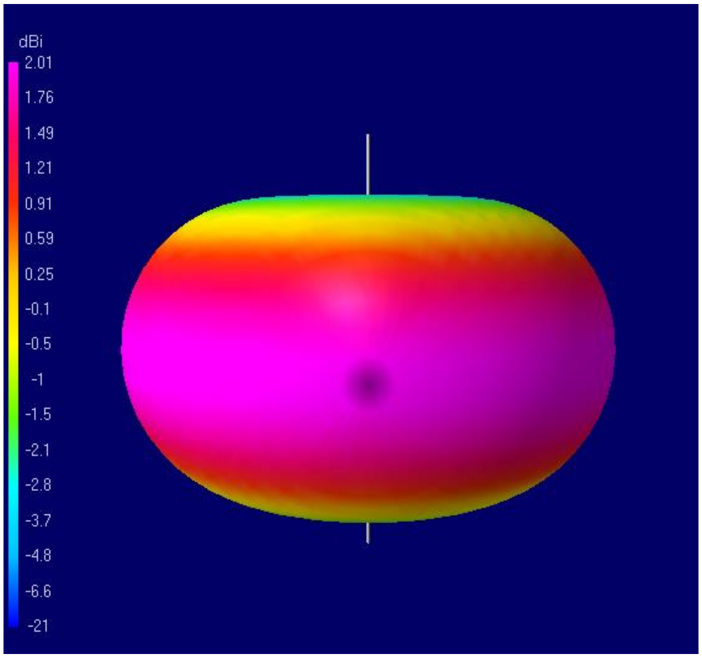

Fig. 6.29: Total gain of omnidirectional antenna modelled with 4NEC2.

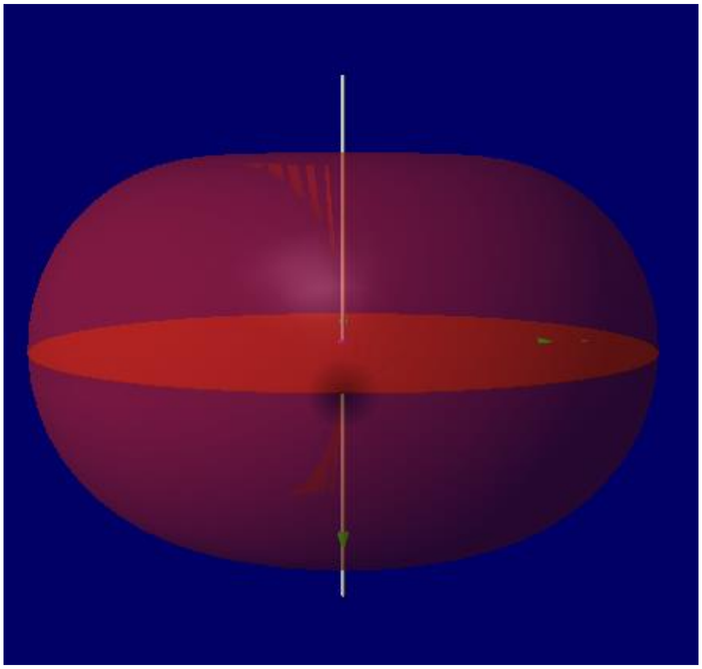

Fig. 6.30: Total gain (transparent view) of omnidirectional antenna modelled with 4NEC2.

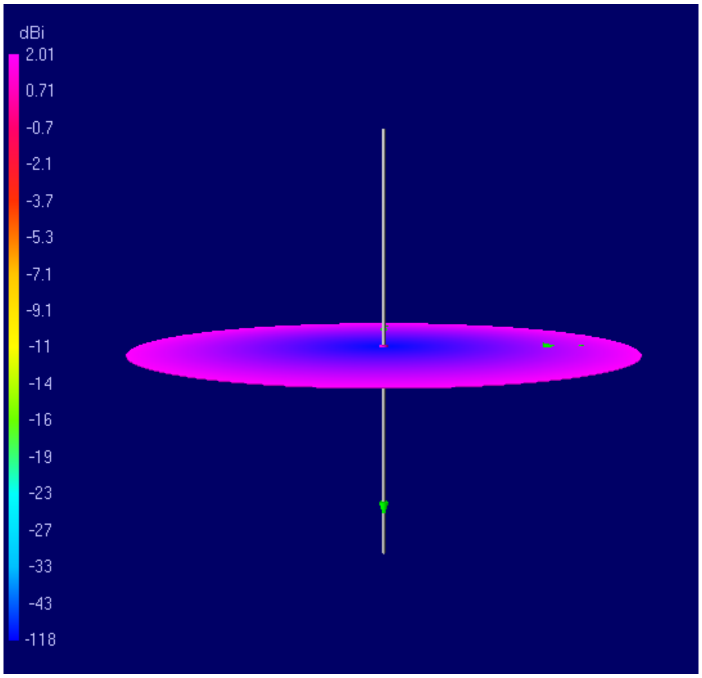

Fig. 6.31: Total gain (2D slice view) of omnidirectional antenna modelled with 4NEC2.

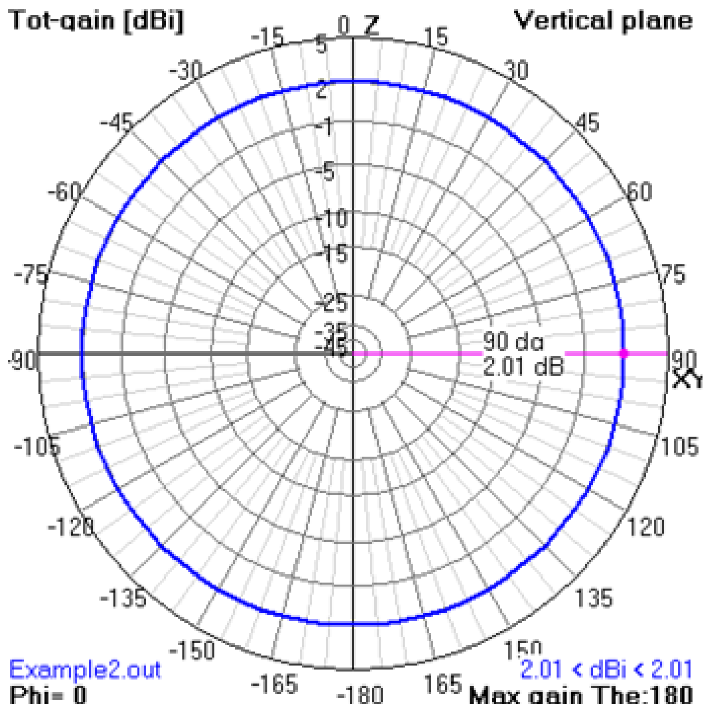

Fig. 6.32: Vertical gain of omnidirectional antenna modelled with 4NEC2.

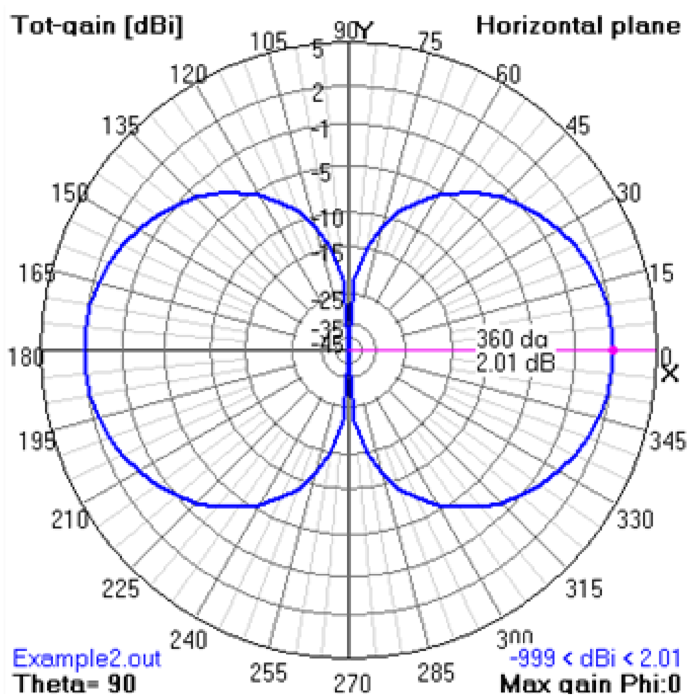

Fig. 6.33: Horizontal gain of omnidirectional antenna modelled with 4NEC2.

6.3.1.2. Relationship of Nakagami Shape Parameter with Propagation Distance

In this experiment, the relationship between the Nakagami shape parameter (m) and the propagation distance between the transmitter and the receiver is investigated. During this experiment, the spherical angle and polarization loss factor of the antennas are kept constant as the distance between the UAV and ground control station is varied. A linear regression model is derived from experiment data which is able to explain the variation in m as the distance increases. The model can be given by

$$\boldsymbol{m = a\, ln(d) + b} \tag{6.8}$$

where, a and b are model dependent parameters with values of $a = -5.241$ and $b = 35.48$. d is the distance between the transmitter and the receiver. The experiment data and the fitted model can be seen in Fig. 6.34.

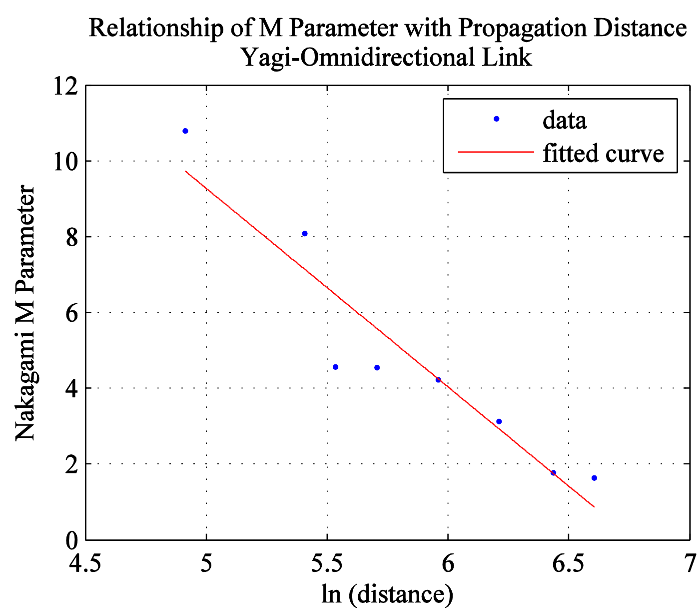

Fig. 6.34: Relationship of m parameter with propagation distance for Yagi-omnidirectional link.

The goodness of fit parameters for the regression analysis are given below.

- *sse: 7.3408*
- *rsquare: 0.8939*
- *dfe: 6*
- *adjrsquare: 0.8762*
- *rmse: 1.1061*

From Fig. 6.34, we can see that the relationship between the Nakagami shape parameter m with the propagation distance is close to a linear relationship. The m parameter is almost linearly related to the natural logarithm of the distance. Here, a is the intercept and b is the slope. The high value of b implies a steep slope for this model. It is apparent from the figure that the fading parameter decreases as the distance increases. This was also confirmed from our previous experiments where the distance was varied between the transmitter and receiver. This model is an approximation of the complicated fading process which is time-variant and often known as a semi-fixed event. The amount of objects causing this multipath fading in the environment can change any time, especially in urban environments where the UAV is in flight. Thus, the true relationship between fading and propagation distance is very complex. This model is a reasonable approximation to this complex process which provides a linear structure of the change of m parameter according to the distance. This model is confined to a certain range of distance data which was used in our experiments. However, an approximate model is derived which is able to explain the change in m parameter up to 89.39% (r square = 0.8939) as the distance varied. Moreover, an adjusted r squared value of 0.8762 implies that the derived model is a good fit to the experiment data.

6.3.1.3. Relationship of Nakagami Shape Parameter with Gain Factor

In this experiment, the relationship of the Nakagami m parameter with the antenna gain factor is investigated. The distance and polarization loss factor of the antennas are kept constant as the gain factor between the UAV and ground control station antennas is varied. Similar to the previous experiment, a model is derived from the experiment data through regression analysis. The model can be given by

$$\boldsymbol{m = a\, e^{bg^2}} \tag{6.9}$$

where, a and b are model dependent parameters with values of $a = 0.6514$ and $b = 0.02089$. g is the antenna gain factor which is the product of directive gains of the antennas in specific spherical angles. The experiment data with the fitted model can be seen in Fig. 6.35.

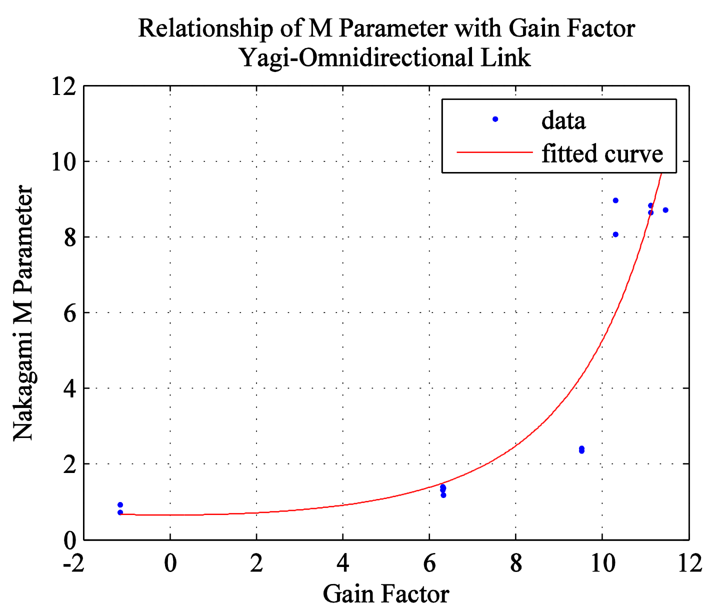

Fig. 6.35: Relationship of Nakagami m parameter with gain factor for Yagi-omnidirectional link.

The goodness of fit parameters from the regression analysis are provided below.

- *sse: 22.9182*

- *rsquare: 0.8584*
- *dfe: 11*
- *adjrsquare: 0.8455*
- *rmse: 1.4434*

From Fig. 6.35, we can see that the fading parameter is exponentially related to the square of the gain factor between the two antennas. When, gain factor between the antennas is low, meaning that the antennas are not aligned with each other, the fading parameter is low, indicating severe fading. This can be explained by the directional nature of the Yagi antenna. As the direction of maximum radiation of the beamwidth is deviated from the UAV node antenna, the total gain decreases which also decrease the system gain. Moreover, as the radiation pattern suggests, an angular displacement of 45 degrees misses the main lobe of the directional antenna completely. In this case, the main lobe is directed in a different direction which is slightly deviated from the correct alignment with the UAV node antenna. The bulk of the main lobe is more susceptible to any multipath propagated signals, scattered and reflected from different objects in the vicinity. Thus, as the gain factor reduces, the fading increases. However, with the increase in gain factor, implying a better alignment with the UAV node antenna, the fading parameter also increases exponentially, indicating less fading. This can be also explained by the reasons mentioned above. With the main lobe of the directional antenna directed directly towards the UAV node, maximum gain can be achieved, increasing the system gain. In addition, the narrow beamwidth of the main lobe is less susceptible to multipath signals propagating from different direction. The high value of adjusted r squared indicates a good fit of the model with the experiment data. Thus, it can be concluded that this model is a reasonable approximation of the change in fading parameter with the variation of antenna gain factors in directional antennas.

6.3.1.4. Relationship of Nakagami Shape Parameter with Polarization Loss Factor

In this experiment, the relationship between the Nakagami shape parameter m and the polarization loss factor between the two antennas is investigated. During the experiment, the distance and antenna gain factor between the two antennas are kept constant as the polarization loss factor between the two antennas is varied. A model is derived from the experiment through regression analysis. This model relates the m parameter with the natural logarithm of the polarization loss factor between the two antennas. The model can be given by

$$\boldsymbol{m} = \boldsymbol{a} + \boldsymbol{b}\,\mathbf{ln}(\boldsymbol{plf}) \tag{6.10}$$

where, a and b are model dependent parameters with values of $a = 9.968$ and $b = 1.492$. plf is the polarization loss factor between the transmit and receive antenna which is described in the theoretical background chapter. The experiment data and the fitted model can be seen in Fig. 6.36.

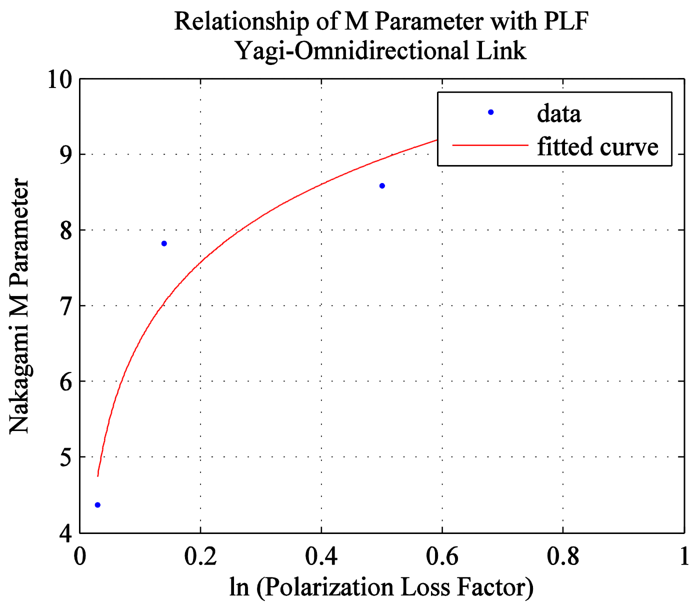

Fig. 6.36: Relationship of Nakagami m parameter with polarization loss factor for Yagi-omnidirectional link.

The goodness of fit parameters from the regression analysis are provided below.

- *sse: 0.8772*
- *rsquare: 0.9440*
- *dfe: 2*
- *adjrsquare: 0.9160*
- *rmse: 0.6623*

From Fig. 6.36, we can see that the fading parameter is related to the natural logarithm (ln) of the polarization loss factor between the two antennas. As the polarization loss factor increases, the fading parameter also increases, indicating less fading. This can also be attributed to the directional nature of radiation for Yagi antennas. As stated before, the polarization loss between two antennas contribute to the degradation of received signal. This in turn affects the overall fading phenomenon of the wireless channel. From this model, it is apparent that the polarization loss factor also affects the small scale fading. The adjusted r squared value of 0.9440 indicates that the model is a good fit to the experiment data. Therefore, this model can be stated as a reasonable approximation to the change in fading parameter as the polarization loss factor varies.

6.3.1.5. Relationship of Nakagami Shape Parameter with Distance, Gain Factor & Polarization Loss Factor

In the previous sections, it is seen that the three delimiting factors in the wireless communication between a UAV and ground control station has significant effects in the fading of the channel. The fading parameter varies considerably when distance, gain factor and polarization loss factor are changed individually. Moreover, individual regression models are derived which approximates the change in fading parameter as these factors are varied. In this section, the overall effect of these three factors on the fading channel is investigated. The experiment involves measuring the fading parameter m as distance, antenna gain factor and polarization loss factor are varied. The measured m parameter and the variation data are then used in a multiple regression analysis to derive a regression equation that estimates the change in m parameter as these three factors are varied. The main objective of this model is to estimate the level of fading the wireless channel suffers when the distance, antenna gain factor and polarization loss factor changes between the UAV node and ground control station node. This model is also able to analyze which of these three delimiting factors impacts the fading parameter, the most.

In this regression analysis, the dependent variable is selected as the m parameter which provides the severity of fading the channel is suffering. This is estimated by the model. The independent variables, or the regressors, are the distance, antenna gain factor and polarization loss factor. The multiple regression model can be given by

$$m_i = \beta_0 + \beta_1 x_{1i} + \beta_2 x_{2i} + \beta_3 x_{3i} + \epsilon_i \quad (6.11)$$

where, m is the dependent variable which gives the estimation of fading parameter. β_0 is the intercept and $\beta_1, \beta_2\ and\ \beta_3$ are the coefficients of the independent variables. ϵ_i is the error term in the regression model.

Before running the multiple regression analysis, the independent variables are checked for overfitting. The term overfitting refers to fitting the regression model with independent variables which do not have any significant effect in the dependent variable. This is detrimental to the analysis and can produce faulty regression data. As seen in the previous section, all of the three independent variables has significant effect in the fading parameter. Therefore, it can be assumed that the independent variables are not overfitted. Another important factor to consider before running multiple regression is multicollinearity. Multicollinearity refers to having independent variables in the regression analysis which are related to each other. This prohibits the analysis to figure out which variable is contributing to the change in the dependent variable, as they are strongly related to each other. Through visual inspection of the data and common sense, we can find out that the independent variables we used in this analysis are not related to each other. The propagation distance between the UAV and ground control station is independent of the antenna spherical angle and polarization. The antenna spherical angle is also independent from the distance and polarization. The polarization too, is independent from the other two variables. During the experiments, these factors are varied independently of the other factors when the fading parameter is measured. Thus, it is safe to assume that multicollinearity do not exist in our regression analysis.

The multiple regression model is fitted to the experiment data and the regression coefficients are calculated. The regression analysis is conducted by using the statistical toolbox provided in MATLAB 2012a.The regression equation can be given by

$$\boldsymbol{\hat{m}} = \mathbf{10.778 - 1.6339\,ln}(\boldsymbol{distance}) + \mathbf{0.16342}(\boldsymbol{gainfactor}) + \mathbf{0.38371\,ln}(\boldsymbol{PLF}) \quad (6.12)$$

where, $\hat{m}$ is the estimated value of the fading parameter m. 10.778 is the first intercept. The coefficient for the first independent variable (ln of distance) is -1.6339. This means that when the ln of distance increases by 1 unit, the fading parameter decreases by 1.6339 units. The coefficient for the second independent variable (gain factor) is 0.16342. This means that with an increase of antenna gain factor by one unit, the fading parameter increases by 0.16342 units. The coefficient for the third independent variable (polarization loss factor) is 0.38371. This implies that for an increase in antenna polarization loss factor of 1 unit, the fading parameter increases by 0.38371 units. From this data, it is apparent that the distance between the ground control station and the UAV has the highest impact on fading in the wireless channel. Secondly, the polarization loss factor between the two antennas effect the fading and lastly, the antenna gain factor between the transmit and receive antennas least impact the fading wireless channel.

This model is an important observation for aerial communication between UAVs and ground control stations. As fading is detrimental to the wireless communication, its estimation and prediction is important for an uninterrupted communication. Moreover, the channel between a UAV and ground control station is time-variant and dynamic in nature due to its high mobility and complex aerial maneuvers. This complex propagation environment poses a severe challenge in prediction and estimation of fading that is suffered. Therefore, this model can be used to design algorithms to predict and estimate the level of fading the propagation environment will suffer from, given the distance, antenna gain factors and polarization loss factors of the transmitting and receiving nodes.

6.3.1.6. Statistical Evaluation of the Multiple Regression Model

Figures 6.37 and 6.38 show the regression statistics and Analysis of Variance (ANOVA) from the MATLAB Statistics Toolbox. From these figures we can see that the overall model has a high F value of 133.99 and a very low P value of $3.4314e^{-64}$. This means that the independent variables are significant to the variation of dependent variable. The R-squared value of 0.438 means that the model is able to explain 43.8% variation of the dependent variable. The lower R-squared value is due to the non-linear nature of the individual relationships of the independent variables to the dependent variables as seen in the previous section. However, through this multiple regression model, we are trying to approximate the change in fading parameter as the impacting factors are changed. Therefore, R-squared value of 0.438 is acceptable for this case. If we observe the P values of the independent variables, we can see that they are very small which means that the independent variables are very significant in explaining the variation in fading parameter. Moreover, the *standard errors* (SE) for the coefficients are also very low which confirms the acceptability of this model.

```
Linear regression model:
    y ~ 1 + x1 + x2 + x3

Estimated Coefficients:
                   Estimate     SE          tStat      pValue
    (Intercept)     10.778      0.67806      15.895    1.3587e-46
    x1             -1.6339      0.11359     -14.385    1.0753e-39
    x2             0.16342     0.014623      11.176    4.0654e-26
    x3             0.38371     0.045818      8.3745    5.2636e-16


Number of observations: 520, Error degrees of freedom: 516
Root Mean Squared Error: 1.37
R-squared: 0.438,  Adjusted R-Squared 0.435
F-statistic vs. constant model: 134, p-value = 3.43e-64
```

Fig. 6.37: Regression statistics of the multiple regression model with the experiment data.

	SumSq	DF	MeanSq	F	pValue
x1	390.75	1	390.75	206.93	1.0753e-39
x2	235.85	1	235.85	124.9	4.0654e-26
x3	132.43	1	132.43	70.132	5.2636e-16
Error	974.36	516	1.8883		

	SumSq	DF	MeanSq	F	pValue
Total	1733.4	519	3.3399		
Model	759.02	3	253.01	133.99	3.4314e-64
Residual	974.36	516	1.8883		
. Lack of fit	945.82	276	3.4269	28.817	1.1854e-110
. Pure error	28.541	240	0.11892		

Fig. 6.38: Analysis of Variance (ANOVA) of the multiple regression analysis.

Figure 6.39 shows the residual plot of the estimated fading parameter against the propagation distance between the UAV and ground control station. The residual plot is helpful in determining the violation of homogenous variance. The error term ϵ_i in the model is assumed to be a random variable in ideal condition. This error term cannot be seen visually, although it can be estimated by e_i. These are the residuals which provide the error in the estimated value from the true regression line. This can be given by

$$e_i = y_{i-}\hat{y_i} \tag{6.13}$$

These residuals should show a random fluctuation around zero to show that the assumption of homogenous variance is not violated. From Fig. 6.39, it can be seen that as the regressor variable of distance increases, the error variance does increase slightly. Most of the residuals are plotted around the value of zero with a slight increase at the end as the regressor variable increases. This is due to the fact that the individual relationships with two (gain factor and polarization loss factor) of the independent variables to the dependent variable is non-linear. This non-linear relationship is represented by this multiple regression model as a linear relationship. Thus, the residuals are not plotted randomly around the value of zero. A non-linear transformation to this multiple linear regression model will be able to better represent these relationships and provide a true random residual plot around zero. However, this will be a matter of future study. Moreover, from the residual plot it can be seen that most of the variation of the fading parameter can be explained by this model which is sufficient for an approximation of the fading parameter given the channel conditions.

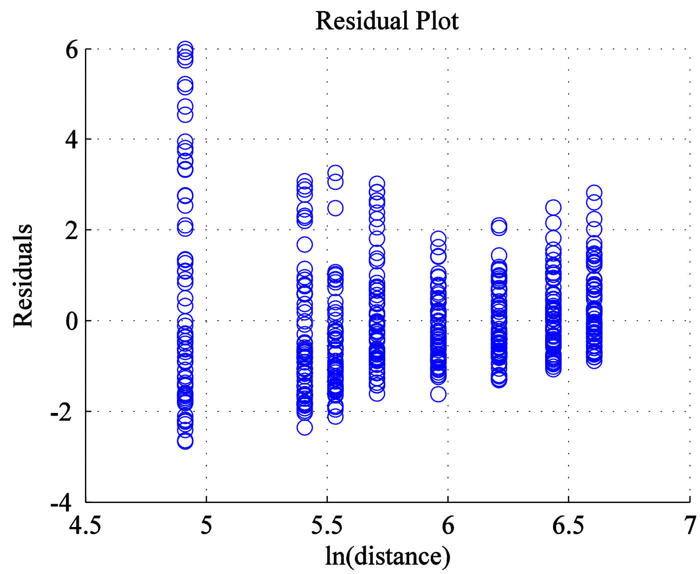

Fig. 6.39: Residual plot.

Figure 6.40 shows the normal probability plot of the residuals. This is also helpful in determining that the error terms are normally distributed or not in the model. The normal probability plot shows the residuals in the horizontal axis and its probability on the vertical axis. If the residuals are truly normally distributed, the plot should resemble a straight line. From Fig. 6.40, we can see that the normal probability plot does show a linear relationship for a certain range of residuals. It deviates from the linear relationship after that range. This confirms the fact that the model is able to explain the fading parameter variation within some boundary conditions. These boundary conditions are confined to the range within which, the experiments are conducted. As stated before, the over simplistic choice of a linear relationship with the dependent variable when the relationship is non-linear is the main reason for this non-linearity in the normal probability plot. However, most of the variation of the fading parameter can be approximated by this model as the normal probability plot shows a straight line appearance within a certain range of residuals.

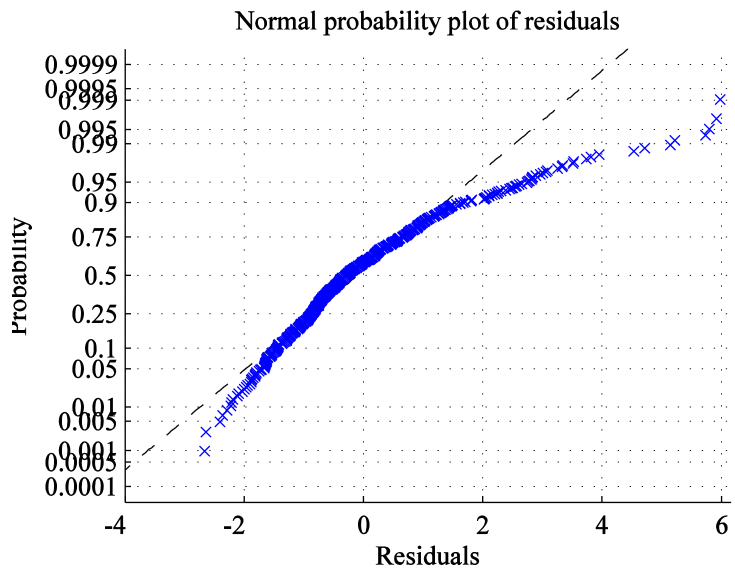

Fig. 6.40: Normal probability plot.

This fact can be reaffirmed by Fig. 6.41 which gives the histogram of residuals for our regression model. The normal distribution of variance can be determined by this histogram of residuals. If the residuals are normally distributed (as it would be in an ideal case), the histogram will resemble a symmetric bell shape which is evenly distributed around the value of zero. From Fig. 6.41, we can see that the histogram of residuals is a little bit skewed and does not show symmetry around zero. This can be also explained by the reasons stated above. However, the skew is very small compared to the data and an approximation can certainly be made from this model about the fading parameter m.

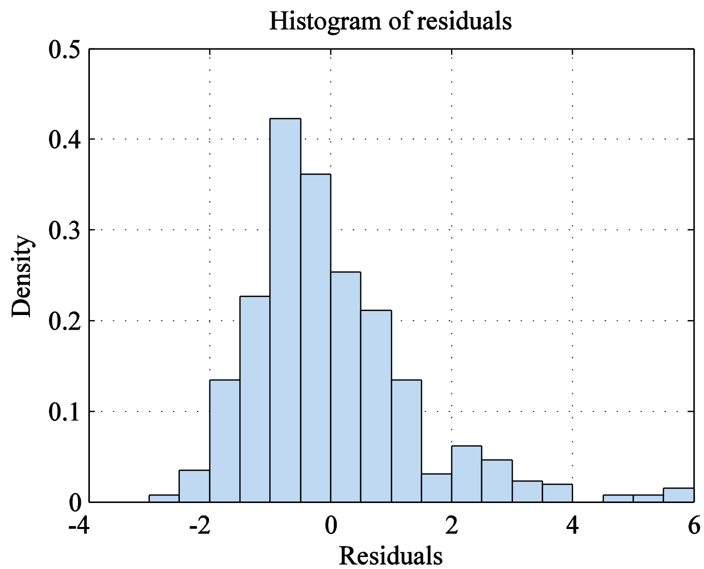

Fig. 6.41: Histogram of residuals.

6.4. Estimation of Model Parameters with Particle Swarm Optimization

In the previous section, we have seen that a multiple linear regression model is developed that is able to estimate the fading parameter m given certain channel conditions. In this section, this model is used in an optimization algorithm that is able to optimize the underlying coefficients of this model which characterizes the channel conditions. The main objective of this algorithm is to estimate the coefficients of the channel conditions (distance, antenna gain factor and polarization loss factor) given the instantaneous fading parameter. Thus this novel algorithm is able to accurately estimate the model parameters that contribute to the fading of the channel.

In this algorithm, a modified version of multidimensional particle swarm optimization technique is employed. The function to be minimized by this optimization algorithm can be given below.

$$\min \; |m - \widehat{m}| = \min \; \left|\left(\beta_0 - \widehat{\beta_0}\right) + x_1\left(\beta_1 - \widehat{\beta_1}\right) + x_2\left(\beta_2 - \widehat{\beta_2}\right) + x_3\left(\beta_3 - \widehat{\beta_3}\right)\right| \tag{6.14}$$

The values of model parameters $\beta_0, \beta_1, \beta_2, \beta_3$ are optimized with boundary conditions given as

$$6 \leq \beta_0 \leq 11$$

$$-3 \leq \beta_1 \leq 0$$

$$0 \leq \beta_2 \leq 3$$

$$0 \leq \beta_3 \leq 3 \tag{6.15}$$

These boundary conditions are confined to the range of values used during the experiments conducted. The algorithm is provided below.

<u>*Algorithm*</u>

(i) *Radio receiver computes initial fading parameter m during a training period*

(ii) *Minimize the function*

(iii) $|m - \widehat{m}| = \left|\left(\beta_0 - \widehat{\beta_0}\right) + x_1\left(\beta_1 - \widehat{\beta_1}\right) + x_2\left(\beta_2 - \widehat{\beta_2}\right) + x_3\left(\beta_3 - \widehat{\beta_3}\right)\right|$

(iv) *Here,* $\widehat{m}$, $\widehat{\beta_0}$, $\widehat{\beta_1}$, $\widehat{\beta_2}$, $\widehat{\beta_3}$ *are predicted estimates from regression model*

(v) *After each iteration of the PSO algorithm, the global best value of the particles are evaluated if* $<|m - \widehat{m}|$

(vi) *If true, the algorithm is stopped and the optimized value of* $|m - \widehat{m}|$ *and coefficients are recorded*

(vii) *Steps i-iv are repeated with these new values until* $|m - \widehat{m}| \sim 0$

(viii) *The optimized coefficients for this* $|m - \hat{m}|$ *value are the optimum coefficient values that closely resembles the actual fading channel*

6.5. Summary

This chapter provides a detailed discussion on the experiments conducted and the results observed for a point-to-point wireless link between a low altitude UAV and a portable ground control station in an urban environment. The channel behavior in terms of large scale and small scale fading is analyzed and compared with different fading channel models. The critical parameters of these models are calculated for this propagation environment. The channel behavior is investigated for two different antenna configurations and the results are provided. Moreover, the effects of some key impacting factors on this wireless channel are analyzed when the ground control station is equipped with a directional Yagi antenna. A multiple regression model is derived from these investigations which estimates the level of fading considering these impacting factors. In addition, a particle swarm optimization based algorithm is developed which is able to predict the underlying channel conditions given the level of fading existent in the channel. In the next chapter, the thesis is concluded by providing an overview on what this thesis achieved. The contributions of this thesis to the scientific community are described along with the findings related to the research questions posed in this thesis. Moreover, some of the limitations of this thesis are talked about which leads to some possible future extensions of this work.

CHAPTER 7

CONCLUSIONS

This chapter provides conclusions drawn from the results, an overview of the observations and findings, a discussion on contributions made, limitations, and some possible future extensions.

7.1. Overview

This thesis presents a comprehensive analysis of large and small scale fading for a time-variant wireless channel between a UAV and a portable ground control station. The large scale fading is analyzed in this wireless channel for a densely populated urban environment. This analysis is conducted for two different antenna configurations. The small scale fading in this wireless channel is also investigated for two antenna configurations. This small scale fading is parameterized by Nakagami fading parameter and its variations due to three factors (propagation distance, antenna gain factor in specific spherical angles and polarization loss factor) are investigated. A multiple regression model is derived which is able to estimate the fading parameter given the channel conditions. This model is statistically evaluated by various measures to investigate its validity. Furthermore, a particle swarm optimization based algorithm is devised that employs this model to optimize the model coefficients that characterizes the underlying channel conditions.

This thesis is motivated due to the technical challenges that arise in predicting the extent of fading in a wireless channel between a UAV and a ground control station operating in an urban environment. This time-variant, dynamic wireless channel poses severe challenges in estimating the small scale fading due to a densely populated urban environment, as well as high mobility of the UAV. From the literature review chapter, it is apparent that multipath fading is one of the key impacting factors that affect the stability and quality of wireless communication in an urban environment. The uncertainty of the propagation environment in an urban scenario poses severe technical challenges in estimation of this fading due to a vast number of buildings, edges, cars, trees densely packed together. Employing a directional antenna in the ground control station increases the range of communication between the UAV and ground control station. However, it has its own set of technical challenges as precise tracking of the UAV antenna is necessary in order to have a stable communication between the two nodes. Highly directional antennas like Yagis provide a high gain which is dependent on the specific spherical angles the antenna is facing. In the case of a directional antenna employed in the ground control station and a UAV equipped with an omnidirectional antenna, deviation in antenna tracking and complex maneuvers of the UAV can cause severe degradation to the antenna gains. This in turn, has a major impact on the performance of the communication. Moreover, micro UAVs (e.g. quadrotors) employ complex aerial maneuvers in its flight dynamics (e.g. roll, pitch and yaw). Therefore, the orientation of the omnidirectional antenna on-board the UAV is constantly changing. This introduces polarization losses in the communication system and degrades the performance of the communication. These factors also add up to the large scale and small scale fading effects of the channel. To ensure the stability and maximum performance gain, these factors need to be considered when estimating the channel fading parameters.

This thesis analyzes this point-to-point wireless link between a UAV and a ground control station which is tested in an urban environment as described above. The large scale and small scale fading parameters are investigated for two antenna configurations (directional-to-omnidirectional and omnidirectional-to-omnidirectional) to determine which configuration gives the optimum performance for this channel environment. Three impacting factors are also investigated for this channel and individual relationships are developed with the fading parameter. The overall effects of these factors on the channel fading are also investigated and a multiple regression model is developed. This model is employed in an optimization algorithm that is able to estimate the underlying channel conditions given the instantaneous fading parameter of the propagation channel.

The individual relationships of these factors with the fading parameters are statistically evaluated through regression analysis and goodness of fit analysis. They show an acceptable performance on the fitting of the data with the model in a certain range. The multiple regression model is also statistically evaluated and shows good performance under certain conditions. This model is further evaluated with normal probability plot, residual histogram and residual plot to provide its validity. The results show a good measure of fit of the model to the data although the fit was not perfect. It can be concluded that, a linear representation of the overall effect of these three impacting factors on the fading parameter is not optimum. As the individual relationships show non-linear correlation, a linear approximation of these factors do not fit the data perfectly.

However, in this thesis, an attempt is made to develop an approximation of the effects on the fading by these three factors which is sufficient to estimate the underlying channel conditions, given the fading information. Moreover, the fading coefficients calculated through regression analysis for this propagation environment, can be validated by previous results published in the literature.

7.2. Thesis Contributions

This thesis makes some unique contributions to the scientific community regarding the propagation characteristics of a point-to-point link between a UAV and a portable ground control station in an urban environment. The introduction chapter provides the critical research questions addressed in this study. This section provides the key observations and findings related to those questions which provide some major contributions in this area of study.

First, the signal propagation between a portable ground control station equipped with a directional Yagi antenna and a UAV equipped with an omnidirectional antenna is investigated. From the results and observations of the experiments conducted, it can be concluded that the received signal amplitude drops from approximately –40 dBm to more than –60 dBm as the propagating distance between the UAV and ground control station increases from 0 to 800 meters. This degradation of amplitude is, however, not linear. The line-of-sight of the propagation path plays a huge role in this variation of amplitude. Paths partially obstructed by building edges suffer more degradation due to signal scattering than paths with longer distances and clearer line-of-sight between the two antennas. This deviation is almost up to 10 dBm for two consecutive ground control station positions spaced within a 100 meters. Moreover, experiments done on different days produced different variations in amplitude in the same distance due to this signal scattering. It can be concluded that the scattering and reflection of the signal in this partially obstructed propagation path is severe and unpredictable which should be taken into account when designing a wireless system between a UAV and a portable ground control station. Moreover, the average received signal amplitude shows a gradual decrease as the distance increases with the standard deviation increasing as the distance increases. The average amplitude drops from –40dBm to –60dBm as the distance increases from 0 to 800 meters and the standard deviation increases from an approximate value of 0.5 to almost 2. However, the standard deviations are very high (approximately 2.25) in very low distances (223 and 301 meters) due to the signal scattering from partial obstructions in the line-of-sight propagation path. This confirms that the obstructions situated in the line of sight of a communication system play a huge part in the fading analysis of the channel. For a communication scheme involving a fast moving UAV and a portable ground control station, this can be very detrimental in achieving a maximum performance gain.

However, when the ground control station and the UAV node are both equipped with omnidirectional antennas, the received signal amplitude decreases considerably as the distance increases. The amplitude drops from approximately –50 dBm to as low as –110 dBm as the distance increases from 0 to 800 meters. But, this decrease has a more linear fashion than its directional antenna counterpart. The average of the signal amplitude also shows a gradual decrease from –56 dBm to little less than –100 dBm and this too, has a linear resemblance. The standard deviation of the signal amplitude increases considerably in this configuration from 1.2 dB to as much as 4.1 dB as the distance increases. This also shows a more linear correlation with the distance. This confirms the fact that omnidirectional antennas perform more predictably in low propagation distances for partially obstructed line of sight operations. As the distance increases, the performance degrades due to low gains of these antennas. On the other hand, directional antennas show better performance in further distances due to its high directionality and gain. However, it is more prone to signal scattering in lower distances due to partial obstructions in the line-of-sight path. This makes the small scale fading analysis and estimation of this channel, a major technical challenge.

For a portable ground control station equipped with a directional Yagi antenna and a UAV node equipped with an omnidirectional antenna operating in an urban environment, the propagation channel closely resembles a Dual Slope Piecewise Linear model for path loss and shadowing. The experiments are conducted with both directional antenna and omnidirectional antenna in the ground control station for performance comparisons. From the results, it is shown that for both antenna configurations, a critical distance of 253 meters is found for a propagation distance of 0 to 800 meters. For the directional antenna configuration, the path loss exponents are found as $\gamma_1 = 3.111$ and $\gamma_2 = 2.559$. For the omnidirectional antenna, these path loss exponents are found as $\gamma_1 = 1.727$ and $\gamma_2 = 8.819$. This proves that directional antennas provide better performance in larger distances but perform poorly in close proximity due to partial obstructions in the propagation path. The path loss and shadowing is also represented with a widely used Log Normal Shadowing model with both antenna configurations to compare against the Dual Slope Piecewise Linear model. For the Log Normal Shadowing model, the directional-to-omnidirectional antenna setting provides path loss exponent of $\gamma = 2.346$ where the omnidirectional-to-omnidirectional antenna configuration provides a path loss exponent of $\gamma = 5.293$. This result confirms our observations and assumptions stated above.

The small scale fading of this wireless channel is also analyzed and investigated for directional-to-omnidirectional and omnidirectional-to-omnidirectional antenna configurations.

This multipath fading is represented by two widely used models, its parameters calculated and compared with both antenna configurations. First, the small scale fading is modeled with a Gaussian fading model and its standard deviations are calculated through regression analysis. For the Dual Slope Piecewise Linear model, the directional antenna provides standard deviations of $\sigma_1 = 0.3159$ dB and $\sigma_2 = 0.5121$ dB. However, the omnidirectional antenna provides standard deviations of $\sigma_1 = 1.826$ dB and $\sigma_2 = 2.569$ dB. This data proves that the directional-to-omnidirectional antenna configuration provides better performance in small scale fading against the omnidirectional-to-omnidirectional link. For the Log-Normal Shadowing model, the directional and omnidirectional antenna provides standard deviations of $\sigma = 3.854$ dB and $\sigma = 7.189$ dB, respectively.

The small-scale fading is represented by Nakagami fading model and the severity of fading is parameterized by a fading parameter m. This m parameter is calculated as the propagation distance is varied from 0 to 800 meters. For a directional antenna, the fading parameter varies from 10.7851 for a distance of 136 meters to 1.62976 for a distance of 739 meters. For an omnidirectional antenna this m parameter varies from 3.96352 to 0.398284 for the same distances. This further confirms the fact that the directional antenna performs much better than its omnidirectional counterpart.

The individual models relating the Nakagami fading parameter m with the propagation distance, antenna gain factor in specific spherical angles and polarization loss factor provide some critical observations for this wireless channel. The fading parameter decreases in a linear fashion against increasing propagation distance. The fading parameter increases exponentially as the antenna gain factor is increased between the two antennas. Moreover, when the polarization loss factor increases, the fading parameter also increases. Here, the polarization loss factor is given as a value from 0 to 1 with 1 being no polarization loss and 0 being complete polarization mismatch.

Multiple regression analysis is conducted on the experiment data to develop a linear approximation model on the overall impact on fading by these three impacting factors. This model suggests that propagation distance has the biggest impact on the fading parameter due to increase in multipath propagation by objects in the environment. The second biggest impact is caused by the polarization loss factor between the two antennas. The third impacting factor is the antenna gain factor in specific spherical angles of the transmit and receive antennas. This model is statistically evaluated and the results suggest that it is able to account for almost 43% of variations in the fading parameter from the experiment data. An analysis of variance (ANOVA) is conducted on the model and fitting of data which gives good results for an approximation of the channel conditions by this model. Lastly, a modified particle swarm optimization based algorithm is developed which uses this model to estimate the underlying channel conditions from instantaneous fading information. The modifications made to the original particle swarm optimization technique along with the algorithm are provided in the results and discussions chapter.

This thesis provides some major contributions to the study of the wireless channel between a low altitude UAV and a portable ground control station operating in an urban environment. The large scale fading of this link is analyzed and the Dual Slope Piecewise Linear model is concluded as the best model that characterizes this channel. The path loss exponents for this model is also calculated which would be crucial to the wireless link design for a micro UAV system. The small scale fading is also analyzed for this link with the path loss exponents calculated. This will be critical in the correct estimation and prediction of multipath fading that exist in this type of propagation environments. Moreover, for a micro UAV and portable ground control station, the best antenna configuration is investigated which provides maximum performance gain for this link. This will be a key factor when designing the communication system between UAVs and ground control stations. In addition, the three major impacting factors for the wireless link (distance, antenna gain factor and polarization loss factor) are investigated and their relationships with the small scale fading parameter are developed. This will be also very important in estimation and prediction of fading in the wireless link in these systems. This can be beneficial to the implementation of an optimum power control strategy for cognitive radio systems employed in UAV communications to increase the range and operation time of this communication link.

7.3. Limitations and Future Work

This thesis provides some key contributions to the area of wireless communications between a UAV and a portable ground control station. However, there are some limitations in this study which can be improved to provide a better analysis. These limitations and areas for possible extension to this research work are provided below.

(i) In the experiments conducted, a UAV in flight is simulated by placing a transmitting node in a certain altitude. The position and orientation of this node are kept constant by physical means. However, as stated before, a micro UAV (especially quadrotors) employ complex maneuvers in its flight dynamics. Even in a stable flight position, the orientation of these UAVs is constantly changing to preserve its balance on air. These minute but rapid orientation shifts can affect the orientation of the on-board antenna which in turn will affect the communication as well. Having a real quadrotor UAV in flight during the experimentation phase will provide sufficient data to investigate these effects. This can be a possible extension to this work and will be able to provide further analysis of the fading channel.

(ii) This study uses an omnidirectional antenna on board the UAV node to measure the path loss, shadowing and multipath fading effects on the wireless channel. A combination of directional-to-omnidirectional and omnidirectional-to-omnidirectional antenna configurations is analyzed. Although, mounting a directional antenna on-board a micro UAV is challenging itself, directional antennas with advanced gimbal system can increase the range of communication drastically for this point-to-point link. The impacts of different delimiting factors on this directional-to-directional link can be an interesting area of possible extension of this work.

(iii) Employing multiple antennas on both the UAVs and ground control station to implement MIMO (Multiple Input Multiple Output) based techniques can provide a better solution to mitigate the effects of multipath propagation. This can be an area of future exploration.

(iv) The transceivers used in the experiments employ a Frequency Hopping Spread Spectrum (FHSS) technique to transmit and receive signals. For these systems, it is often found that there is an offset in frequencies. Moreover, the hopping sequence also plays an important role in its performance. The effects of these phenomena in this communication scheme needs to be analyzed and can provide significant findings.

(v) One possible extension of this research is to employ *Direct Sequence Spread Spectrum* (DSSS) radios in the communication scheme and to investigate the effects of processing gain control to mitigate adverse effects.

(vi) In this study, the experiments are conducted by manually changing the orientation of the ground control station antenna in different spherical angles. These spherical angles are measured by an android application which uses the sensors in a Samsung Note III mobile phone to measure the azimuth and elevation angles. However, this system can be improved by using high precision sensors, integrated with the ground control station system to provide the specific spherical angles the antenna is facing towards, during experiments. This can be regarded as a future work in this thesis.

(vii) This study is confined to a low altitude UAV operating in an urban environment and communicating with a portable ground control station. For high altitude UAVs and balloons communicating with a ground based control station, this point-to-point communication link will be affected by ionospheric absorption of electromagnetic waves. Investigation of these effects can be a valuable extension to this work.

This page intentionally left blank

REFERENCES

[Theu09] The UAV. (2009, Aug. 23).*UAV* [Online]. Available: http://theuav.com/ [November 5, 2014].

[Wiki14] Wikipedia. (2014, Apr. 11). *Unmanned Aerial Vehicle* [Online]. Available: http://en.wikipedia.org/wiki/Unmanned_aerial_vehicle [November 1, 2014]

[Mahm07] Shahid Mahmood, ”Unmanned Aerial Vehicle (UAV) Communications,” M.S. thesis, Dept. Electrical Engineering, Blekinge Institute of Technology, Sweden, 2007

[Myli07] Alicia K. Mylin,”A Communication Link Reliability Study for Small Unmanned Aerial Vehicles,” M.S. thesis, Dept. Electrical Engineering, University of Kentucky, 2007

[RFGL13] Steven Recoskie, Atef Fahim, Wail Gueaieb, and Eric Lanteigne. “Experimental testing of a hybrid power plant for a dirigible UAV,” *Journal of Intelligent & Robotic Systems*, vol. no. 69:69, issue no. 81, 2013.

[LIED08] Mariano I. Lizarraga, David M. Ilstrup, Gabriel Hugh Elkaim, and James Davis, “Aerial photography using a nokia n95,” in *World Congress on Engineering and Computer Science*, October 2008.

[Mamm13] Elchin Mammadov,”Long-range Communication Framework for Autonomous UAVs,” M.S. thesis,Dept.Electrical and Computer Engineering,University of Ottawa, Ottawa, 2013

[Qine10] QinetiQ. (2010, Jul. 16). *QinetiQ’s Zephyr solar powered unmanned aircraft soars to new world records* [Online]. Available: http://www.qinetiq.com/media/news/releases/pages/zephyr-2010.aspx [September 20, 2014]

[Gold04] Andrea Goldsmith, *Wireless Communications*. Cambridge University Press, Cambridge, 2004

[Roch99] Wolfgang W. Rochus, “UAV data-links: Tasks, types, technologies and examples,” in *Development and Operation of UAVs for Military and Civil Applications*, September 1999.

[ZhZa07] Guoqing Zhou and Deyan Zang, “Civil UAV system for earth observation,” in *Geo-science and Remote Sensing Symposium*, 2007. IGARSS 2007. IEEE International, 2007.

[ShKS00] D. H. Shim, H. J. Kim, and S. Sastry, “Hierarchical control system synthesis for rotorcraft-based unmanned aerial vehicles,” in *American Institute of Aeronautics & Astronautics Guidance, Navigation and Control Conference*, 2000.

[Sarr01] Z. Sarris, “Survey of UAV applications in civil markets,” in *IEEE Mediterranean Conference on Control and Automation*, June 2001.

[GoDW10] Niklas Goddemeier, Kai Daniel, and Christian Wietfeld, “Coverage evaluation of wireless networks for unmanned aerial systems,” in *IEEE GLOBECOM Workshops*, 2010.

[WzLD06] Mariusz Wzorek, David Landen, and Patrick Doherty, “GSM technology as a com-munication media for an autonomous unmanned aerial vehicle,” in *21th Bristol UAV Systems Conference*, 2006.

[CHSB07] L. Cheng, B. Henty, D. Stancil, F. Bai and P. Mudalige,"Mobile vehicle-to-vehicle narrow-band channel measurement and characterization of the 5.9 GHz dedicated short range communication (DSRC) frequency band,"in *IEEE Journal on Selected Areas in Communications*, vol. 25, no. 8, pp. 1501 — 1516, 2007.

[CHBS08] L. Cheng, B.E. Henty, F. Bai, and D. D. Stancil, "Highway and Rural Propagation Channel Modeling for Vehicle-to-Vehicle Communications at 5.9 GHz," in *IEEE Antennas and Propagation Society International Symposium*, 2008.

[GPRB10] G. P. Grau, D. Pusceddu, S. Rea, O. Brickley, M. Koubek, D. Pesch,"Vehicle-2-vehicle communication channel evaluation using the CVIS platform," *in IEEE Communication Systems Networks and Digital Signal Processing (CSNDSP) symposium*, July, 2010.

[BeCh01] N. C. Beaulieu and C. Cheng, "An Efficient Procedure for Nakagami-m Fading Simulation," in *Proc. of IEEE Globecom 2001*, volume 6, pp.333, Nov 2001.

[Isla13] Tarikul Islam,”Statistical Modeling of Intelligent Transportation Systems Communication Channels,” M.S. thesis, Dept. Telecommunications, Delft University of Technology,Delft, Netherlands, 2013

[StTh98] W. L. Stutzman and G. A. Thiele, *Antenna Theory and Design*, 2nd Ed. USA: John Wiley & Sons, Inc., 1998.

[Bala97] C. A. Balanis, *Antenna Theory: Analysis and Design*, 2nd Ed. New York: John Wiley & Sons, Inc., 1997.

[PaJu10] MyungGu Park and Jaeil Jung, “An analysis of communication performance ac-cording to antenna directionality in UAV operation environment,” in *2nd IEEE International Conference on Network Infrastructure and Digital Content*, 2010.

[CHKV06] Chen-Mou Cheng, Pai-Hsiang Hsiao, H. T. Kung and Dario Vluh, "Performance Measurement of 802.11a Wireless Links from UAV to Ground Nodes with Various Antenna Orientations," in *15th International conference on Computer Communications and Networks*, Arlington, VA,9-11 October.2006,pp-303-308.

[AHPP07] J. Allred, A. B. Hassan, S. Panichsakul, W. Pisane, P. Gray, J. Houang, R. Han, D. Lawrence, and K. Mohseni ,"SensorFlock: An Airborne Wireless Sensor Network of Micro-Air Vehicle," in *Proceedings of SenSys2007*, 2007, pages 117-129.

[Cana07] Industry Canada. Radio Standards Specification 210, Issue 7, Low-power Licence-exempt Radiocommunication Devices (All Frequency Bands): Category I Equipment., 2007.

[SPSM12] V. Shivaldova, A. Paier, D. Smely and C.F. Mecklenbrauker, "On roadside unit antenna measurements for vehicle-to-infrastructure communications," in *IEEE 23rd International Symposium on Personal Indoor and Mobile Radio Communications (PIMRC)*, 2012, pp.1295,1299, 9-12 Sept. 2012.

[JaYe06] H. Jasani and K. Yen, "Performance improvement using directional antennas in ad hoc networks," in *International Journal of Computer Science and Network Security*, vol. 6, no. 6, pp. 180–188, 2006.

[RRSW05] R. Ramanathan, J. Redi, C. Santivanez, D. Wiggins, and S. Polit, "Ad hoc networking with directional antennas: A complete system solution," *IEEE JOURNAL*, vol. 23, no. 3, pp. 496–506, 2005.

[BRMD07] Quirino Balzano, John Rzasa, Stuart Milner, and Christopher Davis, "High capacity tactical networks with recongerable, steerable, narrow-beam agile point-to-point rf links," in *IEEE Military Communications Conference*, 2007.

[JeGH07] Jenvey S., Gustafsson J., and Henriksson F, "A portable monopulse tracking antenna for UAV communications," in *22nd International Unmanned Air Vehicle Systems Conference*, 2007.

[TMCH08] S. Teh, L. Mejia, P. Corke, and W. Hu. "Experiments in Integrating Autonomous Uninhabited Aerial Vehicles (UAVs) and Wireless Sensor Networks.", in *Proceedings of The 2008 Australasian Conference on Robotics and Automation (ACRA 08)*, 2008

[Mems14] Memsic, Inc. (2005, Feb. 13). *Wireless Sensor Networks* [Online]. Available: http://www.memsic.com/wireless-sensor-networks/ [September 26, 2014]

[Lee12] Hyeon-Cheol Lee, " UAV Position Estimation Using Remote Radio Head With Adaptive Power Control," *International Science Index*, vol.6, issue.3, pp 284-288, March, 2012

[NBRG02] J. Neel, R. M. Buehrer, J. H. Reed, and R. P. Gilles, “Game theoretic analysis of a network of cognitive radios,” in *Midwest Symposium on Circuits and Systems*, 2002

[MaSW01] MacKenzie, Allen B. Stephen B. Wicker, “Game Theory in communications: Motivation, explanation, and application to power control,” in *Globecom*, 2001

[Hayk05] S. Haykin, “Cognitive radio: Brain-empowered wireless communications,” *IEEE Journal on Selected Areas in Communications*, vol. 23, no. 2 , pp.201-220, Feb. 2005.

[HoSa05] N. Hoven and A. Sahai, “Power scaling for cognitive radio,” in *IEEE 2005 International Conference on Wireless Networks, Communications and Mobile Computing*, vol. 1,pp. 250-255, June 2005.

[WaFW06] J. Wang, Y. Fang, and D. Wu, “Syn-dmac: A directional mac protocol for ad hoc networks with synchronization,” *IEEE JOURNAL*, vol. 4, no. 3, pp. 2258–2263, 2006.

[KoSV00] Y.-B. Ko, V. Shankarkumar, and N. H. Vaidya, “Medium access control protocols using directional antennas in ad hoc networks,” in *INFOCOM 2000. Nineteenth Annual Joint Conference of the IEEE Computer and Communications Societies. Proceedings. IEEE)*, 2000.

[TMRB02] M. Takai, J. Martin, A. Ren, and R. Bagrodia, “Directional virtual carrier sensing for directional antennas in mobile ad hoc networks,” in *ACM MOBIHOC*, 2002.

[CBTA08] J. M. de la Cruz, E. Besada-Portas, L. Torre-Cubillo, B. Andres-Toro, and J. A. Lopez-Orozco, “Evolutionary path planner for uavs in realistic environments,” in *GECCO'08*, pages 1477{1484, Atlanta, Ga, July 2008.

[RiWB05] M. D. Richards, D. Whitley, and J. R. Beveridge,”Evolving cooperative strategies for uav teams,” in *GECCO '05*, pages 1721-1728, Washington, D.C., June 2005.

[MiDJ07] D. Miller, P. Dasgupta, and T. Judkins, “Distributed task selection in multi-agent based swarms using heuristic strategies,” Lecture Notes in Computer Science, 2007.

[BaOS08] G. J. Barlow, C. K. Oh, and S. F. Smith, “Evolving cooperative control on sparsely distributed tasks for uav teams without global communication,” in *GECCO'08*, Atlanta, Ga, July 2008.

[InTU13] International Telecommunication Union. (2013, November). *Propagation Data and Prediction Methods required for the design of terrestrial line-of-sight systems*. ITU-R. Geneva, Switzerland. [Online]. Available: http://www.itu.int/dms_pubrec/itu-r/rec/p/R-REC-P.530-15-201309-I!!PDF-E.pdf

[August 4, 2015]

[AdKe51] Arthur I. Aden and Milton Kerker. (1951, October). “Scattering of Electromagnetic Waves from Two Concentric Spheres,” *Journal of Applied Physics* [Online], vol. 22, pp. 1242-1246. Available: http://dx.doi.org/10.1063/1.1699834 [January 9, 2015]

[GuEa54] K.L.S. Gunn and T.W.R. East, ”The Microwave Properties of Precipitation Particles,” *Quarterly J. Meteorolog. Society,* vol. 80, pp.522-545, 1954.

[TaNa66] M. Takada and S. Nakamura, ”Attenuation of 11 Gc Waves by wet snow-fall,” *Rev.Elect.Commun.Lab.*, vol. 14, no.1-2, pp. 27-42, Jan. 1966.

[Nish71] A. Nishitsuji, “Method of Calculation of radio-wave attenuation in snowfall,” *Electron.Commun.Jpn.,*vol. 54-B, no. 1, 1971.

[KOSM83] M. Kharadly, N. Owen, J. Van der Star, D. Michelson and T.Energren,”Observations of abnormal microwave propagation phenomena during melting layer conditions,” in *International Conference on Antennas and Propagation(ICAP),*Norwich, U.K., April 12-15, 1983, vol. 12, pp. 503-509.

[HASO81] A. Hendry, Y. M. M. Antar, J.J. Schelesak, and R.I. Olsen,”Melting layer attenuation at 28.6 GHz from simultaneous Comstar beacon and polarization diversity data,” *Electron.Lett.*, vol. 17, no. 5, pp. 190-191, Mar. 5, 1981.

[InTU02] International Telecommunication Union, *Development Towards a Model for Combined Rain and Sleet Attenuation,* ITU-R, Geneva, Switzerland, ITU-R Document 3M/62F, 2002.

[Rapp01] T.S. Rappaport, *Wireless Communications - Principles and Practice*, 2nd Edition, Prentice Hall, 2001.

[Patz02] M. Patzold, *Mobile Fading Channels*. New York: Wiley. 2002.

[EGTP99] V. Erceg, L. J. Greenstein, S. Y. Tjandra, S. R. Parkoff, A. Gupta, B. Kulic, A. A. Julius, and R. Bianchi, “An empirically based path loss model for wireless channels in suburban environments,” in *IEEE Journal on Selected Areas in Communications*, pp. 1205–1211, July 1999.

[GGKS03] S.S. Ghassemzadeh, L.J. Greenstein, A. Kavcic, T. Sveinsson, V. Tarokh, “Indoor path loss model for residential and commercial buildings,” in *Proceedings of Vehicular Technology Conference*, pp. 3115–3119, Oct. 2003.

[CoTh91] T. Cover and J. Thomas, *Elements of Information Theory*. New York: Wiley, 1991.

[Pons15] Rafael Pons. (2015, Jan. 13). *Understanding Azimuth and Elevation* [Online]. Available: http://www.photopills.com/articles/understanding-azimuth-and-elevation [August 5, 2015]

[Sats04] Satsig. (2004, Oct. 24). *Explanation of Azimuth and Elevation* [Online]. Available: http://www.satsig.net/azelhelp.htm [August 5, 2015]

[Mhed07] Mheducation. (2007, Oct. 19). Antenna Basics [Online]. Available: http://highered.mheducation.com/sites/dl/free/0072321032/62577/ch02_011_056.pdf [August 04, 2015]

[Wiki15] Wikipedia. (2015, Jul. 18). Numerical Electromagnetics Code [Online]. Available: https://en.wikipedia.org/wiki/Numerical_Electromagnetics_Code [August 4, 2015]

[Lewa09] Sam LeWallen. (2009, Aug.02). Eznec Antenna Software by W7EL [Online]. Available: www.eznec.com [August 4, 2015]

[ReCo06] Margarita Reyes-Sierra and Carlos A. Coello Coello,"Multi-Objective Particle Swarm Optimizers: A Survey of the State-of-the-Art," *International Journal of Computational Intelligence Research*, vol. 2, No. 3, pp. 287-308, September, 2006

[BoYo11] Charles W. Bostian and Alexander R. Young. (2011, June). *The Application of Cognitive Radio to Coordinated Unmanned Aerial Vehicle (UAV) Missions*. Air Force Research Laboratory. Blacksburg, Virginia, USA [Online]. Available: http://www.dtic.mil/dtic/tr/fulltext/u2/a546145.pdf [August 5, 2015]

[WaRS09] Manish Wadhwa, Min Song, Vinary Rali and Sachin Shetty. (2009, August). "The Impact of Antenna Orientation on Wireless Sensor Network Performance," in *IEEE International Conference on Computer Science and Information Technology* [Online], Beijing, 2009, vol. 3, pp. 143-147. Available: http://ieeexplore.ieee.org/xpl/login.jsp?tp=&arnumber=5234978&url=http%3A%2F%2Fieeexplore.ieee.org%2Fxpls%2Fabs_all.jsp%3Farnumber%3D5234978 [August 5, 2015]

[BAFB06] J. Buckley, K. Aherne, B. O' Flynn, J. Barton, A. Murphy and C.O. Mathuna,"Antenna Performance Measurements Using Wireless Sensor Networks," in *IEEE International Conference on Electronic Components and Technology*, San Diego, California, USA. June 2006, vol. 2, pp.1652-1657.

[JoFH06] R.H. Johnston, I.G. Finvers, J.W. Haslett,"Antenna Optimization for RF Mote Communication," in *IEEE International Symposium on Antenna and Propagation Society*, Singapore City, Singapore. July 2006, vol. 6, pp.2133-2136.

[LyLS06] Dimitrios Lymberopoulos, Quentin Lindsey and Andreas Savvides,"An Empirical Characterization of Radio Signal Strength Variability in 3D IEEE 802.15.4 Networks Using Monopole Antennas," in *International Conference on Embedded*

Wireless Systems and Networks, Zurich, Switzerland. February 13-15, 2006, vol. 1, pp.326-341.

[LZZG06] Shan Lin, Jingbin Zhang, Gang Zhou, Lin Gu, Tian He and John A. Stankovic,"ATPC: Adaptive Transmission Power Control for Wireless Sensor Networks," in *The 4th ACM Conference on Embedded Networked Sensor Systems ,* Boulder, Colorado, USA. October 31, 2006, vol. 5, pp.156-159.

[WaZh08] Wenye Wang and Ming Zhao," Joint Effects of Radio Channels and Node Mobility on Link Dynamics in Wireless Networks," in *IEEE International Conference on Computer Communications*, Phoenix, Arizona, USA. April 15-17, 2008, vol. 3, pp. 1606-1614.

[KJTT08] C. E. Koksal, K. Jamieson, E. Telatar and P. Thiran," Impacts of Channel Variability on Link-Level Throughput in Wireless Networks," in *Joint International Conference on Measurement and Modeling of Computer Systems*, Saint-Malo, France. June 26-30, 2006, vol. 1, pp. 351-356.

[Sain11] Sanja Sain, "Modelling and Characterization of Wireless Channels in Harsh Environments" [Online], M.Sc. thesis, School of Innovation, Design and Engineering, Malardalen University, Vasteras, Sweden, 2011. Available: www.idt.mdh.se/utbildning/exjobb/files/TR1154.pdf [August 5, 2015]

[DuHH00] Alexandra Duel-Hallen, Shengquan Hu and Hans Hallen. (2000, June)." Long Range Prediction of Fading Signals: Enabling Adaptive Transmission for Mobile Radio Channels," *IEEE Signal Processsing Magazine* [Online], vol. 1, pp. 1-26. Available: http://citeseerx.ist.psu.edu/viewdoc/download?doi=10.1.1.86.6838&rep=rep1&type=pdf [August 5, 2015]

[PILS06] Eline Pajala, Tero Isotalo, Abdelmonaem Lakhzouri and Elena Simona Lohan. (2006, March)." An Improved Simulation Model for Nakagami-*m* Fading Channels for Satellite Positioning Applications," in *Proceedings of the 3rd Workshop on Positioning, Navigation and Communication* [Online], Hannover, Germany, 2006, vol. 2, pp. 81-89. Available: http://wpnc.net/fileadmin/WPNC06/Proceedings/15_An_improved_simulation_model_for_Nakagami-m_fading_channels.pdf [August 5, 2015]

[LLSR05] Abdelmonaem Lakhzouri, Elena Simona Lohan, I. Saastamoinen and M. Renfors," Measurement and Characterization of Satellite-to-Indoor RadioWave Propagation Channel," in *Proceedings of the European Navigation Conference*, Munich, Germany, 2005, vol. 2, pp. 349-360.

[LaLS05] Abdelmonaem Lakhzouri, Elena Simona Lohan, I. Saastamoinen and M. Renfors,"On Second Order Statistics of the Satellite-to-indoor Channel based on Field Measurements," in *Proceedings of IEEE 16th International Symposium on*

Personal, Indoor and Mobile Radio Communications, Berlin, Germany, 2005, vol. 4, pp. 154-160.

[LaLo05] Abdelmonaem Lakhzouri, Elena Simona Lohan, I. Saastamoinen and M. Renfors," Interference and Indoor Channel Propagation Modeling based on GPS Satellite Signal Measurements," in *Proceedings of the 18th International Technical Meeting of the Satellite Division of The Institute of Navigation*, Long Beach, California, USA, 2005, vol. 1, pp. 661-670.

[LaLR04] Abdelmonaem Lakhzouri, Elena Simona Lohan and M. Renfors," Statistical Properties of Urban WCDMA Channel for Mobile Positioning Applications," *International Journal of Wireless and Optical Communications*, vol. 2, issue. 2, pp. 344-352, December, 2004.

[SOSL94] M. K. Simon, J. K. Omura, R. A. Scholtz and B. K. Levitt, *Spread Spectrum Communication Handbook*. New York, McGraw-Hill, 1994.

[TaHo03] Li Tang and Zhu Hongbo. (2003, November)." Analysis and Simulation of Nakagami Fading Channel with MATLAB," in *Proceedings of the Asia Pacific Conference on Environmental Electromagnetics* [Online], Hangzhou, China, 2003, vol. 1, pp. 490-494. Available: http://ieeexplore.ieee.org/xpl/login.jsp?tp=&arnumber=1282377&url=http%3A%2F%2Fieeexplore.ieee.org%2Fxpls%2Fabs_all.jsp%3Farnumber%3D1282377 [August 5, 2015]

[BADD04] T. X. Brown, B. Argrow, C. Dixon, S. Doshi, R. G. Thekkekunel and D. Henkel," Ad Hoc UAV Ground Network (AUGNET)," in *Proceedings of AIAA 3rd "Unmanned Unlimited" Technical Conference, Workshop and Exhibit*, Chicago, Illinois, USA, 2004, vol. 2, pp. 1078-1084.

[AHPP07] J. Allred, A. B. Hasan, S. Panichsakul, W. Pisano, P. Gray, J. Huang, R. Han, D. Lawrence and K. Mohseni," Sensorflock: an airborne wireless sensor network of micro-air vehicles," in *Proceedings of International Conference on Embedded Networked Sensor Systems(SENSYS)*, Sydney, Australia, 2007, vol. 1, pp. 354-358.

[CHKV06] C. M. Cheng, P. H. Hsiao, H. Kung and D. Vlah," "Performance measurement of 802.11a wireless links from UAV to ground nodes with various antenna orientations," in *Proceedings of International Conference on Computer Communications and Networks*, Arlington, Virginia, USA, 2006, vol. 3, pp. 678-689.

[FMTN06] Q. Feng, J. Mcgeehan, E. Tameh and A. Nix," Path loss models for air-to-ground radio channels in urban environments," in *Proceedings of IEEE Conference on Vehicular Technology*, Melbourne, Australia, 2006, vol. 5, pp. 987-992.

[YaKB11] Evsen Yanmaz, Robert Kuschnig and Christian Bettstetter,” Channel Measurements over 802.11a-based UAV-to-Ground Links,” in *Proceedings of IEEE Global Communications Conference, Exhibition and Industry Forum (GLOBECOM)*, Houston, Texas, USA, 2011, vol. 1, pp. 1280-1284.

[Comm14] AFAR Communications. (2014, Nov. 5). *900 MHz versus 2.4 GHz in long distance links* [Online]. Available: http://www.afar.net/tutorials/900-mhz-versus-2.4-ghz/ [August 5, 2015]

[Mura10] Murata. (2010, Aug. 16) *DNT900 Series* [Online]. Available: http://wireless.murata.com/datasheet?/RFM/data/dnt900dk_manual.pdf?ref=rfm.com [April 24, 2014]

[Wiki09] Wikipedia. (2009, Mar. 3). *Raspberry Pi* [Online]. Available: http://en.wikipedia.org/wiki/Raspberry_Pi [May 1, 2014]

[Ftdi14] FTDI. (2014) *FT232R-USB UART IC* [Online]. Available: http://www.ftdichip.com/Products/ICs/FT232R.htm [April 26, 2014]

[Ante08] Antenna-theory. (2008) *Antenna Basics* [Online]. Available: http://www.antenna-theory.com/basics/main.html [April 28, 2014]

[Hamu00] Hamuniverse. (2000) *Basic Antenna Design for the Experimenter* [Online]. Available: http://www.hamuniverse.com/yagibasics.html [April 25, 2014]

[Wiki14] Wikipedia. (2014, Sep. 13) *RF Connector* [Online]. Available: http://en.wikipedia.org/wiki/RF_connector [April 29, 2014]

[Smac14] Wikipedia. (2014, Jul. 31) *SMA Connector* [Online]. Available: http://en.wikipedia.org/wiki/SMA_connector#Reverse_polarity_SMA [April 29, 2014]

[Ncon14] Wikipedia. (2014, Jun. 18) *N Connector* [Online]. Available: http://en.wikipedia.org/wiki/N_connector [April 29, 2014]

[Elec14] Tiptop Electronics. (2014) *Antenna Tripod with Mast* [Online]. Available: http://www.tiptopelectronics.com/home.asp?ProdDetail=TRIPOD [April 29, 2014]

[Adaf14] Adafruit. (2014) *USB Battery Pack for Raspberry Pi* [Online]. Available: http://www.adafruit.com/products/1566 [May 2, 2014]

[Conr14] Conrad. (2014*) PNY SD8G10PER-EF 8GB SD Card Class 10, UHS-I 30MB/s* [Online]. Available: http://www. conrad.com/ce/en/product/562220/PNY [July 2, 2014]

[Adaf13] Adafruit. (2013) *Raspberry Pi Camera Board*[Online]. Available: http://www.adafruit.com/products/1367 [May 2, 2013]

[Wilk12] Wilkerson. (2012) *2.1 dBi Gain*[Online]. Available: www.instrumart.com/assets/wilkerson-antenna_datasheets.pdf [May 3, 2014]

[Arch11] Wikipedia. (2011, Oct. 23) *Arch Linux* [Online]. Available: http://en.wikipedia.org/wiki/Arch_Linux [May 05, 2014]

[Comp08] Anritsu Company," User Guide VNA Master MS2024A/MS2026A and MS2034A/MS2036A," Revision C, Morgan Hill, California: Anritsu Company, 2008.

[Wiki09] Wikipedia. (2009, December). *Antenna Aperture* [Online]. Available: https://en.wikipedia.org/wiki/Antenna_aperture [August 6, 2015]

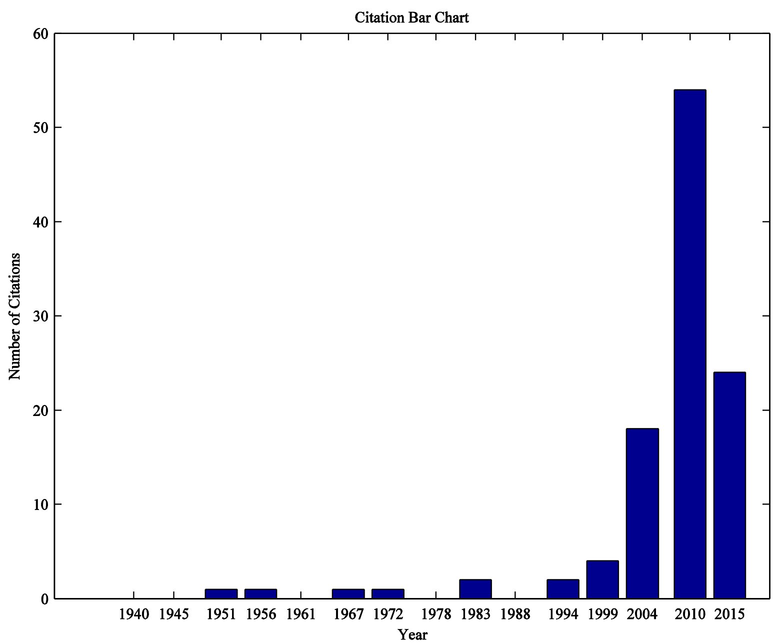

Fig. 8.1: Citation bar chart

Appendices

Table of Contents

List of Figures

Appendix A

Raspberry Pi Schematic

Figure A.1 shows the hardware schematic of Raspberry Pi model B revision 2.0 used in this thesis.

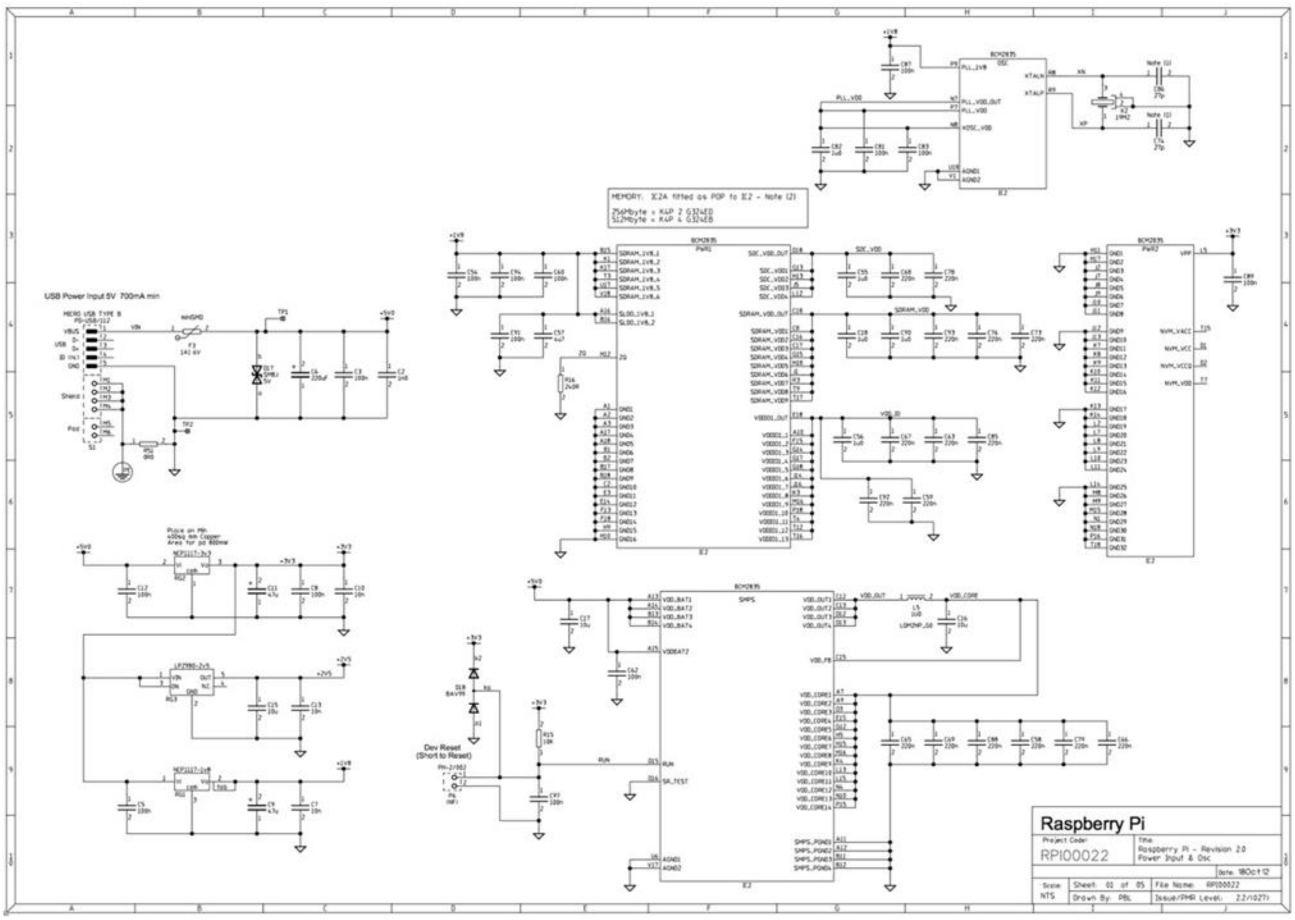

Fig. A.1: Raspberry Pi model B revision 2.0 hardware schematic.

Appendix B

DNT900 Radio Hardware Block Diagram

Figure B.1 shows the hardware block diagram of the DNT900 radio transceiver.

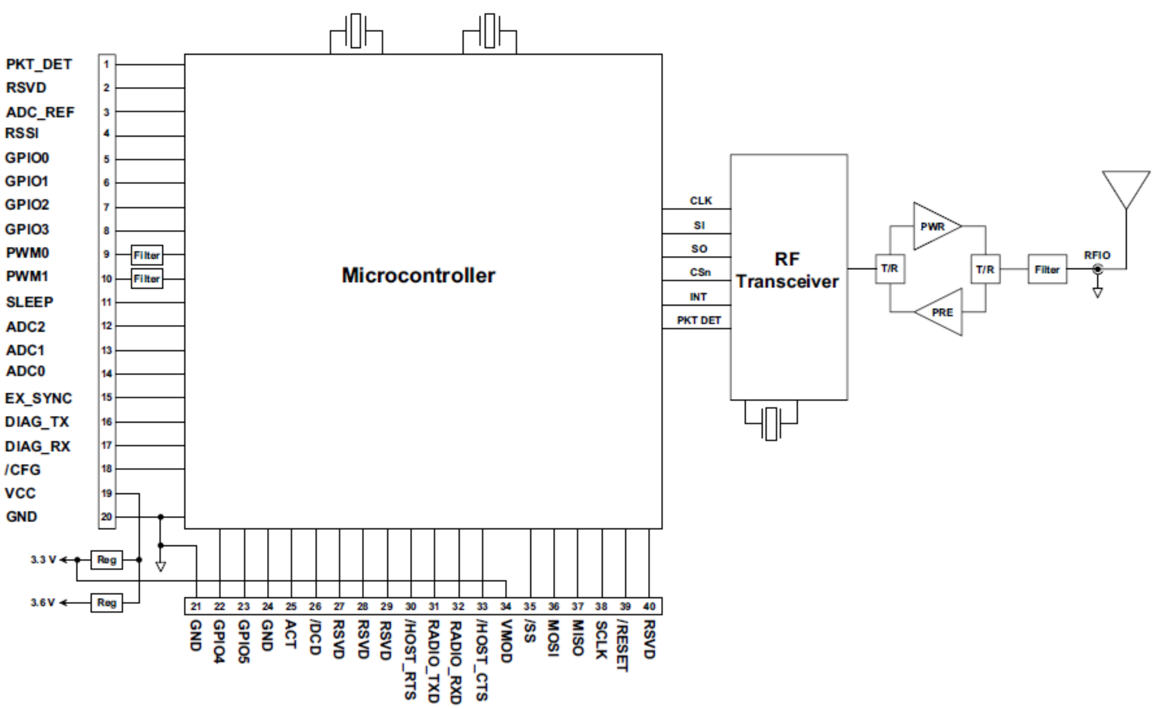

Fig. B.1: DNT900 radio transceiver block diagram.

Appendix C

FTDI FT232RL IC Block Diagram

Figure C.1 shows the block diagram of the FTDI FT232RL integrated circuit.

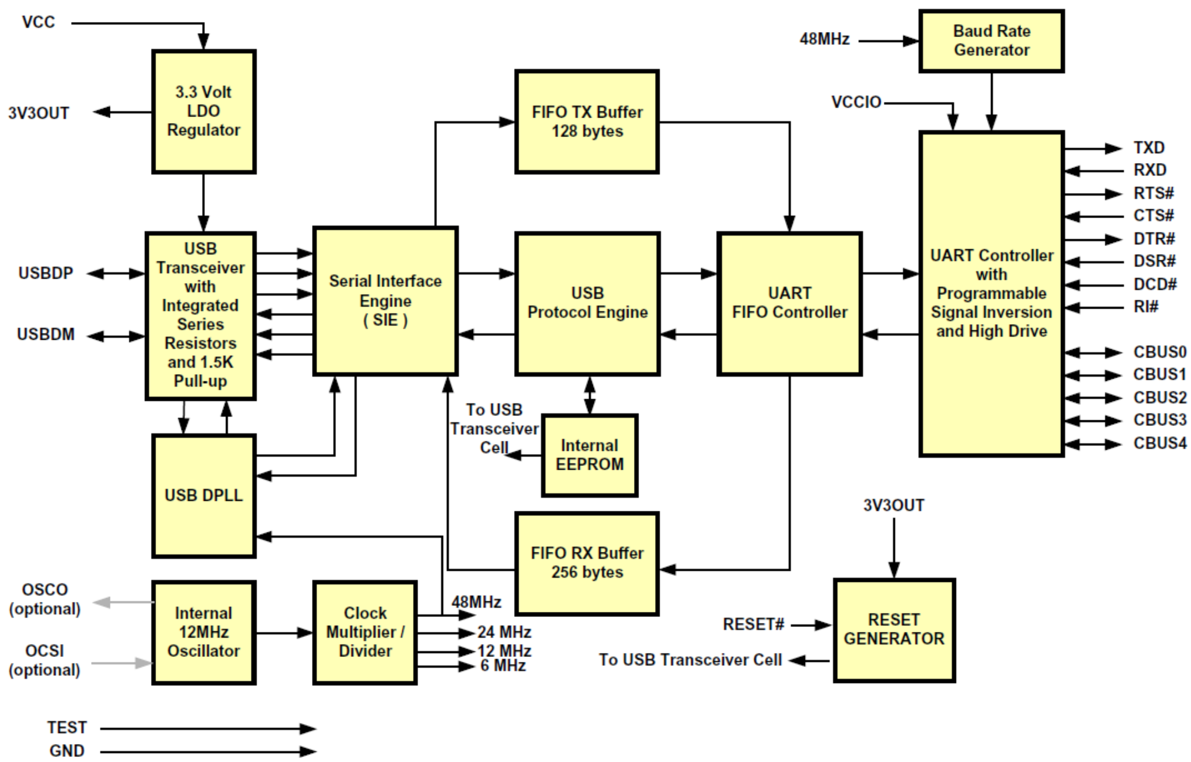

Fig. C.1: Block diagram of FTDI FT232RL integrated circuit.

Figure C.2 shows the pin out schematic of the FTDI FT232RL integrated circuit.

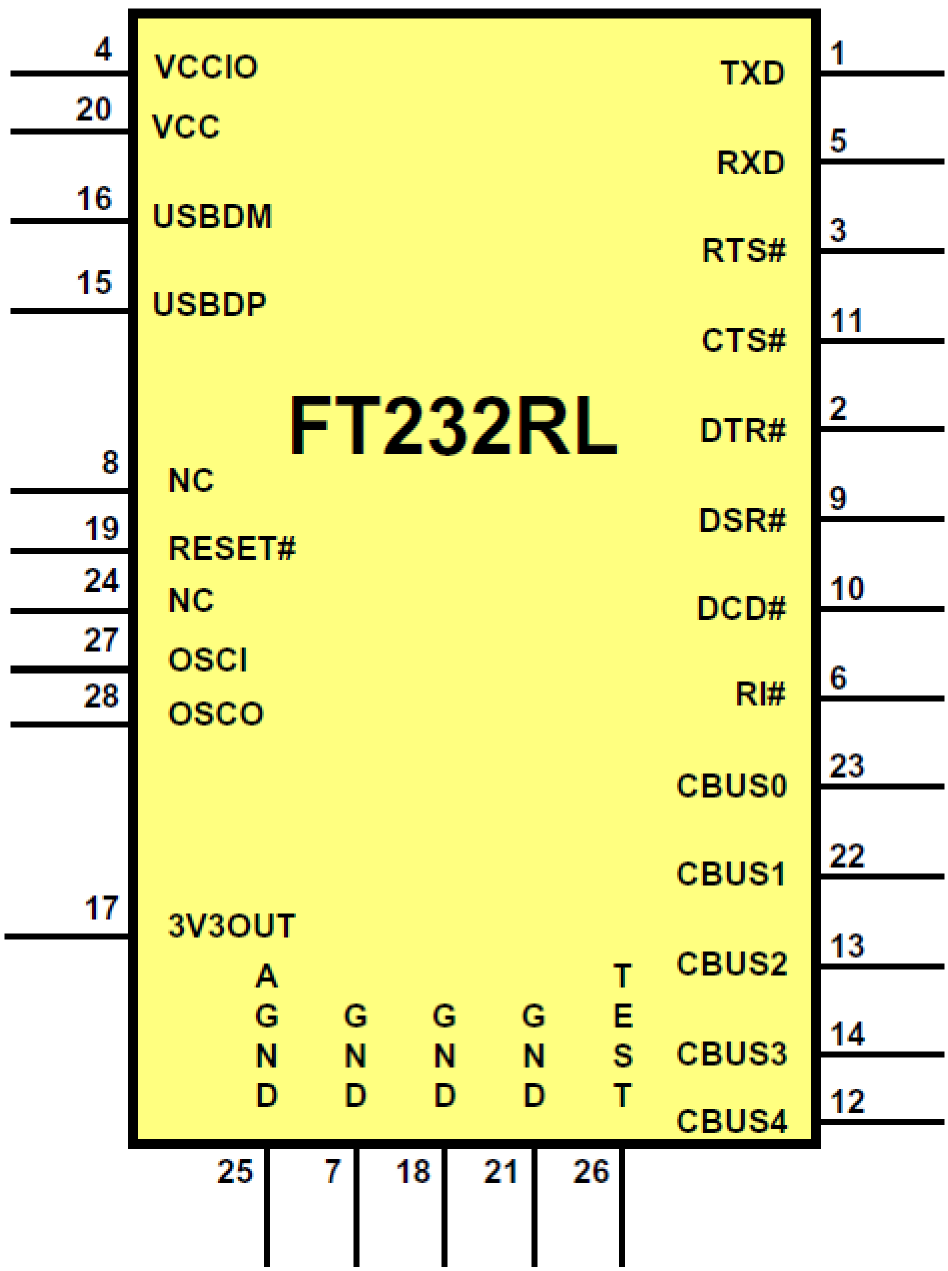

Fig. C.2: Pin out schematic of FTDI FT232RL integrated circuit.

Appendix D

Camera Module Schematic

Figure D.1 shows the hardware schematic of the camera module used in this thesis.

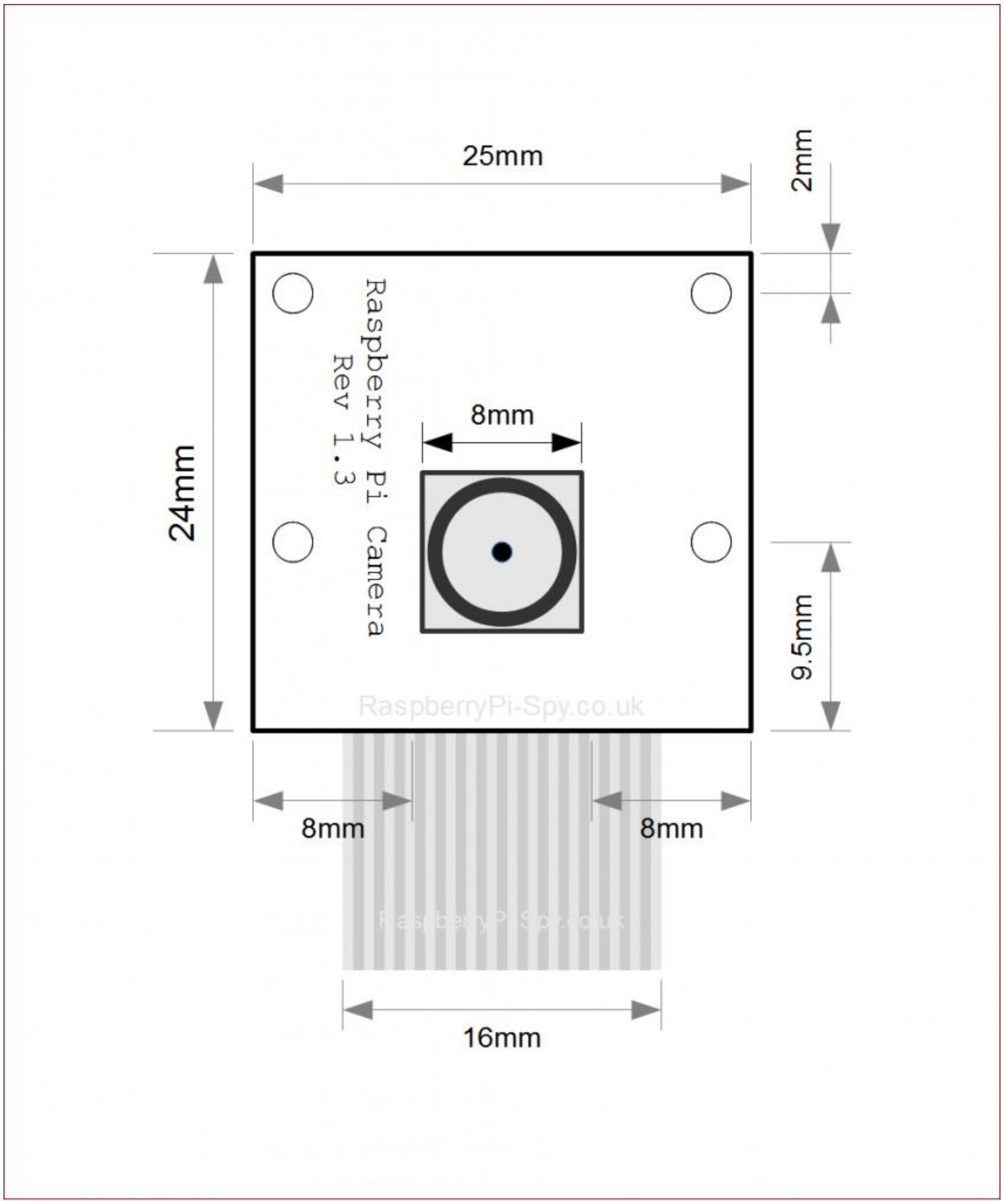

Fig. D.1: Camera module hardware schematic.

Appendix E

Yagi Antenna Data Sheet

Figures E.1 and E.2 show the Yagi antenna data sheet produced by the antenna manufacturer.

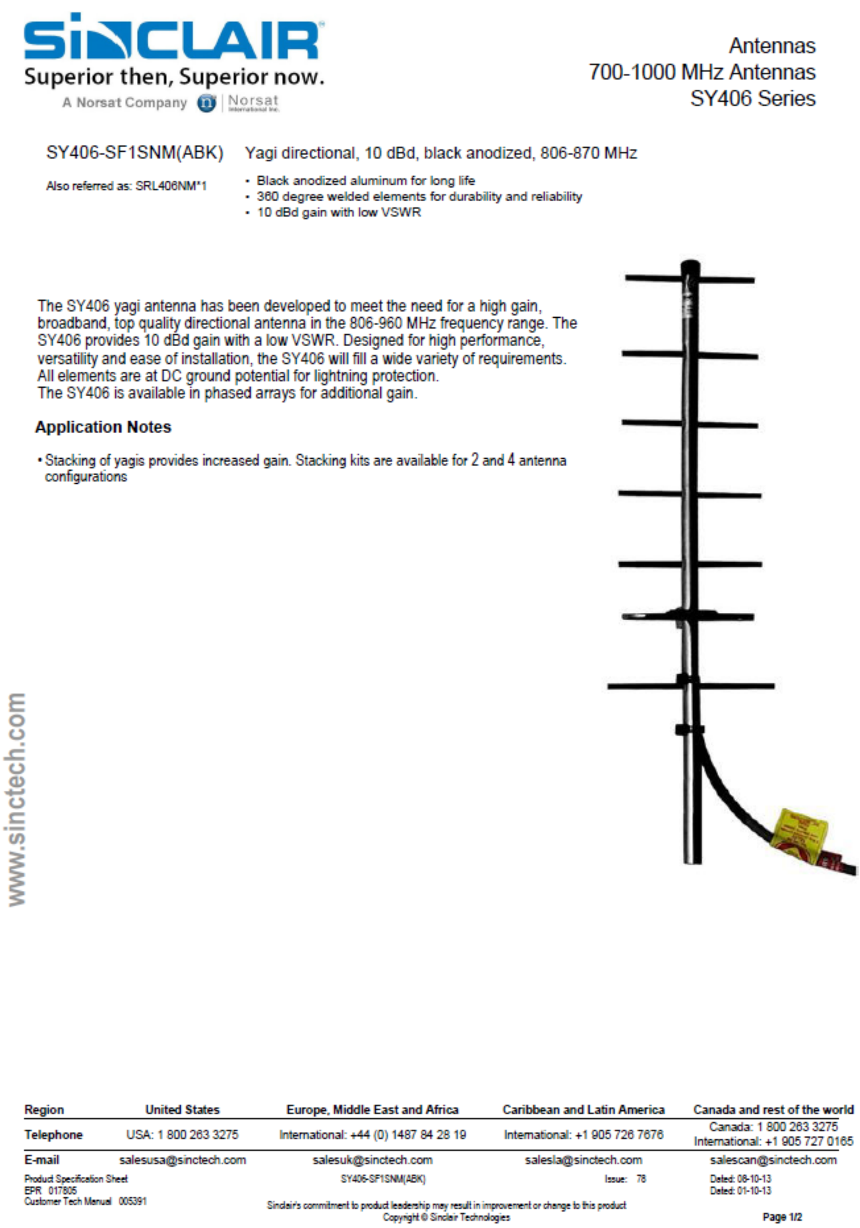

SINCLAIR
Superior then, Superior now.
A Norsat Company | Norsat International Inc.

Antennas
700-1000 MHz Antennas
SY406 Series

SY406-SF1SNM(ABK) Yagi directional, 10 dBd, black anodized, 806-870 MHz

Also referred as: SRL406NM*1

- Black anodized aluminum for long life
- 360 degree welded elements for durability and reliability
- 10 dBd gain with low VSWR

The SY406 yagi antenna has been developed to meet the need for a high gain, broadband, top quality directional antenna in the 806-960 MHz frequency range. The SY406 provides 10 dBd gain with a low VSWR. Designed for high performance, versatility and ease of installation, the SY406 will fill a wide variety of requirements. All elements are at DC ground potential for lightning protection.
The SY406 is available in phased arrays for additional gain.

Application Notes

- Stacking of yagis provides increased gain. Stacking kits are available for 2 and 4 antenna configurations

www.sinctech.com

Region	United States	Europe, Middle East and Africa	Caribbean and Latin America	Canada and rest of the world
Telephone	USA: 1 800 263 3275	International: +44 (0) 1487 84 28 19	International: +1 905 726 7676	Canada: 1 800 263 3275 International: +1 905 727 0165
E-mail	salesusa@sinctech.com	salesuk@sinctech.com	salesla@sinctech.com	salescan@sinctech.com

Product Specification Sheet SY406-SF1SNM(ABK) Issue: 78 Dated: 08-10-13
EPR 017805 Dated: 01-10-13
Customer Tech Manual 005391
Sinclair's commitment to product leadership may result in improvement or change to this product
Copyright © Sinclair Technologies
Page 1/2

Fig. E.1: Page 1 of Yagi antenna data sheet from Sinclair Technologies.

SINCLAIR
Superior then, Superior now.
A Norsat Company | Norsat International Inc.

Antennas
700-1000 MHz Antennas
SY406 Series

Electrical Specifications			
Frequency Range	MHz	806 to 870	
Bandwidth	MHz	64	
Connector		N-Male	*1
Gain (nominal)	dBi (dBd)	12.1 (10)	
Input VSWR (max)		1.5:1	
Polarization		vertical or horizontal	
Impedance	Ω	50	
Pattern		Directional	
Horizontal beamwidth (typ)	degrees	52	
Vertical beamwidth (typ)	degrees	45	
Average Power Input (max)	W	125	
Lightning protection		DC ground	
Front-to-back ratio (typ)	dB	20	

Mechanical Specifications		
Depth	mm (in)	67 (2.63)
Length/ Height	mm (in)	610 (24)
Width	mm (in)	180 (7.08)
Radiating element material		aluminum
Reflector material		aluminum
Weight	kg (lbs)	0.48 (1.06)
Finish		anodize black
Weight iced	kg (lbs)	2.13 (4.7)
Mounting Hardware (Standard)		Clamp115
Actual Shipping weight	kg (lbs)	2.27 (5)
Shipping dimensions	mm (in)	1092x213x81 (43x8.4x3.2)

Environmental Specifications		
Temperature range	°C (°F)	-40 to +60 (-40 to +140)
Wind Loading Area (Flat Plate Equivalent)	m^2 (ft^2)	0.02 (0.18)
Wind Loading Area (1/2" ice)	m^2 (ft^2)	0.05 (0.53)
Rated wind velocity (no ice)	km/h (mph)	242 (150)
Rated wind velocity (1/2" radial ice)	km/h (mph)	137 (85)
Lateral thrust (100 mph No Ice)	N (lbs)	31.1 (7)
Bending moment (100 mph No Ice)	Nm (ft-lbs)	7.1 (5.26)

Notes
*1 : N-Female also available.

Ordering Information
Specify frequency of operation.
Also available with N-female connector.
These antennas can be provided with various cable lengths- see Application notes.

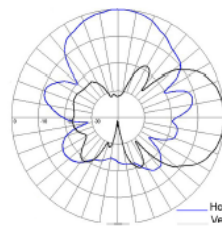

www.sinctech.com

Region	United States	Europe, Middle East and Africa	Caribbean and Latin America	Canada and rest of the world
Telephone	USA: 1 800 263 3275	International: +44 (0) 1487 84 28 19	International: +1 905 726 7676	Canada: 1 800 263 3275 International: +1 905 727 0165
E-mail	salesusa@sinctech.com	salesuk@sinctech.com	salesla@sinctech.com	salescan@sinctech.com

Product Specification Sheet
EPR 017805
Customer Tech Manual 005391

SY406-SF1SNM(ABK) Issue: 78 Dated: 08-10-13 Dated: 01-10-13

Page 2/2

Fig. E.2: Page 2 of Yagi antenna data sheet from Sinclair Technologies.

Appendix F

Spectrum Analyzer Anritsu MS2036A User Manual

The user manual for the spectrum analyzer MS2036A obtained from Anritsu Company is provided in the accompanying compact disc. It resides in the folder named "MS2036A User Manual".

Appendix G

Software Code

The accompanying CD contains the codes for the ground control station user interface, the UAV module server software and the particle swarm optimization based prediction algorithm. The ground control station user interface along with the UAV module server is written and compiled in C++ programming language. The PSO based prediction algorithm is written in MATLAB 2015a. They can be found in the folder named “Codes”.

Appendix H

Raw Experimental Data

The data packets received during the experiments conducted at St. Andrews airport (during the Mitacs Accelerate research internship conducted in partnership with BASI) are provided with the accompanying compact disc. The spectrum analyzer data from the experiments conducted in University of Manitoba campus are also provided. These files can be found in the folder named “Raw Experimental Data” in the accompanying CD.

Appendix I

Hardware and Software Figures

The following figures show hardware used in the implementation of ground control station and UAV communication module for the unmanned aerial system described in chapter 4 of the thesis. Screenshots of various stages of ground control station user interface and UAV module’s server software are also depicted.

Fig. I.1: A standard RP-SMA male antenna connector [Smac14].

Fig. I.2: A standard RP-SMA female antenna connector [Smac14].

Fig. I.3: N-female antenna connector [Ncon14].

Fig. I.4: Co-axial cable with RP-SMA male on one end and N-male on the other end [Elec14].

Fig. I.5: Antenna tripod with mast for ground control station [Elec14].

Fig. I.6: 10000 mAh USB battery pack [Adaf14].

Fig. I.7: 8 GB SD card for storage [Conr14].

Fig. I.8: Briefcase for portable ground control station.

Fig. I.9: Closed view of the ground control station briefcase with all elements inside.

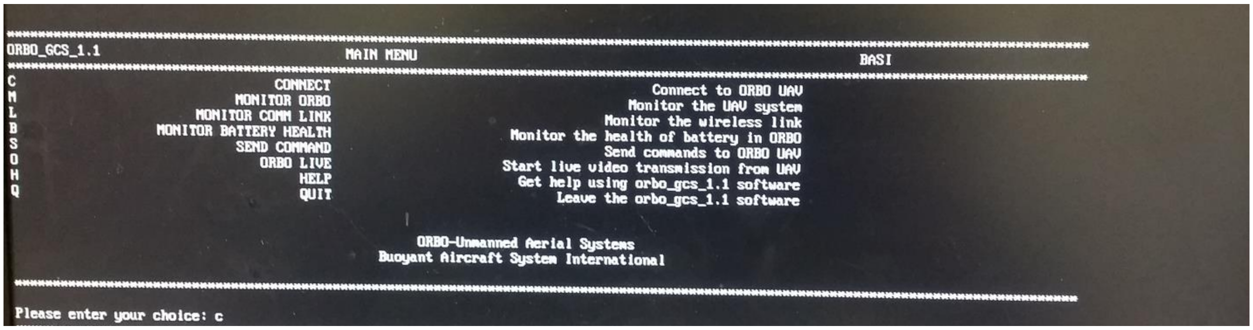

Fig. I.10: Main menu of ground control station command line interface.

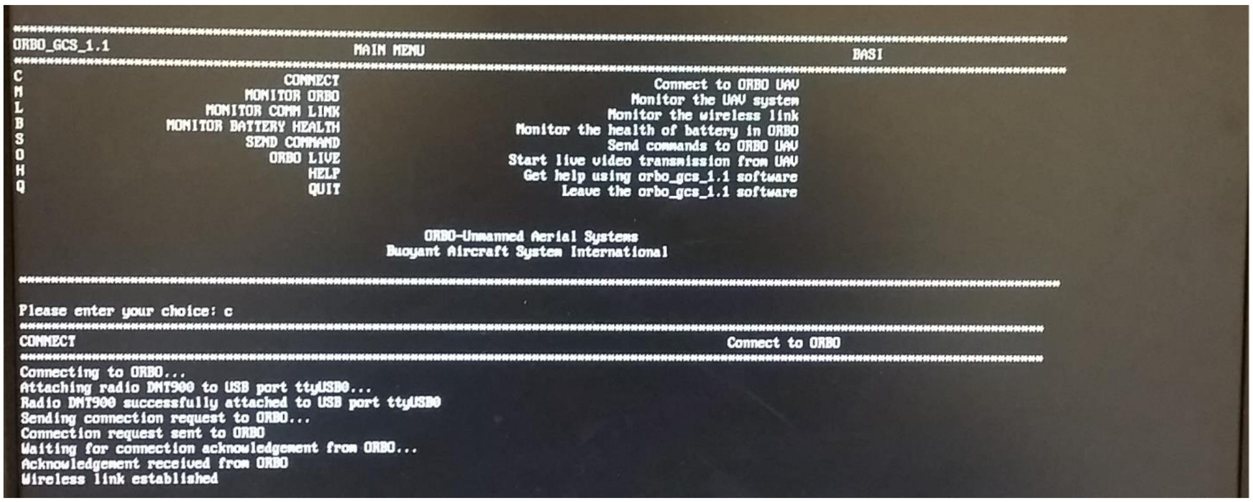

Fig. I.11: RTS/CTS signaling and acknowledgement reception to establish wireless link.

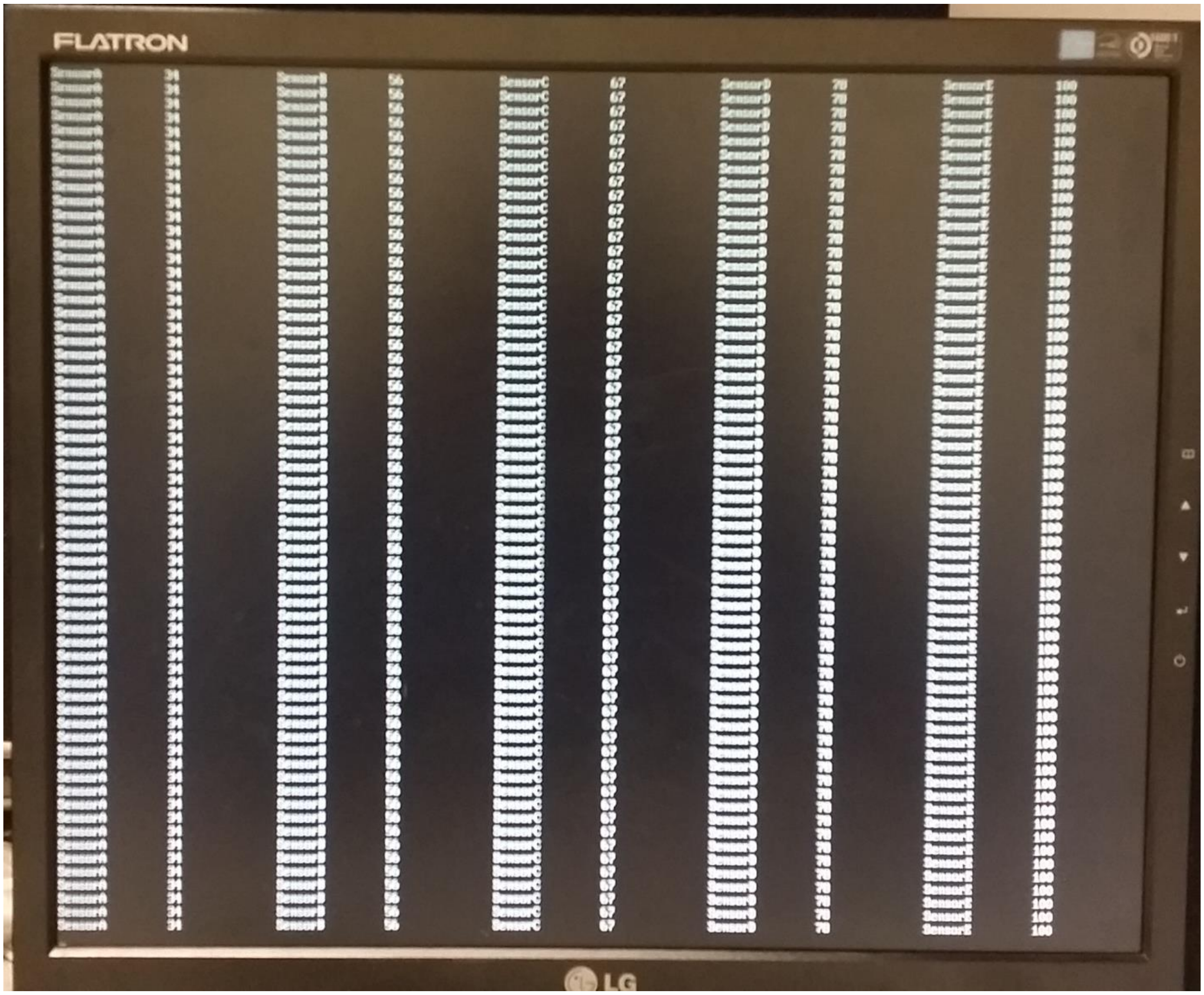

Fig. I.12: Screenshot of ground control station receiving UAV sensor data.

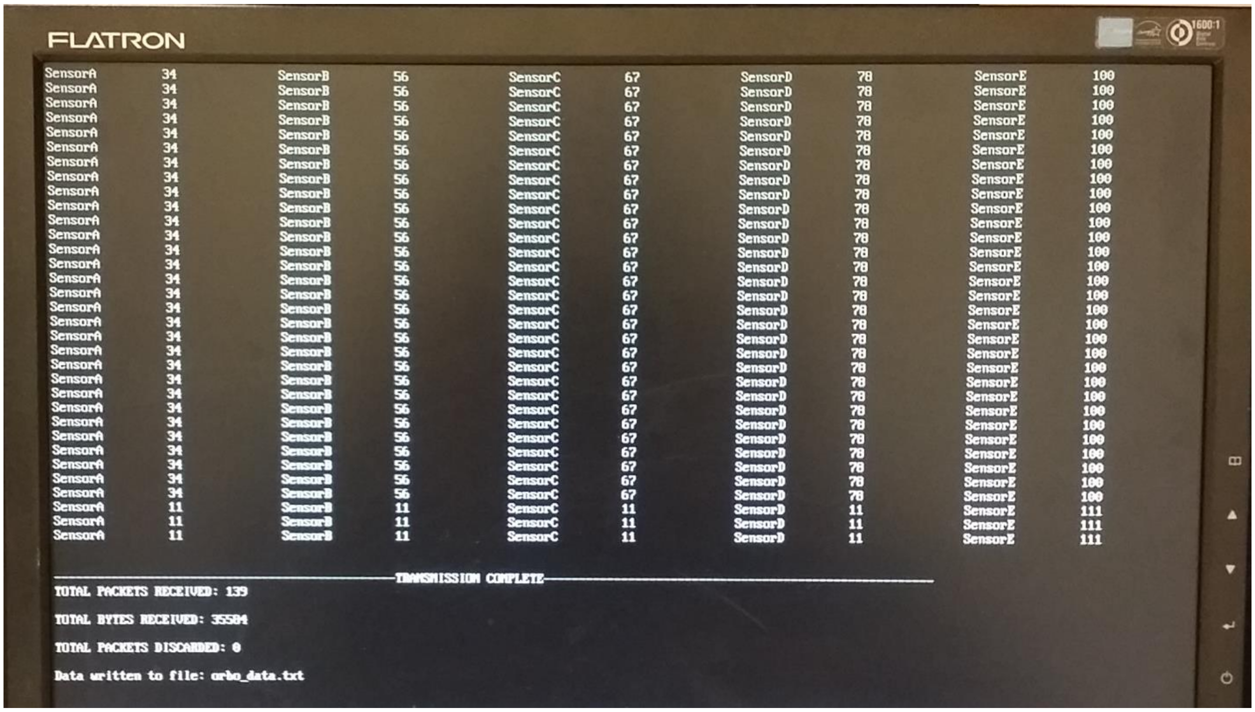

Fig. I.13: Screenshot of report generation after file transmission.

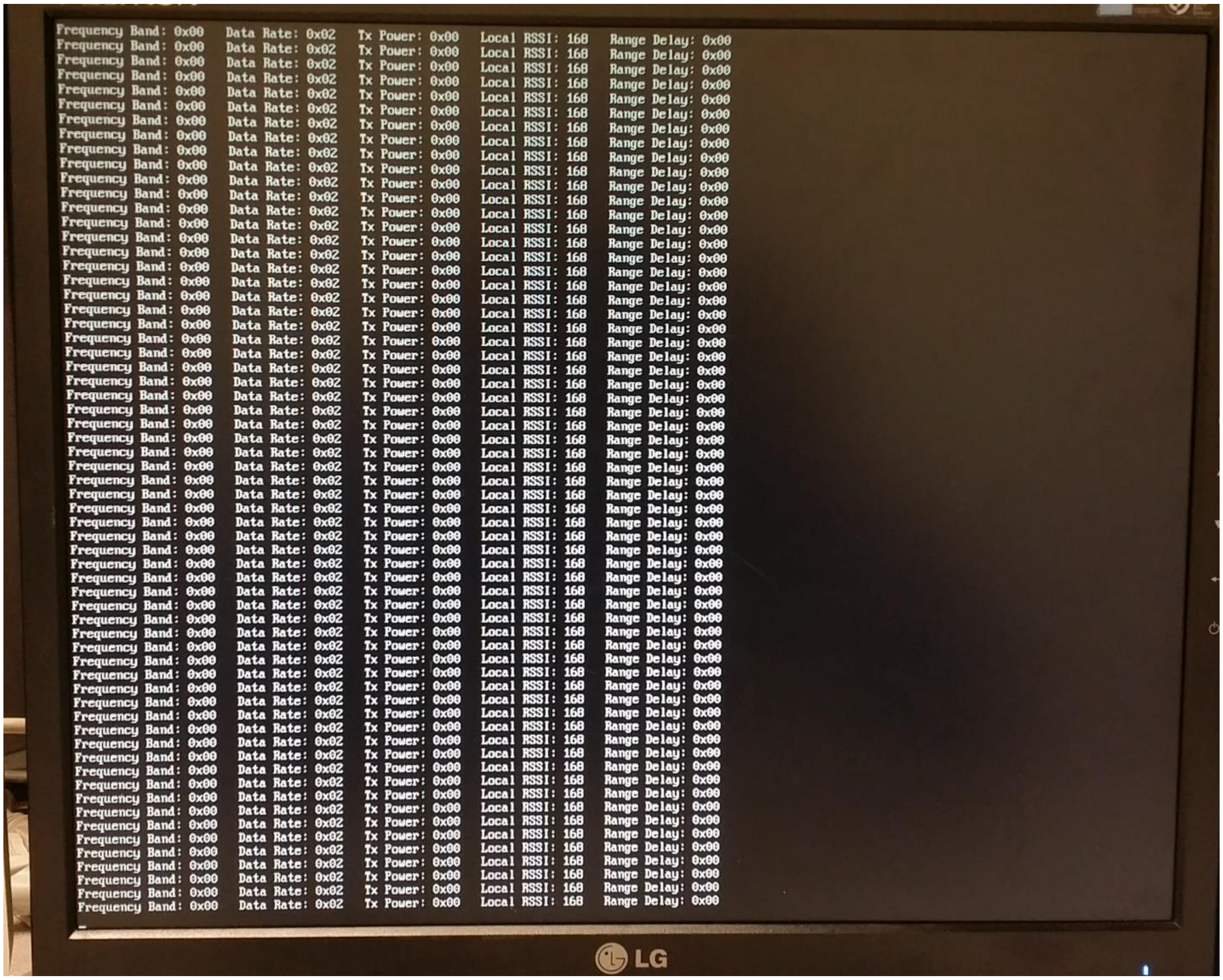

Fig. I.14: Screenshot of real time wireless channel monitoring.

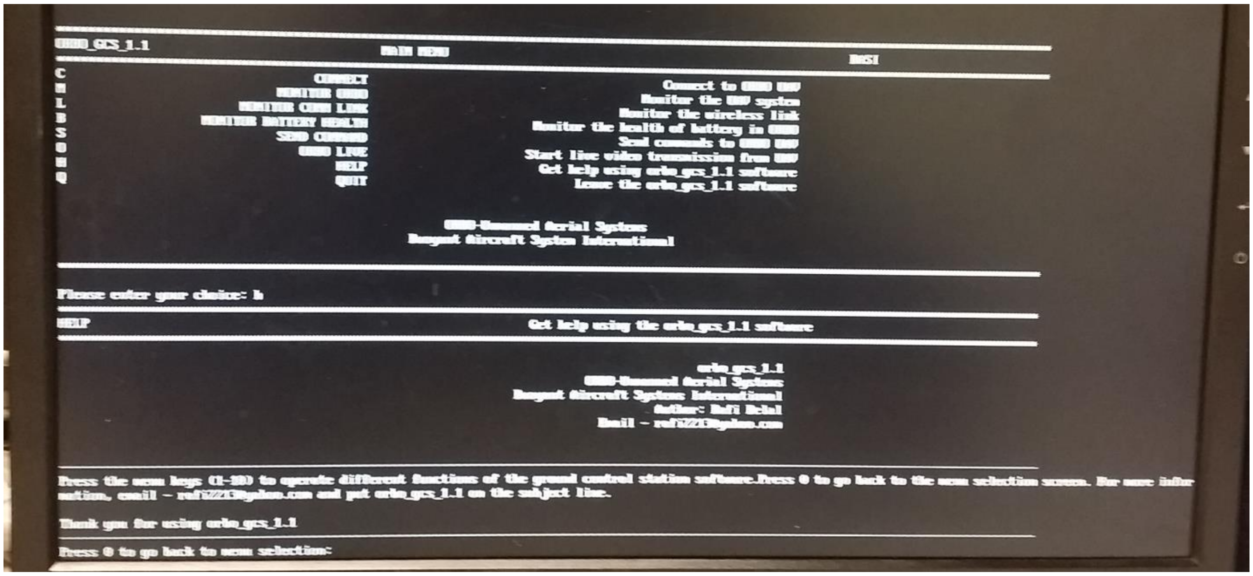

Fig. I.15: Screenshot of the HELP () function.

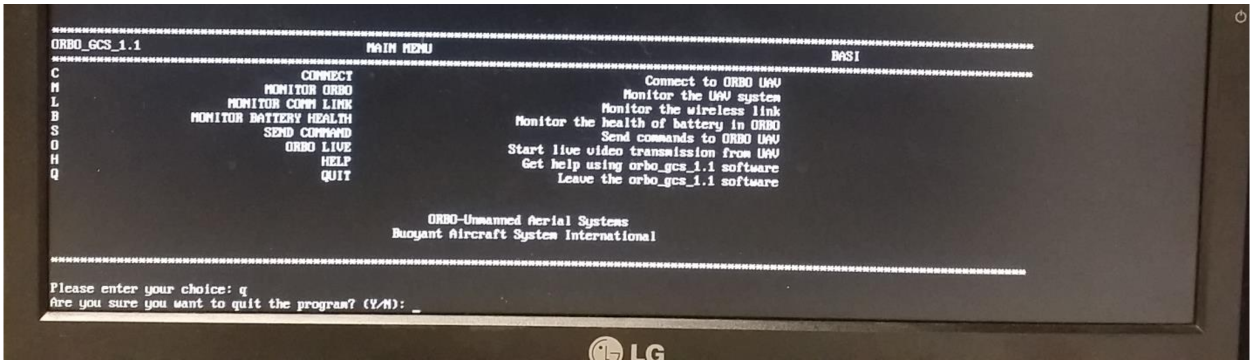

Fig. I.16: Screen shot of the EXIT () function.

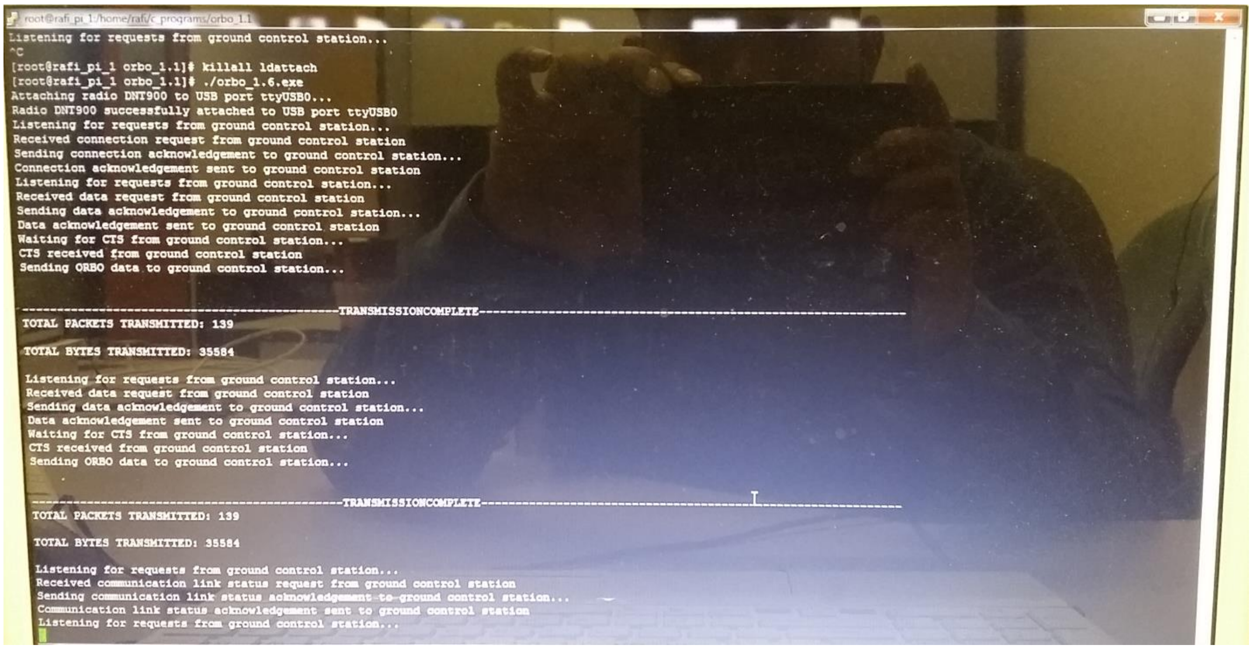

Fig. I.17: RTS/CTS signaling, acknowledgement reception and report generation after flight data transmission by the UAV module.

Appendix J

CD Contents

The accompanying cd contains all the computer generated files relevant to this thesis. The soft copy (*.pdf version) of the thesis can be downloaded from University of Manitoba's institutional repository (MSpace), under the Electronic Theses and Dissertations section. The link to the appropriate web page is provided below.

http://mspace.lib.umanitoba.ca/handle/1993/6/discover

The experimental data can also be obtained from Professor Witold Kinsner, E3-415 Engineering Information and Technology Complex, University of Manitoba, in a compact disc (CD). The contents of the accompanying CD along with the filename, description, file type and size are provided below. All of the files are checked for viruses using AVG Antivirus and Malware Protection software and reported as virus free as of 9th October, 2015. The *.pdf version of the thesis is also embedded with the fonts that were used and checked for portability with IEEE-PDF eXpress.

File Name, Description	File Type	Size [KB]
J.1. Source Codes		
J.1.1. orbo_gcs_1.6, Ground control station command line user interface	.cc	22
J.1.2. orbo_1.6, UAV communication module server software	.cc	9
J.1.3. myfun6, Modified Particle Swarm Optimizer sub-function	.m	1

J.1.4. pso_prac_5, Modified Particle Swarm Optimizer main function	.m	1

J.2. Executable Files

J.2.1. Orbo_gcs_1.6, Ground control station user interface	.exe	36
J.2.2. orbo_1.6, UAV module server software	.exe	22

J.3. Experimental Data

J.3.1. Raw Experimental Data, Received signal amplitude measurement data from MS2036A spectrum analyzer	.spa	24,400
J.3.2. Link Measurement, On-site range test and link performance test for UAV-GCS link	.txt	2,950

J.4. Supplementary Documents

J.4.1. Anritsu VNA Master 2036A, Spectrum analyzer user manual	.pdf	11,168
	Total Size [KB]	**38,609**

List of File Formats

File Extension	Association
.PDF	Portable Document Format
.CC	Source code for C++ compiler
.M	Code for MATLAB environment
.EXE	Executable file format for Windows environment
.SPA	Spectral data file
.TXT	Plain text file